

N66-15543

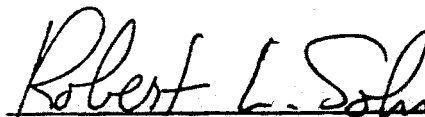
5303-6013-TU000

STUDY OF UNMANNED SYSTEMS
TO EVALUATE THE MARTIAN ENVIRONMENT
Volume I. Sensitivity Analysis
Contract NAS 2-2478

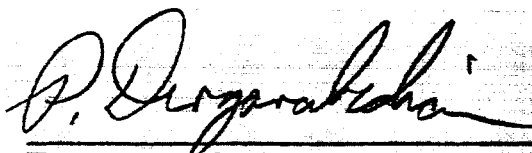
Prepared for:

National Aeronautics and Space Administration
AMES RESEARCH CENTER
Moffett Field, California

23 September 1965



R. L. Sohn
Study Director

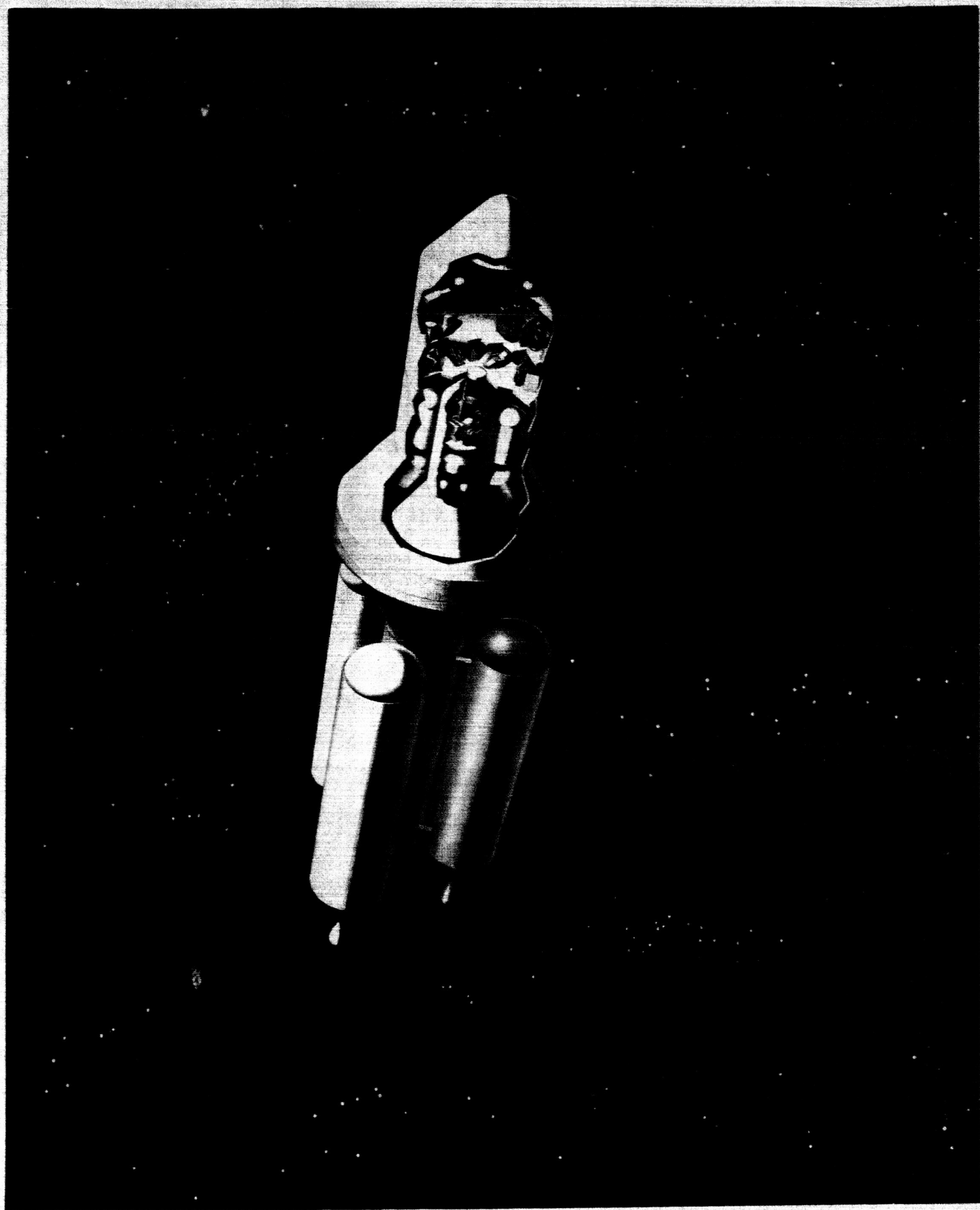


P. Dergarabedian, Director
Systems Research Laboratory

TRW Systems
One Space Park
Redondo Beach, California

The present report is comprised of four volumes:

Volume I	Sensitivity Analysis
Volume II	Experiment Requirements
Volume III	Unmanned Spacecraft Design
Volume IV	Summary



FOREWORD

The following personnel have contributed to the present report:

J. Alper
S. Altshuler
L. I. Dimmick
R. W. Fredricks
A. A. Jensen
R. H. Johns
W. G. Koerner
H. G. Myer
L. D. Simmons
R. L. Sohn

TABLE OF CONTENTS

	Page
1. SUMMARY	1-1
2. INTRODUCTION	2-1
2.1 Study Objectives	2-1
2.2 Study Approach	2-1
3. SCOPE	3-1
4. REFERENCE MANNED MARS SYSTEM	4-1
4.1 General Mission Characteristics	4-1
4.2 Vehicle Design	4-5
4.3 Navigation	4-15
5. ENVIRONMENTAL FACTORS	5-1
5.1 Mission - Environment Interactions	5-2
5.2 Discussion of Environmental Factors	5-4
6. AERO ENTRY SYSTEM ANALYSIS	6-1
6.1 Corridor Analysis	6-1
6.2 Summary of Corridor Capabilities	6-30
6.3 Heat Shield Analysis	6-33
6.4 Effect of Corridor Performance on Vehicle Weight	6-43
7. MARS LANDER SYSTEM ANALYSIS	7-1
7.1 Descent Phase	7-2
7.2 Landing Dynamics	7-15
7.3 Ascent Phase	7-24
7.4 Communications Blackout During Entry	7-27
7.5 Power Breakdown of Antennas in Martian Atmosphere	7-46
8. SURFACE MOBILITY	8-1
8.1 Typical Surface Rover Design	8-1
8.2 Environmental Factors	8-1
8.3 General Mobility Analysis	8-4
8.4 Typical Soil Properties	8-12
8.5 Vehicle Performance	8-13
8.6 Rocket Boost Glide Vehicles for Surface Exploration	8-25
8.7 Surface Range Requirements	8-33

TABLE OF CONTENTS (Continued)

	Page
9. NUCLEAR AND METEOROID RADIATION EFFECTS	9-1
9.1 Nuclear Radiation	9-1
9.2 Meteoroid Flux	9-6
10. POTENTIAL CONTAMINATION HAZARD	10-1
10.1 Introduction	10-1
10.2 The Possibility of Life on Mars	10-1
10.3 The Possibility of Potentially Harmful Organisms on Mars	10-5
10.4 The Study of Martian Organisms by Unmanned Probes .	10-8
10.5 Prevention of Back Contamination	10-10
11. SYSTEM ANALYSIS	11-1
11.1 Mission Modes	11-1
11.2 Mission Sensitivity Factors	11-2
11.3 System Weight Sensitivity	11-12
11.4 System Weight Sensitivity Summary	11-15
12. PRIORITY RATINGS	12-1
12.1 Evaluation Factors	12-1
12.2 Experiment Priorities	12-3
13. CONCLUSIONS	13-1
14. REFERENCES	14-1
APPENDICES	

1. SUMMARY

A study of the sensitivity of the Manned Mars Mission to the Martian and Cismartian environment has been performed under Phase I of Contract No. NAS 2-2478. The primary objective of the Phase I activity was to: identify those environmental factors that can influence the planning and design of the Manned Mars Mission, and to establish the qualitative and quantitative relationships between uncertainties in the environmental factors and the design of the mission. Results obtained from the analyses reported herein are summarized below.

The priorities for the experiments in the order of their importance are: solar cosmic radiation environment, meteoroid environment, and atmospheric properties.

The atmosphere models assumed include the Schilling II Upper Limit (132 mb), the NASA Model 2 (25 mb) and the NASA Model 3 (10 mb) versions. Recent data tend to favor the lower density models. The NASA Model 2 (25 mb) version was selected for the nominal case. A review of available data on the Martian atmosphere was made, and probable limits established for the various factors. Analyses were made to support the review where required.

Effects of Atmosphere Uncertainties

The uncertainties in the Martian environment, as bounded by, the Schilling II Upper Limit Model (132 mb) and the NASA Engineering Model 3 (10 mb) can reduce the entry corridor in the worst case from 74.5 km to 21.9 km for a spacecraft having a lift-to-drag ratio capability of 0.3. Corridor reductions due to roll requirements are negligible, but uncertainties in diurnal effects on atmosphere scale height and density, which were not calculated directly for the Martian atmosphere, could reduce the corridor by an additional 10 km, based on earth reentry analyses. The corridor accuracies attainable with state-of-the-art navigation systems is estimated to be 5.4 km (3σ), which is within the capabilities of the $L/D = 0.3$ aero entry system, unless the diurnal effects are greater than 10-15 km. An increase in L/D to 0.4 increases the corridor (for the worst combination of atmosphere properties) to 46 km which is adequate to cover the above uncertainties.

Recent Mariner IV occultation experiments, and results obtained by recent earth-based spectroscopic analysis by Munch and others, indicate that the band of uncertainties on the Martian environment probably are covered by the Model 2 and Model 3 atmospheres (25 to 10 mb), in which case the corridors attainable with $L/D = 0.3$ are more than adequate.

Aero heating shield requirements are not stringent (amounting to about 7 percent of the spacecraft weight at Mars entry) and do not vary greatly with L/D , up to about $L/D = 0.3$ to 0.4 . About 4000 lbs additional shielding is required if L/D is increased from 0.1 to 0.3 . The greatest effect on shielding is due to uncertainties in scale height, which determine the length of time the shield is retained after entry until a safe jettisoning altitude is reached. Uncertainties in composition are not important, except for the effect of composition on density variation with altitude. Radiative heating effects are reduced to a minimum by sharply pointing the forebody of the spacecraft. Atmosphere surface density can affect the design of the Mars Excursion Module in the areas of decelerator sizes and weights, and in ascent trajectory shaping and propellant requirements. Decelerator (parachute plus retro) weights can be increased by 1.8 percent in the worst case, leading to 0.1 percent increase in spacecraft gross weight. Ascent trajectory losses are affected appreciably because of parking orbit altitude variation with atmosphere density. Increases of 2.3 percent in spacecraft gross weight are incurred in the worst case.

Radiation Environments

Nuclear radiation dosages appear to be within limits prescribed for the Apollo mission, assuming a shield of 22 gm/cm^2 . Recovery effectiveness, if realizable, could reduce the shield to 10 gm/cm^2 , resulting in a 4.8 percent reduction in spacecraft gross weight. The Mars atmosphere contributes somewhat to shielding against nuclear radiations and does not cause peaking of total secondary radiations. Uncertainties in the solar radiation environment and shielding effectiveness could increase shield thickness from 22 gm/cm^2 to 35 gm/cm^2 , resulting in an additional spacecraft gross weight penalty of 3.5 percent. The overall effects of uncertainties in recovery factor, and flux and shielding effectiveness could increase gross weight by 8.3 percent.

Uncertainties in meteoroid flux mass models can amount to one order of magnitude, resulting in shielding weight increases of about 100 percent. The resulting increase in spacecraft gross weight is 7.5 percent. It is noted that meteoroid flux and shielding effectiveness uncertainties have a relatively large effect on mission weight, and should be reduced by precursor missions.

Winds

Winds can have a substantial effect on landing operations, due to reduced vision because of dust, excessive drift rates, which must be nulled before impact, and propulsion requirements to null drift velocity and drift range. In the worst case spacecraft gross weights could increase by 0.7 percent due to winds. Drift meters must be installed to effect drift cancellation. The effects of winds on MEM ascent are small because of the small dynamic pressures generated.

Biocontamination

Possible contamination of the lander crews by pathogens on the Martian surface cannot be predicted in advance of the manned missions based on the results of precursor missions. Decontamination procedures have been devised to reduce the possibilities of contamination to acceptable levels; this effect should not pose a strong hazard to the crews, but may constrain surface operations on the early missions.

Soil and Terrain Properties

The lander touchdown dynamics can be affected by soil conditions and terrain characteristics, but to a minor degree. Landing gear designs can be adopted which minimize these effects with little increase in weight. Surface rover performance could be seriously affected by unusually weak or sticky soils. These effects can be minimized by proper design techniques, particularly the use of wide track techniques, but range performance would be reduced.

Ionization at Surface

The presence of a strong ionization belt at the surface of Mars has been predicted. This belt could affect the proper functioning of electrical equipment and communication radiators. It also interjects an uncertainty in Mariner 4 measurements of the atmosphere by radio occultation techniques.

Experiment Priorities

A summary of the sensitivity analysis is given in Figure 1.1. A recommended list of experiment priorities is given in the following table.

	DESIGN FEASIBILITY	WEIGHT PENALTY	OPERATIONAL CRITERIA	DEVELOPMENT CRITERIA	EXPERIMENT ACCURACY
ATMOSPHERE					
THERMO					
PRESSURE					
TEMPERATURE	2	2	1	1	50%
CHEMICAL COMP					
ELECTRICAL PROP	-	2	-	-	
IONOSPHERE	-	2	2	-	
SURFACE IONIZATION	1	1	1	1	
DIURNAL AND SEASONAL EFFECTS	2	2	1	-	
METEOROLOGY					
WINDS	2	1	2	-	50%
CLOUDS	-	-	1	-	
DUST STORMS	1	1	1	-	
CLIMATE	1	-	1	1	
SURFACE CONDITIONS					
SURFACE COMP	2	1	2	2	
SOIL PROPERTIES	2	1	2	2	25%
TOPOGRAPHY	1	1	2	2	
RADIOACTIVITY	1	-	1	1	
SEISMIC ACT	1	-	-	-	
AREOLOGY		(SEE SURFACE CONDITIONS)			
BIOLOGY	2	1	2	2	
RADIATION ENVIRONMENT					
COSMIC RAD SURFACE	2	1	2	1	20%
COSMIC RAD - CISMARTIAN	3	3	3	3	
UV RAD AT SURFACE	1	-	2	-	
METEOROID ENVIRONMENT	2	3	1	1	60%
GENERAL					
ALBEDO - ABSORP	1	1	-	1	
MAG FIELD	1	-	-	-	
GRAV FIELD	1	1	1	-	
	3	HIGH PRIORITY			
	1	LOW PRIORITY			

Figure 1.1

C ARRIVE EARTH - AERO
 A DEPART MARS - CHEM
 C ARRIVE MARS - AERO
 A DEPART EARTH - CHEM

% CHANGE IN EARTH ORBIT WEIGHT

	AERO AT MARS		RETRO AT MARS			FLYBY		DIRECT	
	CACA		NANA			CA		CACA	
	1982	1986							
UNCERTAINTY IN ATMOSPHERE CAPTURE MEM	1.8	1.4	1.3	0	0			1.8	1.7
	2.5	2.3	2.1	1.7	2.1	--	--	4.2	3.8
COMBINED	5.3	3.7	3.4	1.7	2.1	<1.0	<1.0	6.0	4.6
	0.3(0.4)*	0.3(0.4)*	0.3(0.3)*	0.2(0.2)*	0.3(0.3)*			2.4(2.8)*	2.4(2.8)
EFFECT OF WINDS 50% WINDS (GRADIENT) MAX WINDS (NO GRADIENT) MAX WINDS (GRADIENT) MAX WINDS (GRADIENT, NO RANGE MAKEUP)	0.3(0.2)	0.3(0.2)	0.3(0.2)	0.2(0.1)	0.3(0.2)			2.3(1.6)	2.3(1.6)
	0.7(1.1)	0.7(1.0)	0.6(0.9)	0.5(0.7)	0.6(0.9)			5.6(8.0)	5.6(8.0)
	0.2(0.2)	0.2(0.2)	0.1(0.1)	0.1(0.1)	0.1(0.1)	<1.0	<1.0	1.3(1.2)	1.3(1.2)
MICROMETEOROID DOUBLE THICKNESS	7.5	5.4	4.8	8.9	10.1	14.6	7.9	21.4	20.8
MSC/STL (Cometary)	7.4	5.7	4.8	6.8	7.1	10.0	6.5	14.5	14.3
SOLAR COSMIC RADIATION HALF THICKNESS (90% RECOVERY)	-4.8	-6.5	-3.9	-6.5	-5.0	-9.1	-9.1	-5.2	-5.8
UNCERTAINTY IN SHIELD EFFECTIVENESS & FLUX TOTAL UNCERTAINTY	3.5	4.7	2.8	4.7	3.6	6.6	6.6	3.7	4.2
	8.3	11.2	6.7	11.2	8.6	15.7	15.7	8.9	10.0

* Sch Upper Limit

2. INTRODUCTION

Recent studies of the Manned Mars Mission, including those conducted by Space Technology Laboratories for the NASA Ames Research Center (Reference 1.1), have indicated that it may be possible to perform the early manned mission during the early 1980's. Unfortunately, many gaps exist in our knowledge of the environment of Mars, to the extent that many decisions in the selection of basic mission modes cannot be made with certainty, and specific designs for any given mode are difficult to prepare because of lack of realistic design criteria. The Manned Mars Mission advance planning study programs will suffer similar shortcomings until more complete data on the planet become available.

Based on the foregoing considerations, two key requirements can be placed upon unmanned precursor missions to Mars: first, the precursor programs should be targeted for the near future so that they can contribute most effectively to the early manned mission planning and development programs, and secondly, the precursor programs should be capable of performing those measurements which are of most importance to design and development of the manned missions.

2.1 Study Objectives

The objectives of the proposed study program can be clearly stated as:

- o Those environmental factors that can influence the planning and design of Manned Mars Mission systems are to be identified, and sensitivity analyses performed to establish the quantitative relationship between uncertainties in the determination of the environmental factors and the system implementation.
- o The design of unmanned systems to obtain the necessary environmental information are to be analyzed and compared.

2.2 Study Approach

The sequence of study analyses tasks is shown in Figure 2.1. The study program is divided into two phases: the first deals with the determination of the sensitivity of the manned mission systems to the environmental factors, and culminates with the tabulation of the pertinent factors and the relative importance of each; the second phase of the study is devoted to the analysis of unmanned spacecraft systems designed to acquire the necessary environmental data.

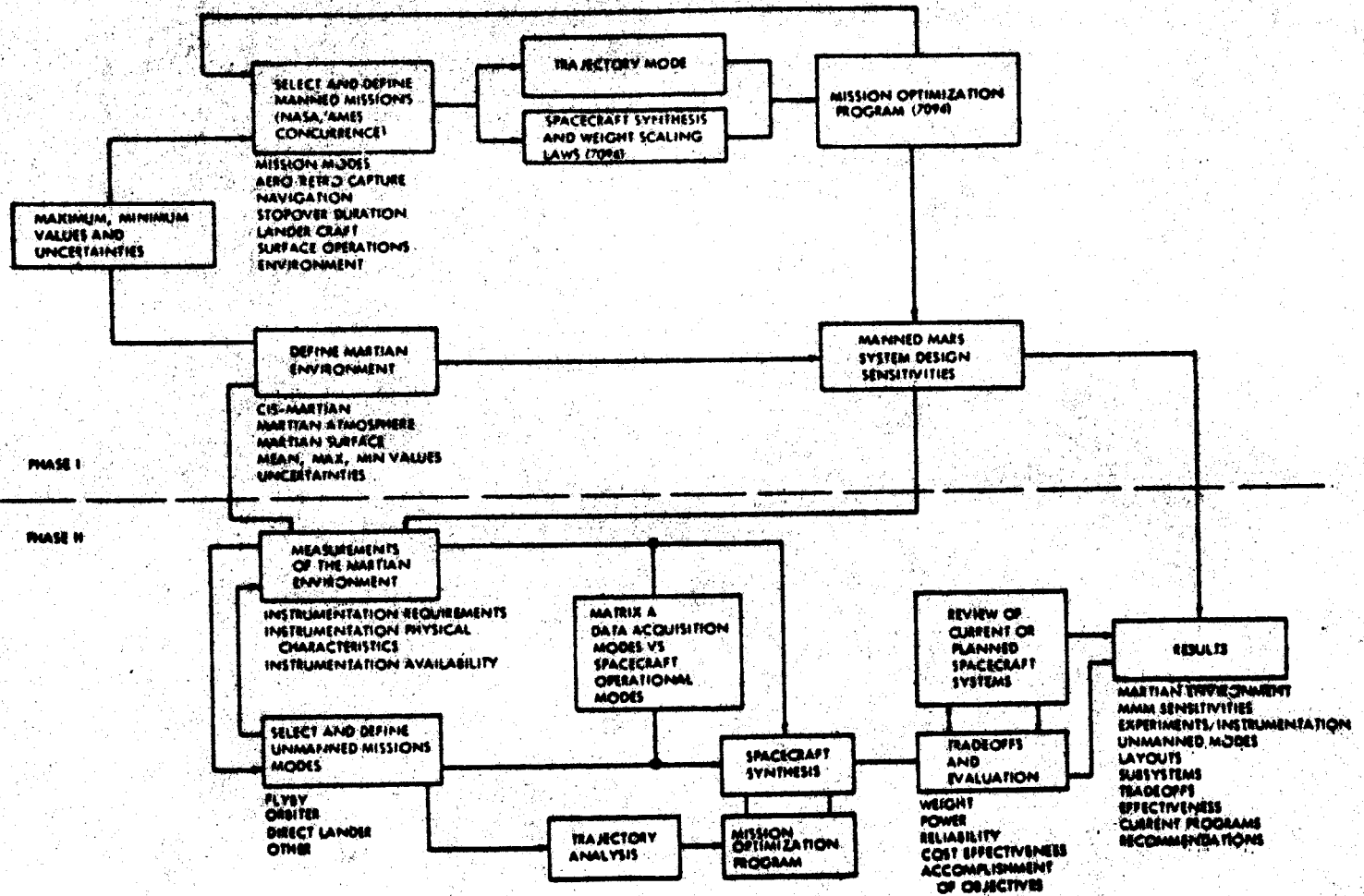


Figure 2.1 Sequence of Study Analysis Tasks

Reference Manned Mars Mission profiles have been selected with the concurrence of NASA/Ames, and are used as a basis for the system sensitivity analyses. System weight scaling laws developed at TRW (Reference 1.1), available on computer set ups, were used to compute the changes in system weight and design as a result of variations in selected environmental factors. Environmental factors were selected after a survey and analysis of known or estimated environmental data.

A TRW mission optimization computer set up was used to establish best trajectory paths and calendar dates for each mission analysis case. This step is vital to the sensitivity analysis because small deviations from the optimum path can cause significant increases in spacecraft gross weight, completely obscuring the effects of variations in environmental factors.

The results of Phase I are used as the basis of establishing the functional requirements for instrumentation and unmanned spacecraft operating modes analyzed in Phase II of the study. A suitable matrix of cases was prepared, combining data acquisition modes and spacecraft operating modes, including flyby, orbiter and direct lander techniques.

Spacecraft designs generated for the selected modes are sufficiently detailed to permit an evaluation and comparison of the various approaches. The mission optimization technique described above for the Phase I sensitivity analyses was used to select the best trajectory paths and calendar dates. The trade-offs and comparisons include weight, power, reliability, relative cost, and effectiveness in accomplishing mission objectives.

An important task in Phase II is the selection of a matrix of data acquisition modes and spacecraft operational modes, including flyby, orbiter and direct landing modes. Certain of these modes cannot accommodate all data acquisition functions, and require a sequence of missions to obtain the necessary environmental data, (e.g., Martian atmosphere). Other spacecraft modes are complex, or cannot easily satisfy the sterilization criteria. Each spacecraft operational mode requires that measurements be made with different techniques or different instrumentation.

The present report contains the analyses and results of the Phase I study. The environment is described, and environmental factors selected that have an influence on the design of the manned system. Vehicle design analyses are

presented to establish the quantitative relationships between parametric changes in the environmental factors and the design implementation. Where possible, upper and lower limits are assigned to the pertinent environmental factors to bound the parametric analyses. The sensitivity of the complete manned planetary spacecraft to the environmental factors was computed using existing mission optimization techniques; the results are presented in terms of changes in overall system gross weight on earth orbit. It is noted, however, that in many areas, environmental factors do not have a significant effect on system gross weight, but do influence the system design in an important way. These interactions are noted as well.

3. SCOPE

A wide range of Manned Mars Mission modes was analyzed for sensitivity to the martian and cismartian environment. The modes examined include Flyby, Mars Orbiting Rendezvous (MOR) with landings by a Mars Excursion Module (MEM), and Direct landing. Chemical and nuclear propulsion configurations were included, as well as aerodynamic and retro braking modes at Mars. The matrix of cases is given in Table 3.1 This matrix was adopted for the sensitivity analysis with the exception that the range of mission opportunities extended from 1975 - 1990.

TABLE 3.1 MANNED MARS MISSION MODES

I. Perform Sensitivity Analysis to Establish:

- (1) Effect of environmental uncertainties on nominal manned mission
- (2) Environmental measurements priority for nominal mission
- (3) Nominal mission for detailed investigation:
1982 MOR - Aerobraking - 7 men - 10 day staytime -
chemical propulsion
- (4) Apply scaling laws or other suitable criteria to determine
effect of environmental uncertainties on nominal mission
during 1980-1995 time period
- (5) For comparison with nominal mission determine these effects
on other manned missions including:
 - (a) Flyby (3 men)
Chemical and nuclear
 - (b) Landing (10-day staytime)
Chemical and nuclear
 - (i) Direct (4 and 7 men)
 - (ii) MOR (7 men)
aerobraking (nominal mission)
retrobraking

Three atmosphere models were selected by the Ames Research Center:

NASA Model 3 (10 mb)

NASA Model 2 (25 mb)

Schilling II Upper (132 mb)

Properties of the atmospheres are given in Section 5.

4. REFERENCE MANNED MARS SYSTEM

The following paragraphs present typical mission characteristics and a reference manned Mars system design, based on the results of a recent study conducted for the Ames Research Center (Reference 1.1). The system is analyzed for its sensitivity to uncertainties in the Martian environment. Scaling laws presented in Appendix C are used to adjust the reference design for changes in mission parameters (velocity, duration), design parameters (propellants, micro-meteoroid protection, solar radiation protection), and mission modes (retro braking, aero braking, fly-by and direct lander).

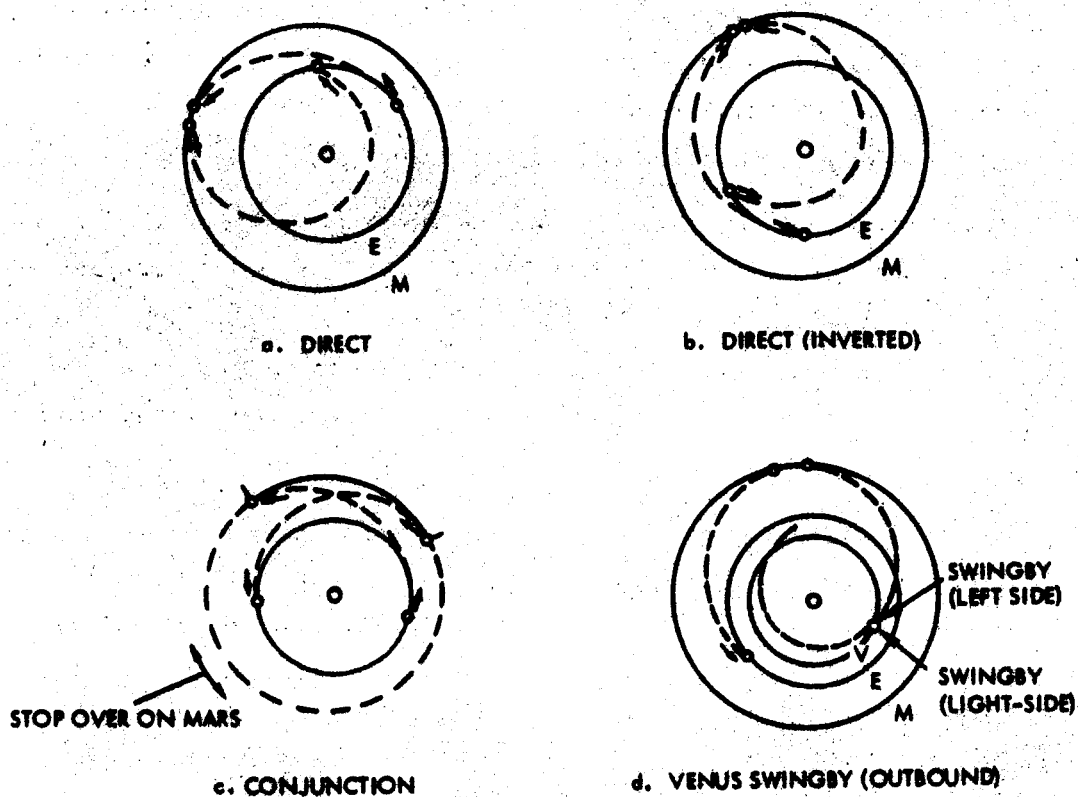
4.1 General Mission Characteristics

Launch opportunities for Mars round trip missions are generally associated with Mars-Earth oppositions, and precede by 3 to 4 months the opposition dates, which occur on the average every 25.6 months. Because of the eccentricity of the Mars orbit, the mission trajectory profiles change from one opposition to the next. Earth entry velocities are particularly sensitive to changes in trajectory profiles, and range from 46,000 fps in a favorable opposition such as 1971, to 70,000 fps in an unfavorable opposition such as 1980. The cyclic pattern of mission profile variations repeats every 15 years, or every 7 oppositions.

Mission Modes

Two general classes of direct-mode round trips to Mars are available: opposition-class modes with short stopover, and conjunction-class modes with long stopover. The opposition-class missions are shortest in duration but are characterized by high earth-return velocities in the majority of mission opportunities. This undesirable situation is avoided in the conjunction-mode missions in which the departure from Mars is delayed in order to achieve a more favorable earth-return path.

Typically, the direct-mode round trip to Mars consists of a short ($>180^\circ$) transfer to Mars, arriving approximately 100 days after opposition, with return to earth via a long transfer ($>180^\circ$). Total trip duration varies between 400 and 440 days, and earth entry velocities range up to 70,000 fps in the unfavorable years. A typical mission trajectory path is shown in Figure 4.1(a) for an unfavorable opportunity, 1975. The return from Mars is made under unfavorable



	Δv LEAVE EARTH (1000 FPS)	Δv LEAVE MARS (1000 FPS)	v ARRIVE EARTH (1000 FPS)	DWELL TIME (DAYS)	TRIP DURATION (DAYS)
a. DIRECT	15	16.5	66	10	430
b. DIRECT (INVERTED)	42	16.5	40	10	430
c. CONJUNCTION	14	8.5	39	480	920
d. VENUS SWINGBY	15.2	12.5	42	10	510

Figure 4.1 Mars Stopover Mission Trajectory Paths

circumstances because Mars "lags" the Earth in heliocentric position; to gain a rendezvous the spacecraft must pass inside the orbit of Earth to develop a higher angular rate of travel than that of the Earth. Unfortunately, rendezvous with Earth occurs when the heliocentric radial velocity components are near maximum, giving rise to high earth approach velocities.

An "inverted" mission mode is possible wherein the long transfer ($>180^\circ$) is followed on the outbound leg, and the short transfer ($<180^\circ$) on the inbound leg. In this case Mars is in a heliocentric "lead" position with respect to Earth as the spacecraft departs Mars, and a more favorable return passage can be taken, as shown in Figure 4.1(b). However, the earth-departure propulsion requirements are increased drastically because of the large radial velocity components at earth depart.

In summary, the opposition-class missions with short dwell times at Mars must accept either high earth-return velocities or high earth-departure propulsion requirements: these two characteristic mission velocities cannot be reduced to near-minimum values simultaneously by trajectory manipulations alone.

An alternate mode is possible if the constraint on dwell time at Mars is removed. Assume that a short transfer is made from Earth to Mars, arriving 3 to 4 months after opposition, as in the optimum opposition mode. As noted previously, the spacecraft now "lags" the Earth in heliocentric position. If we extend the stopover on Mars, a favorable position for earth return will occur shortly before the next opposition, when Mars again is in a "lead" position with respect to Earth, see Figure 4.1(c). Near minimum earth-arrival velocities are achieved, but stay times on Mars are increased to 500 to 700 days.

The Venus swingby mode has been found attractive because: (a) the spacecraft usually passes inside or near the orbit of Venus, either on the return leg of the direct mode, or on the outbound leg of the direct-inverted trajectory mode; (b) the gravitational field of Venus is sufficiently powerful to accelerate or decelerate the spacecraft significantly by proper alignment of the hyperbolic pass around Venus; and (c) the angular rate of travel of Venus is large compared to that of Mars, so that the planet is generally "available" for the job of trajectory energizing or de-energizing. The gravity field of Venus thus can

be used to rectify the shortcomings of the direct-mode Mars round trip missions described previously: to reduce the earth-arrival velocities for the direct-mode return passages, or to reduce the earth-departure propulsion requirements for the direct-inverted-mode passages.

Figure 4.1 demonstrates the usefulness of the Venus swingby mode, as applied to the 1980 mission. Earth-return velocities are reduced from 66,000 to 41,700 fps, although overall trip time is increased by 19 percent. The general applicability of the Venus swingby mode to all mission opportunities has been verified (see Reference 1.1). It is noted that the Venus swingby technique can be applied with even greater benefits to Mars flyby missions, for which earth-departure as well as earth-return velocities can be reduced by significant amounts. The sensitivity of spacecraft design to the variation in trajectory parameters over the cycle of Earth-Mars oppositions is greatly reduced.

Direct-Mode Mission Characteristics

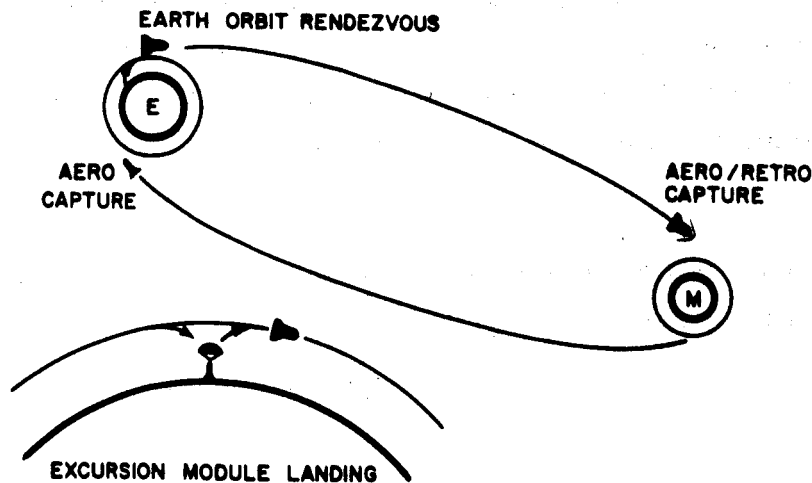


Figure 4.2 Mars Stopover Mission Profile

Characteristics have been established for Mars orbiting stopover missions with profiles similar to that shown in Figure 4.2. The spacecraft departs from a low-altitude earth orbit, decelerates into a 500-km orbit about Mars, using either aerodynamic or retro braking, remains in Mars orbit for 10 to 60 days as a Mars excursion module descends to the surface with a small crew for exploration, and departs for Earth after rendezvous with the lander party. (The mission profile is analogous to that of the manned lunar Apollo mission.) Weight scaling laws were developed from the designs described in Section 4.2 and used as the basis for selecting optimum combinations of calendar dates, total trip time, and leg time to minimize total spacecraft weight on Earth orbit. The results obtained are shown in Table 4.1.

Table 4.1 indicates the optimum launch dates, durations, and leg times and velocities for a complete cycle of opportunities. Overall trip times (for the aerodynamic deceleration modes considered herein) vary from 419 to 436 days. It is interesting to note that optimum earth launch dates occur approximately 100 days before the opposition dates.

Little variation in velocities occurs over the range of favorable to unfavorable opportunities, with the exception of the earth-arrival velocities, which increase rapidly as Mars nears its aphelion. Mars entry velocities range from 22,000 to 29,000 fps. A value of 27,500 fps was selected for the mission sensitivity analysis discussed in Section 10.

4.2 Vehicle Design

A representative vehicle design is presented in the following section, based on the following assumptions:

Propulsion	Hydrogen-Fluorine
Crew	7
Deceleration at Earth	Aero
Mars Landing	Mars Excursion Module (2 or 3-man crew)

Atmospheric braking at Mars has a pronounced effect on spacecraft gross weight (spacecraft gross weights in earth orbit are reduced by a factor of two for the chemical design), and was given serious consideration for that reason.

TABLE 4.1 DIRECT MODE STOPOVER MISSION CHARACTERISTICS

OPPOSITION	DATE LEAVE EARTH	DURATION (DAYS)		TOTAL	(ΔV)**		VELOCITIES (1000 FPS)			
		OUTBOUND	INBOUND		LV EARTH	ARV MARS	LV MARS	ARV EARTH	V	V
		10 DAY STOPOVER								
		NO EARTH HOLD								
10 Aug 1971 (2441174)*	1080*	140	272	422	13.4	24.6	14.1	49.0		
25 Oct 1973 (1980)	1880	160	266	436	14.2	22.0	15.8	59.7		
16 Dec 1975 (2762)	2665	170	250	430	14.9	24.6	16.5	65.6		
22 Jan 1978 (3531)	3436	179	241	430	14.2	24.9	16.3	68.7		
25 Feb 1980 (4295)	4192	185	235	430	13.9	28.5	15.6	66.0		
31 Mar 1982 (5060)	4960	177	232	419	13.4	29.4	14.3	58.2		
11 May 1984 (5831)	5737	168	255	432	12.9	27.2	14.0	53.0		

*Julian Dates

**Gravity losses of 8 and 5 percent included for Earth and Mars depart, respectively.

Aerodynamic deceleration at Mars is feasible with the entry velocities encountered (25,000 to 30,000 fps). Severe radiative heating, due to the presence of CN in the shock, is encountered during Mars entry, and dictates the use of pointed rather than blunt forebody shapes, but overall heat shielding weights are not large. Retro braking versions are considered in the sensitivity analysis presented in Section 10.

System Configuration

The spacecraft design developed in Reference 1.1 is shown in Figure 4.3. The earth-departure tanks are attached aft of the main spacecraft by means of a flared skirt, which serves to decelerate and stabilize the vehicle during Mars entry, and also to house the Mars departure tanks (see Frontispiece). Hydrogen-fluorine propellants are used in both earth-departure and Mars-departure propulsion systems because of the high performance and high propellant bulk density (compared to that of hydrogen-oxygen propellants).

The main spacecraft consists of a central mission module of 260-inch diameter, which contains the basic crew quarters. The Earth entry module and Mars Excursion Module (MEM) are housed in the main spacecraft. The command module is equipped with guidance and navigation gear, communication links with earth, and with adequate life support to perform earth entry and satisfy abort requirements.

A partially closed ecological system is assumed (water and atmosphere are processed and reused, but food is not).

As noted previously, earth entry velocities can reach 70,000 fps, which tends to reduce earth entry corridors and requires higher L/D capsules (up to 1.0). The $L/D = 1.0$ capsule is shown in Figure 4.4.

Earth entry capsules with $L/D = 0.5$ were also considered. This type of module is adequate for a 1971 mission but is not feasible for other direct-return missions requiring higher earth entry velocities. However, the module is feasible for Venus swingby return missions, which characteristically have earth entry velocities below 50,000 fps. The Apollo-type entry capsule installed aboard the spacecraft is shown in the Frontispiece.

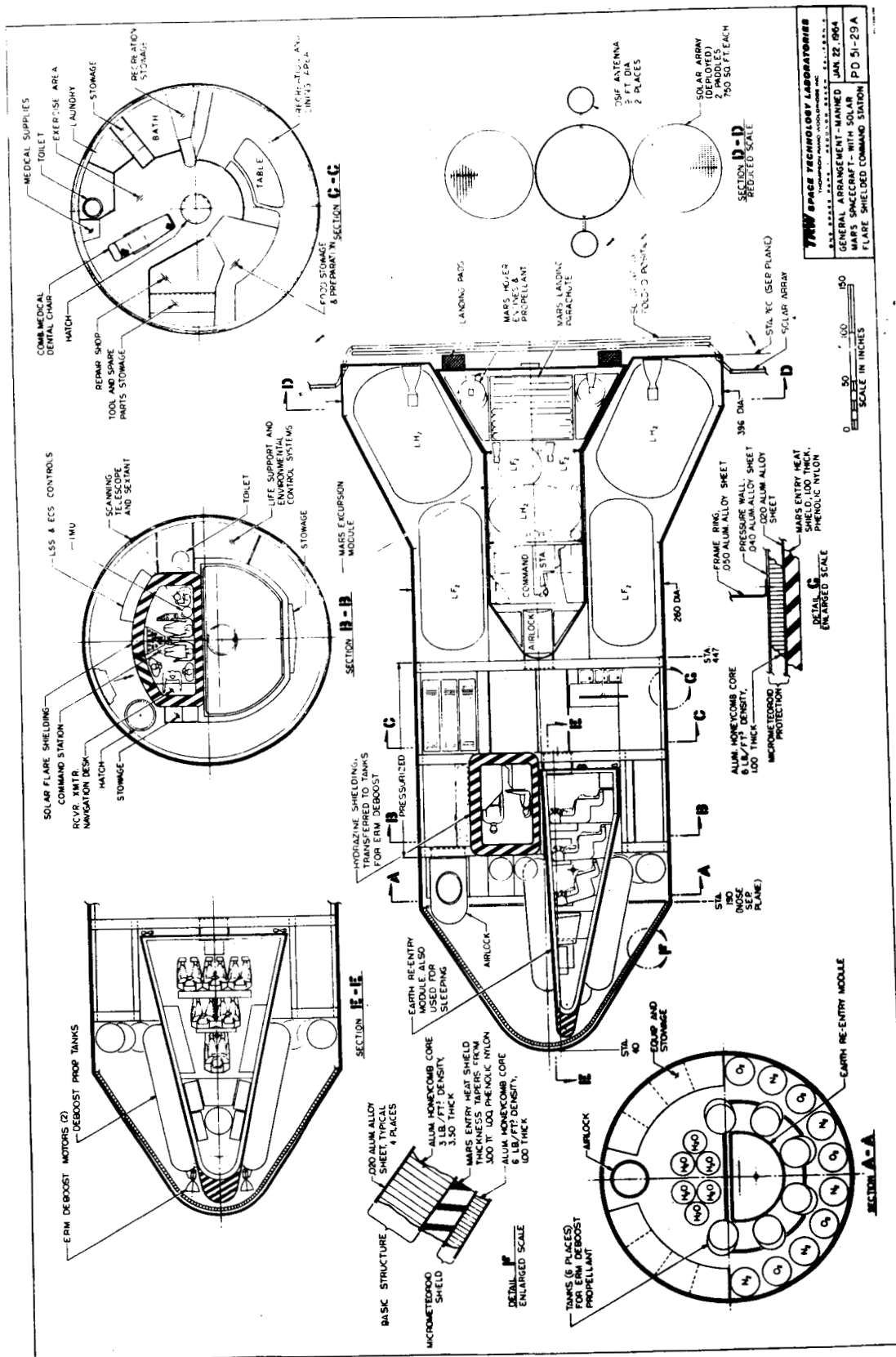


Figure 4.3 Manned Mars Spacecraft - General Arrangement

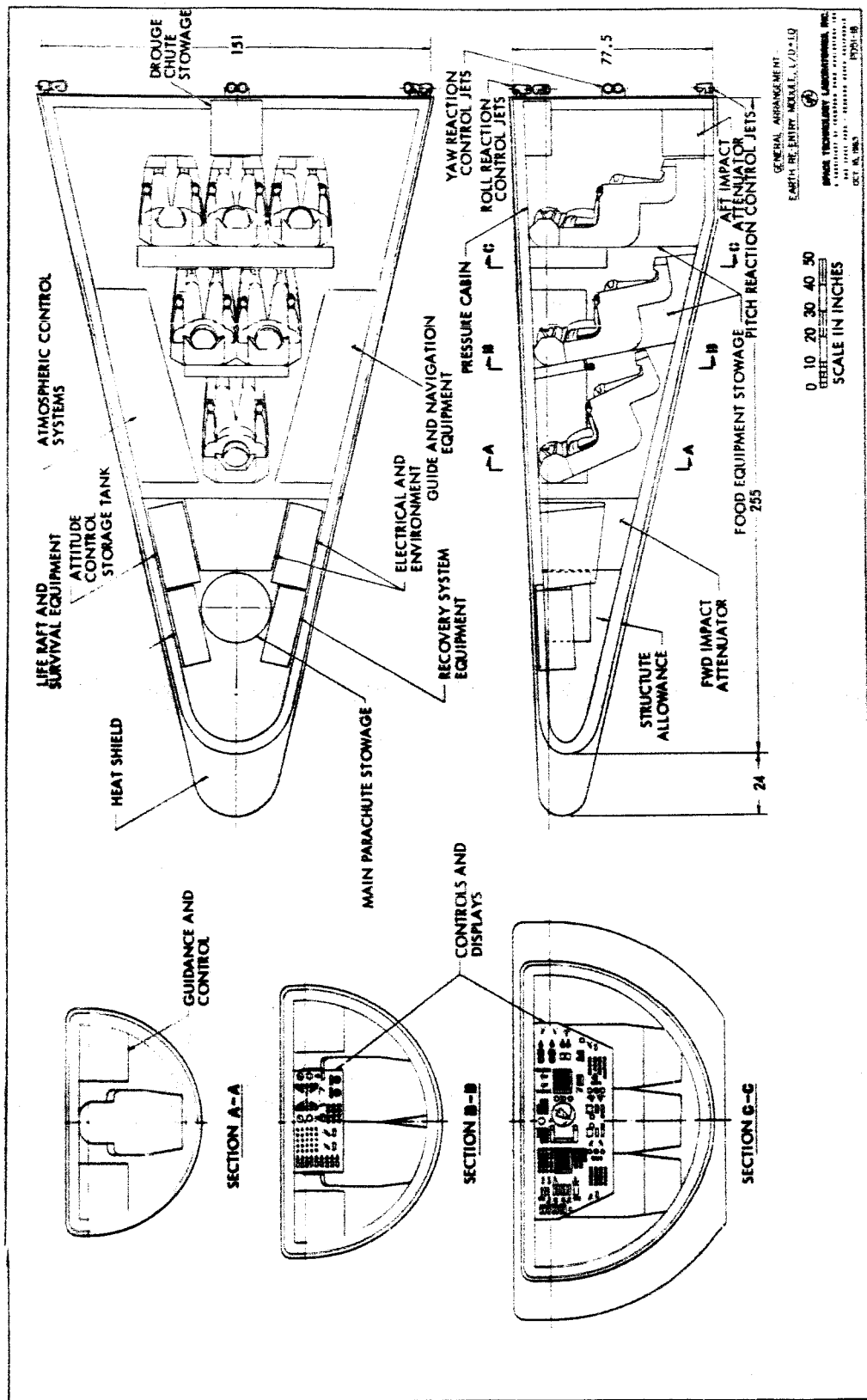


Figure 4.4 Earth Entry Module (L/D = 1.0)

The MEM is designed to land 2 to 3 men on the surface and support their activities for 10 to 15 days. Aerodynamic entry and deceleration in the Mars atmosphere was assumed for the MEM. Terminal touchdown is accomplished with a parachute plus retrorocket; parachute settling speeds range up to 320 fps for the Model 2 (25 mb) atmosphere, but landing system weight is only slightly greater than that of an earth system if an optimum distribution of parachute and retrorocket weights is employed. The external shape is designed to reduce ascent drag and gravity losses, which can be severe (4,000 ft/sec). A hydrogen-fluorine propulsion stage returns the MEM to orbit. The MEM weighs 50,000 lbs.

Thermal control of the Mars departure tanks can be accomplished utilizing passive insulation techniques with weight penalties of about 4 percent. Refrigerator systems are lower in weight but less reliable. Thermal control of the Mars excursion module while on the Mars surface poses a difficult problem because vacuum insulation techniques lose their effectiveness; a double-wall "thermos-bottle" thermal control technique is assumed for the MEM propellant tanks.

Electric power requirements are about 6 - 8 kw, which is in the range suitable for power sources. Solar cell arrays are competitive in terms of weight and devoid of many operational problems associated with nuclear systems. A fuel cell can be used as a power source during solar occult in the Mars orbit. The spacecraft design shown in Figure 4.3 utilizes a solar-static power source, which is folded into the vehicle flare during launch and Mars entry.

An overall spacecraft weight statement is given in Table 4.2 for the 1982 mission, assuming a 6-man crew, aerodynamic braking at Mars and Earth, hydrogen-fluorine propellants, and a 10-day stopover. Allowance for Earth- and Mars-depart holds are not included.

TABLE 4.2 WEIGHT SUMMARY (1975 MISSION)

<u>Component</u>	<u>Weight (1,000 lbs)</u>
Earth Entry Module	15.1
Mission Module	98.2
Midcourse (Inbound), $\Delta V = 320$ fps	4.8
Depart Mars Propulsion ($H_2 - F_2$)	245.0
Mars Excursion Module	50.0
Mars Arrival Heat Shield	65.3
Boiloff and Expendables	11.6
Midcourse (Outbound), $\Delta V = 320$ fps	22.2
Earth Depart Propulsion ($H_2 - F_2$)	<u>1,078.0</u>
	1,590.0

Earth Launch and Assembly

The uprated Saturn V can be employed for earth launch if 4 to 6 shots are used to assemble the complete spacecraft in the parking orbit. Fully-loaded propulsion elements can be brought up and joined with the main spacecraft, thus avoiding the necessity of transferring propellants in orbit. Construction in orbit is not required, or desirable; rendezvous and docking procedures only need be involved.

Artificial Gravity Provisions

An artificial-gravity version of the Manned Mars spacecraft uses spent propellant tanks, suspended from the main spacecraft by means of cables as counterweights. A gravity level of $1/6$ g is provided. This configuration was verified for dynamic and long-term stability on a 9-degree-of-freedom computer program developed for space station analyses (Langley Research Center). The results indicated that no stability problems will be encountered if suitable damping is provided at the cable attach points. Attitude control jets must be provided on both masses.

Mars Flyby Spacecraft Design

A spacecraft design was prepared for the Mars flyby mission based on design approaches developed for the stopover missions. The Mars excursion module was deleted from the spacecraft, and the Mars departure propulsion system capability was reduced to that required for the flyby powered turn, which was assumed to be 3,000 fps. Additional allowances for interplanetary navigation were made (3 corrections of 350 fps each). The total spacecraft weight in earth orbit is estimated to be 440,000 lb, assuming a six-man crew, and hydrogen-fluorine propulsion for earth depart and for the powered turn at Mars. A sketch of the spacecraft is given in Figure 4.5.

Life Support and Environmental Control

Because of the long duration of the cruise phases of the mission, the MMM subsystem regenerates both oxygen and potable water from metabolic waste. General features of this system are the following:

- a. A two-component atmosphere, 52 percent O_2 , 44 percent N_2 , with a total pressure of 7 psia.
- b. Control of CO_2 by conversion to H_2O and methane.
- c. Control of cabin relative humidity to approximately 60 percent at a temperature of $70^{\circ}F$. The water removed from the atmosphere is purified and reused.
- d. Water reclamation from utility water and urine by chemical treatment and vapor compression distillation.
- e. Generation of the major part of the required oxygen by electrolysis of water.
- f. Control of atmosphere contaminants of higher molecular weight by absorption on activated carbon.
- g. Control of lower weight atmospheric contaminants by catalyzed burning.
- h. Stored oxygen and nitrogen to make up cabin leakage losses as well as to provide 10 complete changes of the vehicle's atmosphere.

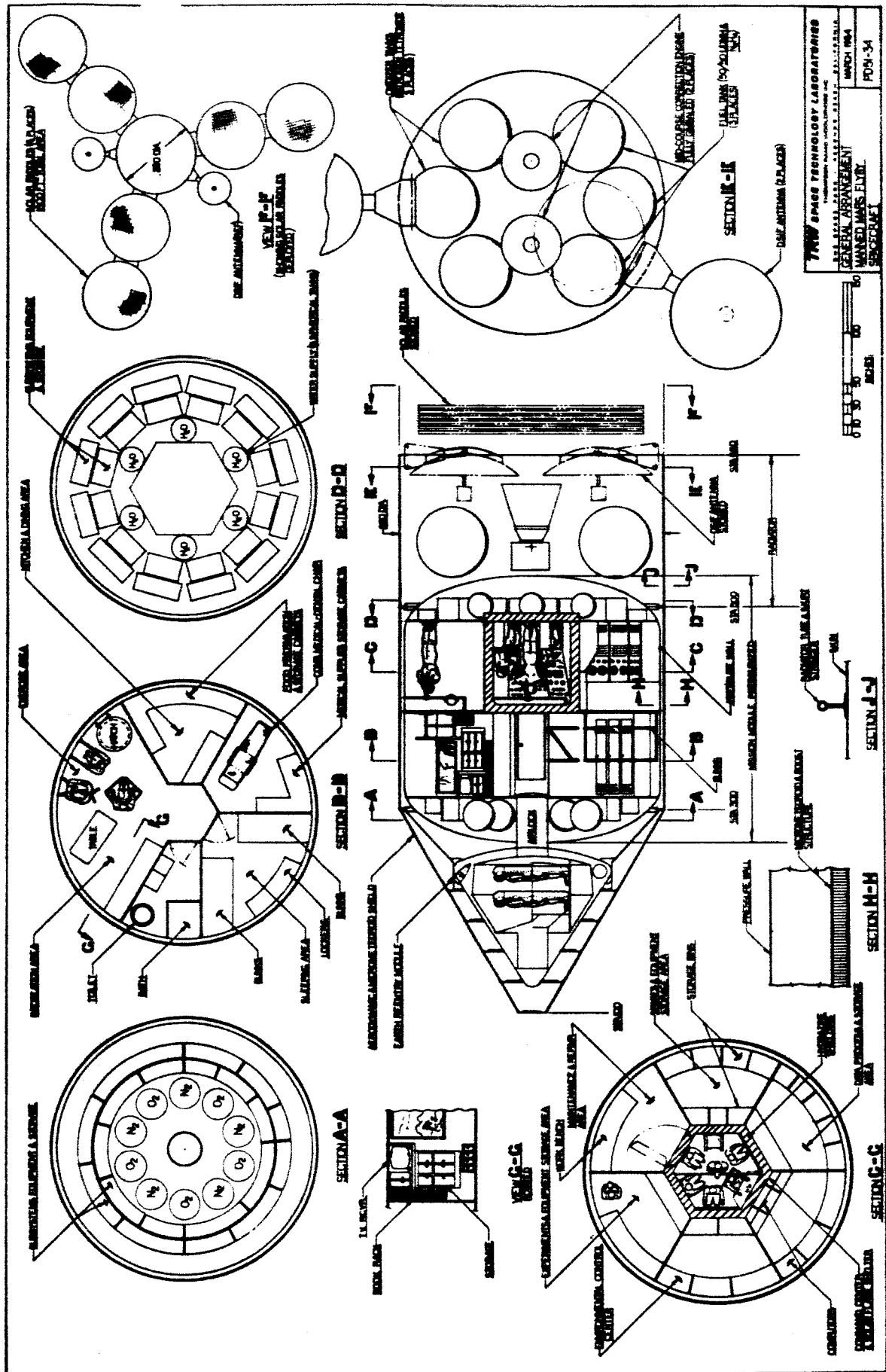


Figure 4.5 Mars Flyby Spacecraft General Arrangement

Communications

For information transmission from the MMM to Earth during trans-Mars, trans-Earth, and near-Mars phases of the mission, the following performance criteria were assumed.

- a. The radio terminals at Earth use 210-ft antennas, operating in the frequency band 2295 mc. The receiver system noise temperature is 100°K , which includes all sources of internal and external noise; the receiver IF bandwidth is 3 mc.
- b. The communication range extends to at least 1.0 AU.
- c. During near-Mars phases of the mission, the communication range does not exceed 0.7 AU.
- d. When transmitting at low-power, the spacecraft equipment must be capable of continuously supporting angular tracking and range-rate (two-way doppler shift) measurements. The maximum duty-cycle for low-power transmission is 100 percent.
- e. When transmitting at high-power the spacecraft equipment must be capable of transmitting either real-time television simultaneously with low-rate telemetry, or one speech channel and medium-rate telemetry, or high-rate telemetry only. During this transmission, the capability of performing angular tracking and two-way doppler measurements must be maintained. The duty cycle of high-power transmission is 10 percent during coast, and 80 percent about Mars.
- f. The television channel must be capable of transmitting one 250-line frame per second during near-Mars phases of the mission (0.7 AU) and every 5 seconds at ranges up to at least 1.0 AU.

The design concept derived includes a transmitter output power of 500 watts in the high-power mode of transmission and 10 watts in the low-power mode. The output power of the high-power transmitter can be raised to

1,000 watts for short periods. The carrier is phase-modulated either directly by digital data or by two sinusoidal subcarriers. The directional antenna at the MMM has a diameter of 12 ft.

The video signal from the television camera directly frequency-modulates a television subcarrier, while the digital telemetry bi-phase modulates the telemetry subcarrier. Both subcarriers phase-modulate the RF carrier. A television video bandwidth of 9.0 kc is obtained, which permits readout of a 250 line TV frame in 3.4 seconds. Camera tubes for this relatively slow readout rate require an erasure phase of about 1.5 seconds after each readout, which increases the total frame period to 5 seconds. Telemetry at a rate of 2,000 bits/second can be transmitted simultaneously with the television.

The telemetry rate is 20,000 bits/second with a bit-error probability of 10^{-3} .

For television, the transmission rate near Mars results in a frame-rate of 1 frame per second. The capability of transmitting at double power, i.e., at 1000 watts, during shorter lengths of time, permits further increase to 2 frames/second. For critical mission phases, such as docking of the MEM with MMM, 8 frames per second is feasible if the picture resolution can be degraded by changing from 250-line frames to 125-line frames.

4.3 Navigation

Simulated flights from Earth to Mars and return were made employing state-of-the-art sensor systems. A 1978 mission was chosen for analysis because of its long duration and relatively high entry velocities.

On both legs of the flight, it was assumed that launch into the inter-planetary transfer orbit was made from a circular parking orbit about the launch planet. The criteria for evaluating the effectiveness of on-board tracking was the crossrange uncertainty at perifocal passage at the target planet. The results of the outbound leg from the Earth to Mars are given in Table 4.3. At perifocal passage the uncertainty of 0.91 km is equivalent to an entry corridor of 5.4 km (3 sigma). This is within the expected required corridor based on aerodynamic entry system performance.

TABLE 4.3

CORRIDORS AND VELOCITY CORRECTION REQUIREMENTS (1978 MISSION)

	TRACKING UNCERTAINTY (KM)	CORRIDOR (KM)
EARTH-MARS		
STAR/SUN SENSORS	0.9 (1 σ)	5.4 (3 σ)
STAR/STAR SENSORS	0.2	1.1
MARS-EARTH		
STAR/SUN SENSORS	3.4 (1 σ)	20.4 (3 σ)
STAR/STAR SENSORS	0.7	4.2
DSIF (AT 210 DAYS)	0.67	4.0
CORRECTION VELOCITIES		
EARTH - MARS	345 FPS (3 σ)	
MARS - EARTH	$\frac{300}{645}$	

BASED ON: DSIF NEAR EARTH
STAR/SUN SENSOR SYSTEM NEAR MARS.

For the return flight from Mars to Earth the perifocal passage uncertainty is 3.42 km, which is equivalent to an entry corridor uncertainty of 20.5 km (3 sigma). This corridor is too wide to meet the aerodynamic and loading constraints anticipated for high speed entry (70,000 fps). A maximum entry velocity of about 56,000 fps, with atmospheric uncertainties can be accommodated.

Further investigation was made of the earth-return navigation problem to reduce perifocal passage uncertainties to a level compatible with entry corridor constraints, using earth based radio guidance. The improved-accuracy optical on-board observational model was achieved by replacing the sun sensor with a second star sensor, which is basically more accurate. The substantial improvement in tracking uncertainty is shown in Table 4.3, and is adequate to meet the requirements for earth entry at velocities approaching 70,000 fps.

The use of earth-based radio tracking (for earth entry) yields very low tracking uncertainties, assuming availability of the 210-ft ground receivers, currently planned for operation before 1970.

Midcourse and terminal velocity correction requirements have been estimated, based on the computed tracking uncertainty characteristics. Conservatively, these requirements are 346 fps for the Earth-to-Mars leg, and 300 fps for the Mars-to-Earth leg (assuming use of the star/sun sensor on-board system).

5. ENVIRONMENTAL FACTORS

Engineering data on the martian and cis-martian environment necessary for the design of the manned Mars mission system are incomplete and inadequate in most areas. In a few instances the amnned Mars mission system is relatively insensitive to selected environmental factors, but in most cases, significant design and system weight penalties must be paid to accommodate the "worst" case. In fact it is often difficult to define a "worst" case, as with surface soil properties, and biological contamination hazards. These shortcomings in our knowledge of key mission environmental factors become apparent as the interfaces between mission and environment are defined and analyzed in the succeeding chapters. The status of our knowledge of the martian environment is indicated qualitatively in Table 5.1.

TABLE 5.1 STATUS OF DATA ON MARTIAN ENVIRONMENT

	Direct Measurement Observation	Inferred From Partial Measurements	Theoretical, Based on Other Measurements	Purely Theoretical	Purely Hypothetical	Not Known to Desirable Accuracy
<u>Atmosphere</u>						
Thermodynamic Properties			X			X
Density vs Altitude			X			X
Surface Density		X				X
Temperature vs Altitude			X			X
Surface Temperature	X			X		X
Chemical Composition				X		X
Electrical Properties				X		X
Ionosphere				X		X
<u>Meteorology</u>						
Winds			X			X
Cloud Cover	X					
Dust Storms		X				X
Climate		X	X			X
<u>Surface Conditions</u>						
Surface Composition			X			X
Soil Strength Properties				X		X
Topography	X					X
<u>Areology</u>						
<u>Biology - Vegetation</u>			X			X
<u>Radiation Environment</u>						
Cosmic Radiation at Surface			X			X
Cosmic Radiation - Cismartian			X			X
UV Radiation Density at Surface			X			X
"Van Allen" Belt						X
<u>Micrometeoroid Environment</u>						
		X				X
<u>General</u>						
Reflectivity - Albedo	X					
Magnetic Field			X			X
Gravitation Field		X				

The following information was obtained from the files of the Department of the Interior, Bureau of Land Management, and the Bureau of Reclamation, and is being furnished to you for your information.

...and
... ..
... ..
... ..
... ..
... ..

Space Technology Laboratories has just completed a preliminary draft of a handbook on the Mars environment (Reference 5.1), which serves as a basis for several of the environmental factors discussed in the following sections. Additional new calculations on the cosmic ray density and electron density at the martian surface are reported herein, the latter being of significant importance to equipment operation. Other data from the Handbook are in Appendices A, B.

Mariner 64 carries a UV scanning spectrometer, magnetometer, IR radiometer, and other instrumentation, and, if successful, will yield information on atmospheric composition, surface temperature, magnetic field, and other factors of great value. The radio attenuation experiment, designed to obtain data on the density and scale height of the atmosphere, may be of questionable value if electron densities near the surface are high, as the new calculations summarized in Section 5.2 predict.

5.1 Mission - Environment Interactions

The martian and cis-martian environment affects many key facets of the manned Mars mission, both in terms of design functions, operational modes and system trade-offs. In many cases, quantitative assessments of mission-environment interactions can be made, at least on a parametric basis; in other cases interactions can be expressed in qualitative terms only because of the complete lack of data.

Table 5.2 lists the environmental factors considered herein, and the mission design and operational elements that are affected by the various factors. The table categorizes the mission by its design, testing and operational elements, and indicates the degree to which the interactions are developed herein, either on a numerical basis, or on a qualitative basis. The biological environment on Mars and its relation to the mission was examined.

Of major importance is the present uncertainty in the martian atmosphere. This single factor has a strong bearing on the feasibility of aerodynamic capture at Mars, including entry corridor tolerances, navigation tolerances, vehicle lift-to-drag ratio, and the basic configuration of the spacecraft; the mode of descent and terminal deceleration of surface landers; surface trans-

N - Numerical Analysis
Q - Qualitative Discussion
I - To be analysed in Phase II

	MISSION MODULE					← MARS EXCURSION MODULE				
	Radiation Shield	Meteoroid Shield	Aero-Entry L/D	Heat Shield	Orbit Alt.	Propellant Storage	Orbital Recon	Radiation Shield	Meteoroid Shield	Aero Entry
<u>Atmosphere</u>										
Thermodynamic Properties			N	N	N		Q			N
Density vs Altitude			N	N	N		Q	N	Q	N
Surface Density								N		
Temperature vs Altitude				N						
Surface Temperature										
Chemical Composition			N	N						N
Electrical Properties										
Ionosphere	Q				Q					
Diurnal & Seasonal Effects			Q ¹	Q ¹	Q ¹					Q ¹
<u>Meteorology</u>										
Winds							Q			Q ¹
Cloud Cover							Q			
Dust Storms							Q			
Climate							Q			
<u>Surface Conditions</u>										
Surface Composition										
Soil Strength Properties										
Topography										
Radioactivity										
<u>Areology</u>										
							Q ¹			
<u>Biology - Vegetation</u>										
							Q ¹			
<u>Radiation Environment</u>										
Cosmic Radiation at Surface								N		
Cosmic Radiation - atmosphere	N									
UV Radiation Density at Surface										
Van Allen Belt	Q ¹				Q ¹			Q ¹		
<u>Micrometeoroid Environment</u>										
		N							Q	
<u>General</u>										
Reflectivity - Albedo						Q				
Magnetic Field	Q ¹				Q ¹			Q ¹		
Gravitation Field					Q ¹					

2

						SURFACE OPERATIONS								
Accelerator	Drift Sensor	Retro	Impact Gear	Propulsion	Propellant Storage	Rover Design	Traverse Range	Contamination Procedures	Experiment Program	Crew Effectiveness	Elec Equip Operation	Stay Time	Navigation	Devel Testing
N	N	N	N	N	D	Q			Q	Q			N	Q ¹
N	N	N	N	N	Q	Q				Q	N		N	Q
					Q	Q				Q	Q	Q		Q
N	N	N	N	N	Q	Q			Q	Q	N	Q		Q
N ¹	N ¹	N	N ¹		Q	Q	Q		Q	Q	Q	Q		Q
	Q	Q							Q	Q		Q		Q
			Q			Q	Q		Q		Q	Q		Q
						Q	Q ¹		Q ¹		Q	Q		Q
							Q ¹	Q ¹	Q ¹					Q ¹
						Q	Q		Q	Q	Q	Q		Q
						Q			Q	Q	Q			Q

portation modes; the design and performance of return-to-orbit vehicles; and the radiation and micrometeoroid environment to which surface crews will be exposed.

The surface environment and mechanical properties affect the lander vehicles, surface transportation modes, and possibly the practical upper limit on surface dwell time.

Of primary importance in the cis-martian environment are solar radiation and micrometeoroid fluxes to which the manned spacecraft will be exposed en route to Mars and during the stopover in the parking orbit about Mars. While many models of these phenomena have been conjectured, the fact remains that much additional experimentation must be performed to properly define these factors. Not surprisingly, uncertainties in cosmic radiation and micrometeoroid fluxes have a major effect on mission spacecraft gross weight, and can lead to costly penalties in mission costs, principally through launch vehicle requirements.

5.2 Discussion of Environmental Factors

Atmospheric Gaseous Composition (Reference 2.1)

The primary gaseous constituents of the martian atmosphere currently are believed to be molecular nitrogen and carbon dioxide, with perhaps a small percentage of argon and with relatively small amounts of carbon monoxide, ozone and oxides of nitrogen formed in the upper atmosphere by photochemical action. The rarefied extreme upper atmosphere also should contain atomic N and O, and some ionic gases and free electrons.

Good determinations of the CO₂ content of the martian atmosphere recently have been made by quantitative spectrographic procedures (References 5.1 and 5.2). The measured CO₂ content is 60 ± 20 meter-atmospheres (that is, if all of the CO₂ gas in the martian atmosphere were reduced to STP (pressure and temperature corresponding to "standard" for sea-level conditions on Earth), it would form a spherical shell layer 60 meters high around the planet).

The most probable N₂ to CO₂ ratio is inferred to lie between 2:1 and 5:1, but this ratio may be significantly lower. The uncertainty is in the estimate of N₂ abundance, since the presence of this molecule in the martian atmosphere is inferred indirectly, and not by spectrographic measurements.

Even for high-altitude balloon operations, the earth's atmosphere is completely opaque to all spectral frequencies characteristic of N_2 absorption. Most of the other gases, with the exception of the inert ones, are too light for Mars to retain or are too photochemically reactive. Argon is the only inert gas that has sufficient cosmological abundance to be considered.

Table 5.3 presents a summary of what is known or suspected concerning the composition of the martian atmosphere. The attribution by Colthup (Reference 5.3) of certain near-infrared absorption bands to the organic molecule acetaldehyde (CH_3CHO) is now considered to be somewhat improbable, and this molecule is omitted from the table. Upper limits on the quantities of some molecules, such as O_2 , have been set by failures to detect these molecules by spectrographic procedures.

Atmospheric Temperature

The martian meteorology is difficult to assess as because surface pressures may be as low as 6-10 mb. The previous conceptions of the martian meteorology were based upon a model associated with a surface pressure of about 85 mb, therefore, the significant meteorological parameters (such as wind velocities) have adjusted where possible for the lower surface pressures (10 mb to 25 mb).

The discussion of temperature, pressure and circulation will be limited to the troposphere and to the lower layers of the stratosphere that are just above it. The distinguishing difference between the troposphere and stratosphere is that the static stability of the troposphere is less than that of the stratosphere. As a result, vertical mixing of the atmosphere is favored in the troposphere and is suppressed in the stratosphere. The height of the tropopause is uncertain; however, one estimate of its height is obtained from the vertical extent of the yellow clouds, which are believed to be dust swept up from the bright surface areas, but confined to the troposphere. According to Slipher (Reference 5.5), the most accurately measured height of the yellow clouds is about 30 km. This is one indication of the height of the tropopause. However, other estimates of the height of the tropopause range from 3 to 45 km (Reference 5.6).

TABLE 5.3 PROBABLE GASEOUS COMPOSITION OF MARTIAN ATMOSPHERE

<u>Molecule</u>	<u>Quantity</u> (in meter-atmos)	<u>Comments</u>
N ₂	120 to 300; possibly as high as 800	Not detectable spectrographically through earth's atmosphere
CO ₂	60 ± 20	Limits well established. Approx- imately 25 times CO ₂ content of Earth's atmosphere.
O ₂	Probably less than 0.8	Not yet detected spectrographically
H ₂ O	(2 ± 1) × 10 ⁻²	Latest determination (1.4 ± 0.7) × 10 ⁻³ gm cm ⁻³
	10 ⁻¹	Highest current estimate, and probably upper bound 8 × 10 ⁻³ gm cm ⁻²
	6 × 10 ⁻³ to 10 ⁻²	Lowest current estimate 5 × 10 ⁻⁴ to 1 × 10 ⁻³ gm cm ⁻²
A	Possibly 8 to 50	By inference only
O ₃	Probably less than 10 ⁻⁴	Appears from photochemical rela- tions, that total O ₃ content is proportional to <u>logarithm of relative</u> O ₂ content.
CO NO	Undetermined amounts in upper atmosphere	photochemical products
NO ₂	2 × 10 ⁻³ , if 3.45μ band entirely caused by gaseous NO ₂	Possible photochemical products. Some investigators have attributed polar caps to solid N ₂ O ₄ and N ₃ O ₆ , and yellow clouds to NO ₂ released by local surface heating.
N ₂ O	< 2	Kuiper (Reference 5.4) has looked for, but failed to detect these molecules. He set the indicated upper limits to the possible abundances of these gaseous species in the martian atmosphere.
CH ₄	< 0.1	
C ₂ H ₄	< 2 × 10 ⁻²	
NH ₃	< 2 × 10 ⁻²	
C ₂ H ₆	< 1 × 10 ⁻²	
SO ₂	< 3 × 10 ⁻⁵	

If it is assumed that the troposphere is in convective equilibrium, the temperature decreases with increasing height at the rate of approximately $3.7^{\circ}\text{C km}^{-1}$. The true lapse rate may not be adiabatic, especially if the surface temperature is changing. When the ground is warming, the lapse rate in the atmospheric boundary layer may be many times the adiabatic lapse rate. Then the true lapse rate decreases with increasing height and approaches the adiabatic lapse rate at some height above the surface. On the other hand, if the ground is cooling, the lapse rate in the lower atmosphere is expected to be much less than the adiabatic lapse rate. Experience on the Earth shows that over the northern Arctic and in the fall and winter the temperatures up to a height of 3 km exceed the surface temperature (Reference 5.7). Consequently, one expects that the martian temperatures in the winter polar regions would be similar: namely, the air in a deep layer above the surface to be warmer than the surface. Therefore, the assumption that the martian lapse rate for the troposphere is always adiabatic is not expected to be satisfied.

The stratospheric temperatures above the troposphere are conjectural. The stratosphere is assumed to be in radiative equilibrium. As a result, the lapse rate would be different than if it were in convective equilibrium. The temperature of the stratosphere depends on the photochemical reactions that are caused by the direct solar radiation, and also by the infrared radiation that comes essentially from the martian ground. The stratospheric temperatures are difficult to estimate at this time.

Since the lapse rate, γ , is less in the stratosphere than in the troposphere, one needs to know the height of the tropopause in order to place limits on the validity of assuming a constant lapse rate. However, estimates of the thickness of the troposphere vary widely from 3 - 45 km. In order to find the possible range of temperature in the troposphere, then, one has to vary three parameters: the first is depth of the troposphere; the second is temperature of the air about a meter above the ground, which should be used instead of $T(0)$, if the lapse rate is assumed to be constant; and the third is the lapse rate, γ , which is a function of gravity, g , specific heat, c_p , and molecular weight, m . Estimates of these quantities are given in Table 5.4. The specific heats and molecular weights of the various atmospheres in that table are nearly the same, because each of the atmospheres is composed principally of N_2 . Also, the specific heats and molecular weights of the other

Table 5.4 Properties of Model Martian Atmospheres
(10 mb surface pressure)

N_2	
% by volume	66.7
Atmosphere-meters	119.2
CO_2	
% by volume	33.3
Atmosphere-meters	59.6
Molecular weight m	33.3
c_v	6.94×10^6
c_p	9.43×10^6
c_p/c_v	1.359
g	376
Adiabatic lapse rate γ	3.99
P_o	10
T_o	230
Scale height H	16.8
Atmosphere-meters	0.179×10^3

constituents do not differ greatly from the corresponding properties of N_2 . As a result of the similarity of the specific heats, the martian adiabatic lapse rate is reduced from that of the earth by the ratio of the martian to earth acceleration of gravity, the ratio being 0.38.

Pressure and Density Variations

For purposes of the present study a range of possible variations in atmosphere properties with altitude is desired, based upon uncertainties or possible interpretations of existing data. While many approaches to this analysis can be taken, the fact remains that only two quantities are reasonably well known: surface temperature and CO_2 content. Other parameters entering into the formulation of the atmosphere models are subject to data interpretation, such as pressure level, or speculation, such as height of troposphere. As discussed in the foregoing section, atmospheric composition (CO_2 : other) probably can be limited to a 5:1 range, although a 12:1 range is possible; surface temperatures can be measured to within approximately 10 percent, although it is more pertinent to determine temperature immediately above the surface rather than on the surface proper.

Rather than formulate new models of the atmosphere to add to the many max-mean-min model now proposed, the data of Reference 5.8 will be used for the parametric system analyses required in the present study. Reference 5.8 does in fact construct models of max-mean-min atmospheres generally within the tolerances given above. The greatest uncertainties are introduced by the lack of data on tropopause altitude and temperature; tropopause altitude has not been varied from the nominal in Reference 5.8.

Table 5.5 summarizes the pertinent assumptions for the various model atmospheres generated in Reference 5.8. The range of parameters selected for the atmospheric composition is in reasonable agreement with the interpretation of spectroscopic data made by STL. Also shown is the Schilling II Upper Limit model atmosphere, which is used as an extreme maximum for establishing bounds on manned mission sensitivities. This model seems beyond predictable limits as established from recent data measurements.

The Mariner-4 mission is designed to make measurements of the atmosphere by changes in the doppler signal of the spacecraft in an occultation trajectory (Reference 5.9). Discussions of experimental accuracy indicate

TABLE 5.5 SUMMARY OF STANDARD MODEL ATMOSPHERE
PARAMETERS FOR MARS
(Reference 5.8)

Parameter	Units	Maximum (Model 1)	Mean (Model 2)	Minimum (Model 3)	Schilling II Upper Limit
Surface Pressure	mb lbs/sq. in.	40 .0.58	25 0.363	10 0.145	1.92 132.6
Composition	CO ₂ % by Mass	7.5	16	60	
	N ₂ % by Mass	92.5	84	40	
	CO ₂ % by Volume	4.9	10.8	48.8	
	N ₂ % by Volume	95.1	89.2	51.2	
Molecular Weight	---	28.8	29.7	35.85	28.0
Acceleration of gravity at surface	cm/sec ² ft/sec ²	375 12.3	375 12.3	375 12.3	390 12.8
Surface Temp.	°K °R	300 540	250 450	200 360	300 540
Troposphere lapse rate	°K/km °R/10 ³ ft	-3.636 -1.995	-3.89 -2.134	-4.55 -2.496	-3.714 -2.034
Tropopause altitude	km ft	11 36,100	18 59,100	22 72,200	10 32,800
Stratosphere temp.	°K °R	260 468	180 324	100 180	263 472
Top of stratosphere	km ft	150 492,100	150 492,100	150 492,100	-- --
Thermosphere lapse rate	°K/km °R/10 ³ ft	2 1.097	2 1.097	-- --	-- --
Surface density	gm/cm ³ slugs/ft ³	4.62x10 ⁻⁵ 8.97x10 ⁻⁵	3.57x10 ⁻⁵ 6.94x10 ⁻⁵	2.16x10 ⁻⁵ 4.19x10 ⁻⁵	1.49x10 ⁻⁴ 2.89x10 ⁻⁴

that surface density and scale height can be determined to ± 10 percent. This degree of uncertainty may be optimistic if the electron densities near the martian surface are as great as those predicted by recent STL calculations (see Section - Ionosphere).

Diurnal Variations

Diurnal variations in the atmosphere have not been estimated because of the complex relations governing atmospheric circulation due to changes in temperature, heat balance, solar radiation absorption in the upper layers, etc. Similar effects observed on the Earth's atmosphere may not be applicable.

Winds

Wind velocities are estimated on the basis of the movements of dust clouds, which have been observed to drift at the rate of about 25m/sec, and by noting the wind velocities necessary to generate dust clouds. Further estimates can be made from general theories of atmospheric movements, based upon known movements in the earth's atmosphere, although values derived on this basis indicate tidal or gross effects only, and do not predict local, high-velocity winds. Local high-velocity winds are difficult to predict analytically and are usually established for the earth's atmosphere on a frequency-magnitude basis from observations. Application of the frequency-magnitude correlations obtained for the earth's atmosphere to that of Mars is not directly possible because of differences in density levels and thermal gradients. For present purposes, the maximum speed of dust cloud movement (25m/sec) is applied to the assumed mean density atmosphere (Model 2 (25 mb)), and ratioed by dust generation requirements to the max-min atmospheres. The wind velocities thus obtained are given below.

TABLE 5.6 WIND VELOCITIES

Atmosphere	Model 3 (10 mb)	Model (25 mb)	Schilling II
No gradient	200 fps	131 fps	79 fps
Max gradient (at 30,000 ft)	320	251	199

In addition to the surface winds, a maximum gradient of 4 fps per 1000 ft altitude has been superimposed on the surface values, giving the large wind magnitudes noted at 30,000 ft. The assumed gradient is based on those observed occasionally in the earth's atmosphere, and is approximately four times greater than that predicted by studies of circulation of the martian atmosphere (Reference A. 6).

Surface Temperature

Martian surface temperatures are based on the measurements of the intensity of the infrared radiation from Mars. Gifford (Reference 5.10) published the most recent data that give the martian surface temperatures for each season. These data are frequently used to describe the seasonal variation of surface temperature (References 5.11, 5.12). However, Gifford's data contains unexplained inconsistencies. First, Gifford shows the summer temperatures in the northern hemisphere to exceed the southern hemisphere summer temperatures. Northern hemisphere summer occurs at aphelion; whereas that of the southern hemisphere occurs at perihelion. The aphelion solar constant is 0.68 of the perihelion solar constant. Since the northern and southern hemisphere albedoes are approximately the same, the aphelion insolation should be less than the perihelion insolation, resulting in cooler northern hemisphere summers. The same type of reasoning shows that the hottest part of the southern hemisphere (latitude -20°) during its summer should become cooler during the winter; but the temperature is the same during the summer and winter. Another example of Gifford's apparent inconsistencies is that the northern hemisphere seasonal temperatures do not change as one would expect them to. Gifford shows the summer (northern) to be the warmest as one would expect. However, the next season (fall) is the coldest. The following winter is about 20°C warmer than the fall. The succeeding spring and then summer warm in the expected sequence. But there appears to be no reason for the sudden drop from the maximum summer temperatures to minima in the fall. Another unusual feature of Gifford's data is the character of the temperature curve for the southern hemisphere in its spring. However, Gifford suggests this curve does not represent the average spring temperatures.

de Vaucouleurs (Reference 5.13) has given a more consistent picture of the average diurnal and seasonal surface temperature. These data are reproduced on Figure 5.1. de Vaucouleurs estimates the probable error of the

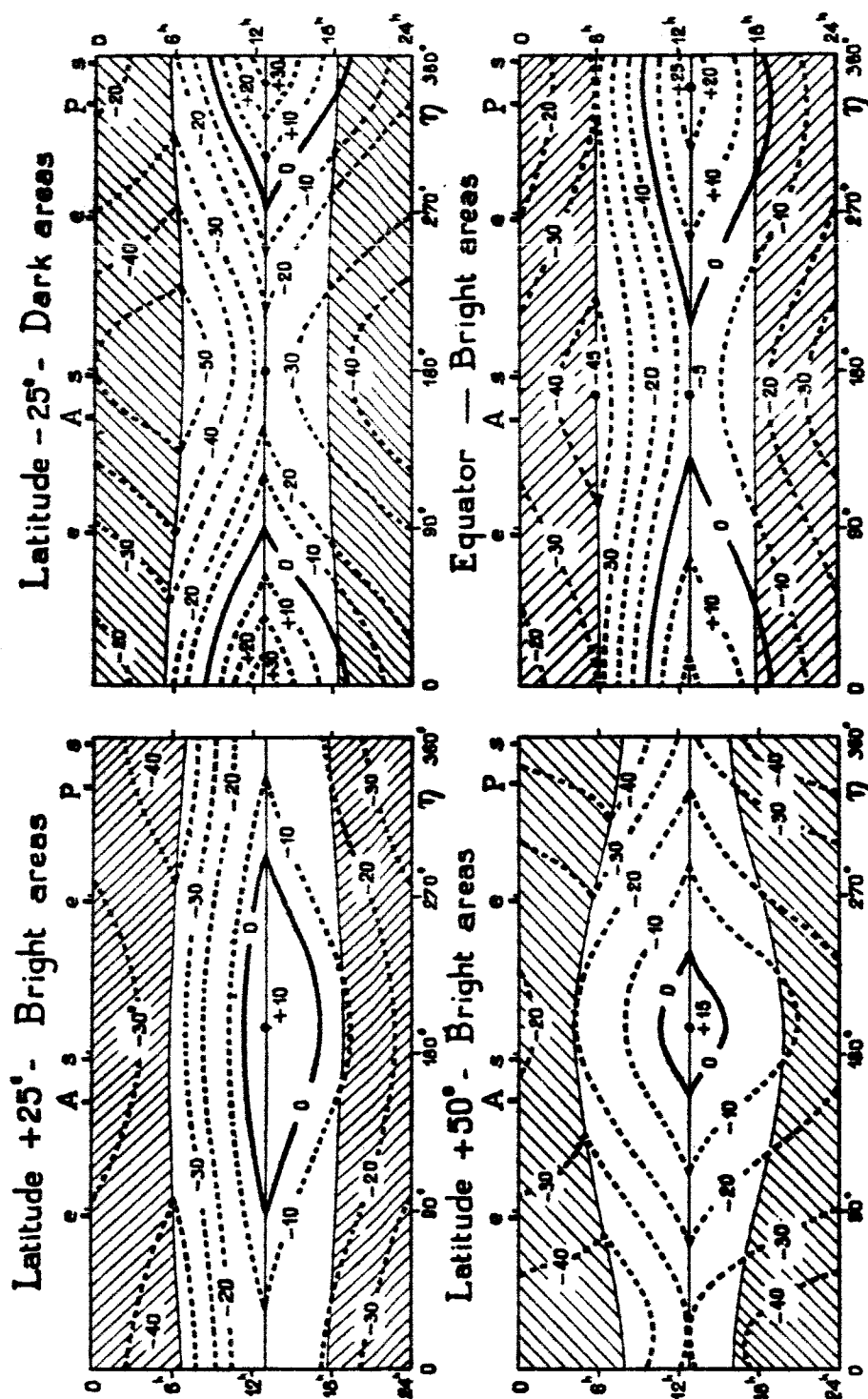


Figure 5.1 Average surface temperatures ($^{\circ}\text{C}$) based on empirical data. (Shaded area represents night) Reference 5.14.

temperatures to be $\pm 5^{\circ}\text{C}$. The time of day is given on the ordinate, and the season is given on the abscissa. Along the top of the separate illustrations appear letters, which have the meanings of e for equinox, s for solstice, A for aphelion, and P for perihelion. The figure shows the expected diurnal trend of temperature, except that the maximum temperature does not occur exactly at noon, but one-half to one hour later.

The seasonal maximum and minimum temperatures occur one to two months after the corresponding maximum and minimum of solar insolation. In the equatorial region (lower right illustration of Figure 5.1) the perihelion maximum temperature is 30°C higher than aphelion maximum temperatures. At the same time of day the perihelion temperatures are 15° to 30°C warmer than the aphelion temperatures. Also, the seasonal variation in the mean temperature for a given time of the day is less than the diurnal variation, which reaches a maximum value of 55°C at perihelion. This estimate of the diurnal variation seems to be low. Sinton and Strong (Reference 5.14) have given surface temperature data that indicate that the diurnal variation in the equatorial regions near the time of perihelion is 100°C .

The two top illustrations of Figures 5.1 show that the dark areas become both hotter and colder than the bright areas. The mean noon-time temperature varies during a martian year by 60°C over the dark areas, but only by 25°C over the bright areas. At a high latitude of $+50^{\circ}\text{N}$ (lower left illustration), which lies near the edge of the polar white cap, the total variation of mean temperature is slightly less than at a lower latitude dark area (upper right illustration).

Enhanced Atmospheric Ionization (Altshuler)

The absence of oxygen molecules in the martian atmosphere implies that the ionization levels due to solar flare disturbances, as well as the background cosmic-ray ionization, can be considerably higher than in the Earth's atmosphere. Furthermore, the radioactivity of the surface can produce a higher level of ionization than in the case of the Earth. The three effects will be discussed below.

a. Solar Flare Ionization in the Martian Atmosphere

Owing to the variability of the solar flare-produced proton spectra, a representative energy spectrum for a class 3^+ flare will be selected to discuss the electron density enhancement produced in the atmosphere of Mars. This representative spectrum is called Bailey's "typical" event, which is a maximum spectrum synthesized from all existing data, and is realistic for the first few hours at the worst possible phase of a flare event. This class 3^+ flare occurred 41 times in 1958, 65 times in 1959, and 70 times in 1960. Shaefer (Reference 5.15) computes the attenuation of this flare-produced proton beam in the Earth's atmosphere. The resulting flux distribution in the atmosphere is shown in Figure 5.2 below.

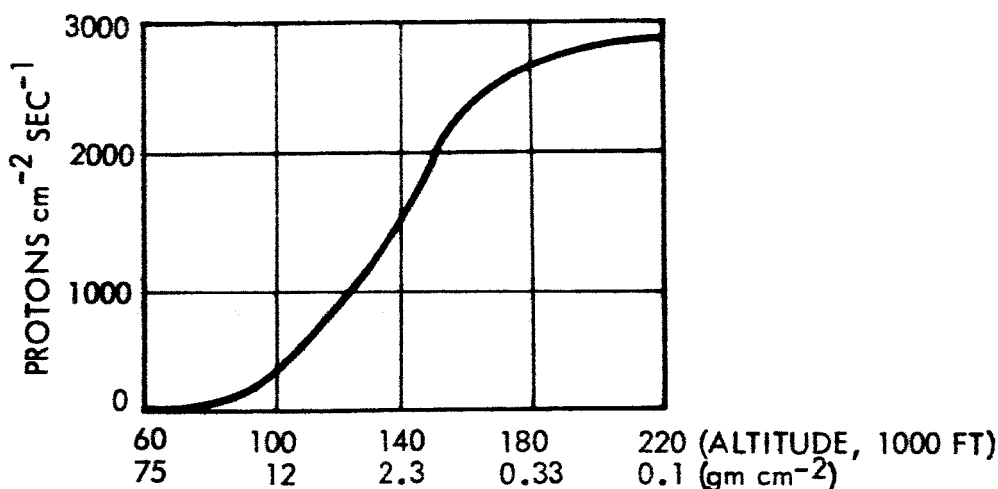


Figure 5.2 Atmospheric Ionization

In computing the total flux associated with this model flare, Shaefer has taken into account the longer path length of the obliquely-incident protons.

We are now in a position to discuss the ionospheric enhancement associated with this flare. First, let us recall that the energy deposition rate \dot{E} at any point in the atmosphere is

$$\dot{E} = \Phi \rho \frac{de}{dx} \quad (1)$$

where Φ is the proton flux, ρ the density in gm cm^{-3} , and de/dx is the stopping power in ergs/gm cm^{-2} . If I is the average energy required to produce 1 ion (~ 32 ev) then the ion production rate R_i is given by

$$R_i = \frac{\Phi \rho}{I} \frac{de}{dx} \text{ ion pairs cm}^{-3} \text{sec}^{-1} \quad (2)$$

and if αn^2 is the electron recombination rate, the electron density is then determined from the equilibrium equation

$$\alpha n^2 = \frac{\Phi \rho}{I} \frac{de}{dx} \quad (3)$$

The first important observation is that the product $\Phi \rho$ has a maximum with respect to atmospheric depth. This is clear from the exponential decay of ρ and the roughly quadratic rise in Φ appearing in Figure 5.2. The peak electron concentration occurs at this point in the atmosphere. Application to the 10 mb (30 gm cm^{-2}) and 29 mb (75 gm cm^{-2}) models of the martian atmosphere yields the data summarized in the table below.

TABLE 5.6 ATMOSPHERIC IONIZATION FROM "TYPICAL"
3+ FLARE

	<u>10 mb (30 gm cm^{-2})</u>	<u>29 mb (75 gm cm^{-2})</u>
Altitude for maximum ionization rate	7 gm cm^{-2} (1.4 x scale ht)	7 gm cm^{-2} (2.3 x scale ht)
Maximum ionization rate	$400 \text{ ion pairs cm}^{-3} \text{sec}^{-1}$	$400 \text{ ion pairs cm}^{-3} \text{sec}^{-1}$
Electron density	$3 \times 10^4 \text{ cm}^{-3}$	$3 \times 10^4 \text{ cm}^{-3}$
Surface ionization rate	$\sim 400 \text{ cm}^{-3} \text{sec}^{-1}$	$100 \text{ cm}^{-3} \text{sec}^{-1}$
Surface electron density	$3 \times 10^4 \text{ cm}^{-3}$	$1.5 \times 10^4 \text{ cm}^{-3}$
Surface electron density (Relativistic Flare)	$3 \times 10^5 \text{ cm}^{-3}$	

Note: The electron recombination rate is $5 \times 10^{-7} \text{ cm}^{-3} \text{sec}^{-1}$ for the reaction $e + N_2^+ \rightarrow N + N$.

For an additional data point concerning this subject of electron density enhancement in the lower martian atmosphere, let us consider the relativistic 23 February 1956 flare. Foelsche (Reference 5.16) estimated an upper limit rate in tissue of 4000 millirad/hr, at a level in the Earth's atmosphere corresponding to 35 gm cm^{-2} . His calculation can be converted from tissue to the density corresponding to the 10 mb martian atmosphere, a density of 10^{-5}

gm cm^{-3} . In this manner an ionization rate of 2×10^4 ion pairs $\text{cm}^{-3} \text{sec}^{-1}$ is obtained. It, therefore, follows that the electron density near the martian surface for a 10 mb atmosphere produced by the 23 February 1956 flare is $3 \times 10^5 \text{ cm}^{-3}$. For a higher martian surface density larger electron concentrations would be expected in the case of such a flare. The electron concentration decays slowly with time. About four hours is required to reduce the electron density by a factor of 100.

b. Background Ionization from Surface Radioactivity

If the surface radioactivity on Mars is similar to that of the Earth, the absence of a strong electron trapping molecule, such as O_2 , suggests the existence of a conductive atmospheric layer adjacent to the surface. In the case of Earth it is known (Reference 5.17) that the ionization rate is 10 to 50 ion pairs $\text{cm}^{-3} \text{sec}^{-1}$ in the lowest 1 meter above the ground. The source of these ionizing radiations are radioactive rocks and radioactive gases, and the cosmic-ray constituent a minor source. On the martian surface the density for a 10 mb model atmosphere is about 10^{-2} that of the Earth. Consequently, the ionization rate ranges from 0.1 to 0.5 ion pairs $\text{cm}^{-3} \text{sec}^{-1}$, if one assumes the same surface radioactivity strength as on Earth. The range, however, is now extended from 1 meter above the ground to 100 meters above the ground. The background electron concentration is 10^3 cm^{-3} for an electron recombination coefficient corresponding to the recombination with the nitrogen molecular ion. It is noteworthy that, unlike the Earth, the galactic cosmic-ray ionization in the lower martian atmosphere is likely to be larger than the background ionization produced from the radioactive sources. For example, about 480 ion pairs $\text{cm}^{-3} \text{sec}^{-1}$ are measured at the 30 gm cm^{-2} level in the Earth's atmosphere using an ionization chamber. Since the ionization chamber gas is at STP and a 10 mb atmosphere amounts to 10^{-2} of the STP density, the ionization rate is reduced to 4.8 ion pairs $\text{cm}^{-3} \text{sec}^{-1}$. Thus, the cosmic-ray ionization rate dominates the radioactivity rates, assuming again the radioactive source strength to be the same for Mars and Earth. The electron concentration near the Mars surface produced by the galactic cosmic rays is $3 \times 10^3 \text{ cm}^{-3}$.

These considerations have so far ignored any possible magnetic shielding. In the event of a substantial magnetic field for the planet Mars, it is then likely that the galactic cosmic rays can no longer dominate the ionization produced by martian radioactivity. If this were the case, simple conductivity

measurements in the atmosphere on a Lander mission would reveal the existence of radioactive sources in the martian crust.

c. Summary of Atmospheric Ionization in the Ground Level Atmosphere on Mars

TABLE 5.8 GROUND LEVEL IONIZATION

<u>Event</u>	<u>Atmospheric Ground Level Ionization cm⁻³</u>	
	(10 mb)	(29 mb)
Relativistic flare	3×10^5	5×10^5
Solar flares (1/wk)	3×10^4	1.5×10^4
Galactic cosmic-ray background	3×10^3	5×10^3
Surface radioactivity	10^3	1.7×10^3

It is important to note that we have assumed that the major constituent in the Mars atmosphere is nitrogen. This has not been verified, and if, as has been suggested, argon should be the major constituent, the electron density levels and the persistence of the ionization could conceivably be much larger, possibly by a factor of 100.

Electrical Breakdown

Because of the possible enhanced ionization near the surface of Mars, electrical breakdown may be encountered unless specific measures and test procedures are taken to avoid it. The breakdown may occur in CW or pulsed electromagnetic radiators, at the frequencies given in Table 5.9. All power generating systems for Mars surface operation should be tested for breakdown in CO₂, N₂ atmospheres at reduced pressures.

It is noted that should the surface ionization reach the levels indicated in Table 5.8, the validity of the data on the atmosphere, to be acquired by Mariner 4 may be in doubt. It is the intent on this flyby to measure the attenuation of rf signals as they travel through the martian atmosphere, thus giving data on the density and scale height of the atmosphere. Surface ionization will affect these measurements.

TABLE 5.9 ELECTRICAL BREAKDOWN

CW BREAKDOWN (10 MB ATMOSPHERE)		BREAKDOWN POWER DENSITY (WATTS/CM ²)		
FREQUENCY (MEGACYCLES)		(10 MB)	(20 MB)	(30 MB)
10,000		600	1,000	2,000
3,000		150	400	2,000
1,000		100	400	2,000
PULSED BREAKDOWN				
PULSE DURATION 3×10^{-6} SEC				
FREQUENCY 8,500 MEGACYCLES				
SINGLE PULSE				
		BREAKDOWN POWER DENSITY (WATTS/CM ²)		
		(10 MB)	(20 MB)	(30 MB)
		1,000	1,500	2,700

Ionosphere

The ionosphere predicted for the upper atmosphere is given in the following table.

TABLE 5.10 IONOSPHERE (11 to 30 MB ATMOSPHERES)

DENSITY (ELECTRONS/CM ³)	ALTITUDE (KM)
6×10^6	470
6×10^5	380
6×10^5	600

Absorption (Reference 2.1)

One of the most significant functions of a planetary atmosphere is the role it plays in the extinction of the solar extreme ultraviolet radiation which would be severely damaging both to unshielded organic life processes and to unshielded electronic apparatus. Figure 5.3 presents a summary of what is known concerning the extinction of solar ultraviolet radiation by the fairly well established minimum CO₂ and N₂ quantities in the martian atmosphere, and by somewhat arbitrarily conjectured quantities of N₂O. The format of the figure is quasi-graphical, but without attempt at uniform scaling. The "ordinate" entries in the first column, represent the percentage of the atmospheric gas, measured from the top, which would be penetrated by a vertical solar beam before virtually complete absorption extinction. $[1 - \exp(-\tau_i^a), \text{ with } \tau_i^a \geq 6]$ occurs for the wavelength interval represented by the "abscissa" entries in the top row. A uniform mixing ratio is assumed for the gaseous constituents. For the sun below zenith, extinction would occur at higher altitudes (corresponding approximately to $\tau_i^a \sec \zeta \geq 6$).

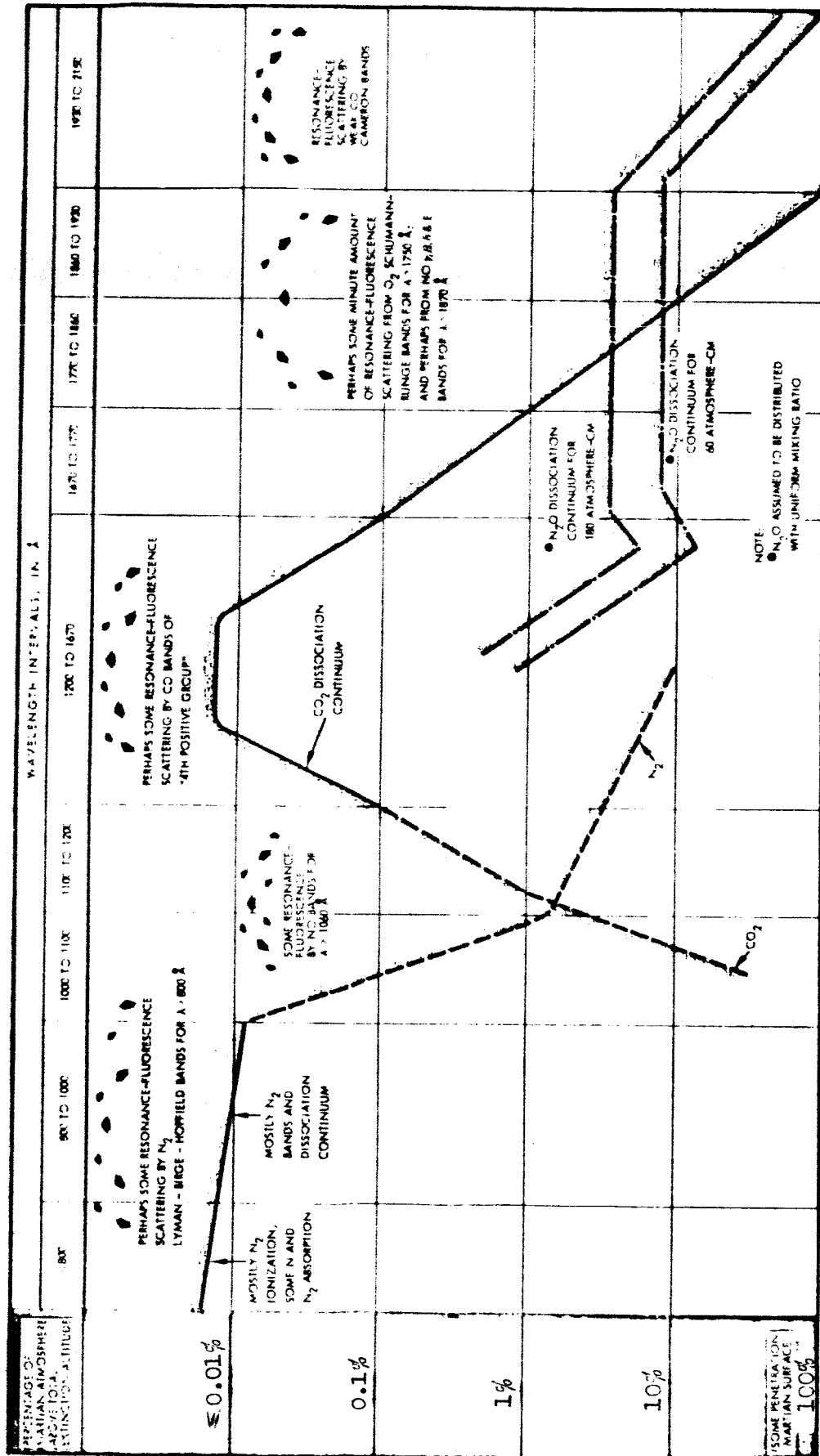


Figure 5.3 Extinction of Solar Extreme Ultraviolet Radiation

Figure 5.3 also indicates the possibility of diffuse outwardly-directed radiation fields arising from resonance-fluorescence scattering by high altitude N_2 , CO and NO molecules that lie above the region of relaxation of electronically excited states by collisional de-excitation.

In Earth's atmosphere, shielding from wavelengths approximately 2100 to 2900 Å is provided by atmospheric ozone. The ozone content of Earth's atmosphere is approximately 0.3 atmosphere-centimeters and is concentrated mostly in an upper atmosphere "shell." It is assumed that the O_3 content of the martian atmosphere also would be concentrated in an upper-atmosphere layer. While some investigators have advanced theoretical arguments to infer as much as 0.1 atmos-cm of O_3 in the martian atmosphere, the best current inferences appear to set an upper bound of 0.01 atmos-cm of O_3 . Figure 5.4 shows the percent transmission spectrum of normally incident sunlight for both 0.1 and 0.01 atmos-cm layer of O_3 . It is seen that, unless the actual O_3 content is appreciably higher than the favored upper bound of 0.01 atmos-cm, there will be a leak-through of potentially lethal solar ultraviolet radiation. An O_3 layer of 0.01 atmos-cm is seen to pass at least 4 percent of normally impinging solar ultraviolet radiation, even in the vicinity of the maximum absorption region near 2500 Å.

The "blue haze" of the martian atmosphere also offers some possibility of shielding the surface of the planet from dangerous ultraviolet radiation. It appears quite probable that the observed extinction in the blue and near-ultraviolet is caused primarily by aerosol particle, or possibly gaseous, absorption rather than by particle scattering. Öpik has inferred that the "blue haze" is an "absorbing smoke," over 70 percent transparent in the red, but with a vertical transmission that drops rapidly in the blue until it levels off at approximately 5 percent between 4050 Å and the 3300 Å limit for which albedo observations were made. If this provisional analysis of Öpik's is correct, then it is possible that this 95 percent shielding absorption by the "blue haze" layer may continue into the shorter wavelength ultraviolet, as shown by the dashed segment of the horizontal line in Figure 5.3. However, even a 5 percent leak-through of hard solar ultraviolet radiation could be dangerous to unshielded apparatus and biological processes. Also, the "blue haze" has been known on occasion to exhibit short time interval planetary wide clearings.

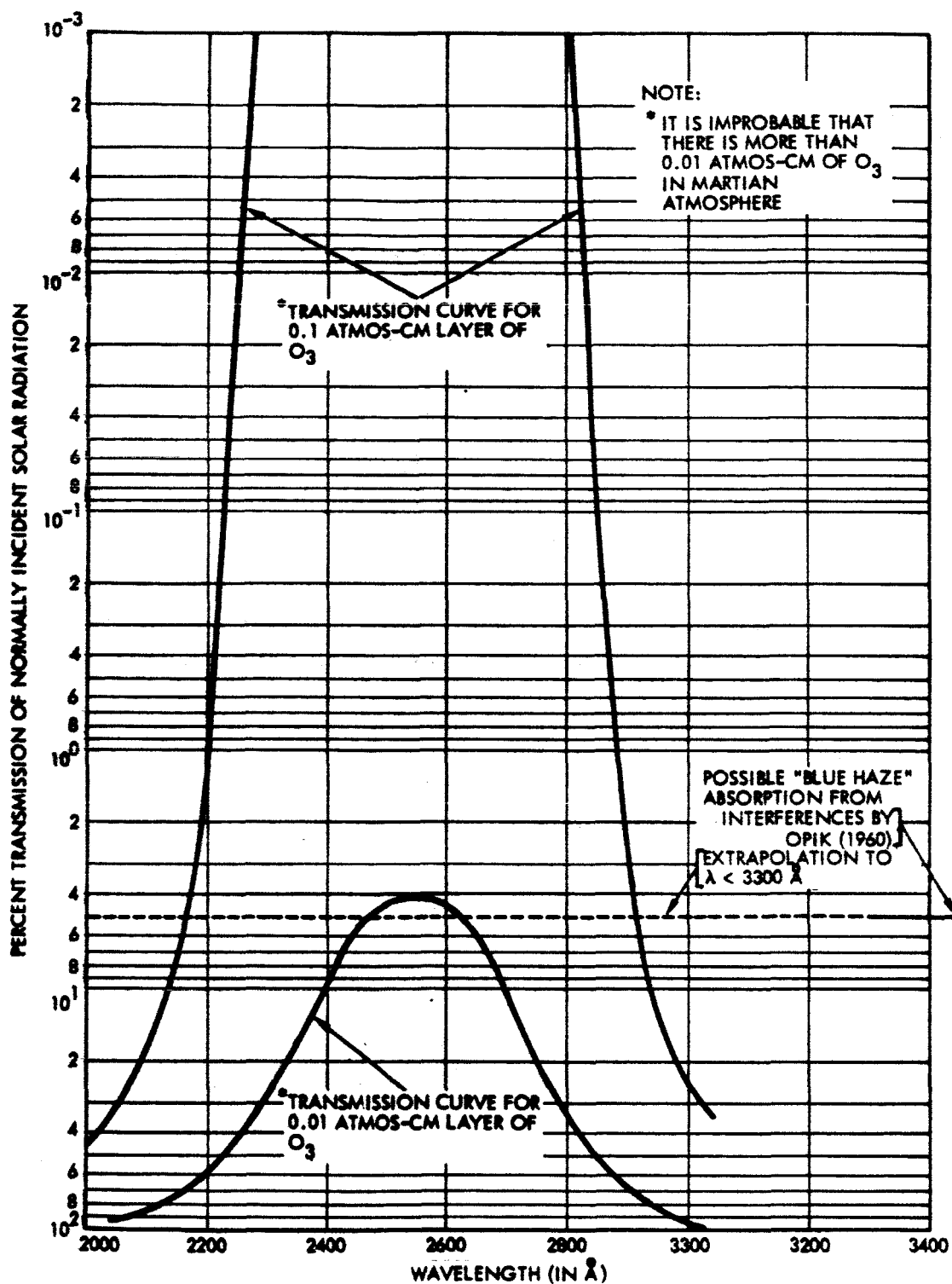


Figure 5.4 Transmissions of Two Arbitrary Ozone Layers and Extrapolation of Blue Haze Absorption

Nuclear Radiation Environment (Altshuler)

There are three regimes of the space environment which require careful consideration as to the shielding precautions on long duration missions.

These are

1. Galactic Cosmic Rays (GCR)
2. Solar Cosmic Rays (SCR)
3. Magnetically Trapped Radiation
(Martian Van Allen Belt)

a. Galactic Cosmic Rays

GCR is a continuous phenomenon. This omnidirectional radiation is composed primarily of protons of energy greater than $1/2$ Bev. The spectrum is well determined near the Earth but may be somewhat greater farther out in the Solar System, near Mars. This will need to be determined experimentally. From Pioneer V measurements (1 gm/cm^2 shielding), the tissue dose rate was determined to be 0.015 rad/day or about 6 rads/yr . However, in large spacecraft this dose may be increased as a result of nuclear cascade multiplication. The question at hand is, for a given incident energy of the primary proton what is the particle flux at any given depth in a nuclear cascade? Such a cascade may develop whenever the incident energy is greater than about 150 Mev . The cascade particles (secondaries) are composed of mesons, gamma rays, neutrons, protons and electrons, and all of these particles contribute to the dosage. The question cannot be answered definitely at present. However, the most extensive data available are to be found in studies of the nuclear cascades produced in the atmosphere by primary cosmic rays. But there is a basic difference between a cascade in the atmosphere and one in condensed matter. In condensed matter the positive and negative pi-mesons will react with nuclei, while in the atmosphere they will not because they will decay before having a chance to interact with nuclei. The main result is that the depth variation of an atmospheric cascade is different from that of a cascade in condensed matter. Nonetheless, the data we now have of the atmospheric cascade do give an indication of what may be expected in the case of shielding material, even though the details may be different. Now an ionization chamber at any point in the atmosphere measures the total energy deposited (absorbed dose) in the sensitive volume of the chamber. Fortunately, extensive measurements of this kind were made during the solar minimum of 1954 (this corresponds to the max. GCR). The result (References 5.18, 5.19) is that at no depth in the atmospheric cascade does the absorbed dose due to GCR exceed 10^{-3}

rad/hr = 8 rad/yr. Figure 5.5 presents the experimental data. It is important to observe how ineffective the Mars atmosphere is as a shield.

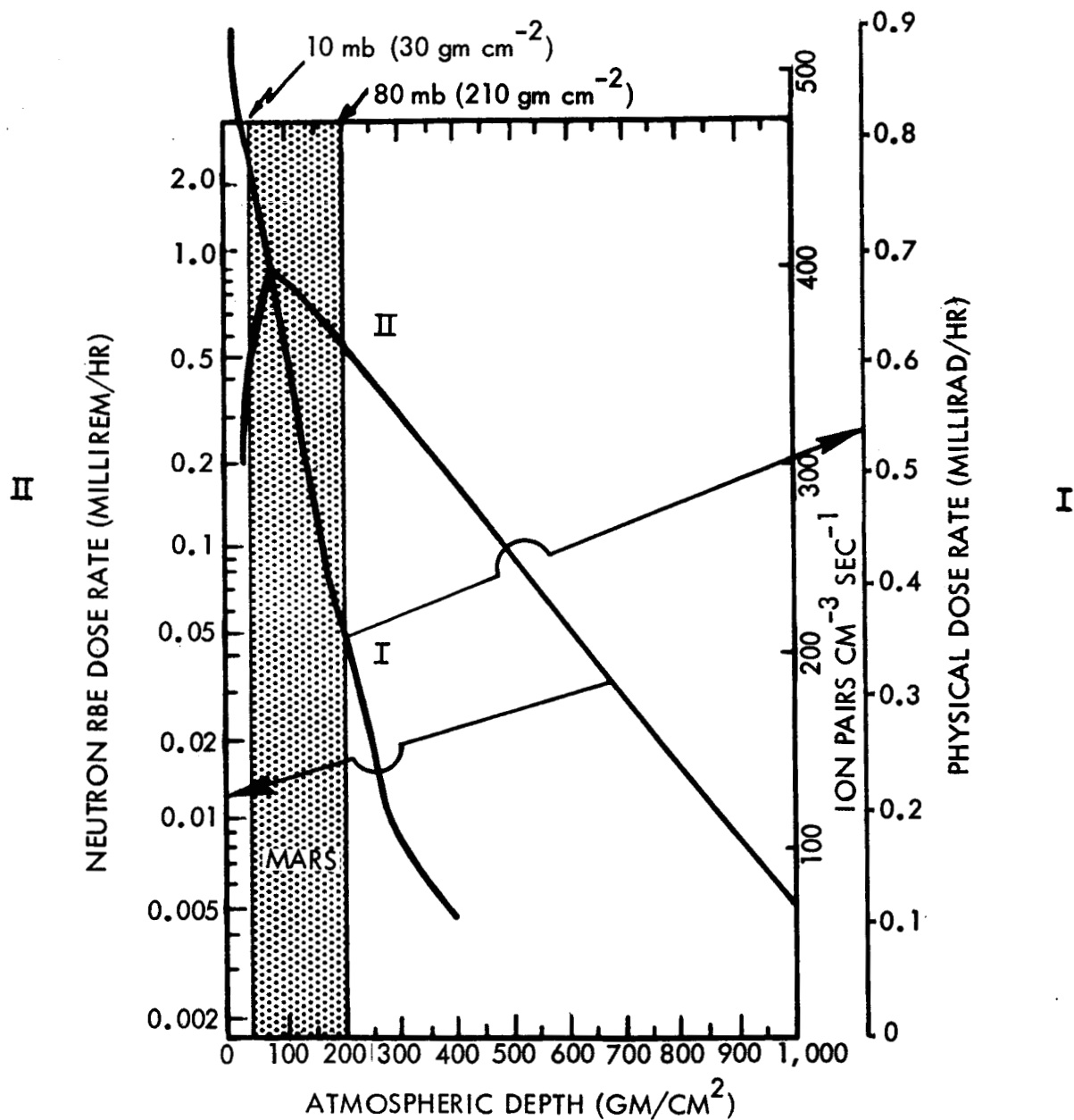
b. Solar Cosmic Rays

This is a complex and elusive phenomena which lasts for hours or days. The intensity of SCR, when they do occur, is several orders of magnitude greater than that of GCR, and the height and shape of the energy spectrum continuously changes with time in the course of a single event. Also, individual SCR events differ greatly from one another as a result of both solar and space propagation effects. Therefore, dosage estimates made from some average event will not resemble what may be experienced in a particular flight. Statistics are very poor, and data prior to 1957 is poor. However, it is possible to establish a synthetic energy spectrum which can be considered representative for a typical large flare. This has been done on the basis of an evaluation of all existing data on flare-produced proton fluxes. Such a spectrum as proposed by Bailey (Reference 5.20) is shown in Figure 5.6. This solar cosmic ray model is adequate for estimating maximum solar proton doses on the martian surface. It is a maximum spectrum which is realistic for the first few hours at the worst possible phase of a flare event. This class 3⁺ flare occurred 41 times in 1958, 65 times in 1959, 70 times in 1960. The frequency declined since 1961. Thus, the average occurrence rate during the last sunspot maximum is about one per week.

Detailed dose rate estimates for this flare have been made by Schaefer (Reference 5.20). Figure 5.7 indicates the associated tissue dosage rates of Bailey's "typical" event as a function of atmospheric depth. The figure also indicates the computed dosages expected from the 3⁺ flare of 20 November 1960. A balloon measurement at 120,000 ft (6 gm/cm²) is also indicated.

The statement that the spectrum of Figure 5.6 and the corresponding dose rates are representative for a maximum event needs some modification. At rare occasions (7 times in the past 20 years, namely, twice in 1947, twice in 1960, and once in 1946, 1949, and 1956) so-called relativistic flares have been observed which show a substantial increase of particle flux up to at least 10 Bev in the energy spectrum. The largest in terms of integrated dose occurred on 23 February 1956. The data below pertains to this particular 1956 flare.

Total shield (gm/cm ²)	10	20	30	35
Dose (rads)	35 - 100	25 - 50	25 - 40	20 - 35



I ABSORBED DOSE RATE IN TISSUE (MEASURED BY IONIZATION CHAMBER) VS ATMOSPHERIC DEPTH.

II NEUTRON RBE DOSE RATE IN TISSUE VS ATMOSPHERIC DEPTH

Figure 5.5 Galactic Cosmic Ray Dosages During Solar Minimum at North Geomagnetic Pole

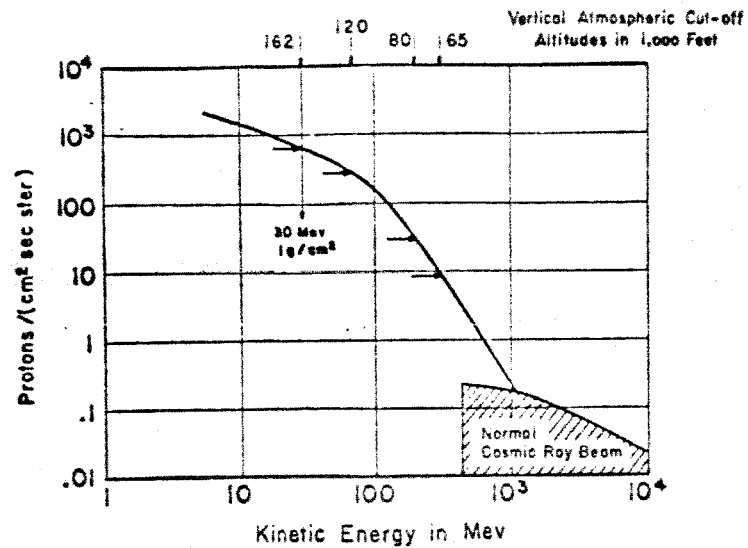


Figure 5.6 Typical Integral Energy Spectrum of Proton Beam from Large Solar Flare

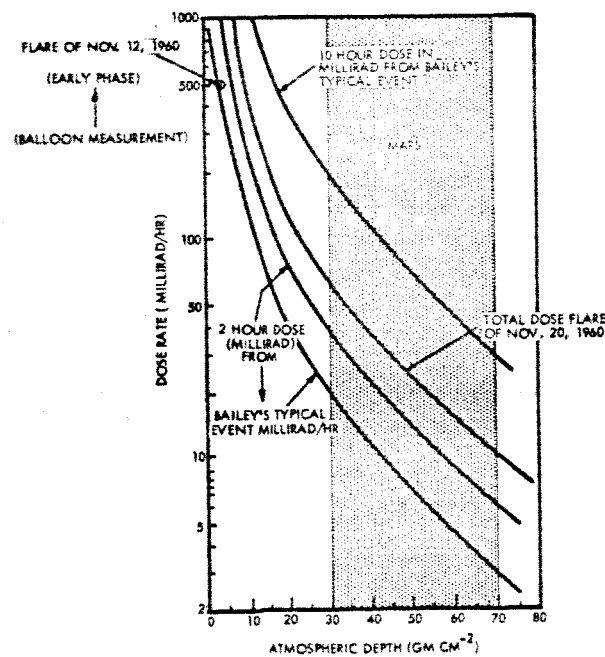


Figure 5.7 Solar Cosmic Ray Dose Rates in Tissue vs Atmospheric Depth

With respect to Bailey's representative event having an occurrence frequency of approximately one per week during high solar activity, detailed dosage calculations have been carried out for the tissue dose behind 1 gm/cm² of shield and a 16 gm/cm² shield. The results in free space as well as upon the martian surface are presented in the following table.

TABLE 5.11 SOLAR COSMIC RADIATION DOSES

Dose (rad/wk)

Shield gm/cm ²	Free Space	On Martian Surface			
		11 mb (30 gm/cm ²)	15 mb (40 gm/cm ²)	22 mb (60 gm/cm ²)	29 mb (75 gm/cm ²)
1	21	0.25	0.13	4×10^{-2}	2.5×10^{-2}
16	2.3	0.13	0.09	4×10^{-2}	2.5×10^{-2}

It is interesting to observe the insignificant effect of the extreme 15 gm/cm² shielding for the denser martian atmospheres. This indicates simply that the low energy protons have been filtered and that negligible attenuation occurs for the remaining very high energy particles.

c. Summary of the Dosages on the Mars Surface

The maximum dosages expected for a one-week residence upon the Mars surface appear in the following table.

TABLE 5.12 EXPECTED DOSAGES

EVENTS	INTEGRATED DOSE
GALACTIC COSMIC RAYS PER WK ON SURFACE	0.17 RAD
SOLAR COSMIC RAYS PER WK ON SURFACE	0.25 RAD (11 MB ATMOSPHERE)
ONE RELATIVISTIC FLARE ON SURFACE	40.0 RAD (30 GM CM ⁻²)
TOTAL WEEKLY TRIP DOSE ON SURFACE	40.4 RAD
DOSE IN TRANSIT (22 GM CM ⁻²)	
GCR	9 RAD PER YR
SCR	104 RAD PER YR
TOTAL DOSE (1 YEAR)	<hr/> 153 RAD

Apparently, the only concern relates to the rarely occurring relativistic flares. Such flares can be detected on Earth to provide a warning to the martian expedition. There is, of course, no way to avoid such a flare during transit.

Meteoroid Flux

Meteoroid flux in cismartian space will have a significant effect on vehicle gross weight, and in general, must be better documented with experimental data, which are very poor in certain critical areas of importance to the designer.

Prediction models of meteoroid flux are based in part on the following sources of data:

1. Satellites operating primarily (to date) in the near-earth environment; few data are available from deep space probes. Data are further limited to small particle sizes, less than 10^{-6} to 10^{-7} grams. The application of these data to interplanetary space is rendered difficult by the apparent dust cloud surrounding the Earth.
2. Radiations of zodiacal light. These faint radiations are observed near the ecliptic plane, and are due to the presence of very small particles, or a dust cloud, between the Earth and sun. These particles tend to spiral in to the sun, and are replaced, probably by asteroid and comet fragmentation and ejection. The mass of particles involved may not exceed 10^{-5} grams.
3. Visual, photographic and radar observations of the relatively larger meteoroids. These observations are made possible by the interaction of the meteoroid with the earth's atmosphere, which gives rise to ionization and visible radiation. The smaller particles are vaporized, and the resulting visible trails and radar echoes used as indications of mass and velocity. Particles as small as 10^{-3} grams can be detected in this manner. These data are most helpful because particles of this size are pertinent to the design of vehicle shielding. Particles of this type are cometary in nature, and probably decrease in flux at greater distances from the sun.
4. Visual and radar observations of asteroids. These are relatively large bodies lying in a belt situated between Earth and Mars. Asteroids of large size have been detected and

correlated for size-flux distribution. The extrapolation of this distribution data to particle sizes of interest in shielding analyses are doubtful, but have been used by Kessler and others to "link" the cometary data of (3) to the asteroid data of (4).

Data obtained from satellites is shown in Figure 5.8, as shown in Reference 5.23. The data extend up to sizes of approximately 10^{-6} grams, and are based on measurements taken mostly in the near earth environment. As discussed by Whipple (References 5.21 and 5.22), there is good evidence of a "dust cloud" attached to the Earth. The origin of this "cloud" is unknown, but may be due in part to the ejection of material from the moon by meteoriteic bombardment, by capture as a result of inelastic collisions between interplanetary particles, and by capture through aerodynamic deceleration. Whipple (Reference 5.22) has proposed a strong altitude dependency for the flux of small particles (10^{-9} grams) near the Earth (see Figure 5.9). The model seems to be substantiated by its agreement with a) the zodiacal flux in interplanetary space, and b) data obtained by Mariner II during transit to Venus. Data from the latter source were very limited, and do not constitute adequate verification of Whipple's altitude scaling law. In general, particles of the size covered in Figure 5.8 are too small to be of significance in determining vehicle shielding thicknesses.

It is doubtful if the "dust cloud" phenomenon and its associated altitude dependency described above apply to larger meteoroids detected by visual or photographic and radar observations as reported by Hawkins and others. In general, these data apply to meteoroids weighing 10^{-3} grams and greater, traveling at velocities on the average of 22 to 30 km/sec (Lowell), which is above the escape velocity with respect to the Earth which is about 11 km/sec. At these velocities, the focusing effect of the gravity field of the Earth is small, hence, the data are representative of the interplanetary environment at the Earth's distance from the sun. In this regard, it might be noted that Whipple's flux-mass law, which is based on Hawkin's observations at mass values from about 10^{-3} to 10^3 grams, tends to merge with the satellite data in the 10^{-6} to 10^{-8} gram region (see Figure 5.8). Since the satellite flux measurements may be influenced to a significant degree by the proposed "dust cloud" surrounding the Earth, Whipple's flux-mass law, as applied to interplanetary space, should not merge with the earth satellite data, but should pass through data points obtained by space probe satellites, which in turn should

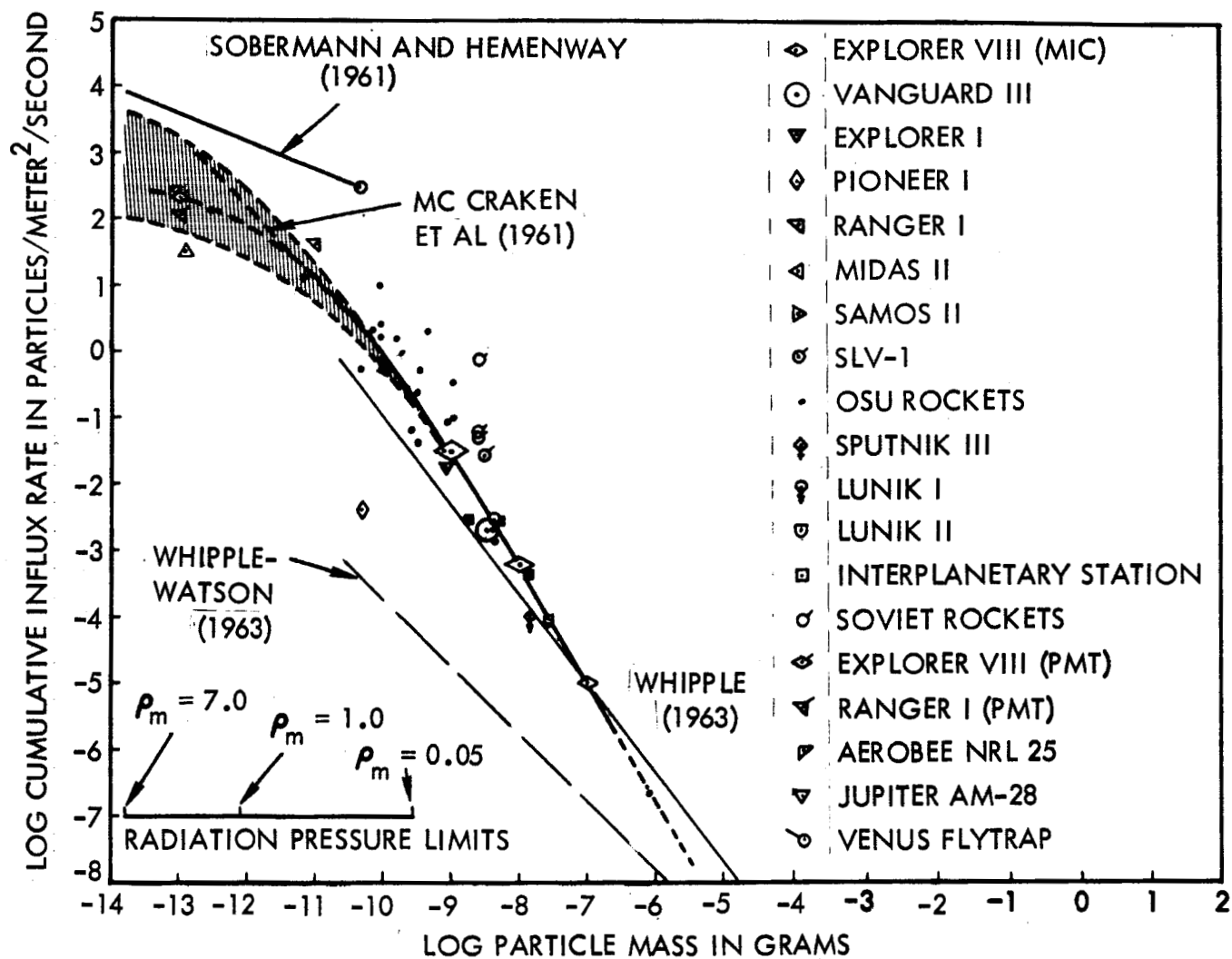


Figure 5.8 Micrometeoroid Flux (Hamermesh, Reference 5.23)

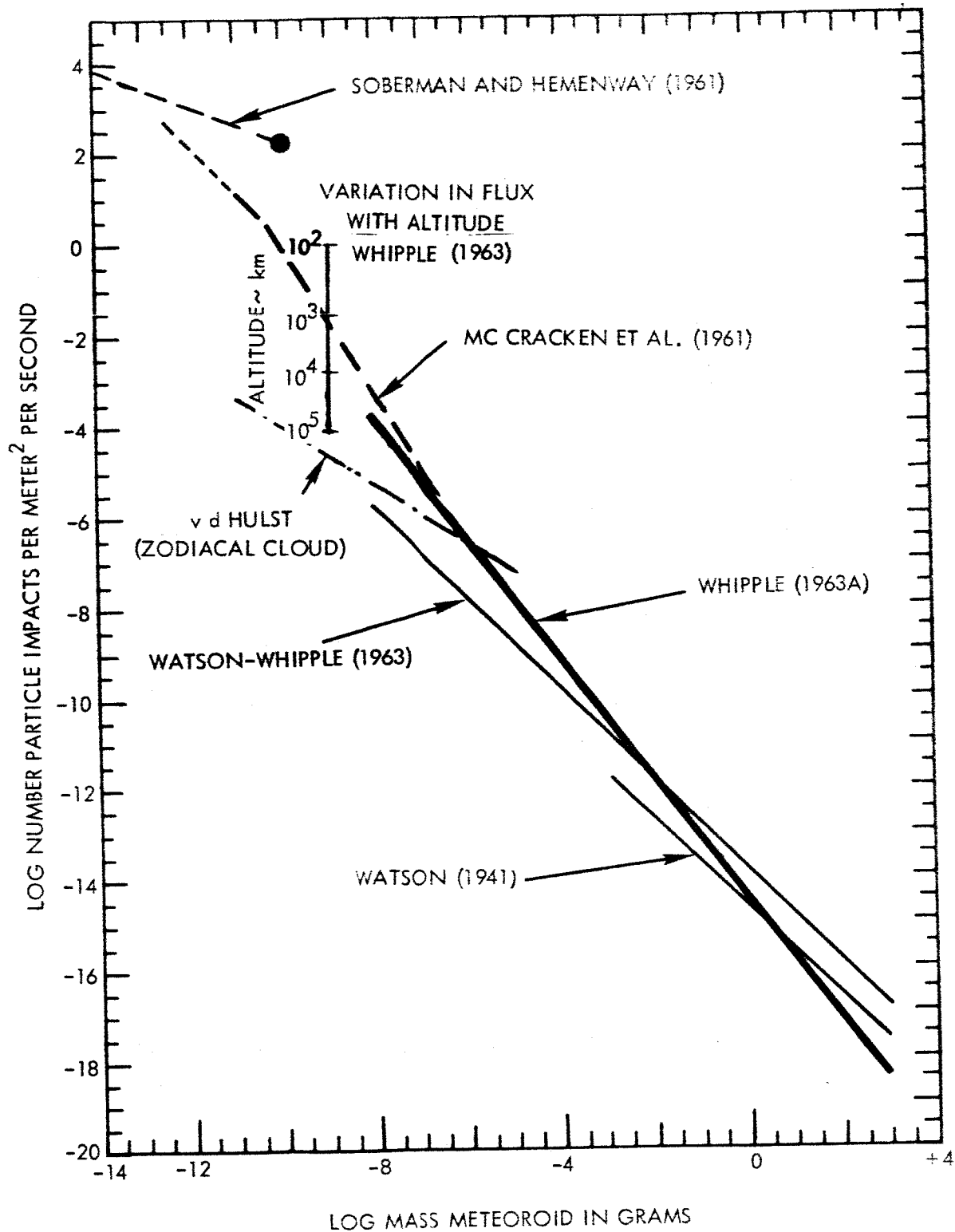


Figure 5.9 Meteoroid Flux Models (Whipple, Reference 5.20)

agree with Whipple's altitude extrapolation through the "dust cloud" to free space. This can be done by adopting Whipple's version of Watson's flux-mass law:

$$N = 1.34 \log m + 2.68 \log (0.433/\rho) - 14.48$$

(Whipple-1963)

$$N = -\log m + 2 \log (0.443/\rho) - 13.80$$

(Watson as modified by Whipple-1963)

These flux-mass laws are in agreement at 10^{-2} grams, but the Watson-Whipple law is in better agreement with the zodiacal flux law and with the Mariner II space probe data in the micrometeoroid range, and is the preferred model.

Whipple's 1963 flux-mass law is about 1.7 orders of magnitude lower than his 1957 law, do largely to new interpretations of mass-visual magnitude relations based on recent data. There remains some uncertainty in the meteoroid laws in the vehicle shielding design range ($\sim 10^{-3}$ grams), but the uncertainty should be no greater than one order of magnitude. Accordingly, this degree of uncertainty is used in the mission sensitivity analysis.

The question is raised concerning the extension of the flux-mass model law to the region of the martian orbit. The meteoroid flux-mass model of Whipple can be adapted rather easily to variable radius missions by incorporating the orbital heliocentric characteristics of the particles as derived from visual-radar observations. Based upon the velocity spectra given by Lovell and others for these particles, which indicate that many of the particles follow highly eccentric paths in heliocentric space, it can be predicted that the flux due to these particles decreases with increasing distance from the sun. No calculations of this reduction have been made, but Hamermesh indicates a reduction to 39 percent of the flux at 1 AU in the vicinity of the Mars orbit. For design purposes, it may be appropriate to use the near-Earth law without modification.

Kessler has developed a flux-mass law for asteroids, which he then shows to have a dominating effect in the region beyond the Earth, at particle sizes greater than 10^{-4} grams, which would include the mass range of concern to the vehicle designer. Essentially, Hawkins' statement that the asteroid flux is equal to the cometary particle flux at Earth in the range from 0 to -5 visual

magnitude, is used to derive a flux-mass relation for asteroids in this size range. This law is then extrapolated through several orders of magnitude in mass range to determine a value of flux for particles 10^9 grams in mass; this flux value is then used in a correlation of flux versus solar radius for asteroids!! This technique is so highly speculative as to render its validity questionable. Many factors such as particle density, velocity spectra, and correlation of visual magnitude to mass for asteroids, which depends heavily on velocity (the velocity spectra of asteroids may be greatly different from that of cometary particles), must be established on a firmer basis before gross extrapolations of this type can be attempted.

6. AERO ENTRY SYSTEM ANALYSIS

The main Mars spacecraft will approach Mars along a hyperbolic path, and must decelerate to below parabolic velocity in order to be captured by Mars. The Mars orbit rendezvous mode makes it desirable to decelerate the spacecraft into a low altitude circular parking orbit to facilitate the subsequent landing operations, although a moderately elliptic orbit tends to reduce the departure propulsion requirements.

The deceleration maneuver can be accomplished by aerodynamic braking if sufficient lift-to-drag ratio is provided in the design to accommodate uncertainties in terminal guidance, and in the properties of the atmosphere. Aerodynamic braking is attractive from an overall mission standpoint because of the relatively low weight of the aero braking system compared to that of a retro braking system; the reductions in overall system weight are especially large for chemical propulsion configurations.

The purpose of this section is to determine the sensitivity of the aero entry system described in Section 4 to uncertainties in the Martian atmosphere, and to compare the corridors attainable with a range of lift-to-drag ratios with guidance corridor requirements. The atmosphere models considered are: Model 3 (10 mb), Model 2 (25 mb), and the Schilling upper limit model (132 mb). The effects of uncertainties in atmosphere density, scale height and composition are considered, both for relatively moderate uncertainties, as well as for gross uncertainties.

6.1 Corridor Analysis

For present purposes, corridor depth is defined as the difference in altitude of the virtual or vacuum periapses of the overshoot and undershoot trajectories. The overshoot trajectory is flown with a given constant negative L/D ratio which allows the vehicle to exit from the atmosphere at the desired velocity. The virtual periapsis of this overshoot trajectory is a function of the exit velocity. The undershoot trajectory is flown with a given constant positive L/D ratio. As with the overshoot case, the periapsis altitude for the undershoot case is a function of exit velocity. The undershoot trajectories found in this study did not have resultant decelerations exceeding 10 g's.

For the purpose of examining the change in corridor requirements with atmospheric characteristics for an aerodynamic braking maneuver in the Martian atmosphere, point mass trajectories for vehicles with lifting capability were computed. These trajectories were computed for three atmospheres specified by the Ames Research Center. These are the Model 2 and 3 atmospheres of the NASA Engineering Models of Reference 6.1 and the upper limit atmosphere of the Schilling Model II atmosphere of Reference 6.2. The density variation with altitude for these atmospheres is given in Figure 6.1. The lifting capability of the vehicles was given at a constant L/D ratio. The overshoot type trajectories were computed for L/D values of -0.3 and -0.1 and the undershoot type trajectories for L/D values of +0.3 and +0.1. A non-rotating planet and an entry velocity of 27,500 ft/sec at an altitude of 800,000 ft were assumed. A value of $W/C_D A = 765 \text{ lb/ft}^2$ was used for the ballistic coefficient. Results of the trajectory calculations are given in Figures 6.2 through 6.7. In Figures 6.2, 6.3, and 6.4, the virtual periapsis altitude is given as a function of the velocity of the vehicle as it leaves the atmosphere at an altitude of 800,000 ft. Figures 6.5, 6.6, and 6.7 are similar, but actual minimum flight altitude is given instead of virtual or vacuum minimum altitude.

Figures 6.2 through 6.7 are of interest in defining L/D requirements. For example, if a given vehicle design must accommodate all three atmospheres, a corridor exists only for an $L/D = 0.3$ and then only if the vehicle is slowed to below 14,000 fps. It is noted that this is an upper bound on corridor depth since certain operational problems will reduce the corridors such as allowing for the ability to maneuver (Reference 6.3).

According to Figure 6.7 the actual minimum altitude of flight for the $L/D = 0.3$ is down around 10,000 ft. Thus a higher L/D capability is not useful for a vehicle with this ballistic coefficient. Lowering the ballistic coefficient while maintaining the same L/D probably requires lowering the overall density of the vehicle, which is undesirable when the initial assembly of the vehicle in earth orbit is considered.

Since accommodating all three atmosphere models with a given design presents an almost prohibitive corridor situation, it is of interest to

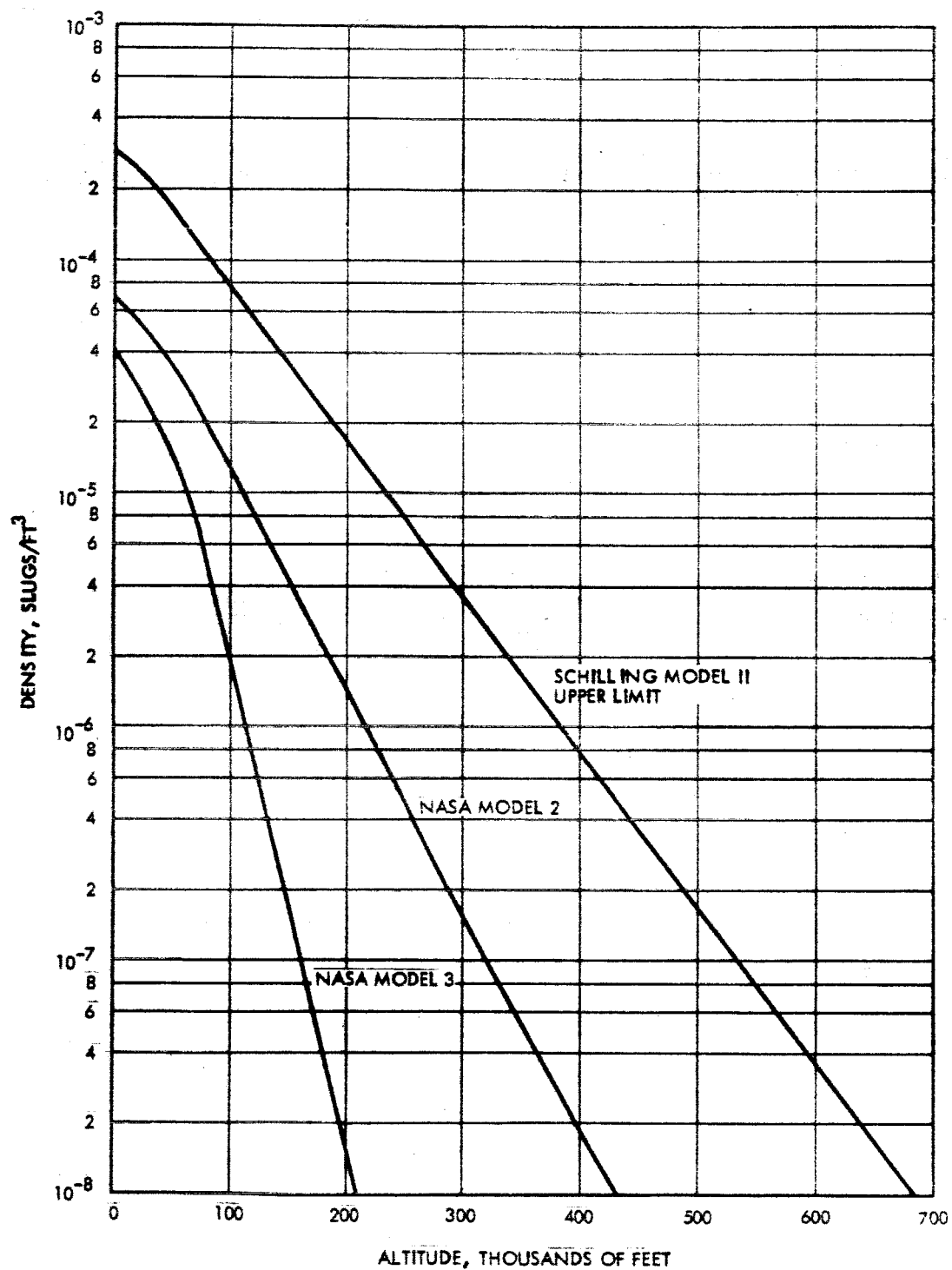


Figure 6.1 Schilling Model II Upper Limit, and NASA Model 2 and Model 3 Mars Atmospheres

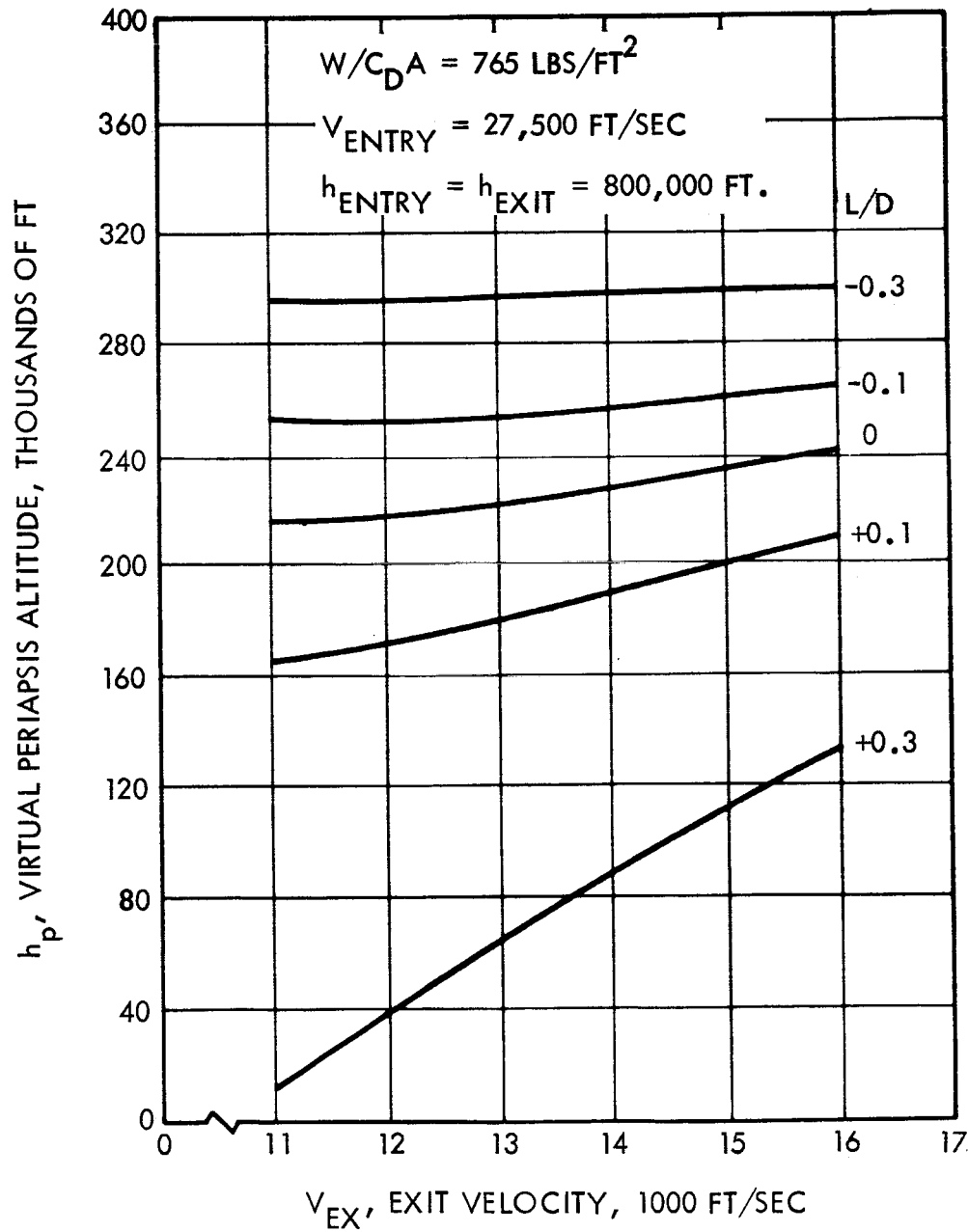


Figure 6.2 Virtual Periapsis Altitude for Schilling Upper Limit Atmosphere Model

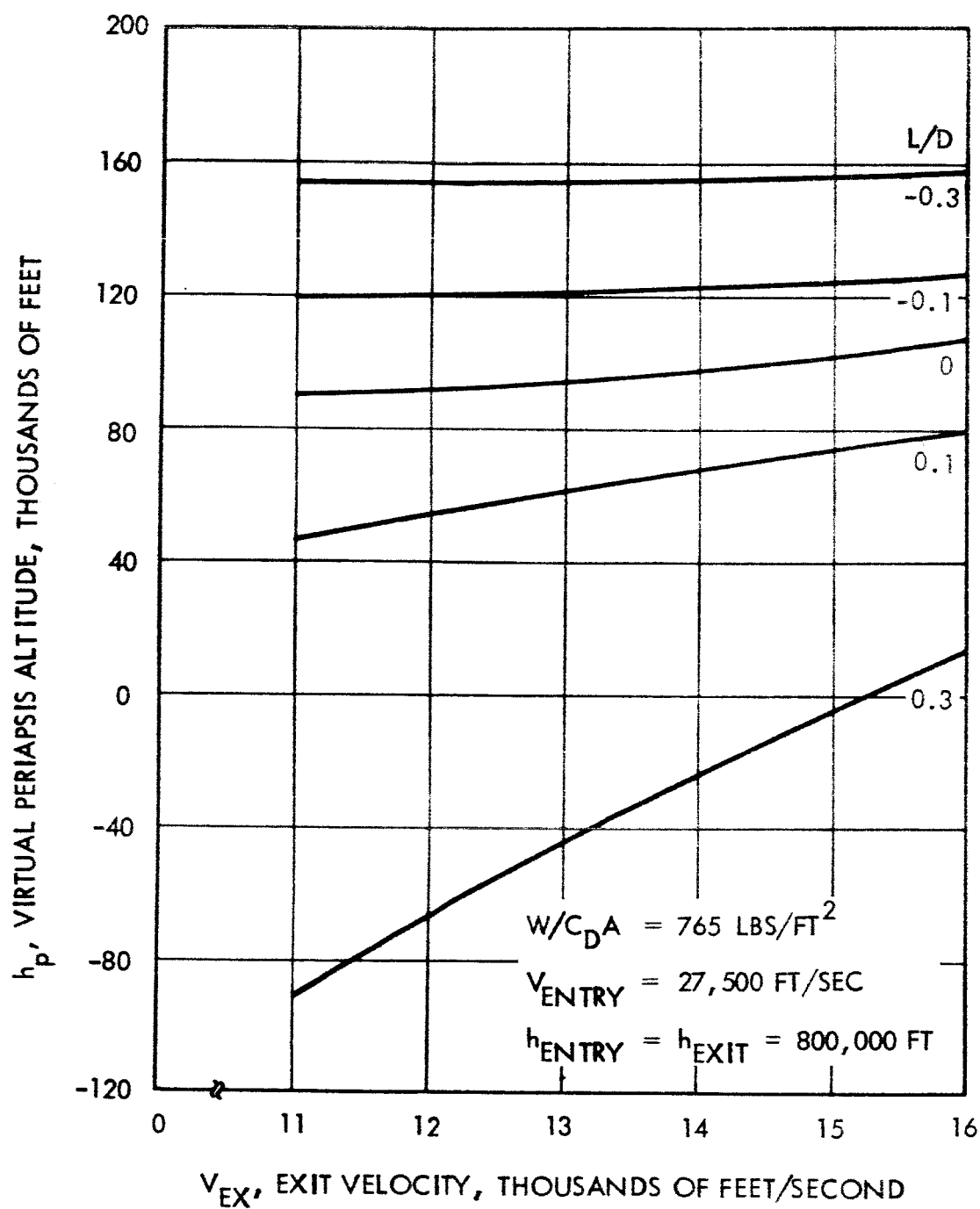


Figure 6.3 Virtual Periap sis Altitude Vs. Exit Velocity and L/D for NASA Model 2 Atmosphere

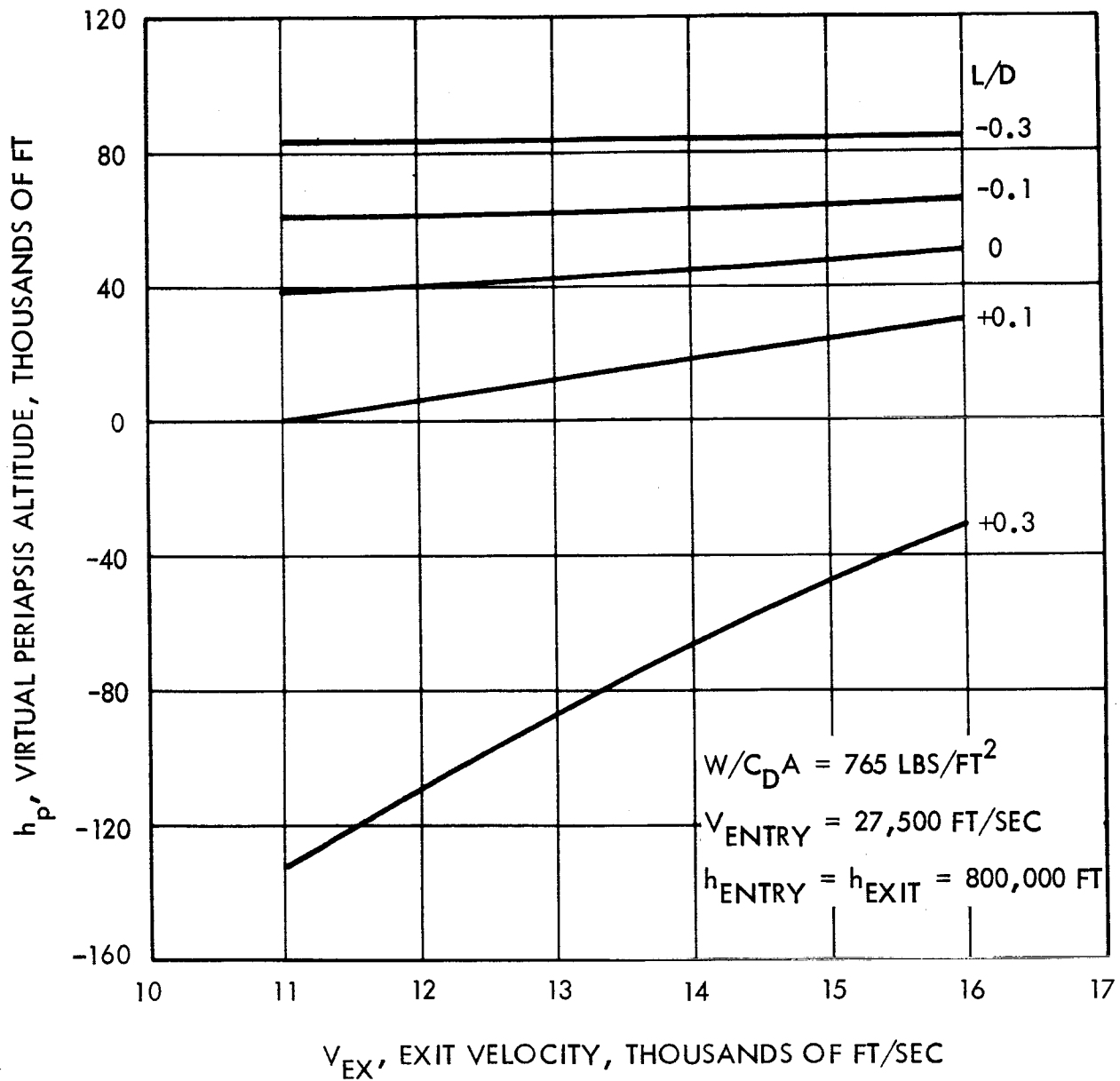


Figure 6.4 Virtual Periapsis Altitude for NASA Model 3 Atmosphere

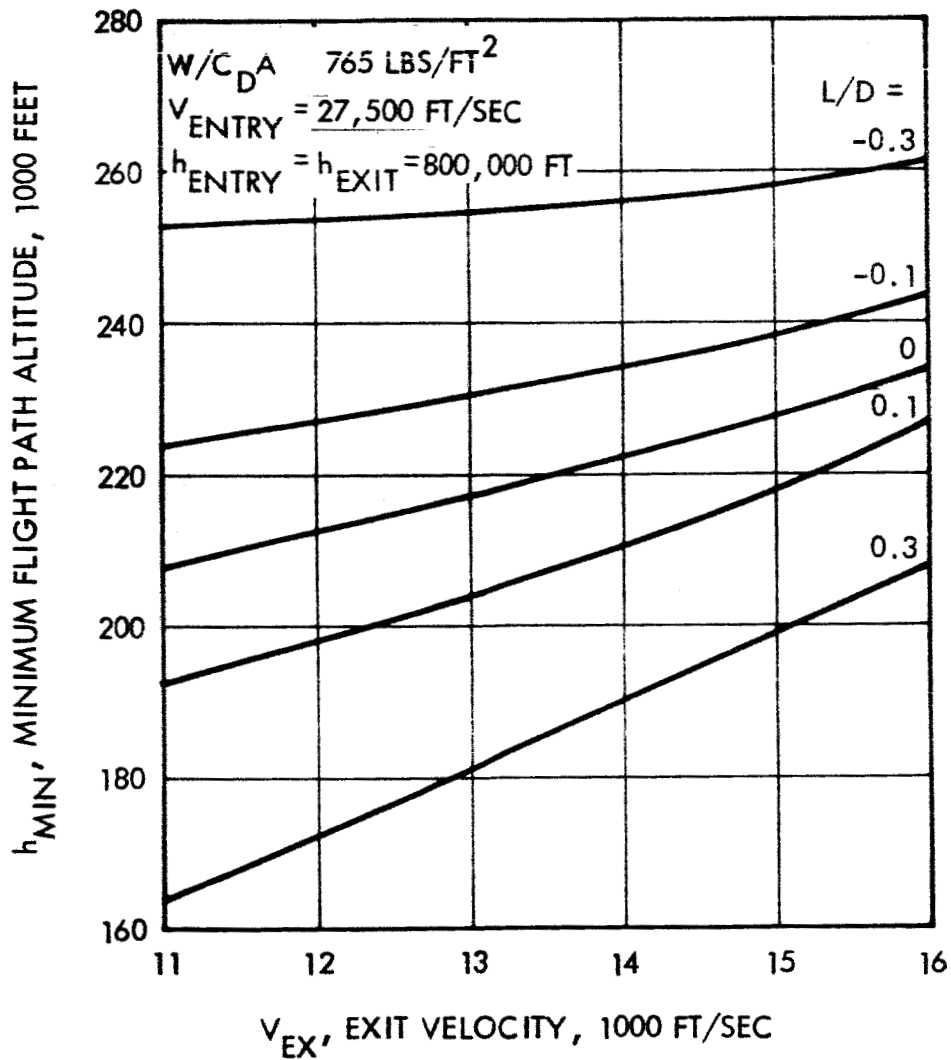


Figure 6.5 Minimum Flight Path Altitude Vs. Exit Velocity and L/D for Schilling Model II Upper Limit Atmosphere

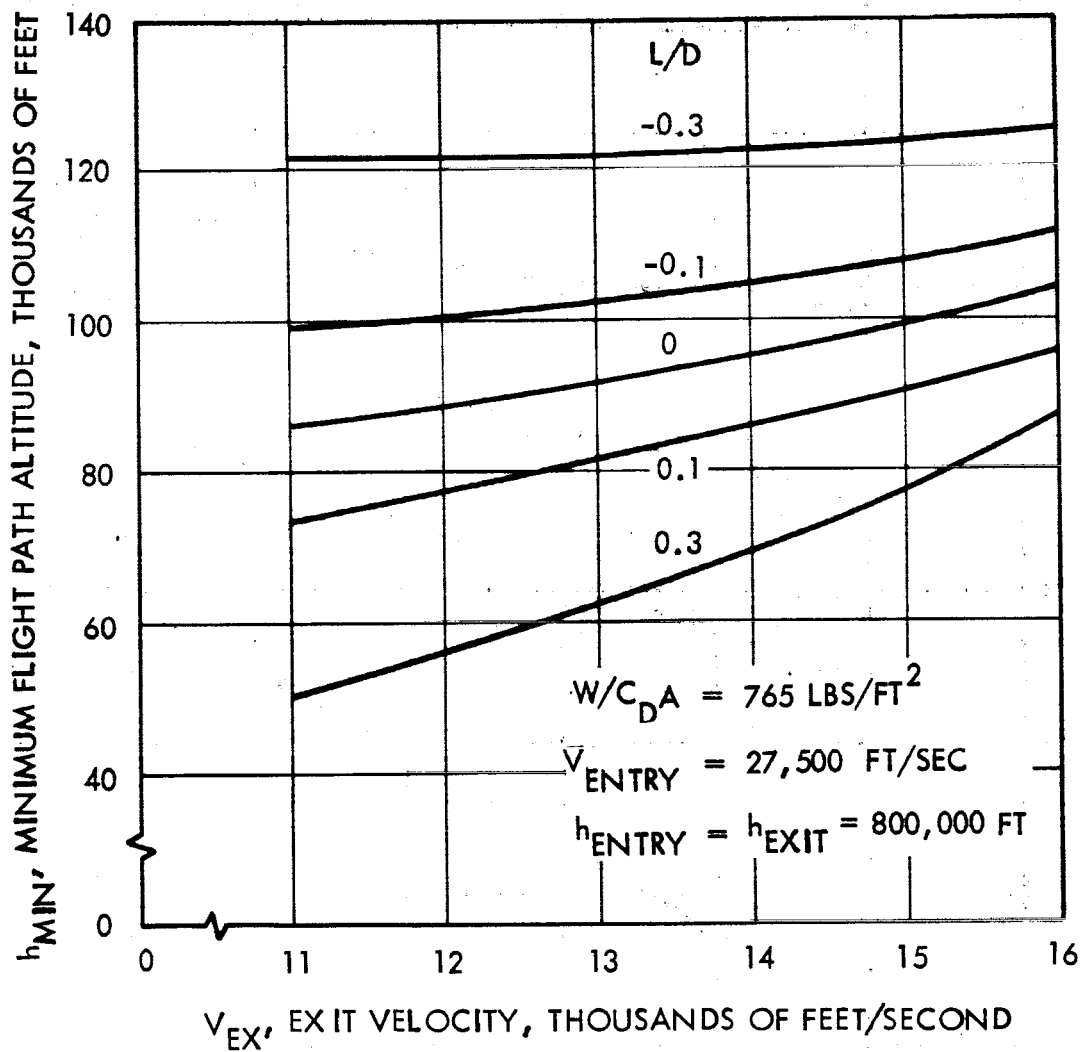


Figure 6.6 Minimum Flight Path Altitude Vs. Exit Velocity and L/D for NASA Model 2 Atmosphere

$$W/C_D A = 765 \text{ LBS/FT}^2$$

$$V_{\text{ENTRY}} = 27,500 \text{ FT/SEC}$$

$$h_{\text{ENTRY}} = h_{\text{EXIT}} = 800,000 \text{ FT}$$

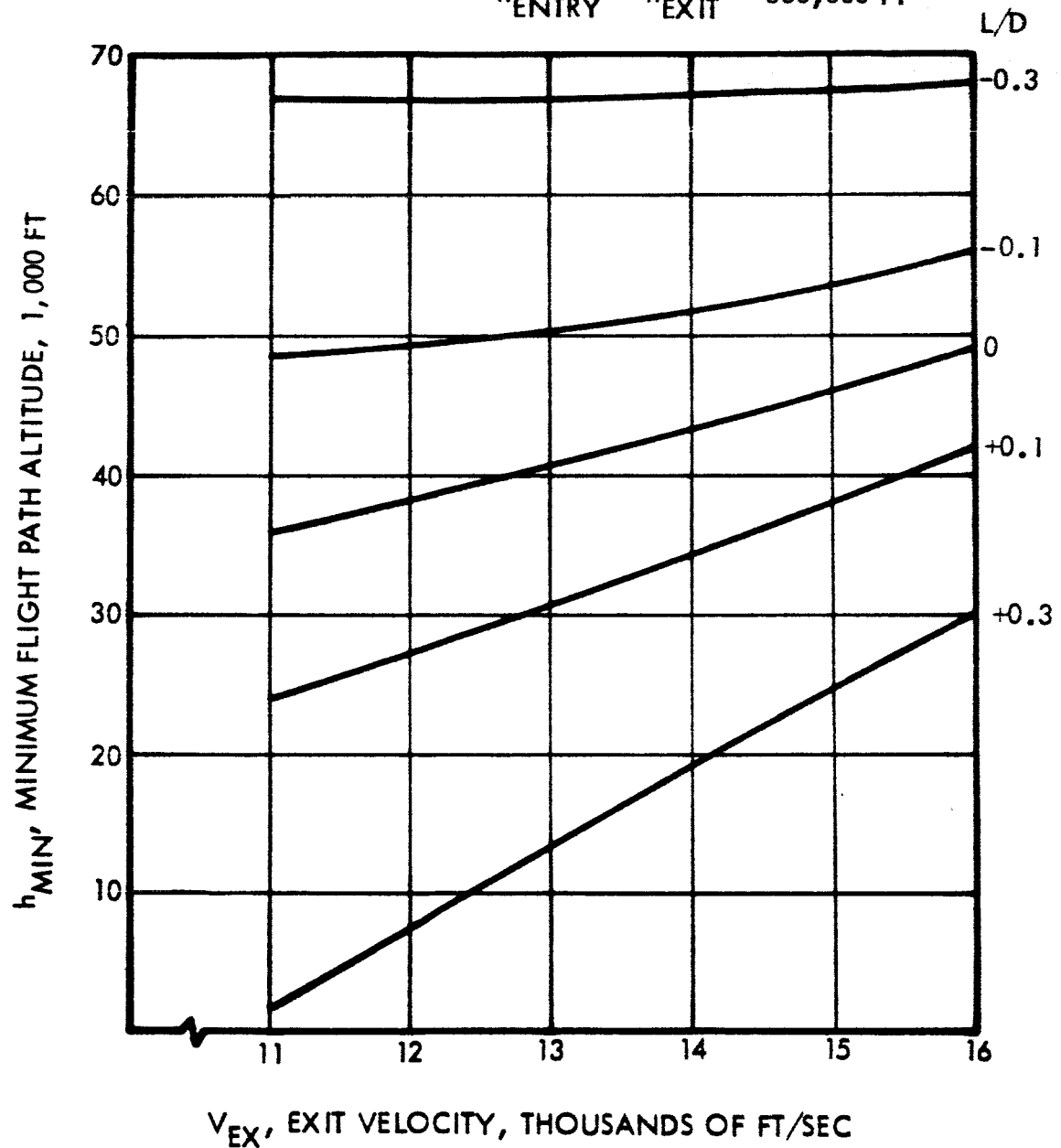


Figure 6.7 Minimum Flight Path Altitude for NASA Model 3 Atmosphere

consider the less restrictive case where the Mars atmosphere is better known. For this purpose the NASA atmosphere Model 2 was taken as a nominal atmosphere and the effect on corridor depth due to variations in surface density and scale height were investigated.

First a variation of $\pm 10\%$ in scale height was investigated. To perform this analysis, Chapman's approach to the entry problem (Reference 6.4) was used. Trajectory solutions which had been computed as discussed above are shown in Figure 6.8, where the L/D parameter,

$$\sqrt{\frac{r}{H \rho}} \bigg|_{\theta} L/D,$$

is plotted as a function of the log of the periapsis parameter, F_p . The periapsis parameter used in this figure applies to trajectories that have an exit velocity of 12,500 fps. The computed points for the Model 3 atmosphere fall off the curve because the trajectories extend into a non-isothermal portion of the atmosphere below the stratosphere. The correlation of Figure 6.8 is used for determining corridor depths as functions of atmosphere scale height and density. The effects on corridor depth of 10 percent variations in scale height and density are given by Figures 6.9 and 6.10. Figure 6.11 shows the variation of density with altitude, which was obtained by taking a variation in the stratosphere scale height of ± 10 percent. Figure 6.12 shows the effect on the virtual periapsis altitude produced by the ± 10 percent variation in scale height.

Next the variation in periapsis altitude due to a 10 percent variation in sea level density was considered. A given corridor depth for the Model 2 atmosphere is decreased by 9,000 ft when the flight takes place in the stratosphere due to a sea level density uncertainty of ± 10 percent. This effect in terms of periapsis altitude is shown in Figure 6.13.

In addition to the consideration of these 10 percent variations in atmospheric properties, the effects of gross variations on corridor depth were also considered. The intermediate NASA Model 2 was used holding surface density constant but using the variation of density with altitude given by the NASA Model 3 and the Schilling atmospheres. The resulting atmospheres are shown in Figure 6.14. The virtual periapsis altitudes

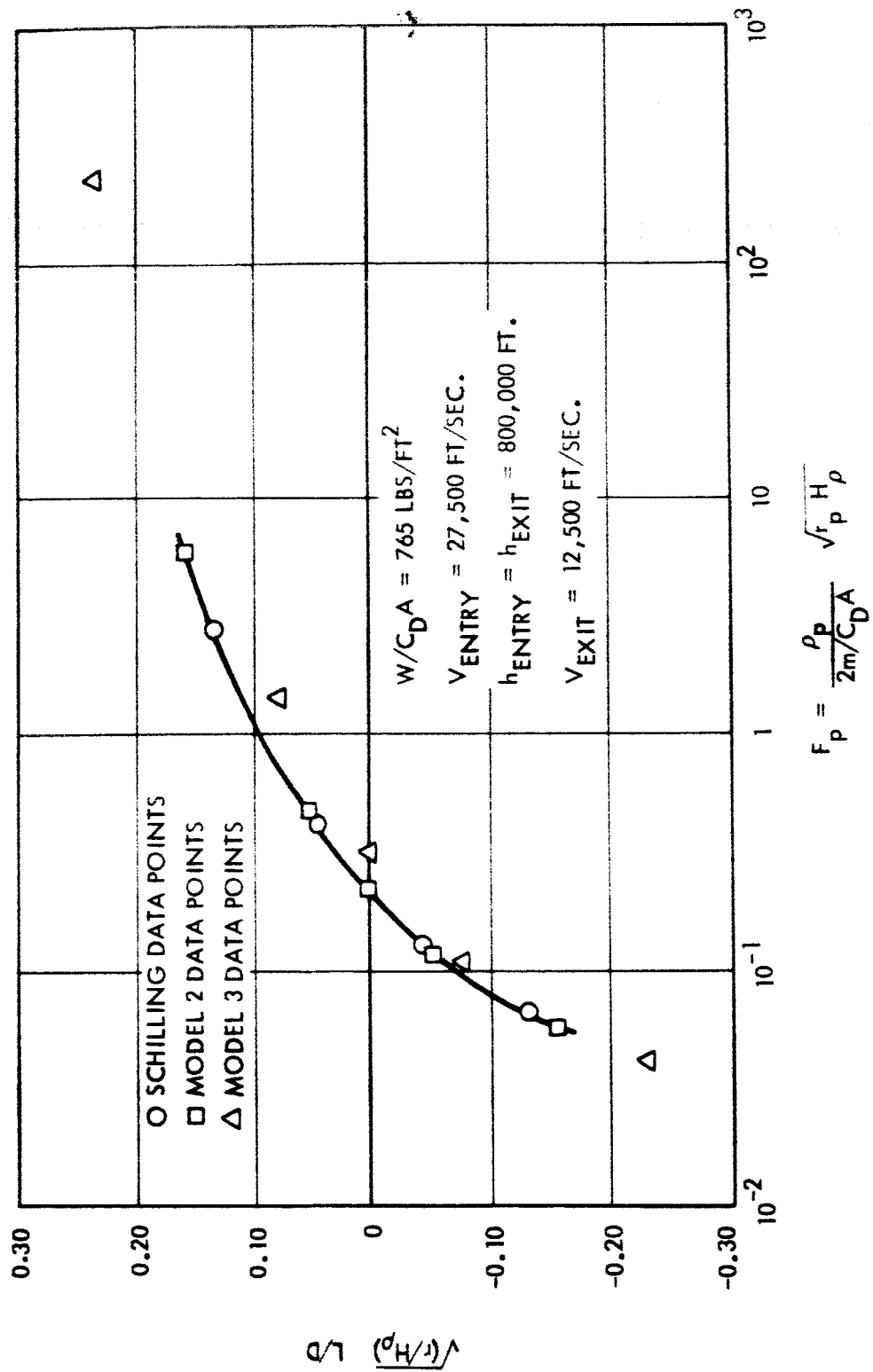


Figure 6.8 Variation of Periapasis Parameter with L/D for $V_{\text{EX}} = 12,500 \text{ fps}$

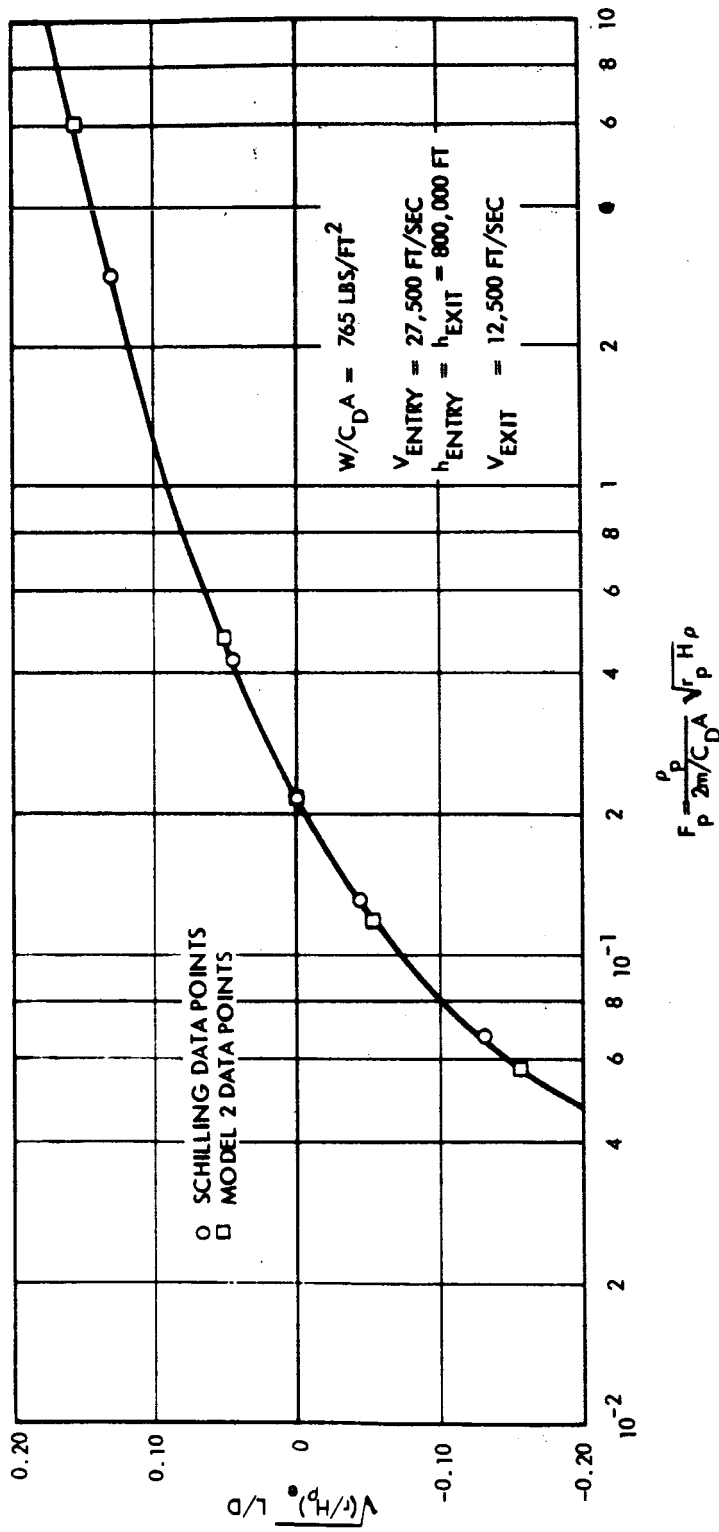


Figure 6.9 Variation of Periapsis Parameter with L/D for $V_{\text{EXIT}} = 12,500 \text{ fps}$

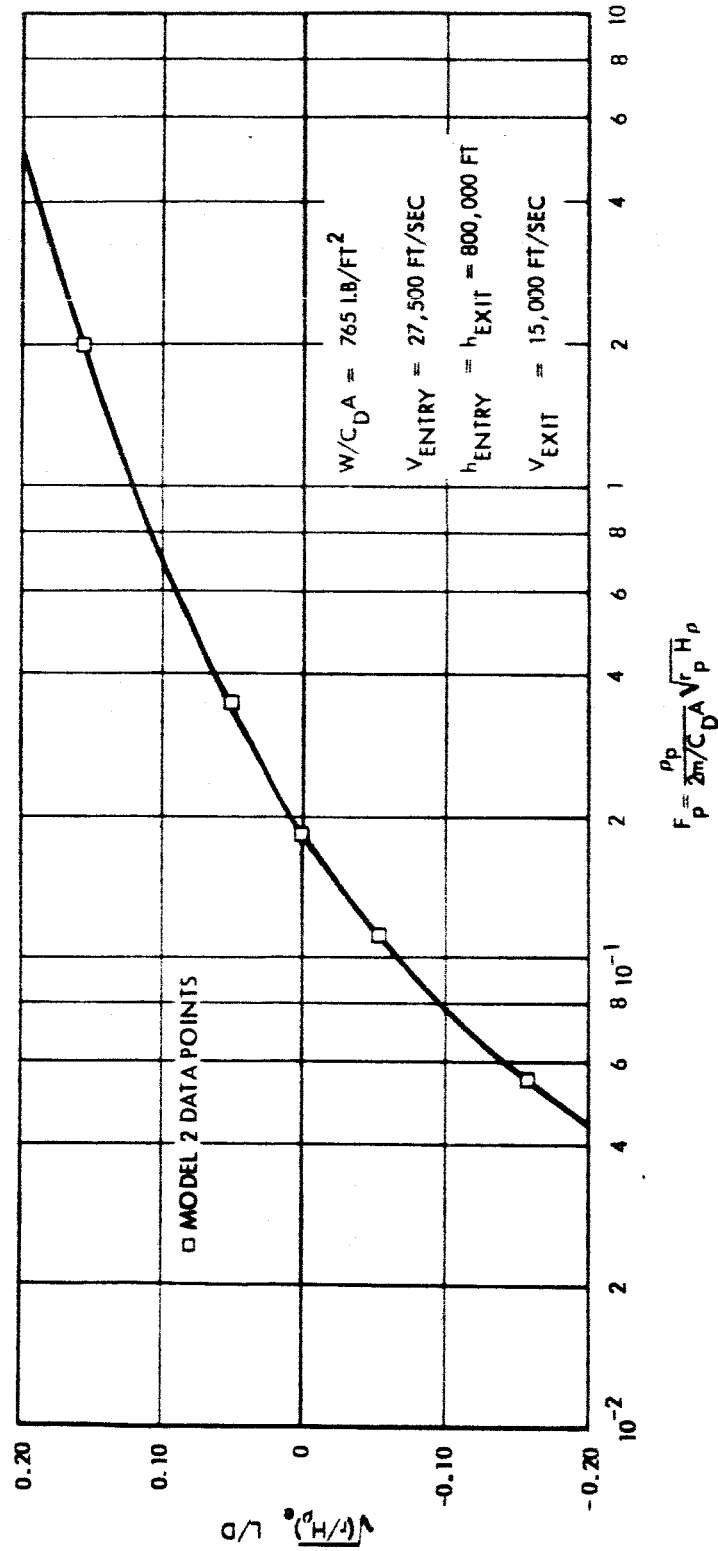


Figure 6-10 Variation of Perlapsis Parameter with L/D for $V_{\text{EXIT}} = 15,000 \text{ fps}$

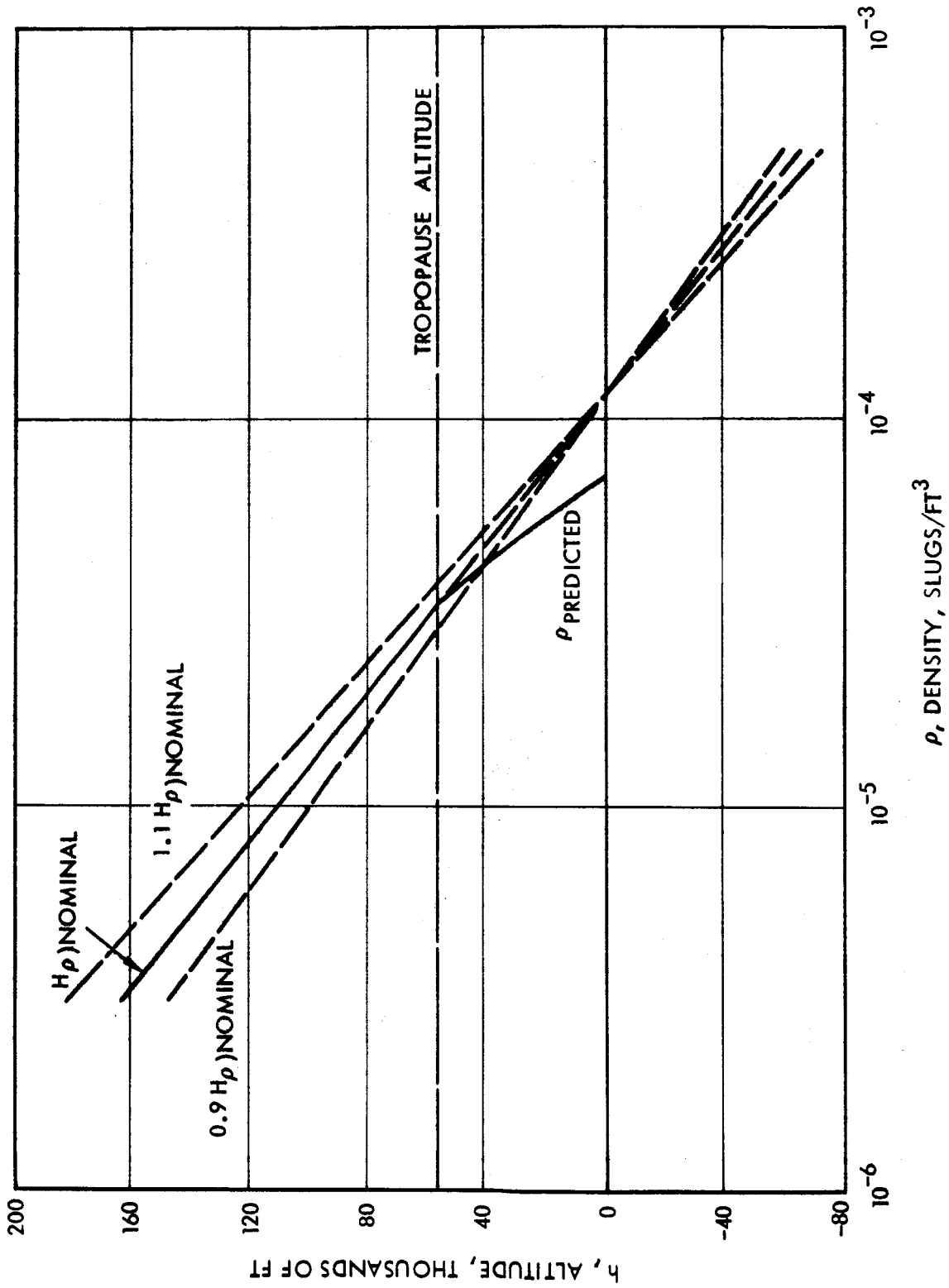


Figure 6.11 NASA Model 2 Atmosphere with $\pm 10\%$ Scale Height Variations

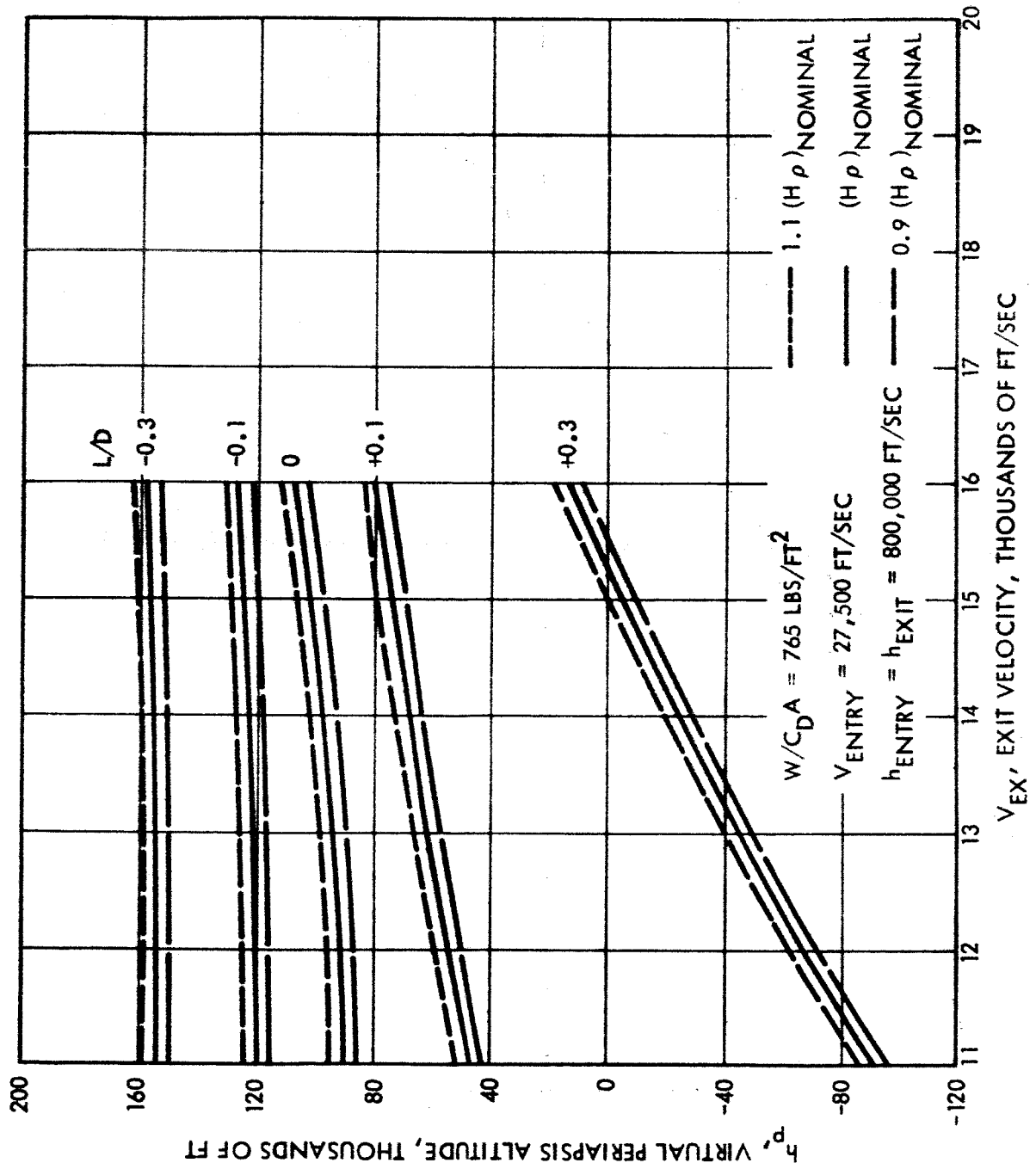


Figure 6.12 Virtual Periapsis Altitude for NASA Model 2 Atmosphere with $\pm 10\%$ Scale Height Variation

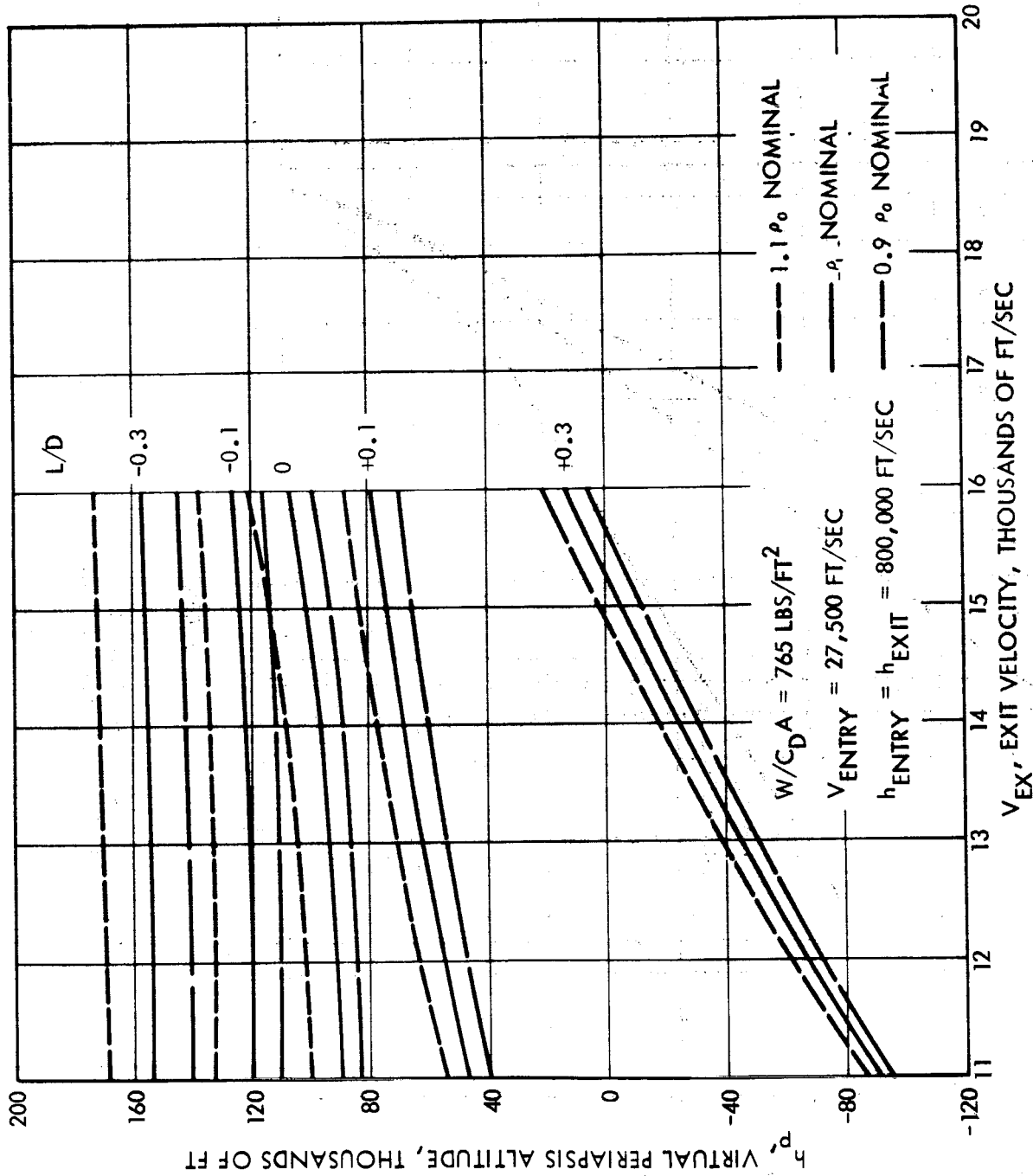


Figure 6.13 Virtual Periapsis Altitude for NASA Model 2 Atmosphere with $\pm 10\%$ Surface Density Variation

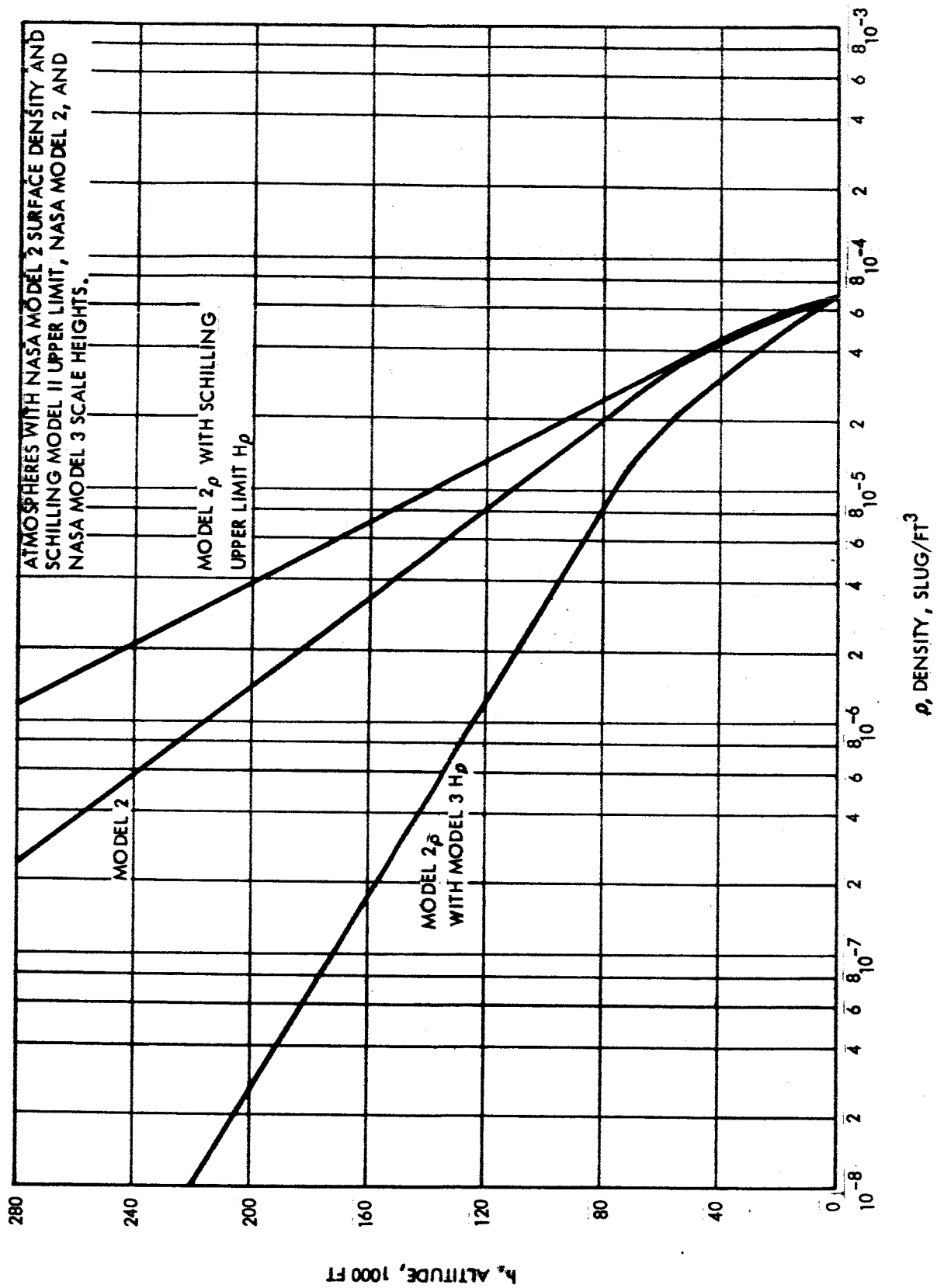


Figure 6.14 Atmospheres with NASA Model 2 Surface Density and Schilling Model II Upper Limit, NASA Model 2, and NASA Model 3 Scale Heights

for these atmospheres and a vehicle with L/D capability of 0.3 are shown in Figure 6.15. An L/D value of 0.1 is not shown because no corridor remains for this case. The figure shows the decrease in corridor depth caused by these gross deviations from the Model 2 atmosphere.

Similarly, the Model 2 atmosphere was varied by shifting the surface density but not its variation with altitude. These atmospheres are shown in Figure 6.16. The resulting variations in virtual periapsis altitude and therefore corridor depth are shown in Figure 6.17 for $L/D = 0.3$. Here again the corridor no longer exists for an L/D of 0.1.

Finally, the net corridor depths are shown in Figure 6.18 for the variation of the Model 2 atmosphere from the Model 3 atmosphere on one side of the Schilling atmosphere to the other. The remaining corridor for $L/D = 0.3$ theoretically exists only for exit velocities below 13,800 ft/sec. It should be kept in mind that this corridor is further reduced by maneuvering requirements such as discussed in Reference 6.2.

A summary of corridor depths is given in Figure 6.19 where the corridor depths are given as a function of exit velocity. The corridors are given for $L/D = 0.1$ without atmospheric uncertainties, and for $L/D = 0.3$ with variations from the Model 2 atmosphere as discussed above.

The results of the above analysis as will be discussed in Section 6.2, indicate that if the worst combination of properties of the three atmospheres is allowed, a lift-to-drag ratio of 0.3 provides a marginal braking maneuver entry corridor. In view of this conclusion, a vehicle with a lift-to-drag ratio of 0.4 has been examined with the following results.

Figures 6.20, 6.21 and 6.22 give virtual periapsis altitude as a function of exit velocity for $L/D = 0.4$ and a ballistic parameter $W/C_D A = 2000 \text{ lbs/ft}^2$. Figures 6.23, 6.24 and 6.25 give minimum flight path altitude as a function of

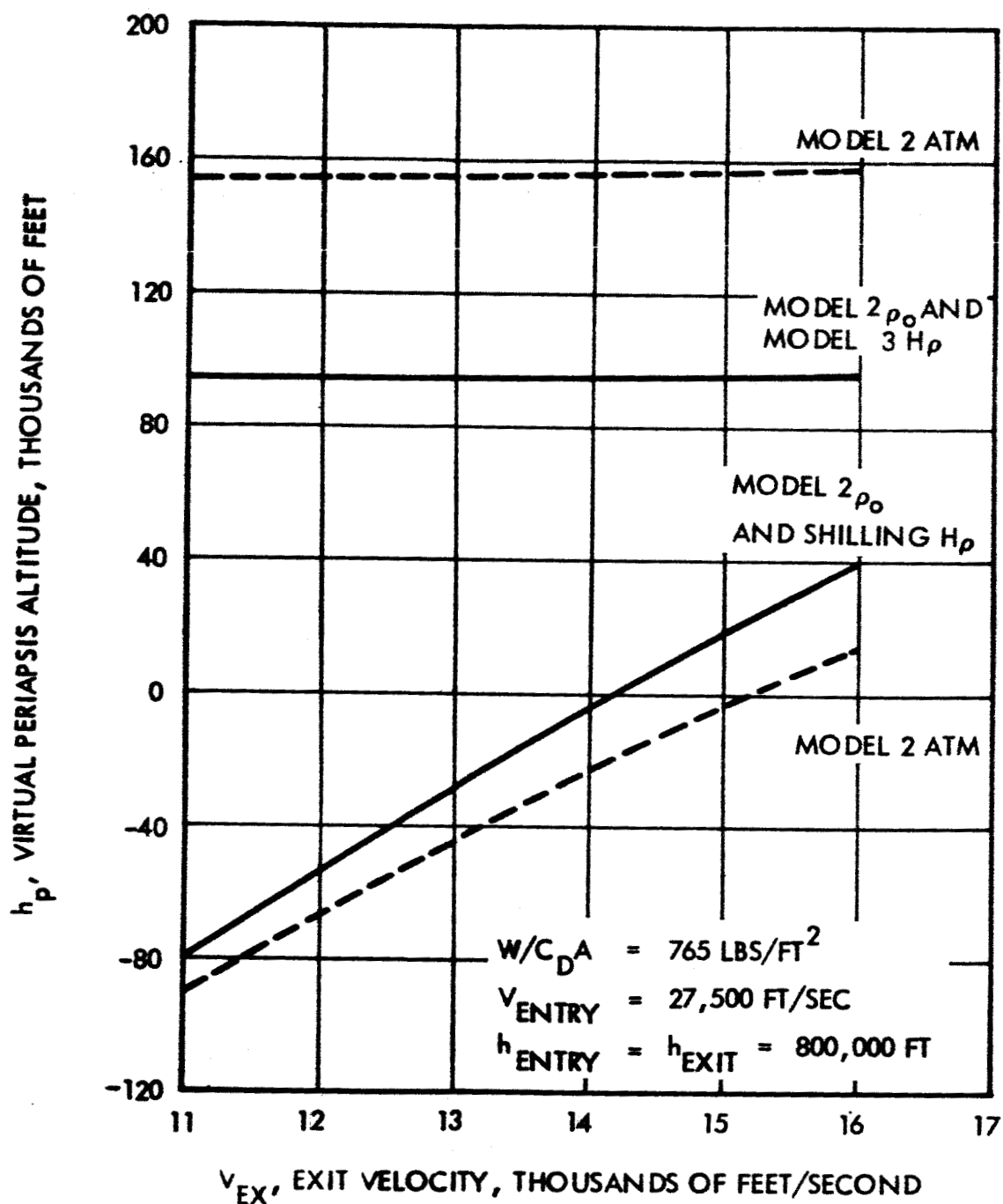


Figure 6.15 Corridor Limiting Virtual Periapsis Altitudes for $L/D = +.3$ for Atmosphere with Model 2 Surface Density and Possible Scale Height Range from Schilling Model II Upper Limit to NASA Model 3

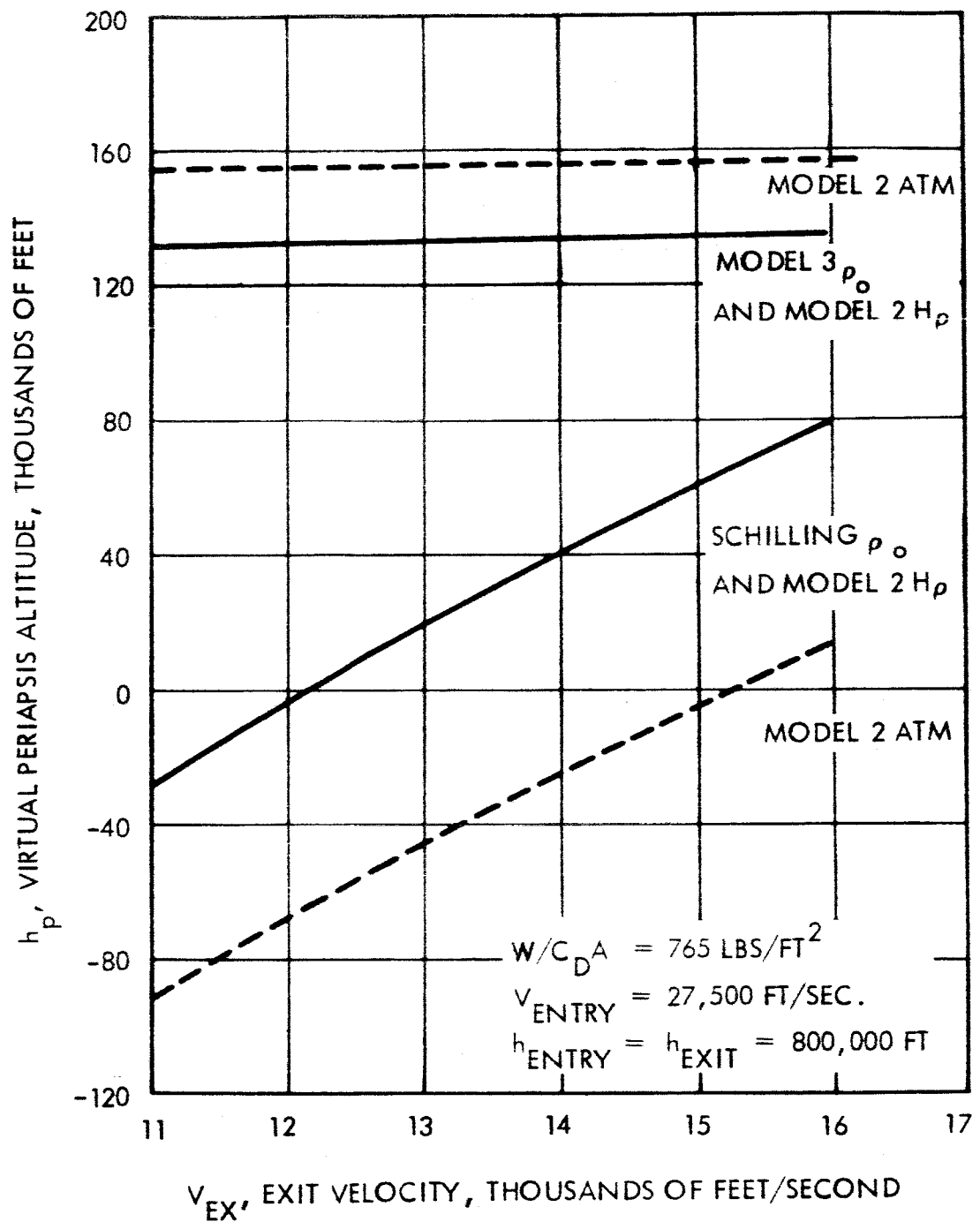


Figure 6.17 Corridor Limiting Virtual Periapsis Altitudes for $L/D = +.3$ for Atmosphere with Model 2 Scale Height and Possible Surface Density Range from Schilling Model II Upper Limit to NASA Model 3

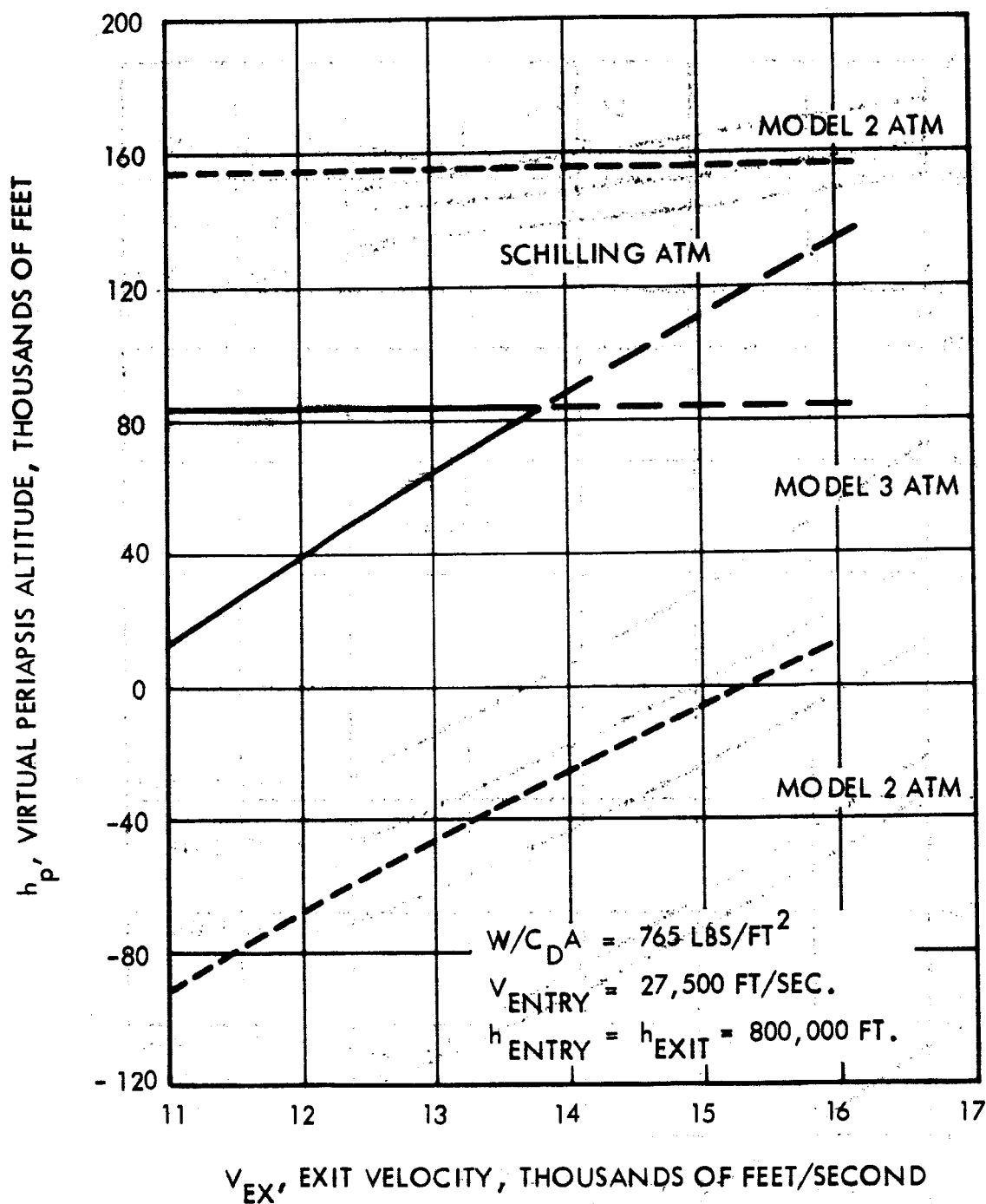


Figure 6.18 Corridor Limiting Virtual Periapsis Altitudes for $L/D = +.3$ for Atmosphere with Possible Surface Pressure and Scale Height Ranges from Schilling Model II Upper Limit to NASA Model 3

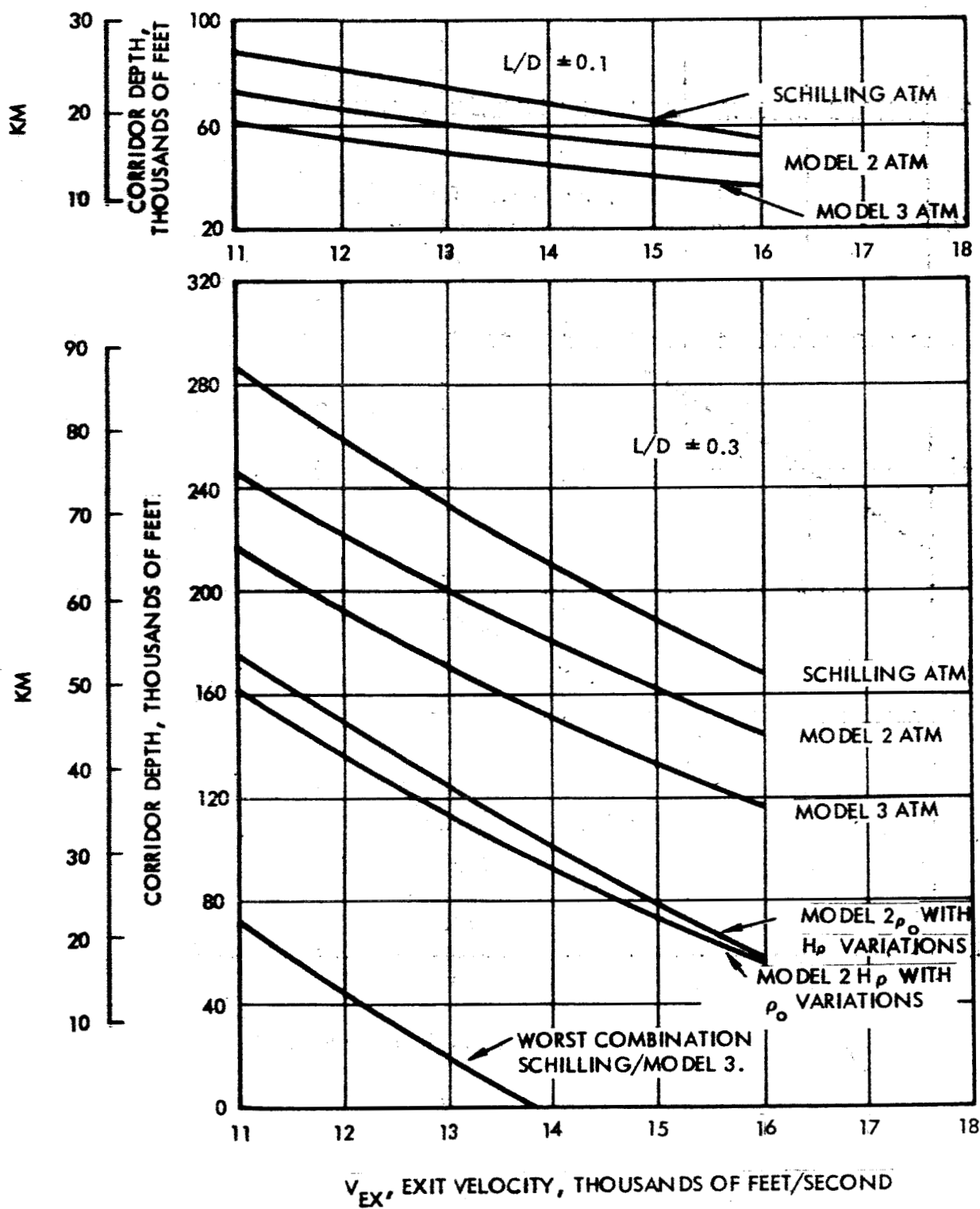


Figure 6.19 Corridor Depths for $L/D = \pm 0.1$ and ± 0.3

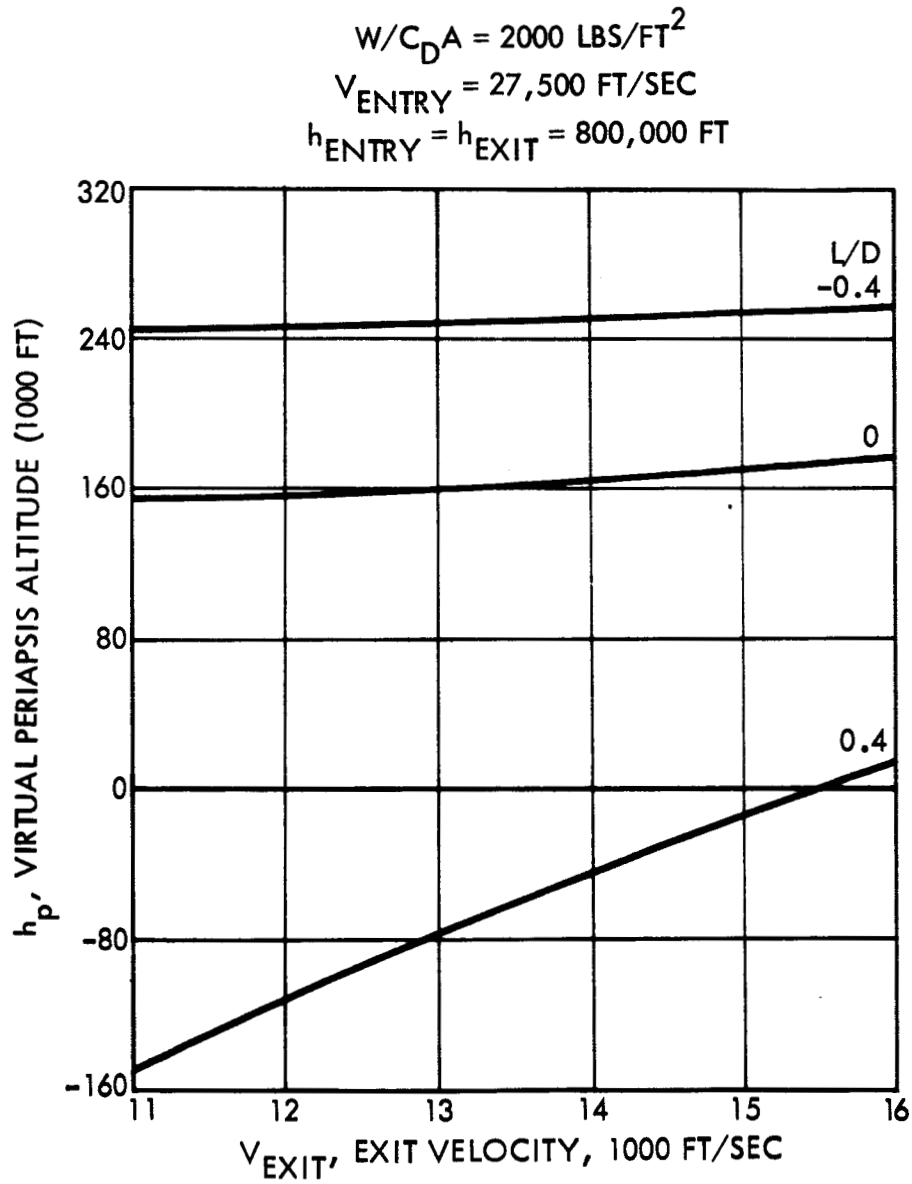


Figure 6.20 Virtual Periapsis Altitude Vs. Exit Velocity and L/D for Schilling Model II Upper Limit Atmosphere

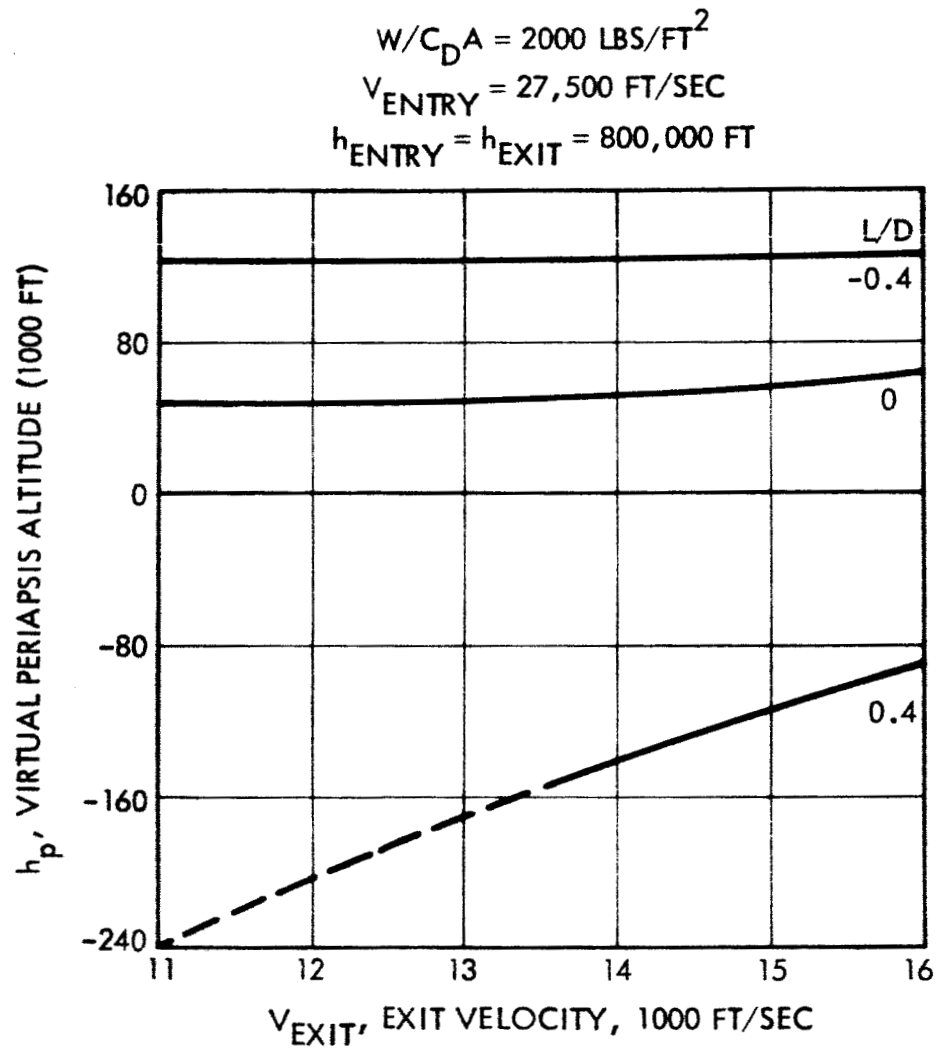


Figure 6.21 Virtual Periapsis Altitude Vs. Exit Velocity and L/D for NASA Model 2 Atmosphere

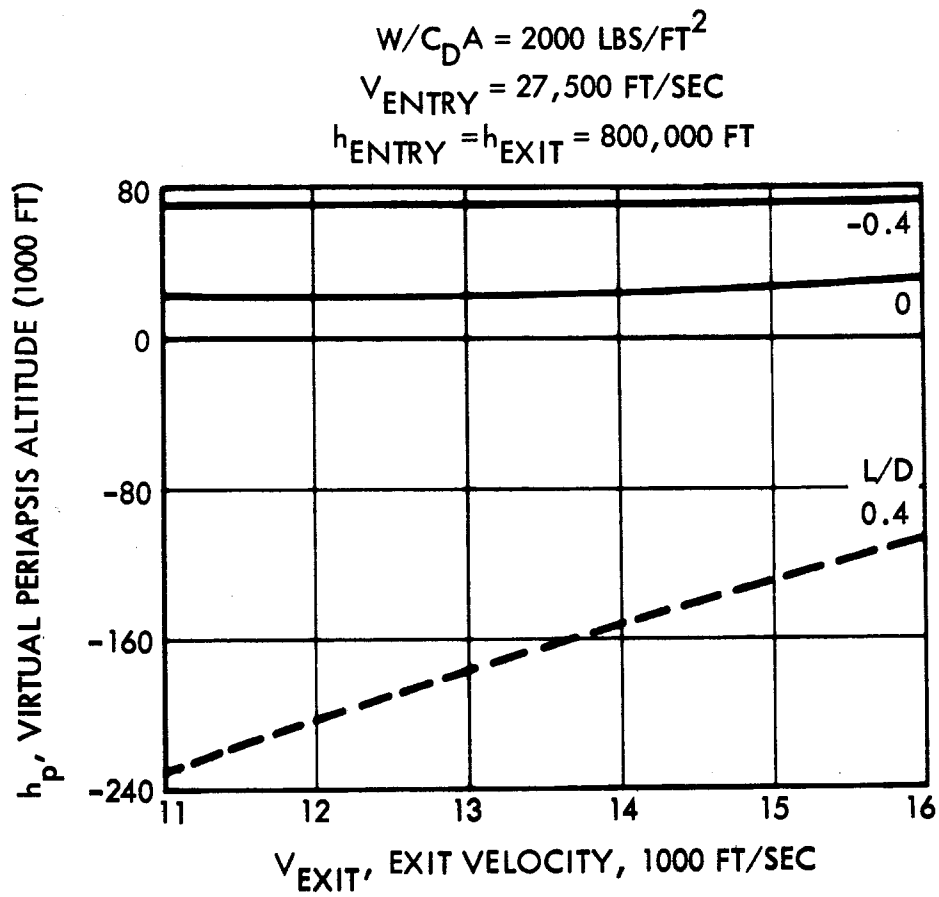


Figure 6.22 Virtual Periapsis Altitude Vs. Exit Velocity and L/D for NASA Model 3 Atmosphere

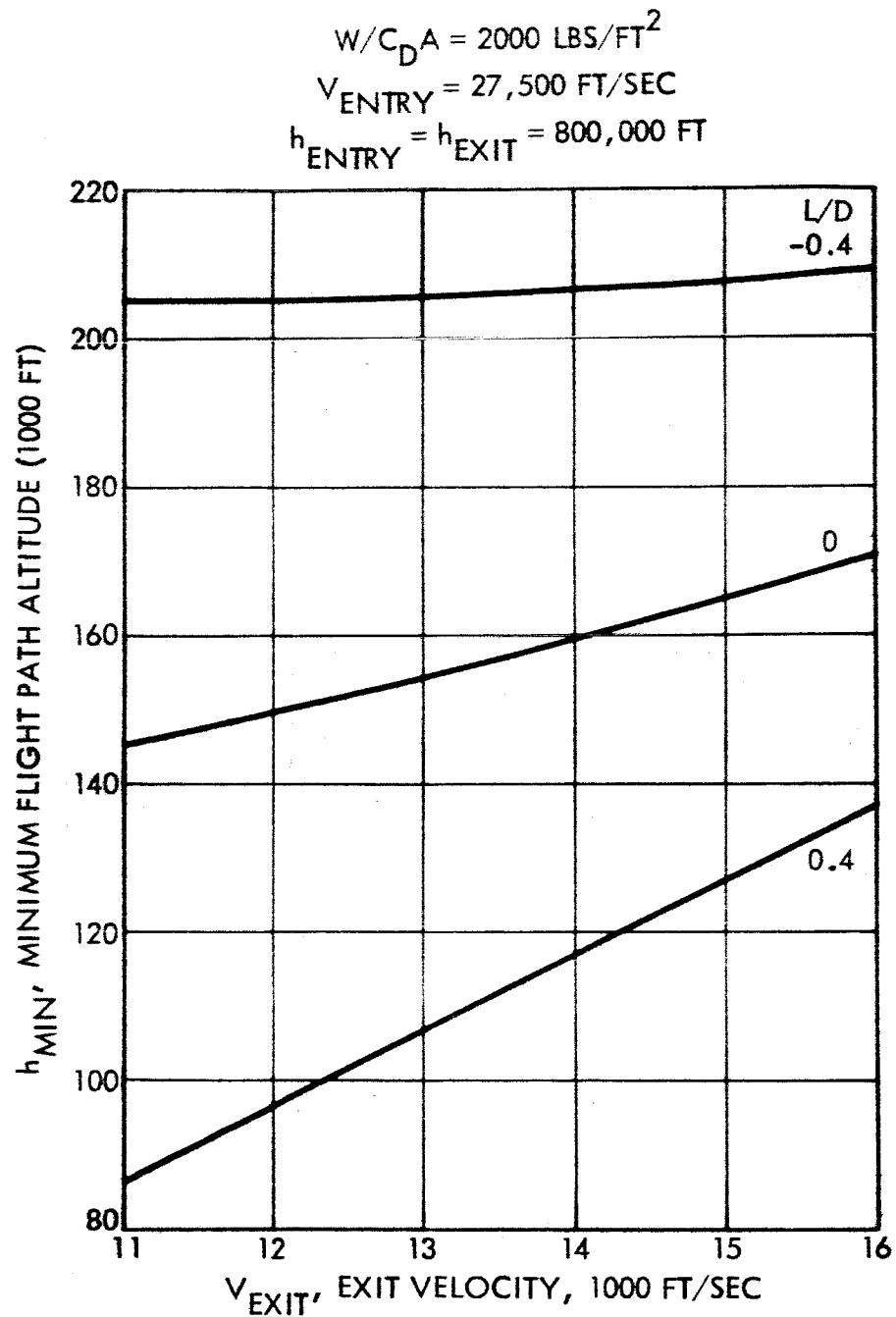


Figure 6.23 Minimum Flight Path Altitude Vs. Exit Velocity and L/D for Schilling Model II Upper Limit Atmosphere

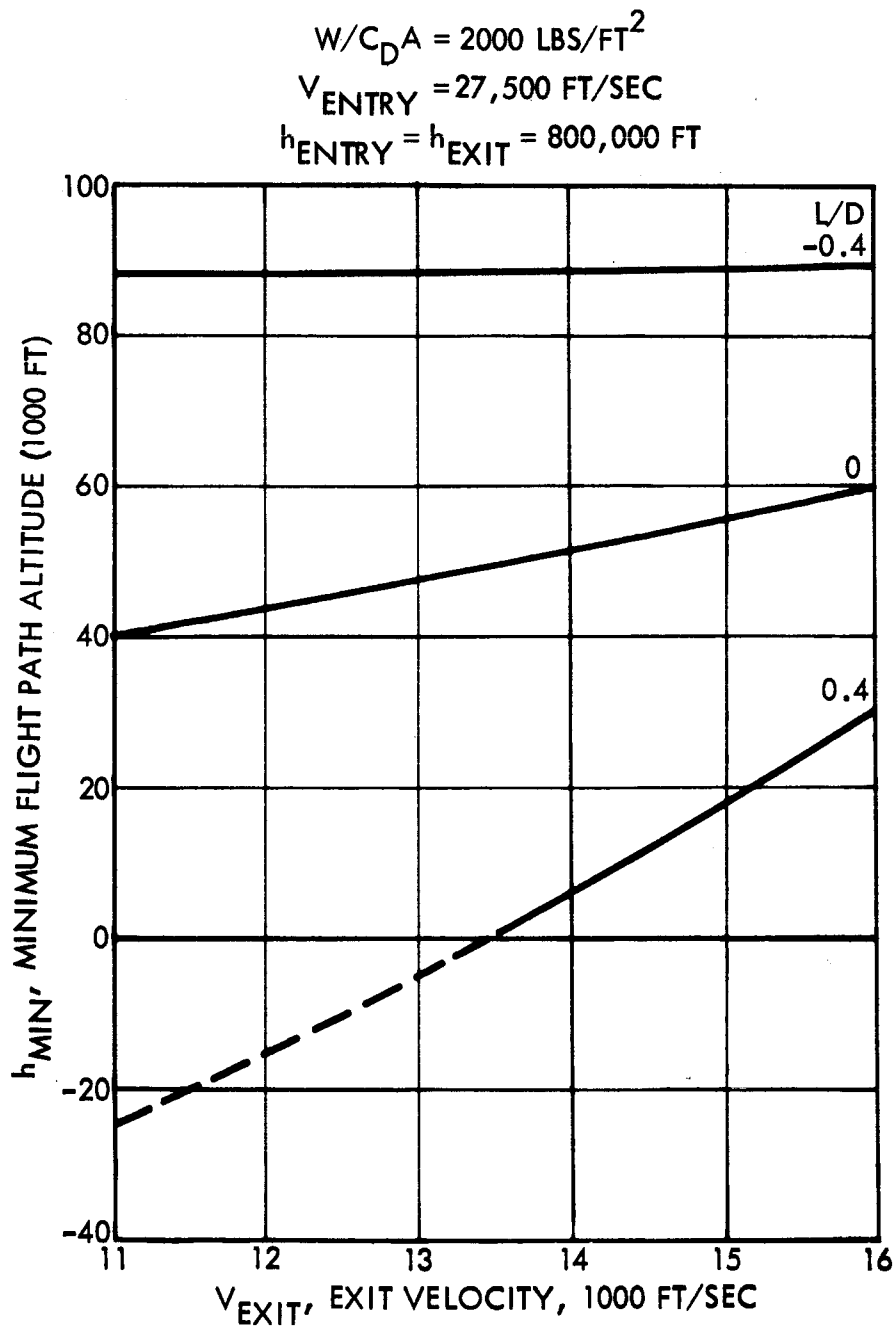


Figure 6.24 Minimum Flight Path Altitude Vs. Exit Velocity and L/D for NASA Model 2 Atmosphere

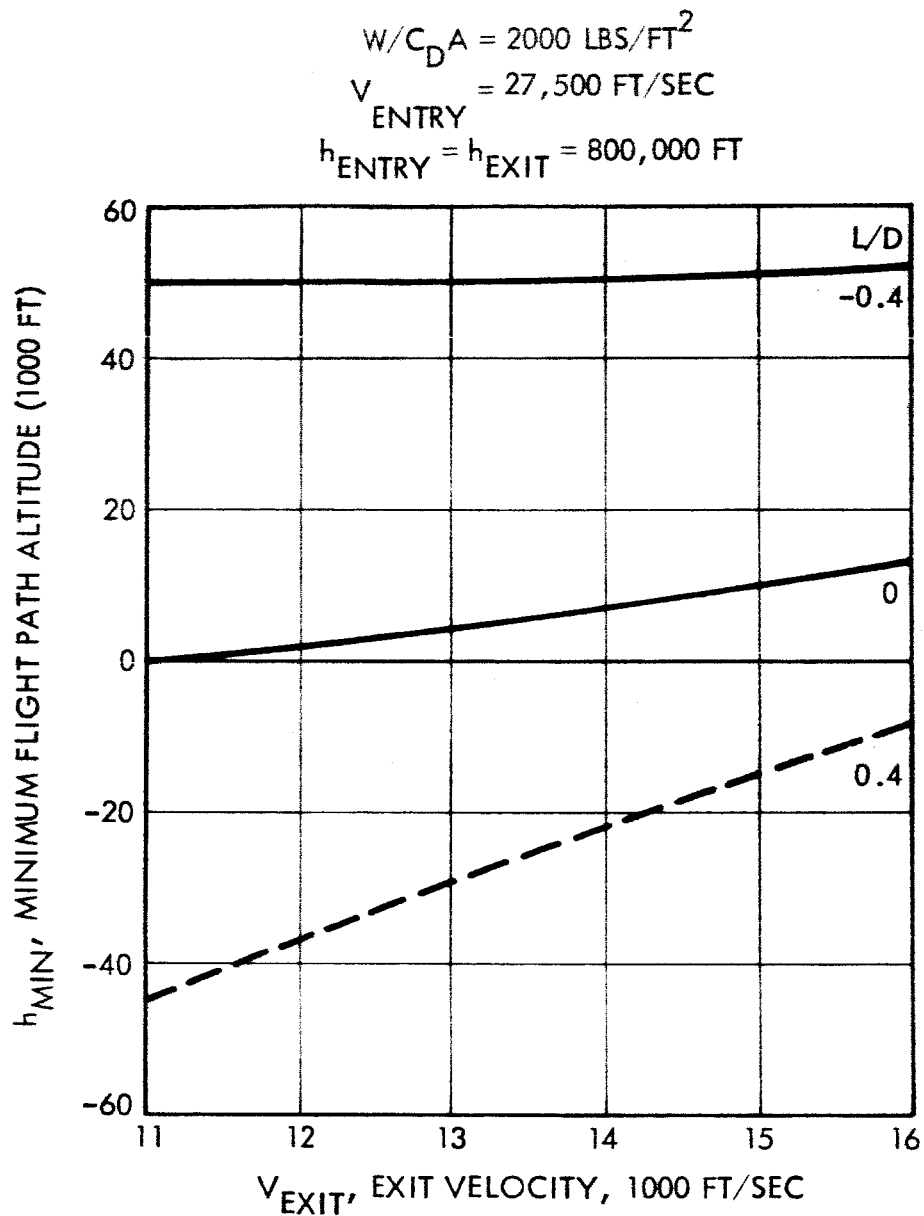


Figure 6.25 Minimum Flight Path Altitude Vs. Exit Velocity and L/D for NASA Model 3 Atmosphere

exit velocity. These curves were obtained by extrapolating the above results for $L/D = 0.3$ to an L/D of ± 0.4 and shifting down to a lower altitude to account for the higher $W/C_D A$. The portions of the curves shown as dashed lines represent trajectories which intersect the planet surface. Corridor depths for the three atmospheres are shown in Figure 6.26. It is seen that corridor depths for NASA Model 2 and 3 atmospheres are limited on the positive L/D side by a restriction on the minimum flight path altitude. In Figure 6.27 is shown the corridor depth for a vehicle braking in an atmosphere whose properties represent the worst combination of the Schilling Model II Upper Limit and the NASA Model 3 atmospheres.

As noted above, the corridor depths in several cases are limited by a minimum flight path altitude restriction. The effect of reducing the $W/C_D A$ is to increase the minimum flight path altitude. Thus, the corridor depths shown in Figure 6.27 would be increased by reducing $W/C_D A$. However, reducing $W/C_D A$ requires a reduction in vehicle weight or an increase in vehicle drag which increases the difficulty of obtaining a specified L/D .

Vehicle layouts were made to verify the L/D capability of the vehicle, and CG locations necessary to achieve the necessary trim angles. Spacecraft configurations satisfying these requirements are discussed in Section 6.5.

6.2 Summary of Corridor Capabilities

A summary of corridor capabilities is given in Table 6.1 for an exit velocity of 11,000 fps, which is applicable to braking into a low altitude circular orbit.

Estimates of allowances for rolling maneuvers have been calculated, assuming sensors capable of detecting 0.03 g deceleration levels, and 10 second rolling time. The effect on corridor performance was found to be negligible. Approximately 75 @ lbs of propellant are consumed by this maneuver; 4 roll engines with thrust levels of 1,000 lbs are required.

As noted in Section 4, the on-board navigation system is capable of steering to a 5.4 km (3σ) corridor with state-of-the-art sensor systems. A 6σ corridor would be 10.8 km. Uncertainties in the diurnal variation in the atmosphere have not been investigated, but require an additional 10

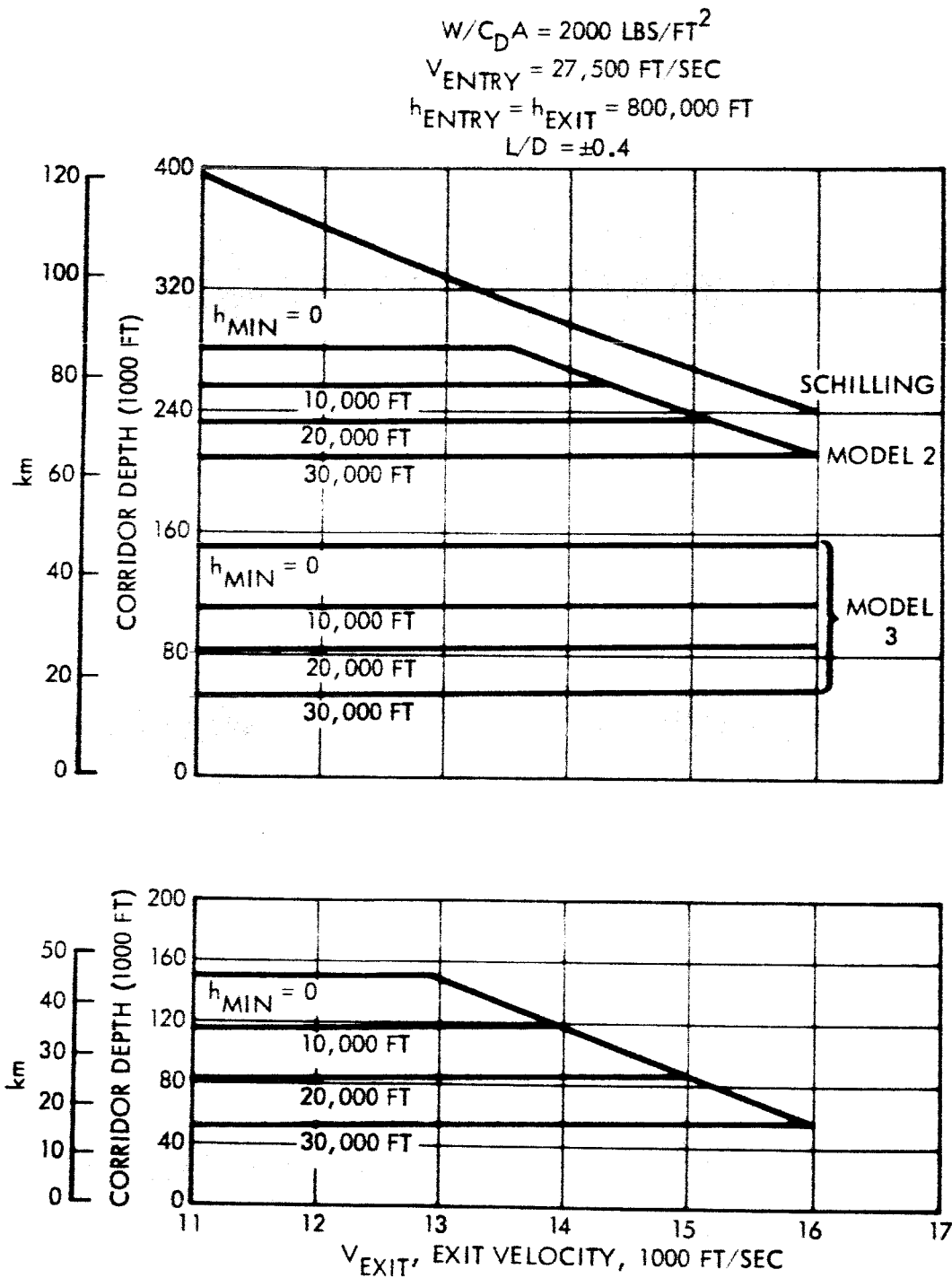


Figure 6.27 Corridor Depth Worst Combination of Atmospheres
Schilling Model II Upper Limit and NASA Model 3

TABLE 6.1 SUMMARY OF CORRIDOR PERFORMANCE (L/D = 0.3)

<u>Model</u>	<u>Uncertainty</u>	<u>Corridor (km)</u>
Schilling	None	87.2
2	None	74.5
3	None	66.0
2	10 percent uncertainty in scale height	69.2
2	10 percent uncertainty in density	71.8
2	10 percent uncertainty in scale height and density	66.4
2	Worst combination of Schilling and Model 3 scale heights	53.7
2	Worst combination of Schilling and Model 3 densities	49.4
Schilling -3	Worst combination of Schilling and Model 3 atmospheres	21.9
Schilling -3	Worst combination of Schilling and Model 3 atmospheres (L/D = 0.4)	46.4

to 20 km for entry into the earth's atmosphere at parabolic velocities. Similar allowances for Mars entry maneuvers should be adequate. Hence, total corridor requirements for 6 σ guidance requirements, diurnal variations in the atmosphere, and rolling maneuver allowances would increase the possible corridor uncertainty to about 30 km. This requirement could be accommodated by an aero entry system with $L/D = 0.3$ except for the gross uncertainty generated by the worst combination of Schilling upper limit and Model 3 atmospheres. More probable uncertainties do not pose as severe a limitation. A vehicle with $L/D = 0.4$ can accommodate the worst combination of atmosphere properties.

6.3 Heat Shield Analysis

The following section presents the results of analyses to determine heat shield weights for the Mars braking vehicle. Heat shield weights are calculated for three model atmospheres. A sketch showing the relevant dimensions of the vehicle is shown in Figure 6.28.

Radiant and Convective Heating

Radiant heat rates were obtained from charts contained in Reference 6.5 which is a study of radiation from a model planetary atmosphere composed of 15 percent CO_2 and 85 percent N_2 by volume. The effect of varying CO_2 concentration in a $CO_2 - N_2$ atmosphere and the effects of additions of argon were studied in the reference work, but the resultant changes in the radiation are not judged to be of a magnitude to warrant inclusion in the present study. The results of an absorption study are also reported in this reference, in which it was shown that for a similar braking trajectory approximately 50 percent of the radiation is absorbed by the radiating gas. This result was applied to the present study, so that the radiant heat rates were divided by the factor 2 in the heat shield design calculations.

It was inferred from results presented in Reference 6.6, a study concerning entry in air, that the equilibrium radiant heating distribution over the body, normalized relative to the value at the stagnation point, is approximated by the distribution of the square of the normalized pressure.

NOSE RADIUS = 50.8 IN.
 FORWARD CYLINDER RADIUS = 130 IN.
 BASE RADIUS = 198 IN.

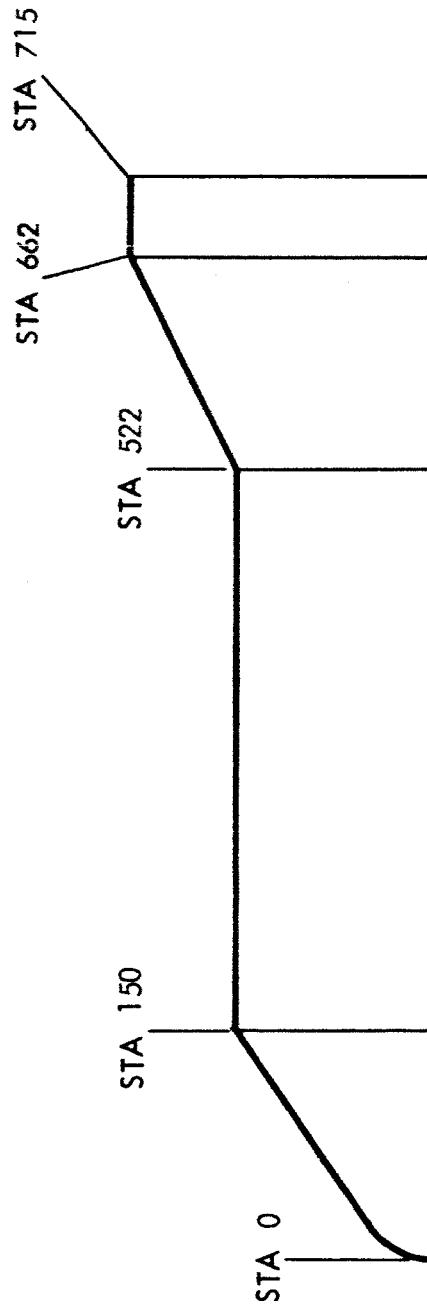


Figure 6.28 Basic Dimensions of Mars Braking Vehicle

This pressure scaling was used in determining the radiant heating distribution around the surface of the nose and forecone sections of the braking vehicle. Since the scope of the study did not permit the determination of the actual flow field around the braking vehicle the pressure scaling represents a reasonable assumption that could be made under the circumstances.

The convective heating on the braking vehicle was determined with the STL Aerodynamic Heating Program (Reference 6.7), which is based on air. However, considering the conclusions of Hoshizaki (Reference 6.8) that the convective heating for CO_2 is close to that for air and considering the fact that the transport properties of nitrogen are close to those of air, the computed results should be sufficiently accurate for this analysis. The heat rates were written on magnetic tape and transferred as input to the Ablation-Conduction Program (Reference 6.9) from which the thermal response was obtained. The heat rates are computed at a number of wall temperatures in the range of temperatures from the initial ambient temperature to the maximum expected surface temperature.

Convective and radiant heating rates at the stagnation point, as well as the corresponding trajectories, are shown in Figures 6.29 through 6.31 for the three model atmospheres. The trajectories correspond to an entry velocity of 27,500 fps, a ballistic coefficient of 765 lb/ft^2 , and lift-to-drag ratio (L/D) of -0.1 . This is on the overshoot side of the corridor where the convective heat pulse is greater and the necessary heat soak time longer, thereby giving the greater weight when compared to the undershoot side with $L/D = +0.1$.

Heat Protection Design

The heat shield material chosen for this study was phenolic nylon, because of its low thermal conductivity, low density, and a relatively high specific heat which are desirable properties for this application. It should not be inferred, however, that phenolic nylon is recommended as the heat shield and insulation material. At the present time the performance of most candidate materials has not been determined for this mission.

An effective heat of ablation of 4,000 Btu/lb was assumed. To keep the backface temperature below 500°F , rather large heat shield thicknesses would be required unless the heat shield is jettisoned before the heat in the

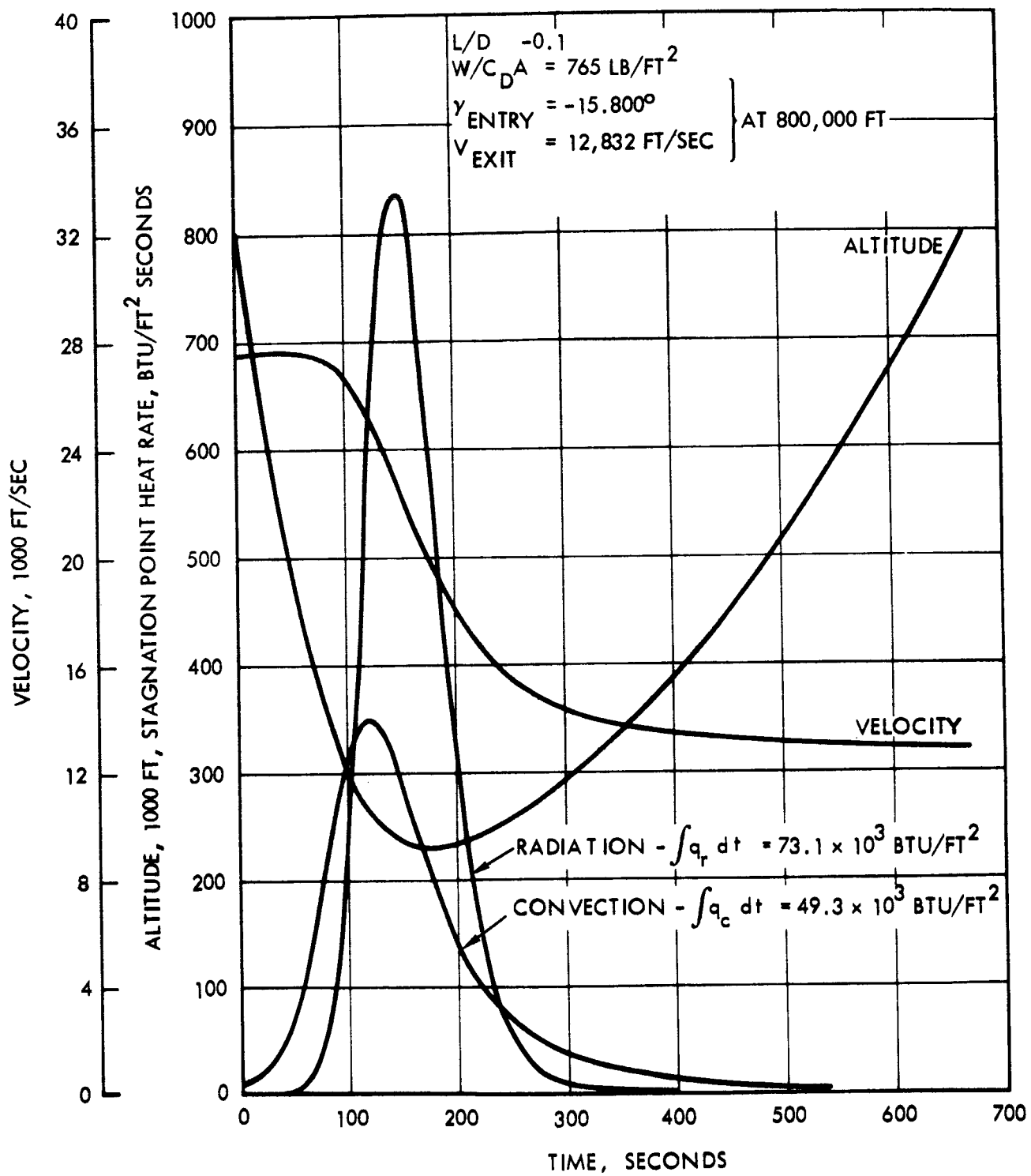


Figure 6.29 Stagnation Point Heat Rates for Schilling Model Atmosphere

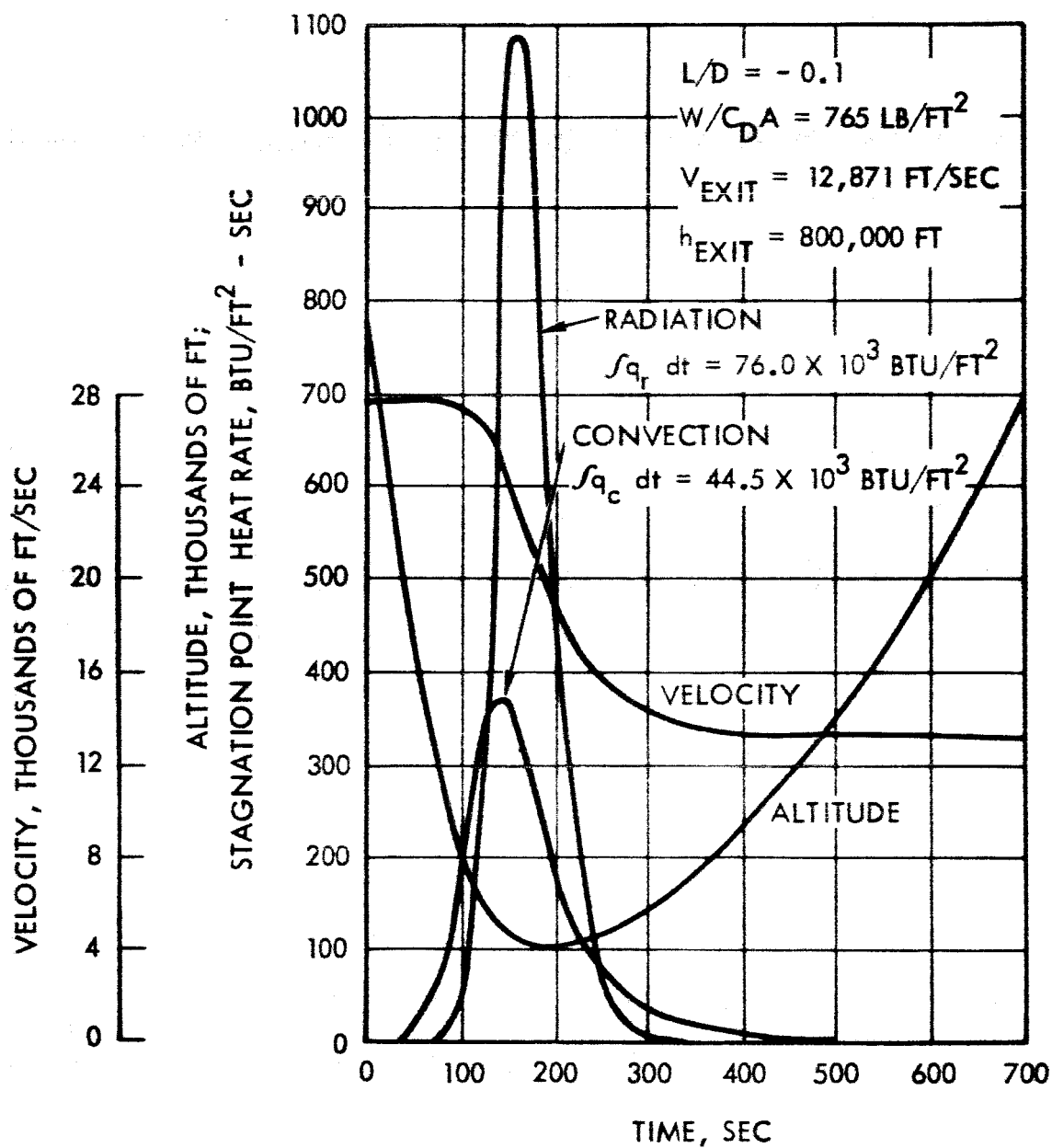


Figure 6.30 Stagnation Point Heat Rates for Model 2 Atmosphere

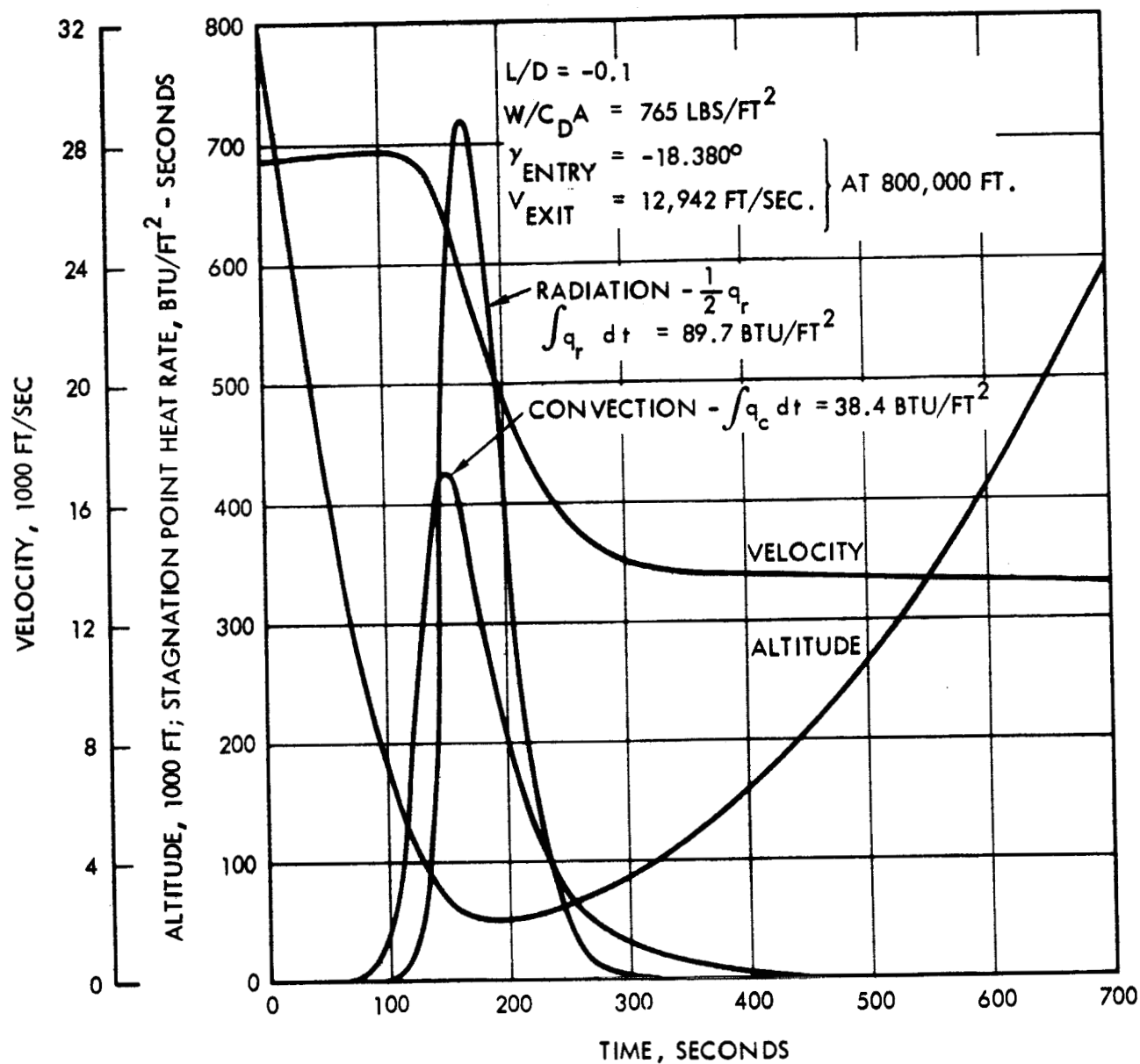


Figure 6.31 Stagnation Point Heat Rates for Model No. 3 Atmosphere

insulation soaks through to the backface. A jettison concept was selected for this reason. From the thermal standpoint it would be desirable to jettison near the end of the heat pulse at a time of approximately 300 seconds. However, this operation must be performed when the vehicle is well out of the Martian atmosphere, hence, a jettison time corresponding to 0.5 lb/ft^2 free stream dynamic pressure was selected. The required thicknesses of phenolic nylon to maintain the backface temperature at or below 500°F at the jettison time and design summaries are shown in Table 6.2. In the case of the spherical nose and the forecone, the thicknesses include the ablated heat shield and 0.6 inches of insulation. No ablation is predicted for the two cylindrical portions of the vehicle and for the flare.

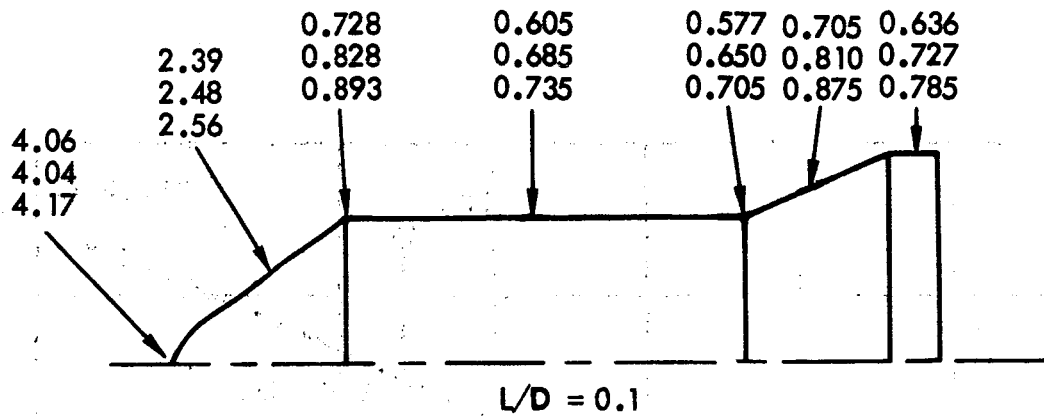
The total heat shield weight was plotted as a function of the atmosphere scale height in Figure 6.32 for $L/D = -0.1$. The scale height directly affects the heat soak time which is the most influential factor in these heat shield calculations. Since the jettison time corresponds to a specified dynamic pressure and the exit velocities are approximately equal, the three jettison times occur at roughly the same atmospheric density; however, it takes more time to travel to this given density in an atmosphere having a large scale height.

Calculations also were made for a lift-to-drag ratio of -0.3 for the Model 2 atmosphere. For this L/D the heat soak time is increased considerably and the total heat shield weight is 30,880 lbs which is 7 percent greater than that obtained for the L/D of -0.1 . The surface pressure corresponding to a given scale height does not appreciably affect the heat shield design, although it is recognized that the surface pressure and scale height of a planetary atmosphere are closely related.

No attempt was made to establish a mathematical relationship for the heat shield weight as a function of scale height or heat soak time. A number of pertinent factors, all of which have a definite bearing on the heat shield weight, are listed in Table 6.3. In this tabulation heating rates and integrals are shown for the stagnation point and STA 360 which is a representative station along the side of the vehicle. The increases in total convective heating and heat soak time with increasing scale height are the dominant factors, and more than compensate for the decreasing total radiant heating and maximum surface temperatures.

TABLE 6.2 HEAT SHIELD WEIGHTS

SHIELD THICKNESS (INCHES)



	Schilling Upper Limit (132 mb)	Model 2 (25 mb)	Model 3 (10 mb)
<u>Insulation Weight</u>			
Nose and Cone	2,350 lb	2,350 lb	2,350 lb
First Cylinder	9,700	9,010	7,950
Flare	5,840	5,410	4,700
Second Cylinder	2,160	1,990	1,750
Aft Closure	<u>2,560</u>	<u>2,560</u>	<u>2,560</u>
TOTAL INSULATION	22,610 lb	21,320 lb	19,310 lb
<u>Ablated Heat Shield Weight</u>			
Nose and Cone	<u>7,880</u>	<u>7,560</u>	<u>7,150</u>
TOTAL HEAT SHIELD WEIGHT	30,490 lb	28,880 lb	26,460 lb

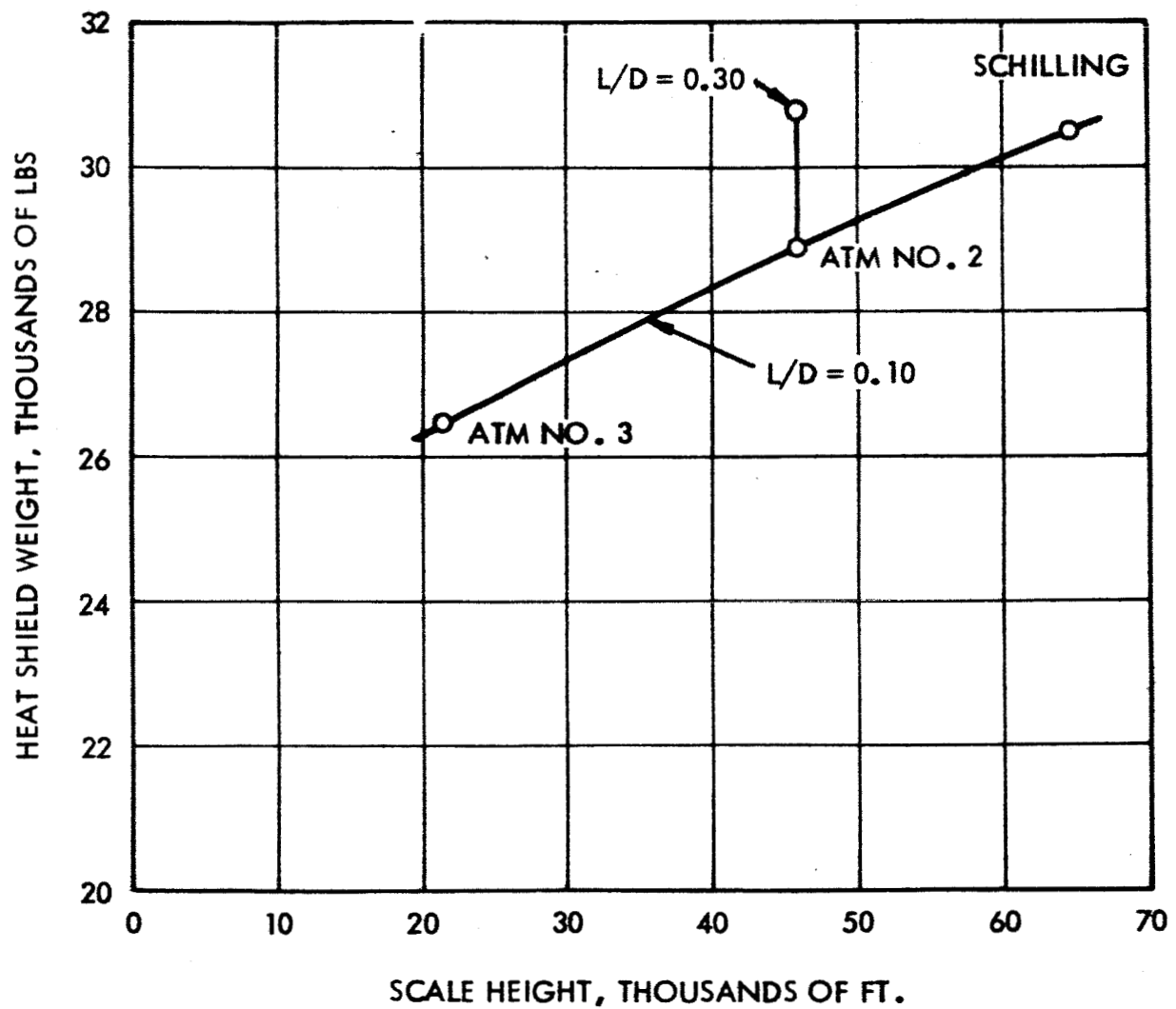


Figure 6.32 Spacecraft Heat Shield Weight vs Scale Height

TABLE 6.3

COMPARISON OF HEATING FOR THREE ATMOSPHERES (L/D = -0.1)

	Schilling Atmosphere	Atmosphere No. 2	Atmosphere No. 3
Stag. Pt Total Convective Heating (Btu/ft ²)	49,300	44,500	38,400
Stag. Pt Total Radiant Heating (Btu/ft ²)	73,100	76,000	89,700
STA 360-Total Convective Heating (Btu/ft ²)	4,010	3,730	3,480
STA 360-Max. Heat Rates (Btu/ft ² - sec)	31.2	33.7	41.0
STA 360-Time at Max Heat Rate (sec)	130	150	160
Time at Heat Shield Jettison (sec)	630	570	464
STA 360-Difference Between Time at Max. Heat and Time at Heat Shield (sec)	500	420	304
STA 360-Max. Surface Temperature (°F)	2,564	2,618	2,760
Vehicle Heat Shield Weight (lb)	30,490	28,880	26,460

6.4 Effect of Corridor Performance on Vehicle Weight

The aero entry system shown in Figure 4.1 is capable of generating lift-to-drag ratios up to about 0.3 to 0.4. In view of the moderate increase in heat protection weight required to accommodate the higher L/D ratios, the vehicle should be given this added protection to provide for uncertainties in corridor requirements.

It is possible, however, to develop a trade-off between aero entry system weight and corridor requirements through the implied change in lift-to-drag ratio. For example, assume that a given corridor width is required, corresponding to a nominal L/D. Uncertainties in the atmosphere will require a higher L/D, which in turn requires added heat protection. Thus, the uncertainties in the atmosphere can lead to added entry system weight. This trade-off is shown in Figure 6.33 for the case of a 10 percent uncertainty in atmosphere density and scale height. The effect on entry system weight is less than 500 lbs. If gross uncertainties in atmosphere properties are considered, such as going from the extremes of the Schilling upper limit to the Model 3 atmospheres, the increase in entry system weight would be approximately 4,000 lbs (assuming an $L/D = 0.3$).

6.5 Vehicle Configuration

An axially symmetric vehicle (without control surfaces) can be trimmed to a non-zero L/D only by a laterally displaced center of gravity. However, vehicle asymmetries can also be employed to vary the trim attitude and L/D. A symmetric vehicle with a laterally offset center of gravity has been selected for this study due to the simplicity of its trim mechanism and its amenability to analysis.

The vehicle center of gravity must be located such that the required lift-to-drag ratio is obtained at trim (see Figure 6.34). The L/D requirement determines the angle between the resultant aerodynamic force vector and the vehicle velocity vector, $\beta = \tan^{-1} L/D$. Since at trim condition the moment about the center of gravity must be zero, the center of gravity must lie along the resultant force. The vehicle attitude relative to the velocity vector for a

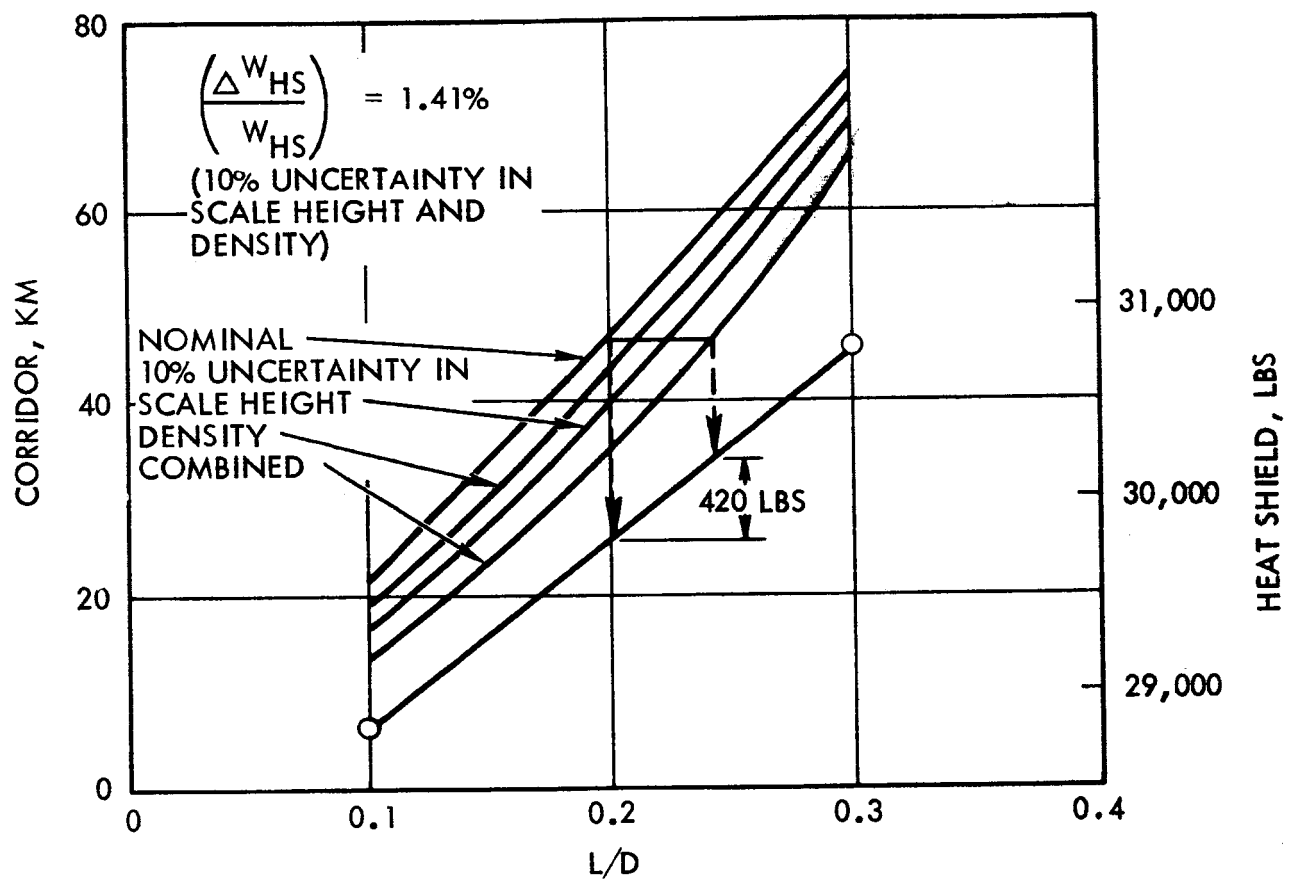


Figure 6.33 Aero Entry System Sensitivity

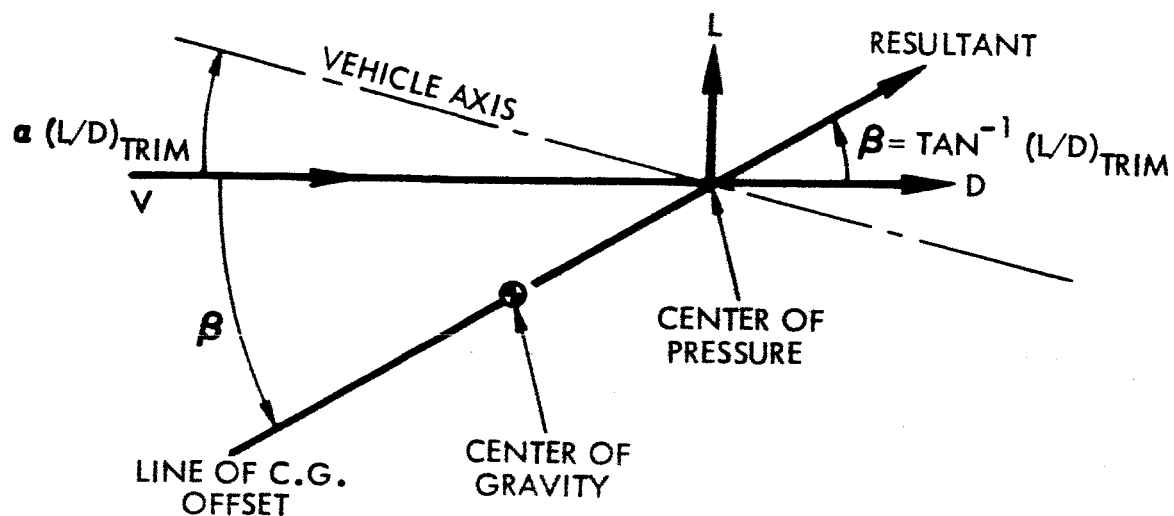


Figure 6.34 Trim with Center of Gravity Offset

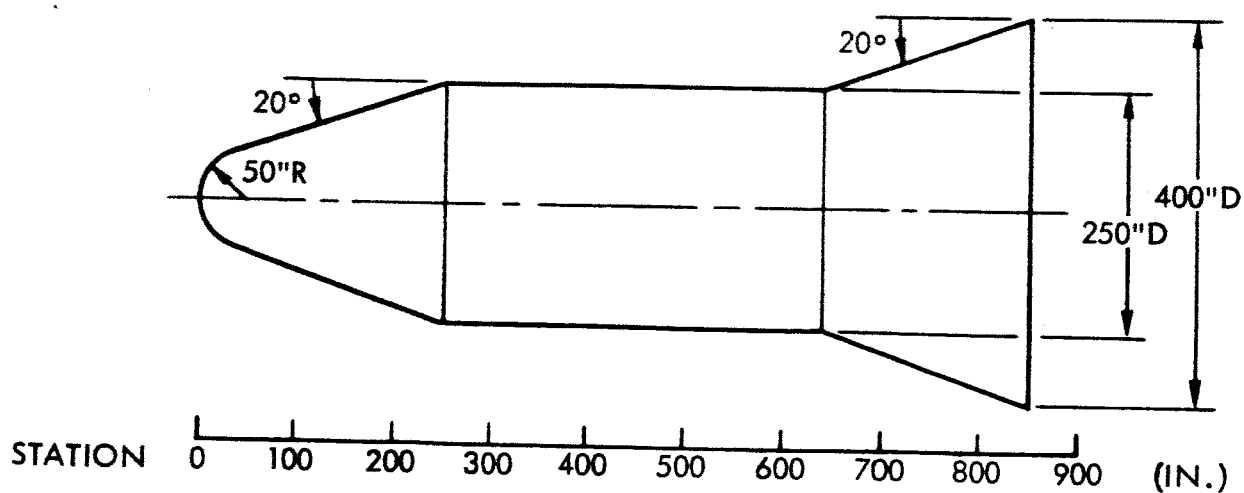


Figure 6.35 Vehicle Configuration

given L/D is determined by the vehicle geometry alone. The angle between the line joining the center of pressure and center of gravity, and the vehicle axis is the sum of the required trim angle of attack and the $\tan^{-1} L/D$. Thus, vehicle geometry and L/D requirement determine the line of the center of gravity offset. The center of gravity must be so placed along this line that sufficient aerodynamic stability is guaranteed.

A preliminary analysis of the configuration shown in Figure PD 51-29A, page 9-5 of Reference 1.1, indicated that an L/D capability of 0.4 would be difficult to achieve. Thus, in order to provide a higher L/D capability, a configuration somewhat more slender than the one cited above has been examined. This configuration is shown in Figure 6.35.

A preliminary aerodynamic analysis of the vehicle shown in Figure 6.35 has been performed. Since the vehicle encounters Mach numbers greater than 10 in the braking maneuver, only the hypersonic aerodynamic properties have been estimated. The aerodynamic properties are shown in Figures 6.36 and 6.37. It is seen that a lift-to-drag ratio of 0.4 is obtained for an angle of attack at 6° . The angle of the center-of-gravity offset line is then:

$$\gamma = \alpha + \beta = \alpha + \tan^{-1} L/D = 6^\circ + \tan^{-1} (0.4) = 28^\circ$$

The center of pressure is shown to be approximately 500 inches aft of the nose. A center of gravity position to trim the vehicle to an L/D of 0.4 with a static margin of approximately 8% is shown in Figure 6.38. At an L/D of 0.4, the drag coefficient is 0.69 and the ballistic coefficient for a vehicle weight of 470,000 lbs. is:

$$W/C_D A = 2000 \text{ lbs/ft}^2$$

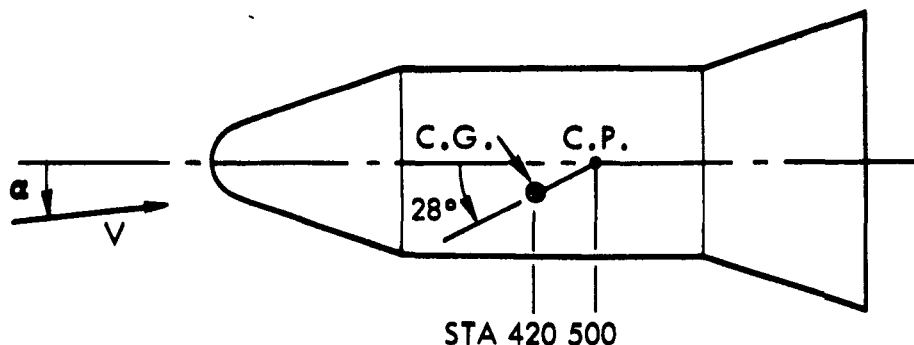


Figure 6.38 Center of Gravity Position for $(L/D)_{Trim} = 0.4$

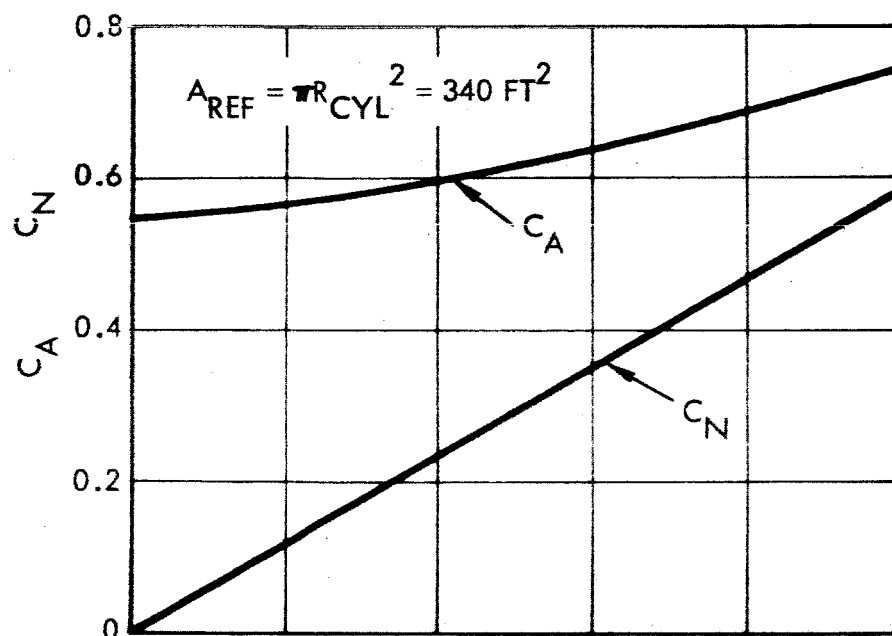


Figure 6.36 Axial and Normal Force Coefficients Versus Angle of Attack

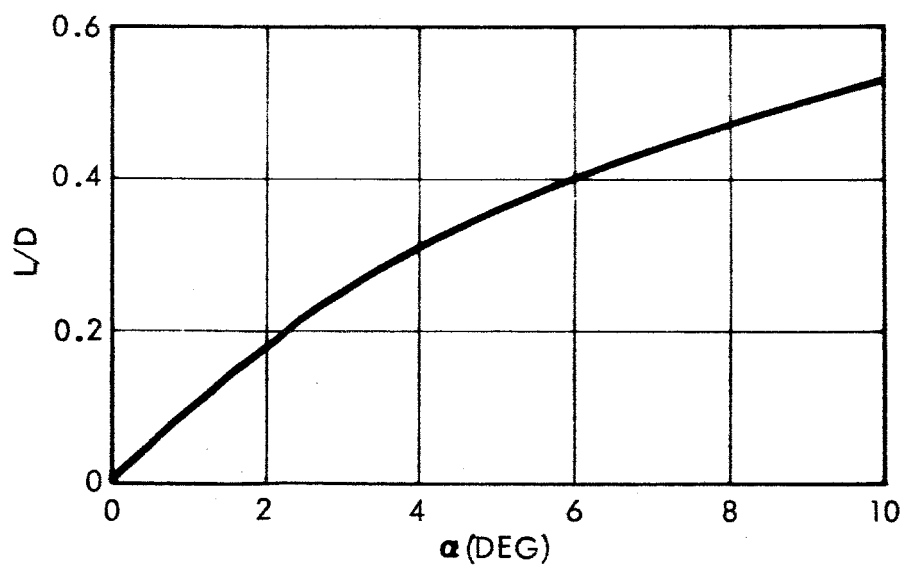
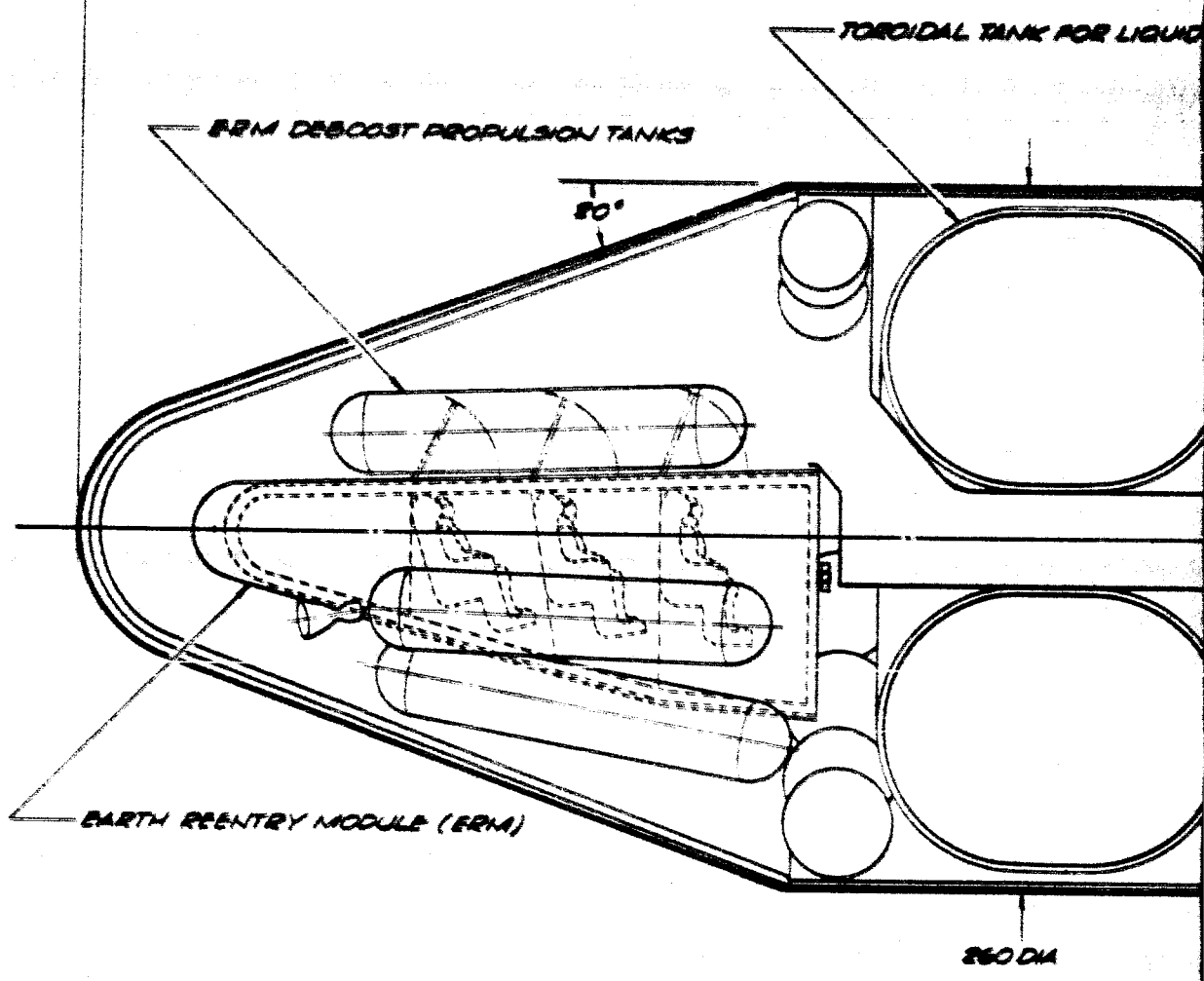


Figure 6.37 Lift-to-Drag Ratio Versus Angle of Attack

Vehicle arrangements that meet the required center of gravity locations are shown in PD 51-36 and -37. In PD 51-36, the fluorine propellant has been shifted forward to a position immediately aft of the nose section, which houses the Earth return module. The fluorine, which is contained in a toroidal tank, is relatively dense, and, because it comprises 58 percent of the total vehicle mass at entry into the Mars atmosphere, causes the center of gravity to shift relatively far forward in the vehicle. The hydrogen is stored in a toroidal tank in the flare of the vehicle. The fluorine must be pumped aft about 36 feet to the propulsion units. Since the fluorine tanks cannot be jettisoned after use, the volume used by the propellant could be converted for crew use after the departure from Mars. About 400 cu ft additional volume could be obtained in this manner for the long-duration voyage home (about 8 months).

A second vehicle arrangement that meets the center of gravity requirements is shown in PD 51-37. Both propellants have been moved to the forward section of the spacecraft, providing a very stable configuration for aerodynamic entry. The earth entry vehicle has been moved into the skirt portion of the vehicle, which serves as a hangar for the Mars excursion module as well. Flare volume utilization is not as efficient in this version, although nose section volume utilization is maximized. Center of gravity location is well forward in the version (Station 400).

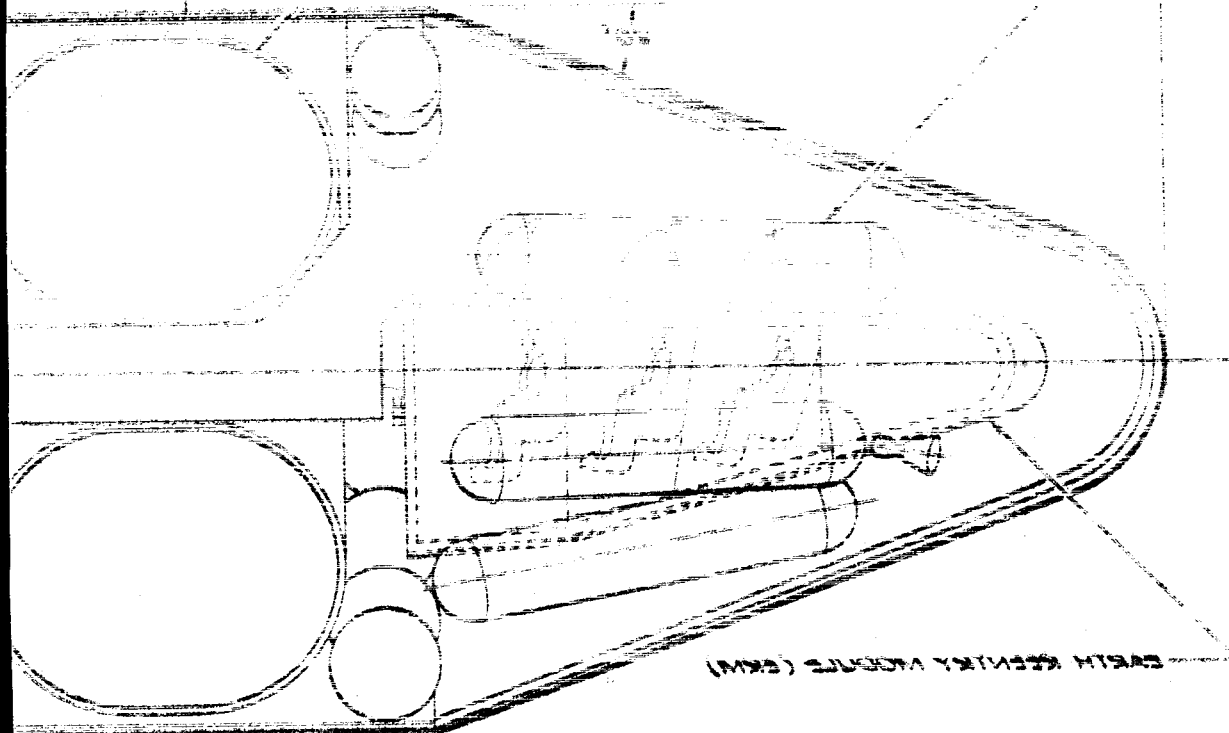
It is apparent from these layouts that difficulties may be experienced with hydrogen-nuclear versions using aero braking at Mars.



100

LONGITUDINAL TANK FOR LIQUID

LONGITUDINAL TANK FOR LIQUID

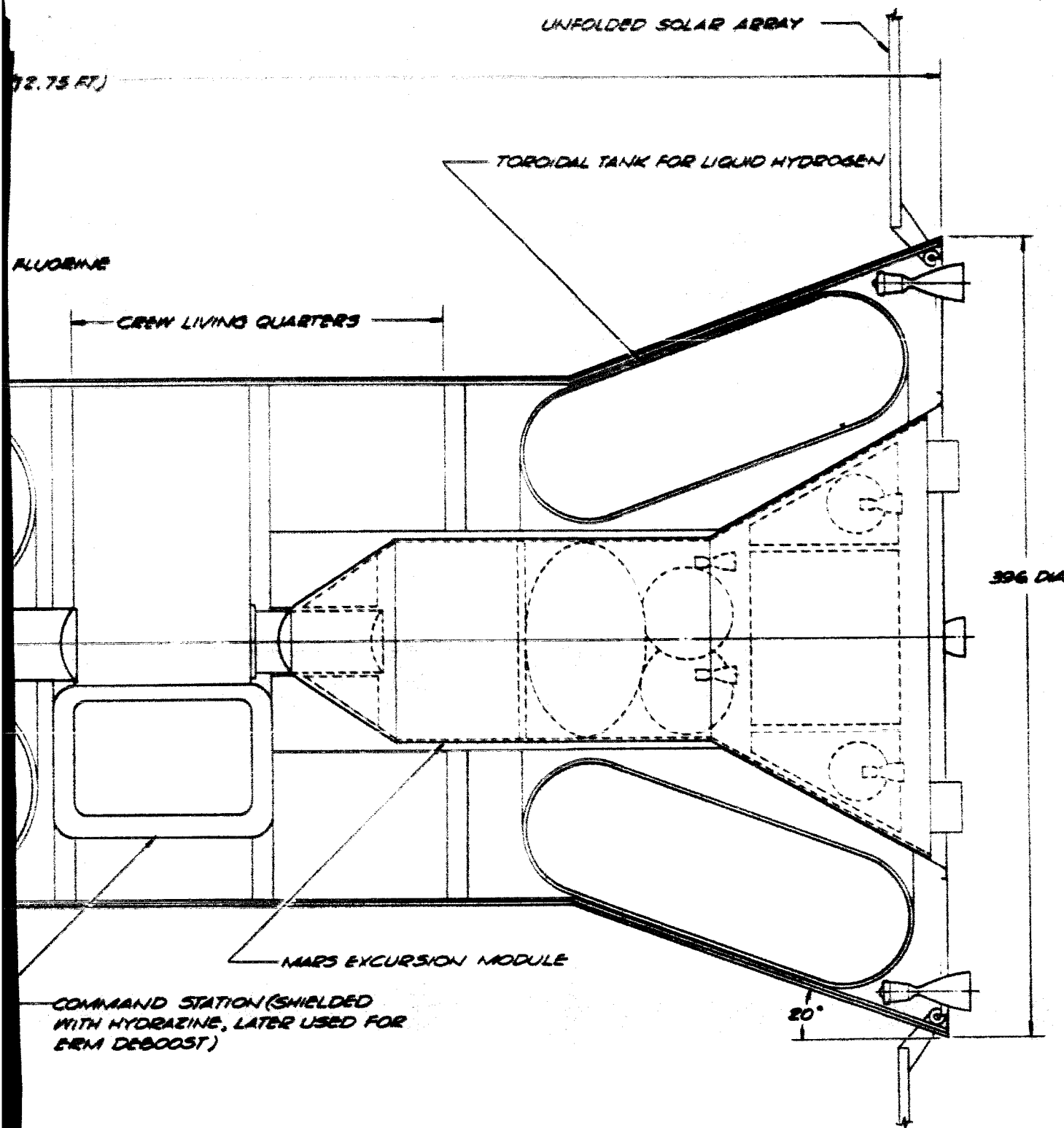


LONGITUDINAL TANK FOR LIQUID

100

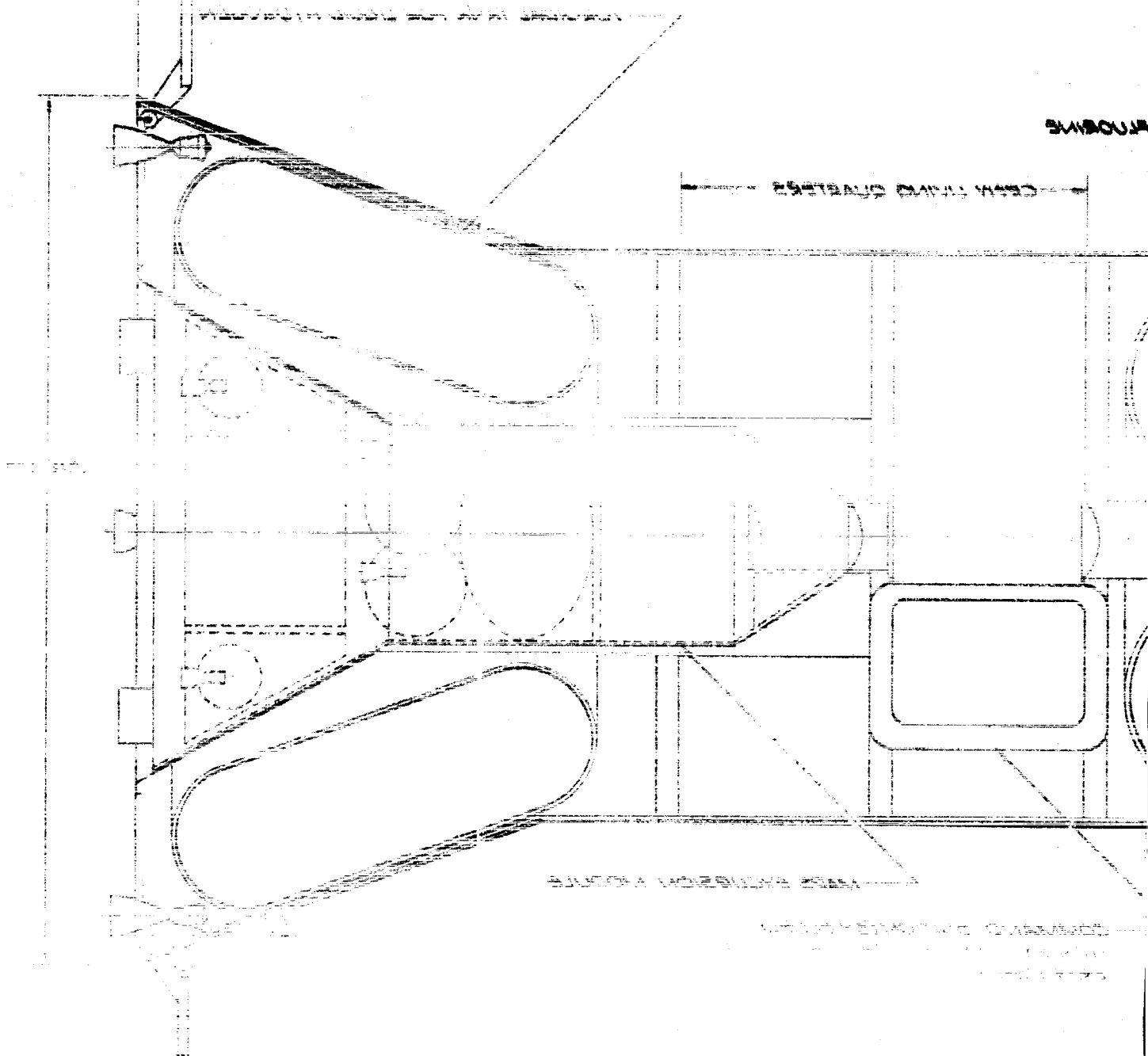
100

2



50 100 150 200
SCALE IN INCHES

TRW SPACE TECHNOLOGY LABORATORIES	
ONE SPACE PARK • REDONDO BEACH, CALIFORNIA	
GENERAL ARRANGEMENT - MANNED MARS SPACECRAFT WITH TOROIDAL PROPELLANT TANKS	JUNE 11, 1965
	PD51-36



Technical drawing of a mechanical assembly, likely a pump or engine component, showing a cross-section or plan view. The drawing includes a central vertical shaft with a large, rounded, bulbous section in the middle. To the right of the shaft is a rectangular component, possibly a valve or a housing. The drawing is annotated with various labels and dimensions:

Top left: "PUMP BODY" (mirrored text)

Top right: "PUMP BODY" (mirrored text)

Center right: "PUMP BODY" (mirrored text)

Bottom right: "PUMP BODY" (mirrored text)

Bottom center: "PUMP BODY" (mirrored text)

Bottom left: "PUMP BODY" (mirrored text)

Left side: "PUMP BODY" (mirrored text)

Right side: "PUMP BODY" (mirrored text)

Top: "PUMP BODY" (mirrored text)

Bottom: "PUMP BODY" (mirrored text)

LIQUID FLUORINE TANK

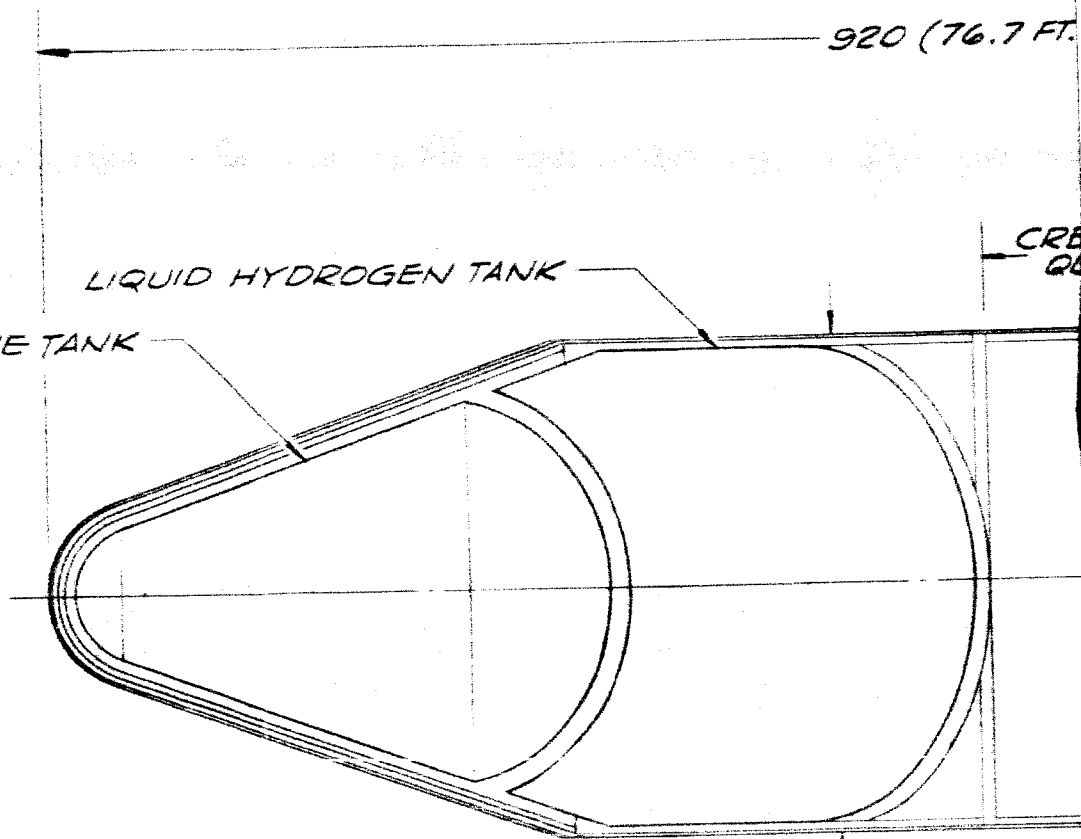
LIQUID HYDROGEN TANK

920 (76.7 FT.)

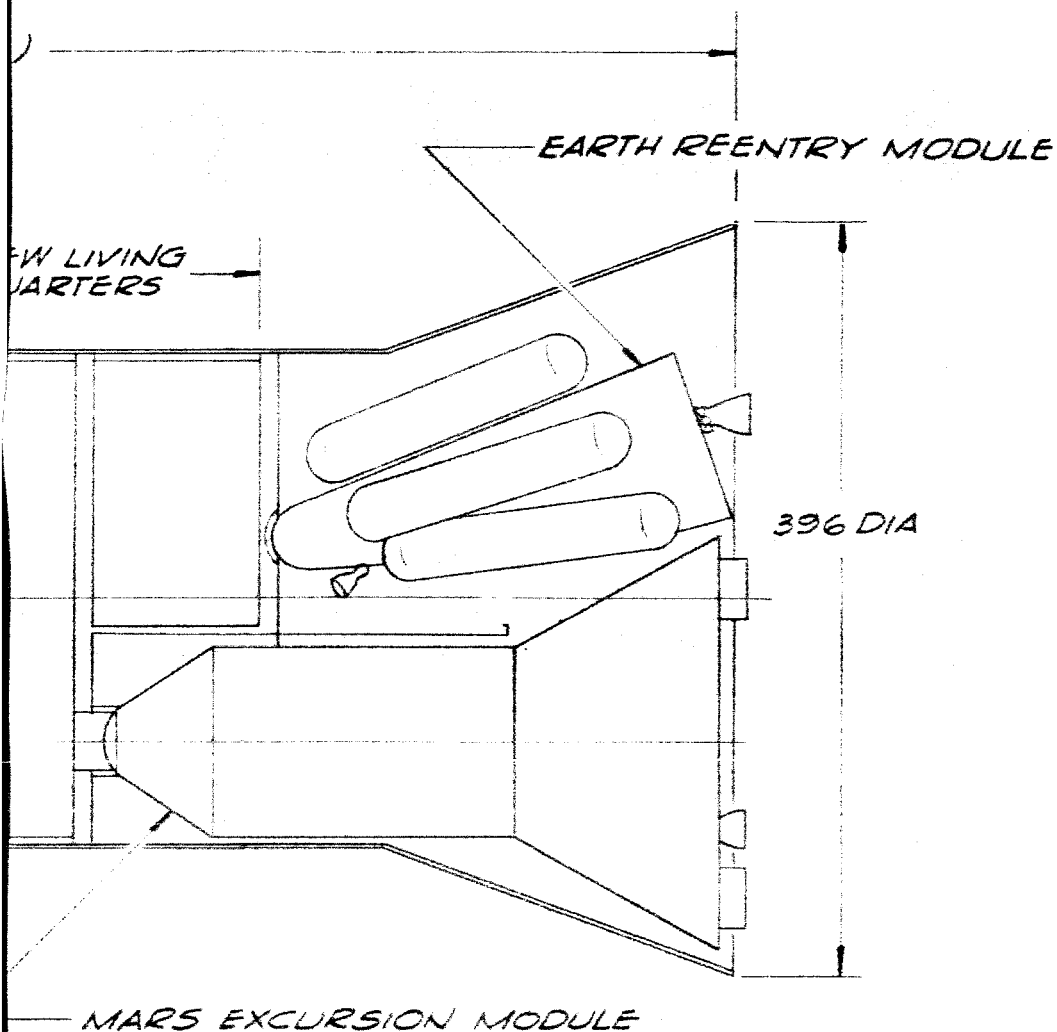
CRB
QB

260 DIA

0



2



100 200 300
SCALE IN INCHES

TRW SPACE TECHNOLOGY LABORATORIES

ONE SPACE PARK • REDDING BEACH, CALIFORNIA

GENERAL ARRANGEMENT -
MANNED MARS SPACECRAFT
WITH PROP. TANKS FORWARD

JUNE 14, 1965

PD51-37

7. MARS LANDER SYSTEM ANALYSIS

The Mars excursion module described in Section 4 is designed to effect a landing on the surface by aerodynamic deceleration to subsonic velocities, followed by parachute descent to the near surface, and retro hover and descent to the surface proper. Return to orbit is accomplished by jettisoning unessential portions of the module and launching the return craft into orbit by means of a hydrogen-fluorine propulsion system. All phases of this operation are affected by uncertainties in the Martian environment, as indicated in the table below:

Phase	Environmental Factor
<u>Descent</u>	
1. Parachute deployment altitude	Density
2. Sink velocity	Density
3. Drift	Winds and wind gradients
4. Visibility for site selection	Dust clouds
5. Retro touchdown	Density, winds
6. Impact absorption	Slope, soil friction, drift due to winds, obstacles
<u>Surface Operations</u>	
7. Thermal protection on surface	Temperature, density, dust
8. Radiation protection	Density
9. Communications and electrical equipment operation	Surface ionization
<u>Ascent</u>	
10. Orbital altitude	Density, scale height
11. Velocity losses	Density, scale height
12. Launch operations	Winds, dust

Not all of the above factors can be treated analytically, although most are amenable to quantification. In many cases it is difficult if not impossible to assign meaningful upper and lower limits on the environmental factors. In such cases, parametric variations were developed to indicate the sensitivity of the design to the environmental factor, and comments made as to possible seriousness of the uncertainties.

Each phase of the operation is discussed in the following sections.

7.1 Descent Phase

The landing system envisioned in this study provides for a drogue parachute for initial deceleration after re-entry followed by a cluster of three main recovery parachutes to reduce the velocity of the Mars excursion module (MEM) to an equilibrium descent velocity. This velocity is then reduced to zero at the surface of Mars through the use of retrograde rockets. This combination is the best approach concomitant with minimum total weight for the system. Crushable material pads on the landing struts provide impact energy absorption for a final touchdown after rocket shutdown. To nullify the effects of wind, an additional rocket can be mounted perpendicular to the MEM vertical. Both rocket engines should be throttleable to effectively match descent and translational velocities.

Provision can be made for the parachute cluster to glide, enabling (with descent and translational rockets) the MEM to home on a chosen landing site. Navigation, drift and altitude sensing instrumentation and displays are a necessary adjunct to gliding descent for landing site choice and "terrain" avoidance.

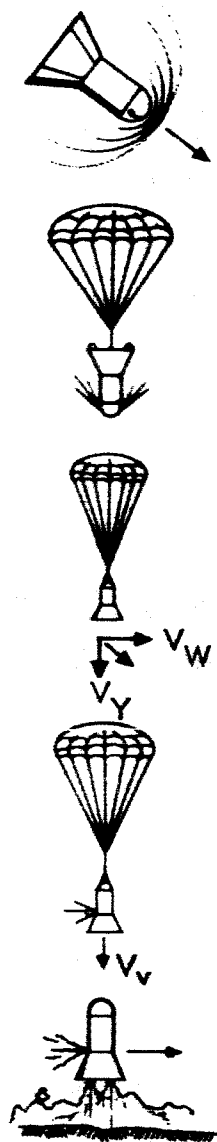
The parachute sizing analyses were carried out for the three atmospheres cited in Section 3: Schilling upper limit (132 mb), Model 2 (25 mb) and Model 3 (10 mb).

Parachute System

The parachute system design is based on a MEM gross weight of 50,000 pounds. The deceleration sequence is as follows (see Figure 7.1):

1. Atmospheric entry - initial deceleration accomplished by aerodynamic drag of the MEM.
2. Mach 2.5 Deploy a single FIST ribbon drogue parachute to stabilize and achieve initial parachute deceleration.
3. Mach 1.2 Deploy a cluster of three solid canopy main recovery parachutes in reefed condition.
4. Mach 0.8 Disreef main recovery parachutes.
5. Decelerate to equilibrium speed.
6. Fire translation rockets at 10,000 ft altitude in conjunction with parachute gliding and turning maneuvers to nullify the effects of drift.
7. Fire descent retro rockets to achieve zero vertical velocity at the Martian surface.

Figures 7.2, 7.3, and 7.4 present main recovery parachute nominal diameter as a function of equilibrium velocity at the martian surface for all three atmospheres



- AERO BRAKING FROM ORBIT

- PARACHUTE DEPLOYED

$$V_{WIND} = \frac{ATMOS (mb)}{SURFACE WIND (fps)}$$

- | | |
|--------------|-----|
| MSC 3(10) | 200 |
| MSC 2(25) | 131 |
| SCH UP (132) | 59 |

- DRIFT CANCELLED WITH IMPULSE
(ALTITUDE = 10,000 FT)

- SINK CANCELLED WITH RETRO

Figure 7.1 Lander System

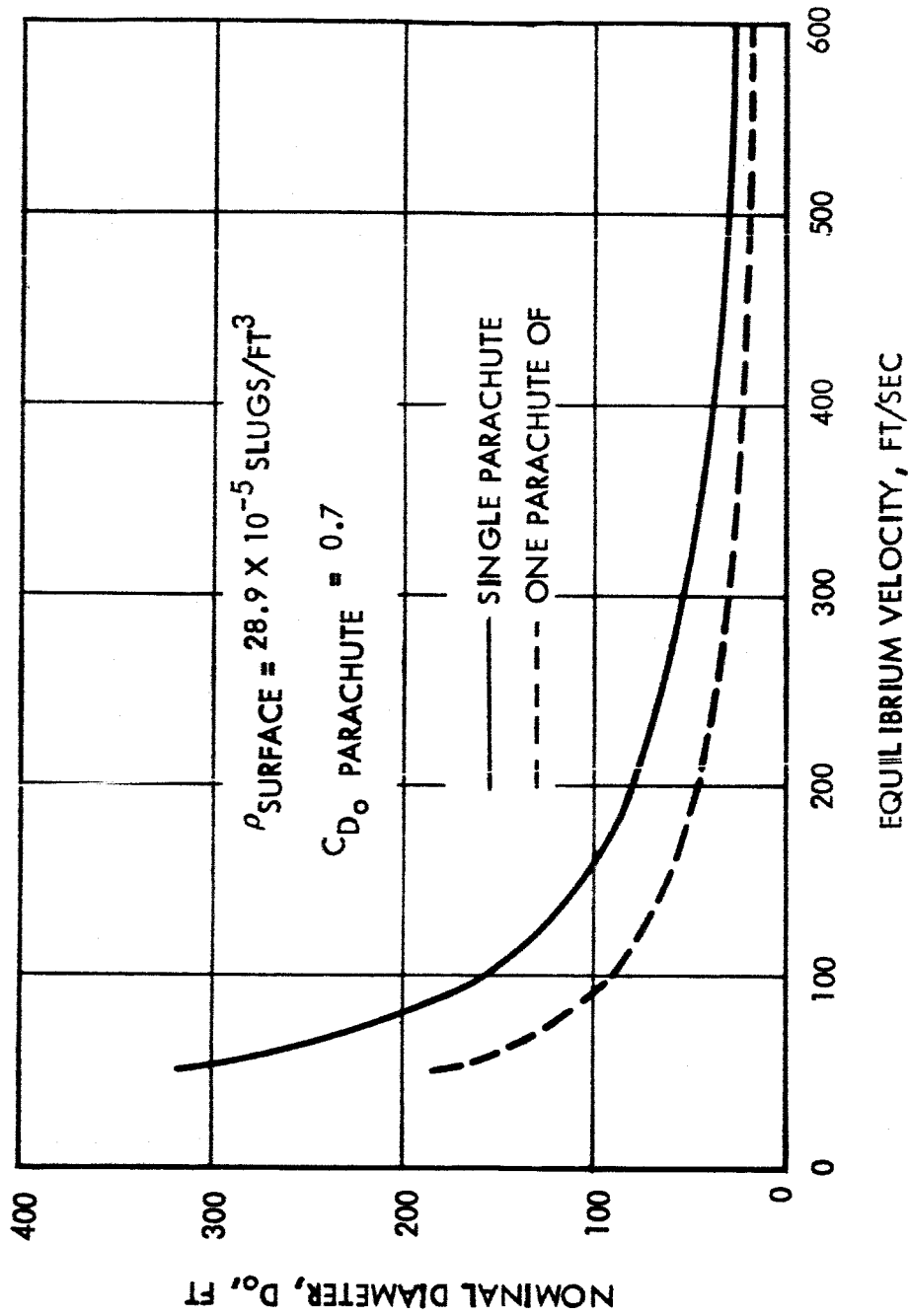


Figure 7.2 Parachute Diameter, D_o , vs Equilibrium Velocity Mars Schilling Atmosphere (132 mb)

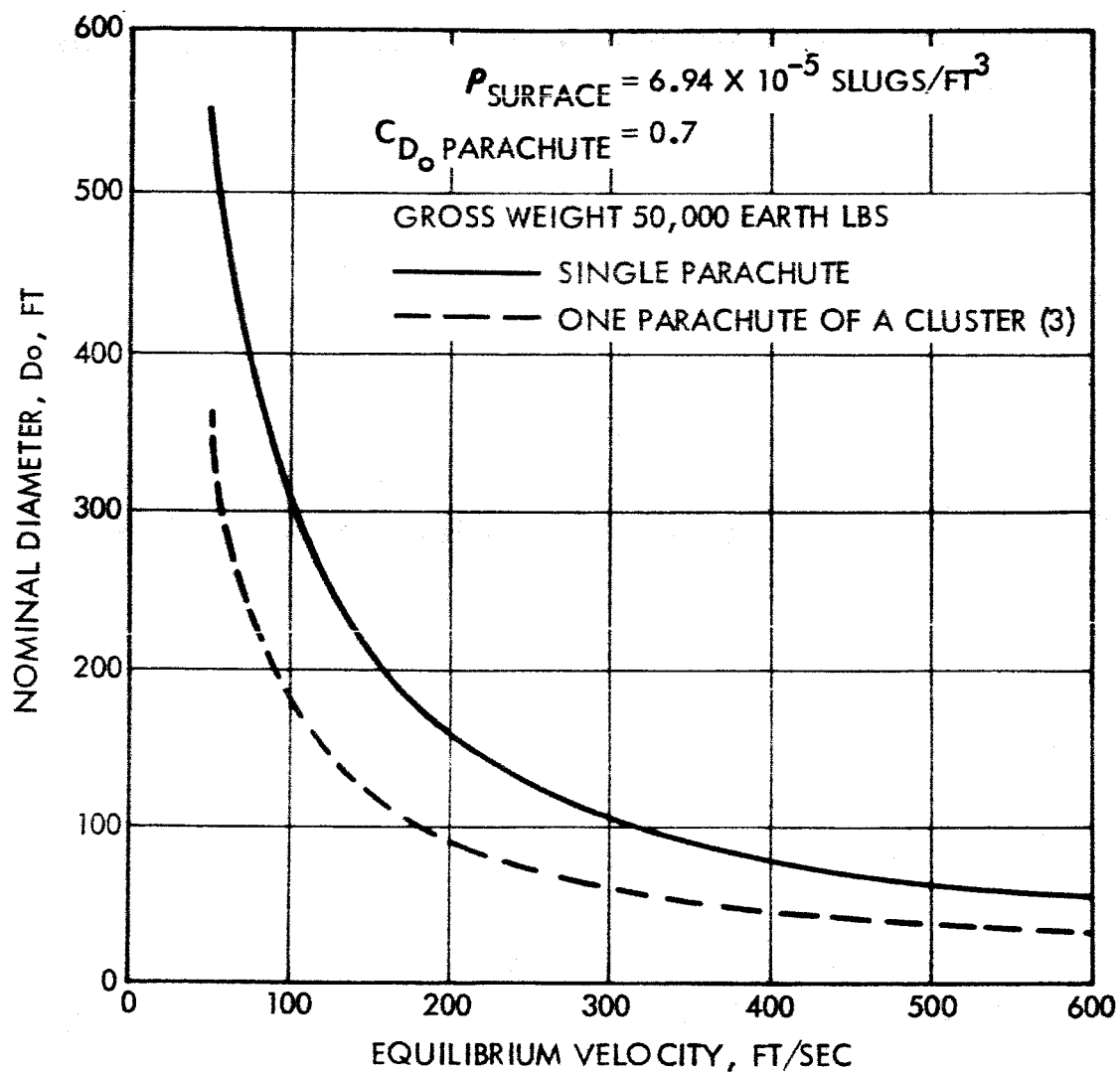


Figure 7.3 Parachute Diameter vs Equilibrium Velocity
Mars Model 2 Atmosphere (25 mb)

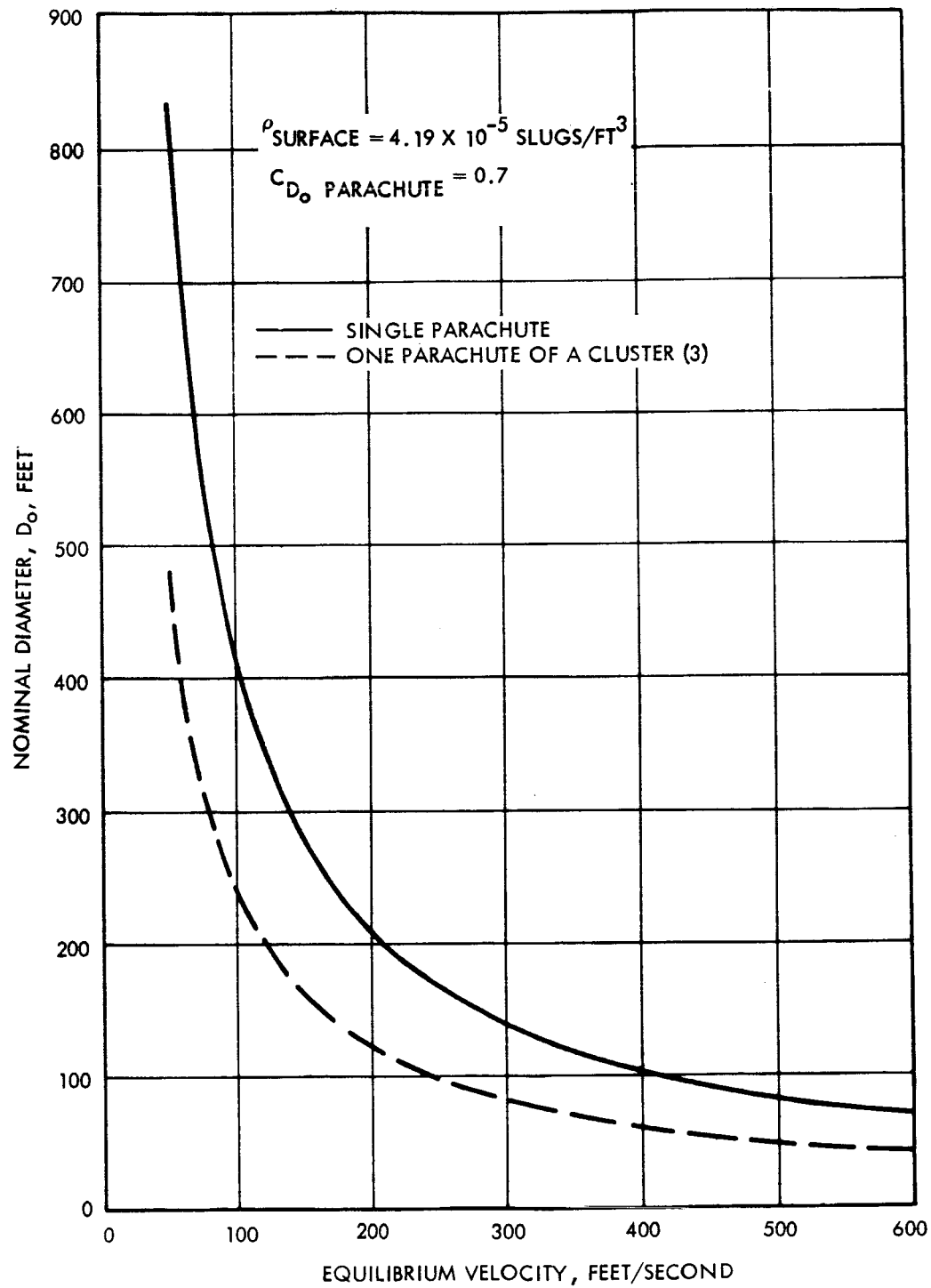


Figure 7.4 Parachute Diameter, D_o vs Equilibrium Velocity Mars
Model 3 Atmosphere (10 mb)

considered. The term nominal diameter means a reference diameter based on the surface area of a parachute converted to a flat circle. Figure 7.5 presents the weight of the parachute system as a function of parachute nominal diameter.

Parachute Retro-Rocket Combinations

From Figures 7.2, 7.3, and 7.4 it is obvious that use of a parachute alone for landing would lead to prohibitive parachute sizes and weights. Figure 7.5 shows that above diameters of 100 feet the weight of the parachute system climbs very rapidly (heavier risers, fittings, and line are required) and it becomes more profitable from a weight consideration, to use a retrograde rocket in conjunction with the parachute system. The amount of propellant (ΔW propellant) necessary to reduce the equilibrium velocity to zero is plotted in Figure 7.6, 7.7, and 7.8 versus equilibrium velocity for all three atmospheres investigated. Presented also are the parachute system weight and the sum of the parachute system plus ΔW propellant. Minimum points on these last curves indicate the minimum weight landing system. Isp assumed for the descent rocket is 300 seconds. In all three atmospheres the minimum weight equilibrium velocity is high, however a reliable retro-rocket system is capable of reducing this velocity to zero with relatively small weight penalty.

Wind Models

Winds have been postulated for the Martin atmosphere, based generally on the movement, or apparent movement, of dust clouds. These clouds have been observed to move at a rate of about 25 meters per second (82 fps).

Other values of wind magnitudes have been postulated by the theory for generation of dust storms. These values are as follows:

<u>Atmosphere</u>	<u>Wind Velocity (fps)</u>
Schilling upper (132 mb)	59
Model 2 (25 mb)	131
Model 3 (10 mb)	200

The value for the Model 3 atmosphere is an extreme upper limit for all theories.

An additional estimate is based on the circulation of the atmosphere required to shift elements from one polar region to the other within a half-year period, in keeping with the observed shift of the polar caps. This theory suggests a wind velocity, which is far less than the value suggested for the 25 mb model atmosphere. The values suggested by the dust generation model will be used.

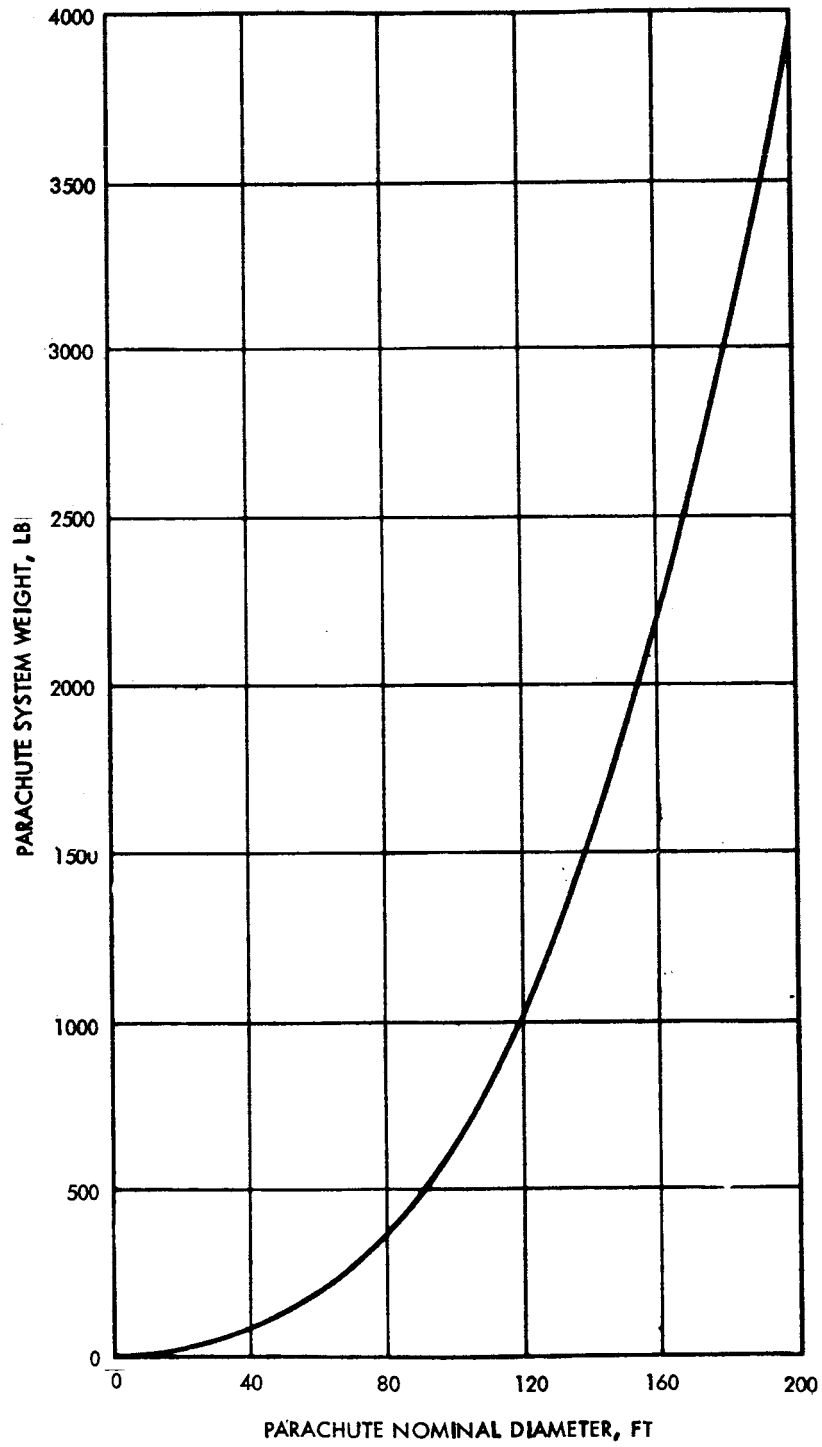


Figure 7.5 MEM Parachute System Weight

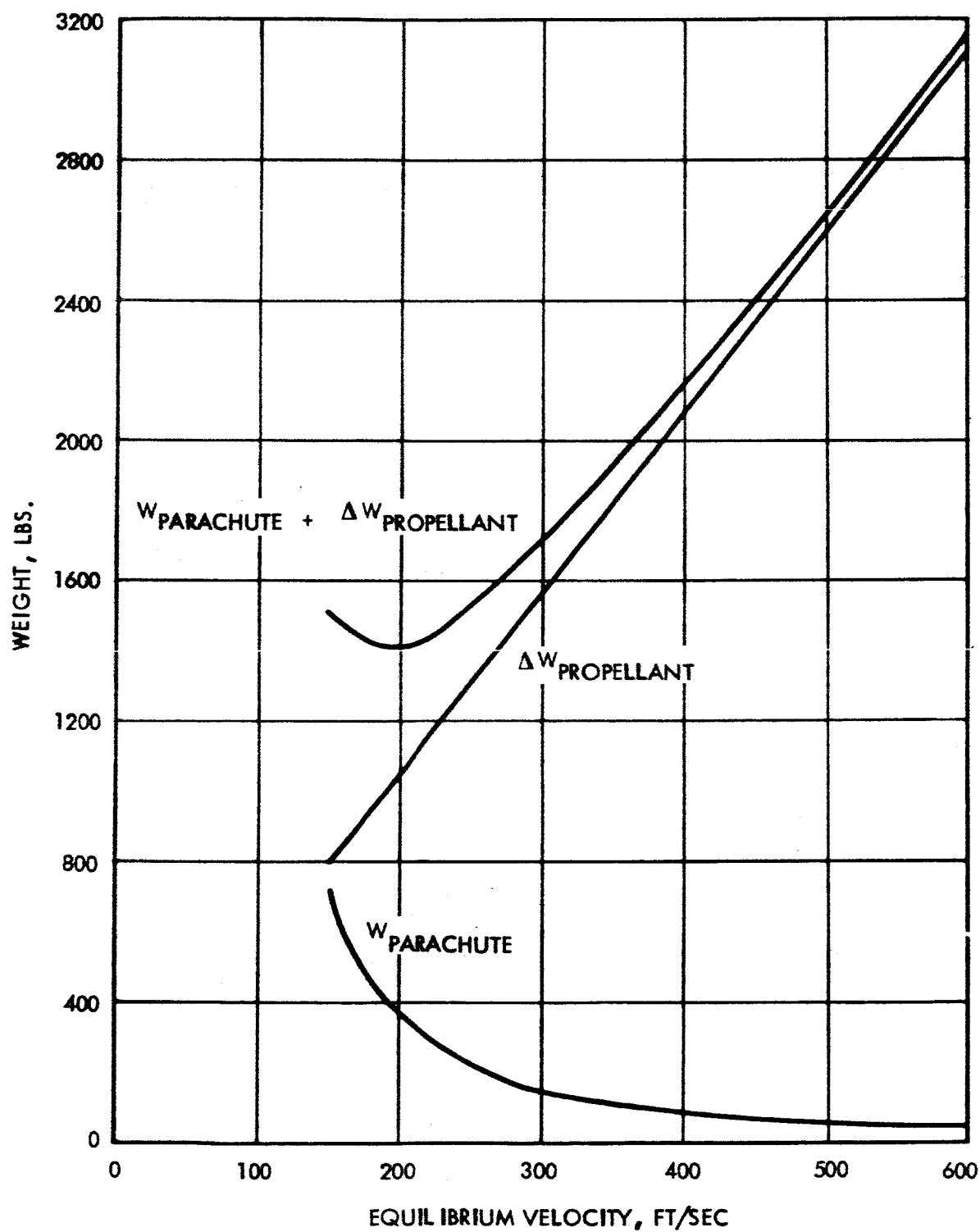


Figure 7.6 Parachute and Δ Propellant Weights vs Equilibrium Velocity
Mars Schilling Atmosphere (132 mb)

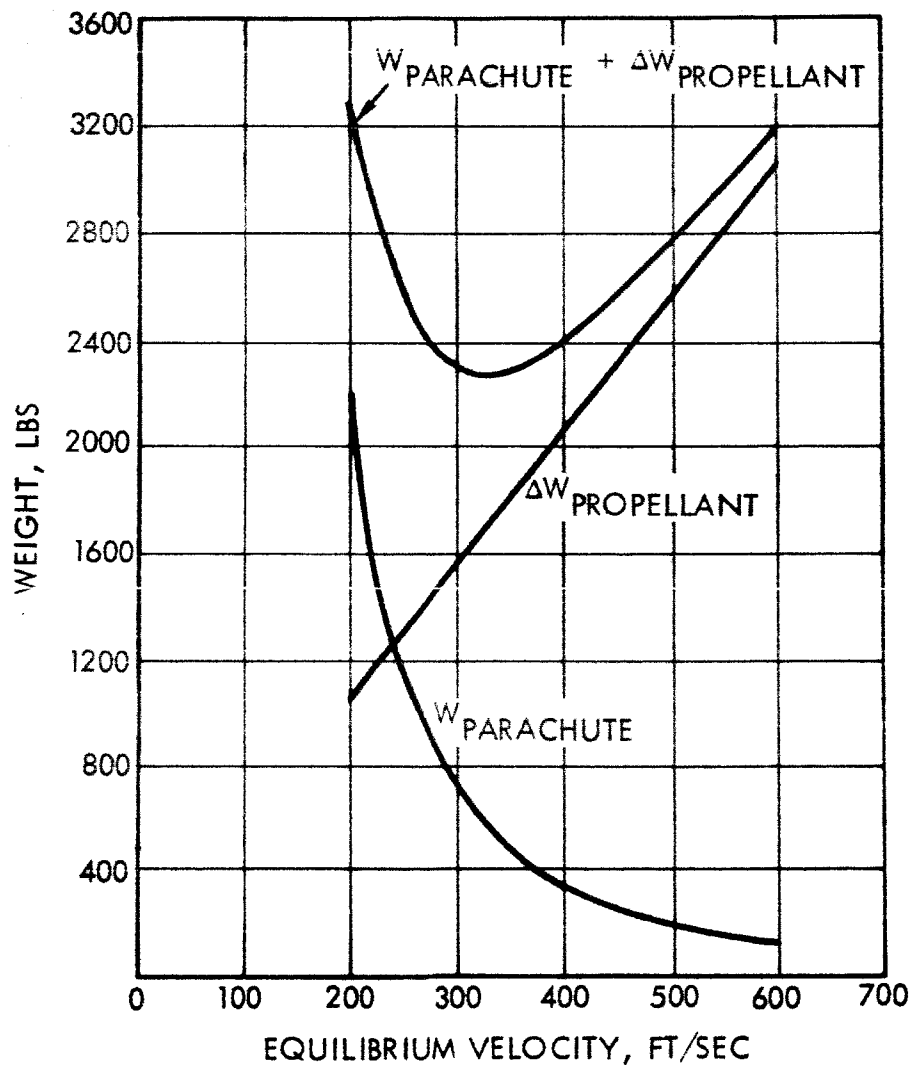


Figure 7.7 Parachute and Δ Propellant Weights vs Equilibrium Velocity Mars Model 2 Atmosphere (25 mb)

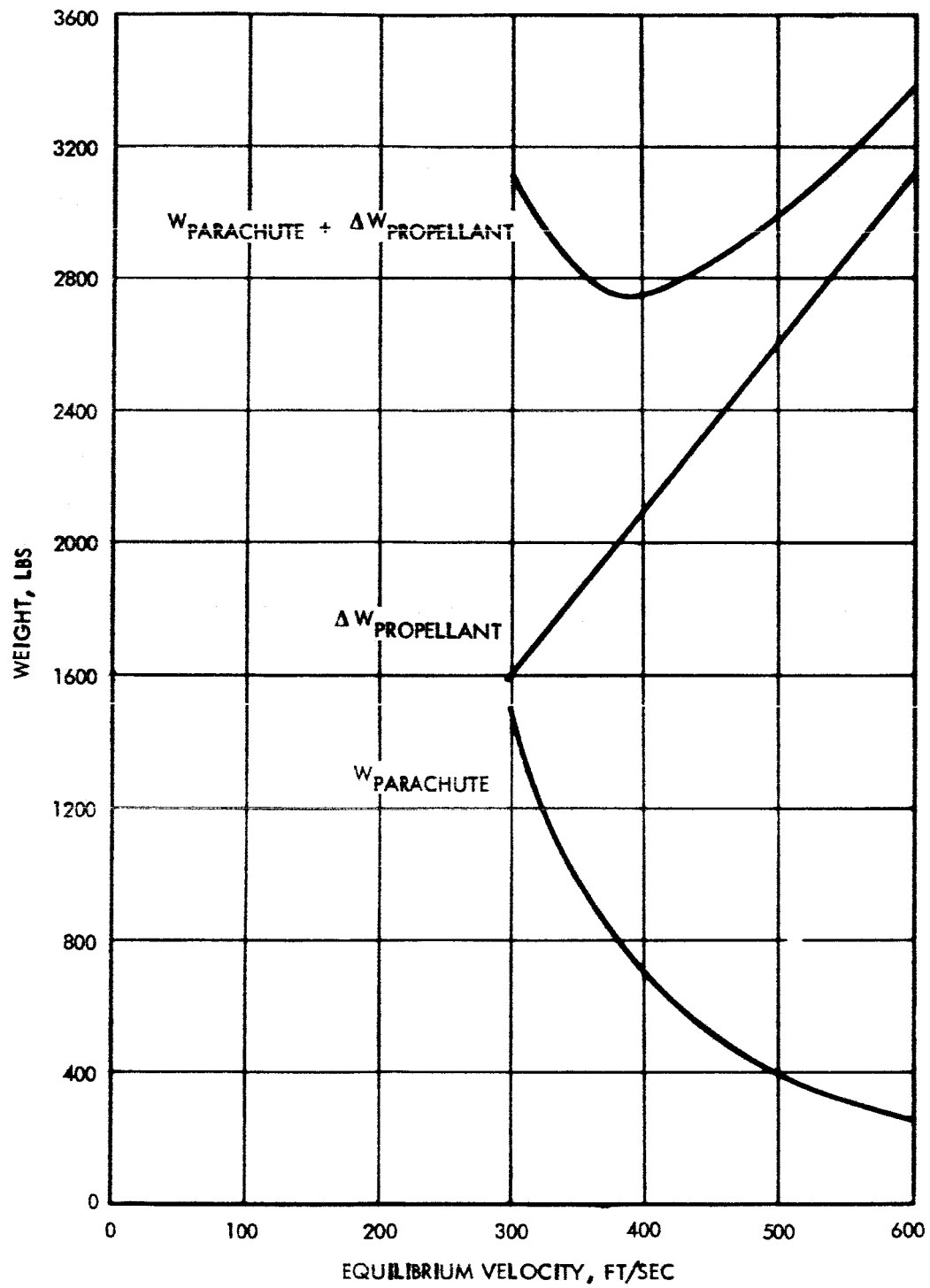


Figure 7.8 Parachute and Δ Propellant Weights vs Equilibrium Velocity
Mars Model 3 Atmosphere (10 mb)

Wind gradients extending to the upper atmosphere are difficult to predict. However, gradients of 4 fps per 1000 ft of altitude have been observed in the earth's atmosphere up to 30,000 ft, and might be assumed for the martian atmosphere.

Figure 7.9 gives the wind models assumed for the following analysis.

Effects of Winds

It is of interest to compute the drift range and drift velocity due to the wind models given in Figure 7.9. Because of the low densities of the atmospheres, the Mars excursion module (MEM) with main parachute deployed requires appreciable time to come into equilibrium with the wind, such that the drift velocity equals the wind velocity. Hence it is necessary to integrate the drift velocity and range from the time of parachute deployment, which is assumed to be 50,000 ft, although a lower altitude could be selected if necessary to reduce the effects of winds. The drift paths were integrated out for the wind models given in Figure 7.9 and the parachute diameters, given in Figure 7.2, 7.3, and 7.4, conservatively assuming that 50 percent of the parachute planform area was exposed to the full side wind. The resulting drift range and drift velocities attained at ground impact are summarized in the table below:

TABLE 7.1 DRIFT VELOCITIES AND RANGES AT IMPACT

(Refer to Figure 7.9 for Wind Models)

<u>Atmosphere</u>	<u>Drift at Impact</u>		<u>Drift Range</u>	
	<u>No Gradient</u>	<u>With Gradient</u>	<u>No Gradient</u>	<u>With Gradient</u>
Schilling Upper (132 mb)	36 fps	114 fps	5,900 ft	27,000
Model 2 (25 mb)	63 fps	129 fps	4,900 ft	12,600
Model 3 (10 mb)	76 fps	130 fps	3,700 ft	7,700

It is noted that in all cases the MEM with main parachute deployed does not come into full equilibrium with the wind, particularly in the case of the low density atmospheres. Drift ranges are appreciable for the Schilling atmosphere with strong wind gradients. As mentioned previously, drift range can be nullified by gliding the parachute, which has ample lift-to-drag ratio capability for this purpose. Alternatively, drift range can be cancelled by translational rockets, firing at 10,000 ft altitude (a lower altitude requires a high translational velocity, with attendant penalties in propellant weight; reacceleration due to the wind below this altitude is small, less than 8 fps). Propellant weights to cancel drift velocity and drift range are given in Figure 7.10. The penalties are small except for the Schilling upper limit atmosphere with maximum wind gradients.

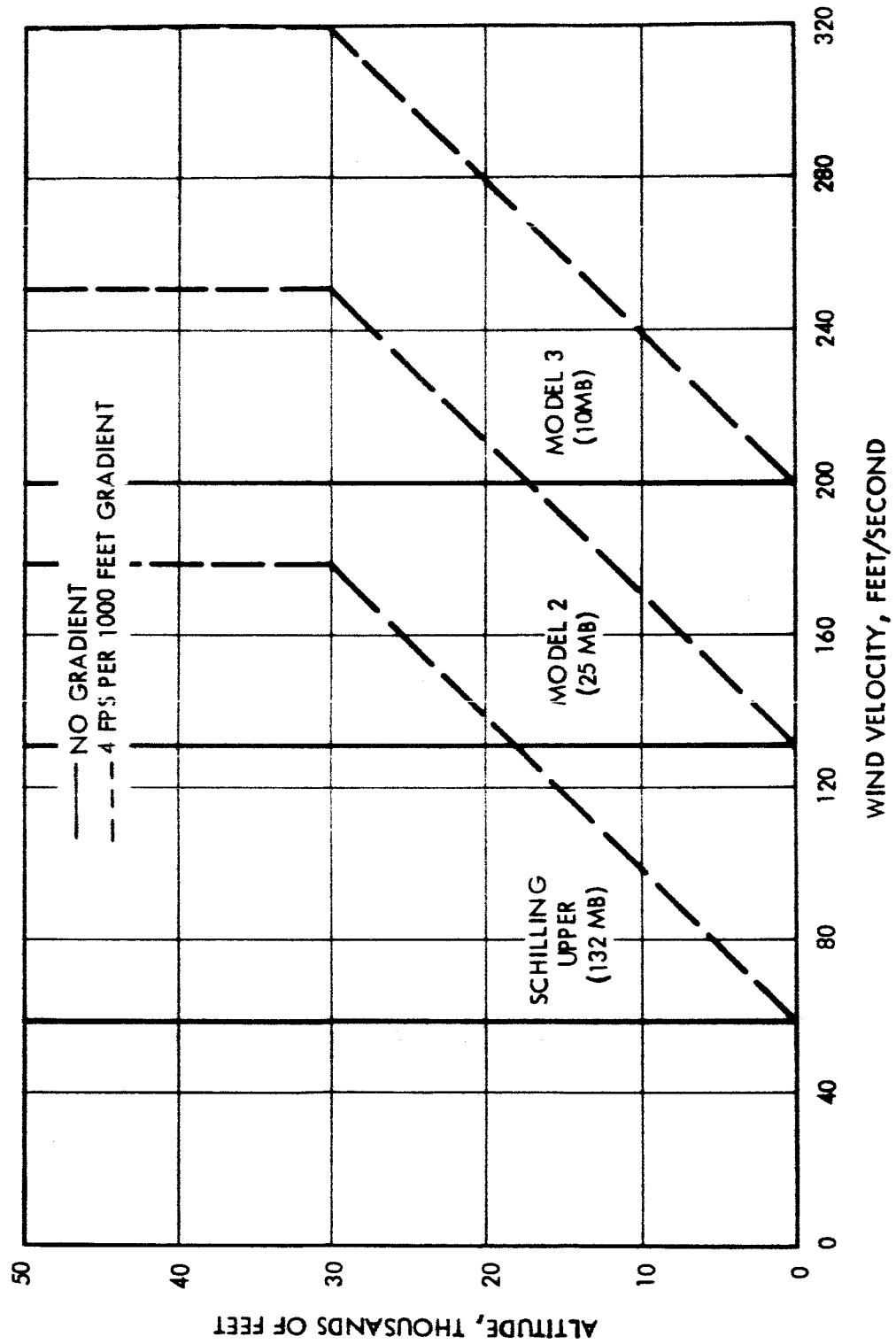


Figure 7.9 Wind Model

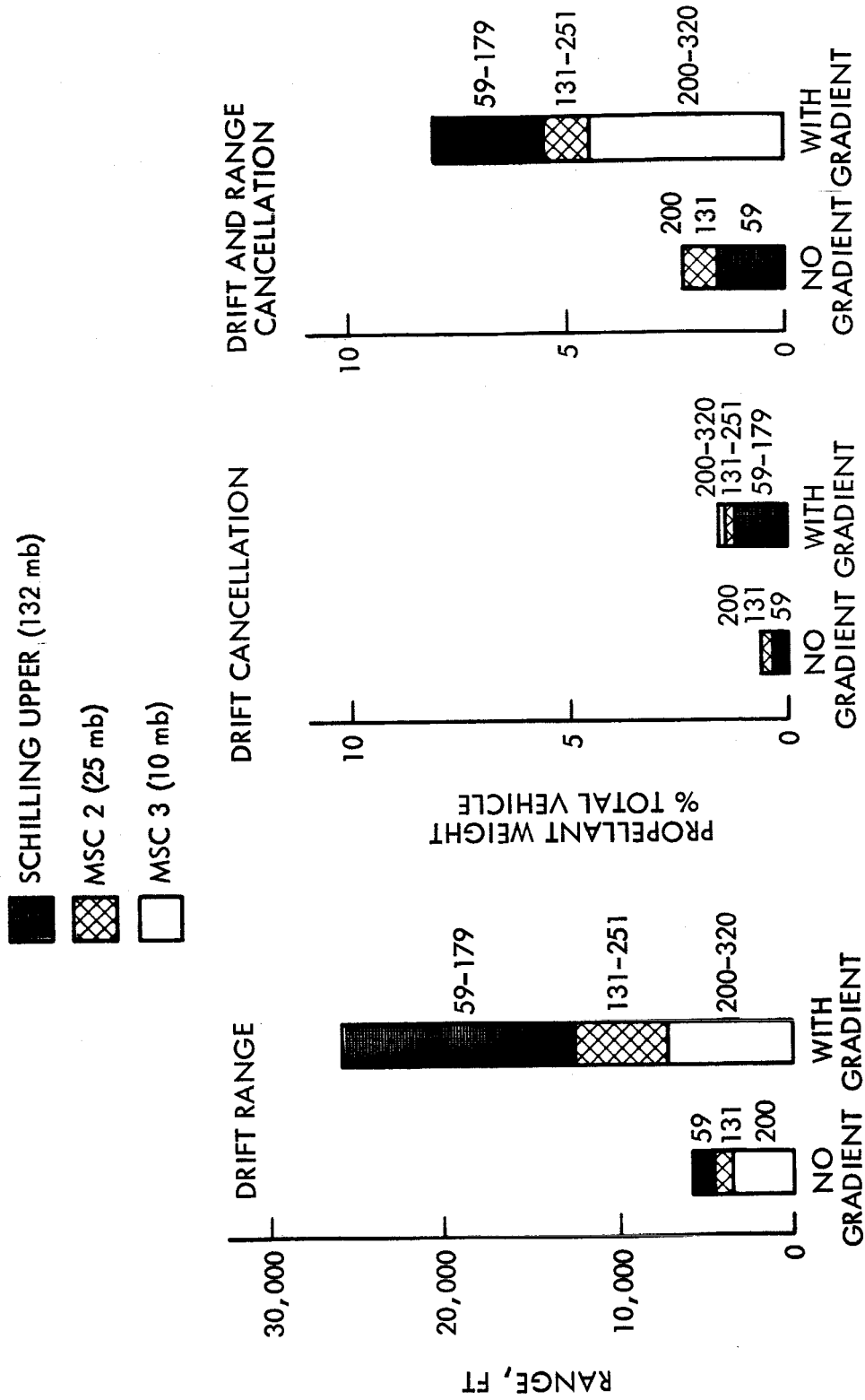


Figure 7.10 Effect of Winds

It must be pointed out that the effects of winds outlined above represent extreme situations. It is unlikely that landings would be attempted in maximum wind conditions, which would likely generate dust storms, clearly visible to the orbiting spacecraft. However, properly equipped with drift meters and translation rockets or steerable parachutes, landing could be effected under severe wind conditions.

Effect of Uncertainty in Density on Descent System Weight

In addition to the effects of winds on descent system design, uncertainties in the density of the atmosphere will require performance margins in the parachute and retrorocket systems. An indication of these margins is given below.

TABLE 7.2 EFFECTS OF UNCERTAINTIES IN DENSITY ON PARACHUTE PLUS RETROROCKET SYSTEM

Atmosphere	Impact Velocity	Weight of Parachute + Retro (% of Gross)	Effect of 10% Uncertainty in Density (% of Gross)
Schilling Upper (132 mb)	200 fps	2.8%	0.10%
Model 2 (25 mb)	325	4.6	0.17
Model 3 (10 mb)	390	5.5	0.20

In the extreme case, an allowance of $5.5 - 2.8 = 2.7$ percent of the gross weight would be required to accommodate both the Schilling upper limit and Model 3 atmospheres. A 10 percent uncertainty in a given model would result in negligible penalties in gross weight.

7.2 Landing Dynamics

After retro firing, the MEM impacts the surface with relatively small residual sink and drift velocities. A shock absorbing landing gear is provided to absorb the impact energy, and prevent overturn. The following analyses illustrate the effects of terrain conditions and impact velocities on landing gear system design.

Computational Technique

The spacecraft system must be designed to accomplish the landing maneuver with the utmost reliability despite environmental unknowns, uncertainties in landing velocities, and uncertainties in vehicle orientation. Because of the present lack of adequate data and the range of uncertainty in the values of these parameters at this time, it becomes necessary to provide a landing system whose performance is predictable and satisfactory over a very wide range of conditions.

The computational technique involves several assumptions. Of prime importance is the assumption that an orientation with the vehicle's touchdown velocity vector in the place of the maximum surface slope represents a critical condition from a stability standpoint. This assumption has been verified by a limited amount of experimental work during the STL Surveyor study effort.

The investigations described in this section are as follows (nominals to left):

TABLE 7.3 LANDING DYNAMICS VARIABLES

Number of legs	4	
Vertical Velocity, fps	19.7	9.8
Drift velocity, fps	3.3	6.6
Slope angle, degrees	10	30
Coefficient of friction	1.0	0.5
Deceleration	6g	2g
Obstacle	No	Yes

The variables were investigated individually, holding the nominal values of the remaining variables. The only exception was the case wherein a combination of low friction coefficient ($\mu = 0.5$) and high slope angle ($\theta = 30^\circ$) was assumed.

Description of Analysis

The analysis technique to be described has evolved from previous work performed on the Surveyor (Reference 7.1) Prospector and Apollo Direct Flight (Reference 7.2) study contracts, and has been slightly extended from work done on the LLS study (Reference 7.3). These studies showed that the spacecraft orientation most likely to cause an overturning is a landing during which the spacecraft is constrained to motion in a vertical plane. Accordingly, the analysis technique to be described considers the rigid body planar motion of a vehicle with an elastic system for the support of the attenuators.

The vehicle is idealized as a rigid body of mass, m , and mass moment of inertia about its center of gravity. Each individual tripod leg system is represented as a single spring with spring constant, K_1 . This spring constant defines the elastic deflection normal to the surface caused by a force applied normal to the surface. The spring constant is maintained at a fixed value as the vehicle rotates, though there will be slight variations in the flexibility of the leg system relative to a force applied normal to the surface for various orientations of the vehicle relative to the surface.

The energy absorbers are attached to the leg ends and assumed to possess a perfect-plastic-force-deflection characteristic. The attenuation system, which is a combination of the flexible legs and perfect-plastic energy absorbers, possesses therefore a bilinear load-deflection characteristic (Figure 7. 11).

The normal force required to crush the energy absorber is assumed constant. Crushing is assumed to occur normal to the surface, although the program computes and prints out the amount of crush (stroke) parallel to the vehicle reference line. The analysis accounts for the elastic and plastic deflection of the attenuation system normal to the surface only. Any motion of the contact point parallel to the surface is due to rigid body motion of the vehicle.

The value of the normal force required to crush the energy absorbers is set either by allowable deceleration forces or stability considerations. The friction force is equal to μ times the normal force when the vehicle is sliding. When sliding ceases, the friction force at each contact point is that value required to prevent sliding and must be computed from the equations of motion. A maximum value for the friction force is specified for each attenuation system, generally taken as μ times the normal force.

The landing surface is assumed to be a rigid included plane with coefficient of friction μ between the pad and the surface. To account for any particular leg striking an obstacle, the coefficient of friction between that leg and the surface is increased to approximately ten. For all cases investigated, this has the effect of immediately transforming any kinetic energy due to sliding into angular kinetic energy. The transfer is impulsive, and represents quite well the phenomena being modeled.

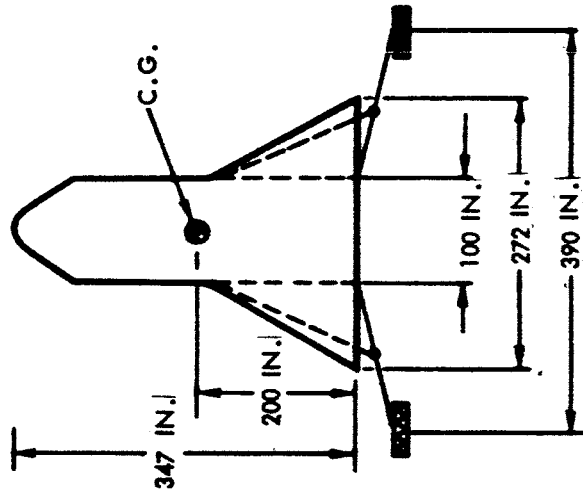
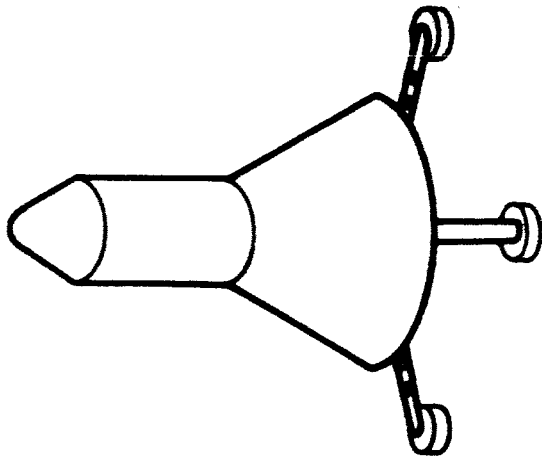
Details of the computational procedures are given in Reference 7. 4.

Vehicle Design

The vehicle design shown in Figure 7. 12 was assumed for the analyses. The shock absorbers for the main landing gear are located inside the flare of the vehicle. These struts are tubular in shape and filled with crushable honeycomb to absorb the impact energy, and limit the deceleration to its nominal value.

Results of Stability Studies

A summary of the basic design studies performed are presented in Figures 7.13 through 7.15.



$W_{LDG} = 41,600 \text{ LBS.}$
 $I = 82,300 \text{ SLUG-FT}^2$
 $= 8.0 \text{ FT}$

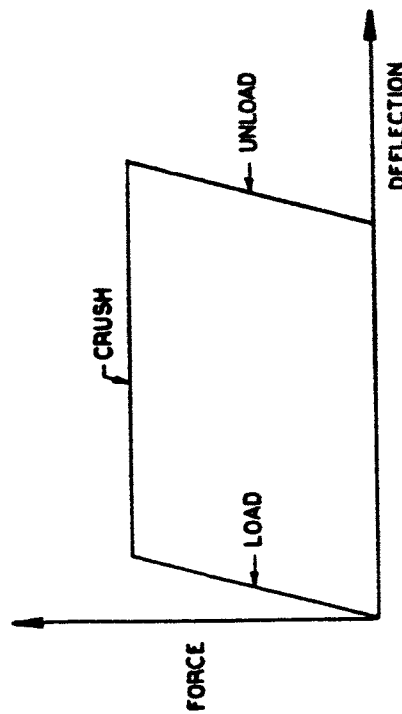


Figure 7.12 Vehicle Arrangement

Figure 7.11 Attenuation System Normal Load -- Deflection Curve

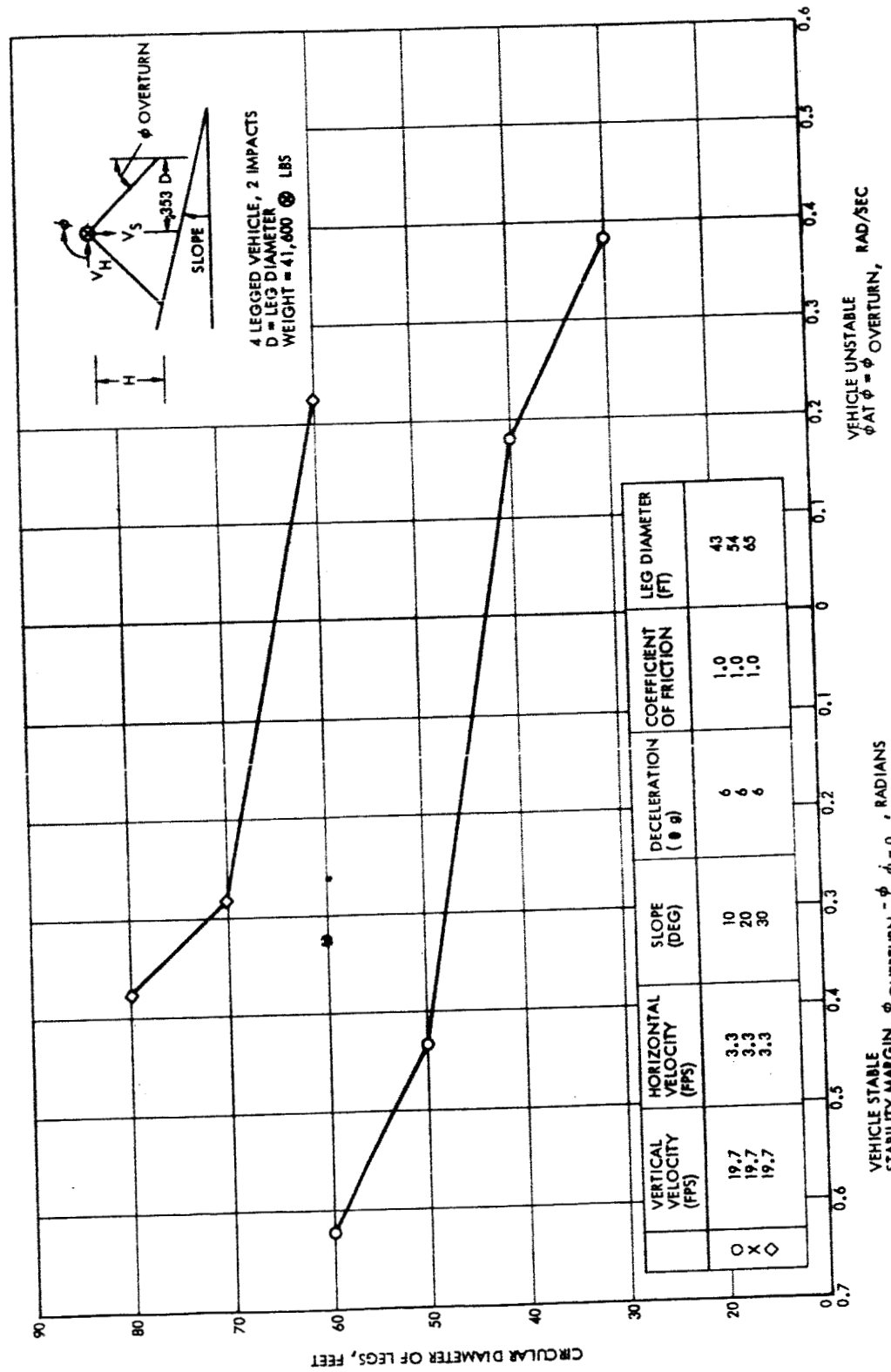


Figure 7.13 Landing Stability of Mars Excursion Module - Effect of Slope

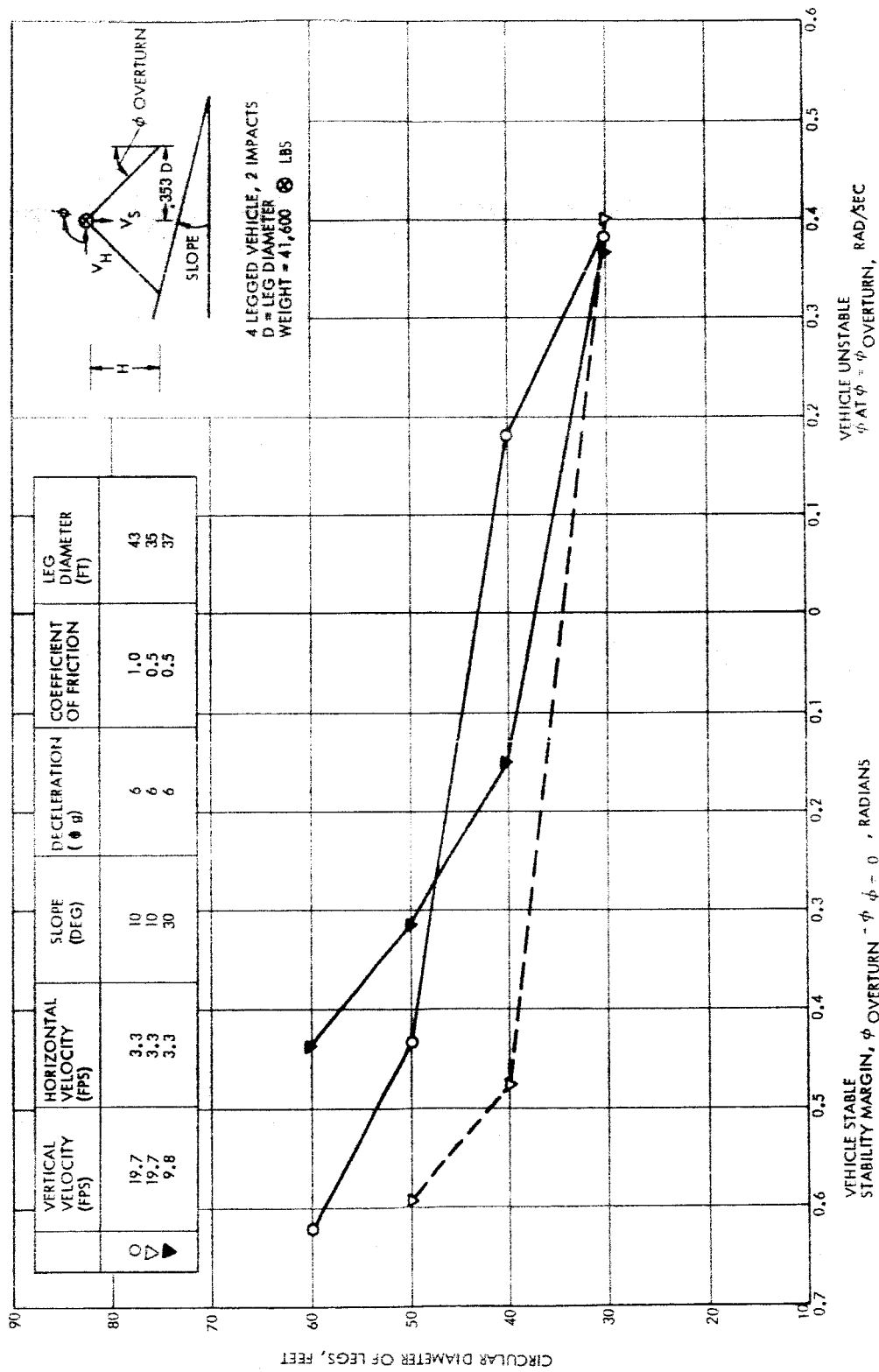


Figure 7.14 Landing Stability of Mars Excursion Module - Effect of Friction

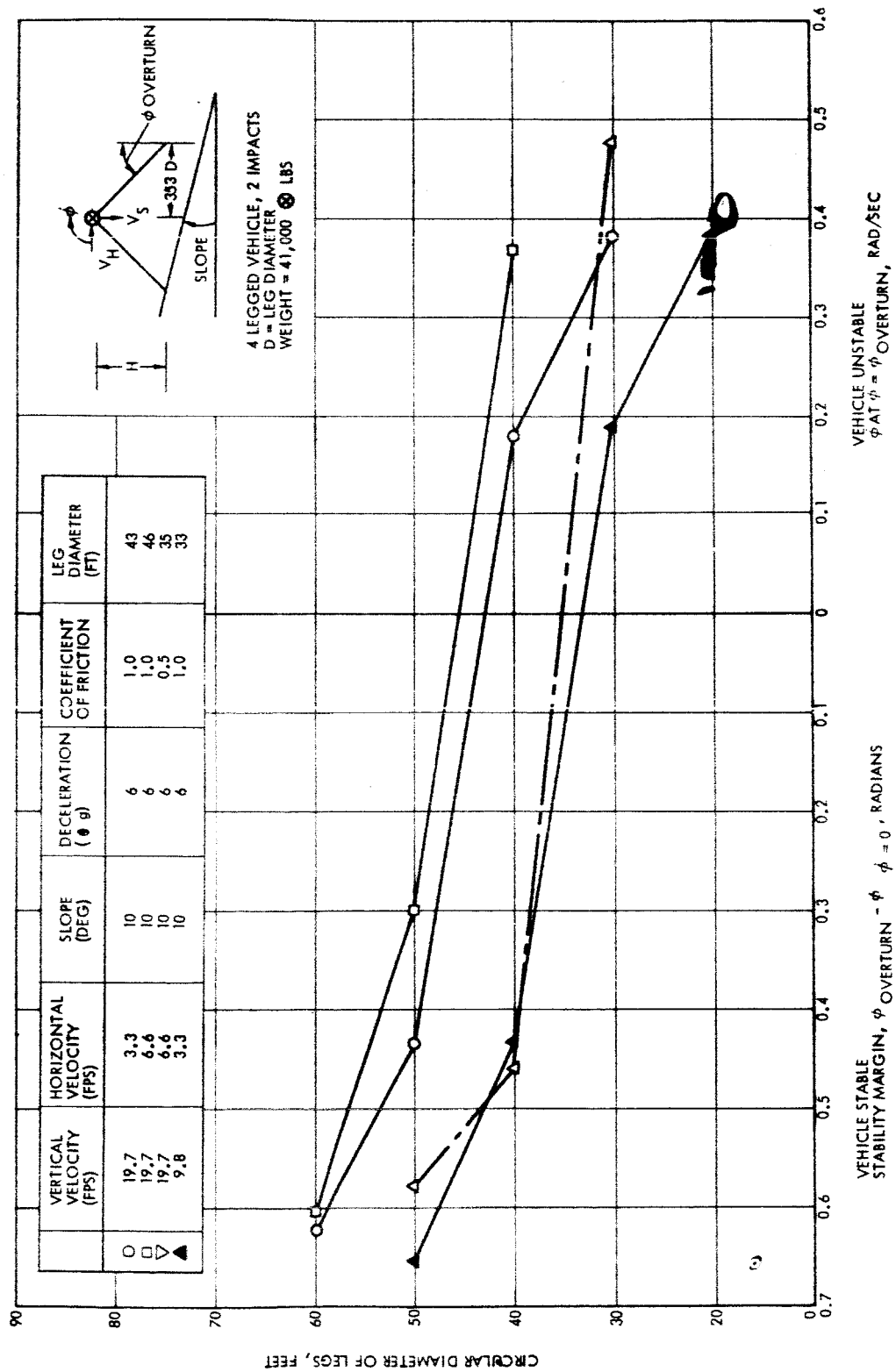


Figure 7.15 Landing Stability of Mars Excursion Module - Effect of Velocities

In an effort to obtain an accurate estimate without undue computational expense, the following method of plotting was adopted: the abscissa is the circular diameter of the landing leg system, and the ordinate is divided, representing two functions of vehicle attitude. The portion of the ordinate below the x axis represents the angular speed at which the vehicle passes the angle of neutral stability. This portion of the curve represents the degree of instability. The portion of the ordinate above the x axis represents the stability margin of the vehicle. Remembering that a vehicle is considered stable if $\dot{\phi}$ changes sign before $\phi = \phi_{\max}$, at the instant that $\phi = 0$ and the angular acceleration is opposing the rotation of the vehicle, the difference $\phi_{\max} - \dot{\phi}_{\phi=0}$ represents the margin on stability. When $\phi_{\max} - \dot{\phi}_{\phi=0} = \dot{\phi}_{\phi=\phi_{\max}} = 0$, the vehicle is in neutral stability. The diameter associated with this condition is the minimum diameter required for stability. The results are summarized in the following table.

TABLE 7.4 SUMMARY OF LANDING STABILITY ANALYSIS

<u>Condition</u>	<u>Vertical Velocity (fps)</u>	<u>Horizontal Velocity (fps)</u>	<u>Slope (deg)</u>	<u>Deceleration (\oplus g)</u>	<u>Coefficient of Friction</u>	<u>Leg Diam. (ft)</u>
1 (Nom.)	19.7	3.3	10	6	1.0	43
2	19.7	3.3	20	6	1.0	54
3	19.7	3.3	30	6	1.0	65
4	19.7	6.6	10	6	1.0	46
5	9.8	3.3	10	6	1.0	33
6	19.7	3.3	10	6	0.5	35
7	19.7	6.6	10	6	0.5	35
8	9.8	3.3	30	6	0.5	37
9*	19.7	3.3	10	6	1.0	43

*Downhill leg strikes obstacle

The results indicate that slope angle has a strong influence on leg diameter if the coefficient of friction is high ($\mu = 1.0$). Leg diameter is increased from 43 to 65 ft if the slope increases from 10 to 30°. An increase in drift velocity does not have a large effect on gear design.

Reducing sink velocity has a pronounced effect, and should be achieved if possible in the final design. The impact velocity of 9.8 fps corresponds to a rocket shut-off altitude of 4 ft.

Reducing the coefficient of friction has a pronounced effect on stability, particularly for large slope angles. Although the coefficient of friction of the natural terrain may not be known, an artificial coefficient of friction can be provided by proper selection of crushable materials in the pads. Such materials are available and are designed to yield under relatively low shear loads, but remain stiff to normal loads.

An obstacle on the downhill slope has little effect on the stability of the system. However, an encounter with an obstacle during free fall could cause a significant increase in angular velocity, and dangerously hinder the chances for a stable landing.

The vehicle design shown in Figure 7.12 will settle approximately 7-12 inches under impact. Hence, about one meter-vertical distance remains under the vehicle to clear rocks or other obstacles. This is assumed to be adequate for initial landings.

It is necessary to provide sufficient stroke in each attenuator to accommodate up to 80 percent of the kinetic energy possessed by the vehicle at touchdown. This stems from the fact that very little energy is absorbed at initial contact -- the bulk of the absorption occurs when the vehicle slams its downhill leg or legs into the surface. For the long base orientation (three impact) of a four-legged vehicle, practically all the energy at touchdown is still available in the form of vehicle velocity when the single downhill leg contacts the surface. This leg must have the capacity to absorb this energy, and since it is not possible to specify which of the legs of the vehicle will encounter such a condition, all must be designed to cope with it.

Rocket Study

A limited investigation of the effect of rockets on stability was performed, using the basic 6 g, 30 degree, four-legged system as a reference case. Individual rockets were located at the perimeter of the legs, one above the elastic portion of each leg. The vehicle was oriented for a two-impact (short base) landing maneuver.

The analysis assumed each rocket fires when the leg to which it is attached contacts the surface, and will continue to fire throughout the maneuver. Preliminary investigations indicated that the downhill rockets hindered the effect of the uphill rockets in rotating the vehicle back uphill.

Subsequent investigations were performed with the rocket thrust on the downhill legs reduced to zero. These indicate that:

- a) 5000 pounds of thrust (total) on the uphill legs acting for about 5 seconds provides sufficient impulse to turn the vehicle back uphill and significantly reduce the three components of vehicle velocity.
- b) If the rocket is not cut off at this time, the vehicle will tumble uphill.

The implications of these results are twofold.

- a) For vehicles required to land on steep slopes, a large reduction in leg diameter can be realized by the implementation of rockets, having a total system weight of less than 200 pounds.
- b) Unless the vehicle's orientation relative to the slope can be sensed and a favored orientation at touchdown achieved, a fairly complex system of logic may be required to control the firing of the leg rockets and assure that they do, in fact, produce stability.

These conclusions are indeed based upon a limited number of investigations. The concept of stability augmentation rockets, however, appears so promising as to merit considerable study in the future.

Conclusions

It is concluded that a reasonably wide range of uncertainties in the martian terrain can be accommodated with small increases in landing gear diameter (of the order of a few feet), resulting in small increases in vehicle gross weight (approximately 400 lbs., or 1 percent of the gross weight). Obstacles up to one meter in height can be accommodated. It is assumed that soil bearing strength is adequate to support the landing. Soft soils will act like the downhill obstacle cases summarized in Table 7.3, which is not critical from a stability standpoint. Vehicle sinkage would be excessive, however.

7.3 Ascent Phase

Surface operations are considered in Section 8. The ascent of the MEM to orbit for rendezvous with the main spacecraft is discussed in the following section.

Ascent trajectories were computed to determine the effects of three different models of the Mars atmosphere. The models are defined in Section 4, and are:

- NASA Model 3 (10 mb)
- NASA Model 2 (25 mb)
- Schilling Upper Limit (132 mb)

Estimates were made of the effects of a 10 percent uncertainty in the density and scale height for the NASA Model 2 atmosphere. The effects of gross uncertainties in the Model 2 atmosphere were also examined, by using the extreme scale height and density variations of the Model 3 and Schilling Upper Limit atmospheres.

Vehicle and Flight Profile

To give a proper comparison of the effects of the three atmospheres, a standard vehicle, mode of ascent, and restriction on final orbit life were assumed for all three atmosphere models. The vehicle was a single stage rocket with the following characteristics:

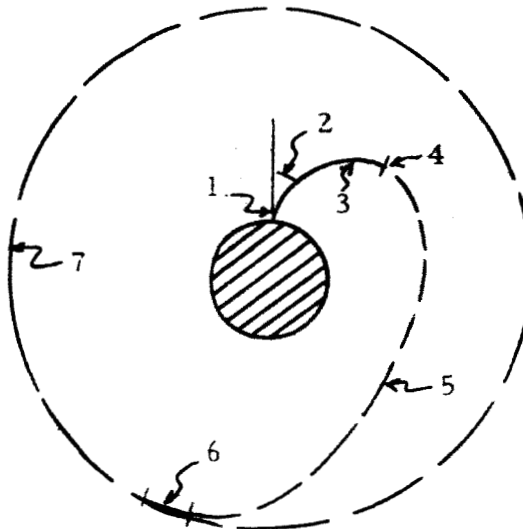
Lift off weight, $W_0 = 50,000 \oplus \text{lbs}$

$W/C_D A = 760 \oplus \text{lbs/sq. ft.}$

Thrust to weight ratio = 1.25 at lift off (Mars weight)

$I_{sp} = 450 \text{ seconds (vacuum)}$

Because of the high orbit altitudes required a dual burn ascent was employed. The first burn was terminated at an altitude where drag effects had dropped appreciably, after which the vehicle coasted to orbital altitude where an impulsive second burn added the small additional velocity required to achieve circular orbit. * The coast phase was essentially a Hohmann transfer from first injection to final injection into orbit. No other optimization of the ascent was attempted. However, according to Helgostam (Reference 7.5) the mode of ascent used here will approach very closely maximum payload performance.



* For a rendezvous at injection into circular orbit a low-thrust long burn injection will probably be preferable for terminal maneuvering. However, this should not affect payload on orbit appreciably.

The above sketch describes the ascent maneuver:

1. Vertical lift-off
2. Small "kick" angle
3. Gravity turn followed by appropriate program of thrust turn rate to achieve proper cut off conditions
4. Thrust cut off
5. Coast
6. Impulsive burn, ΔV_2
7. Circular orbit

The orbital altitude was selected for each atmosphere to give a minimum life on orbit of 100 days (using the method of Reference 7.6), which leads to a relatively high orbit altitude, and reduces payload on orbit considerably. This requirement may be unnecessary when actual missions are planned. However, for the present comparative study this requirement tended to emphasize the difference in effects of the three model atmospheres.

The results of this analysis are summarized in Table 7.5, which presents the effects of the atmospheres on required orbit altitude and final orbit weight. The intermediate effects of the various losses are also shown for comparison.

TABLE 7.5 COMPARISON OF MARS ASCENT TO ORBIT FOR
VARIOUS ATMOSPHERE MODELS

($W_o = 50,000 \text{ @ lbs}$)

Atmosphere	Orbit Altitude (km)	W_o (Earth lb)	ΔV_{total} (ft/sec)	Losses (ft/sec)				ΔV_2 ft / sec
				V_F	V_g	V_d	V_T	
NASA Model 3 (10 mb)	141	45,400	15,170	23	3478	24	3525	41
NASA Model 2 (25 mb)	375	50,000	16,020	153	3690	113	3956	195
NASA Model 2 (27.5 mb) + 10% uncert.	490	50,900	16,520	178	3710	260	4148	276
Schilling Max (132.6 mb)	610	58,700	17,810	242	4269	853	5365	332
Hybrid (CO at 500,000 ft)	454	54,700		239	4235	478	4952	227
Hybrid (CO at 600,000 ft)	454	56,600		382	4527	451	5361	203

where the losses are as follows:

V_F	= Thrust losses
V_g	= Gravity losses
V_d	= Drag losses
V_T	= Total losses

Figures 7.16 to 7.31 give a more detailed comparison of the losses and other effects of the atmosphere models.

The results emphasize that the denser atmosphere models require higher orbit altitudes and greater expenditures of fuel to overcome the higher drag forces and reach orbit. It can be seen that orbital altitude has a much greater effect on payload in orbit than the drag losses. This is apparent by comparing V_g (the losses in gaining altitude and speed) to V_d (the losses in drag). Also comparing V_g among the various models indicates the direct effect of orbit altitude on the losses and, therefore, payload in orbit. If orbit altitude had been held constant for all the atmosphere models, the gravity losses would have been essentially the same for all the models, and the only appreciable difference would have been the drag losses, which are a small part of the total losses, but vary significantly with atmosphere density level.

7.4 Communications Blackout During Entry

In order to analyze the worst possible effect of the Martian atmosphere on S-band radio transmission, it was assumed that the entry module maintained the entry velocity (11,000 fps) down to impact. From the standpoint of electron generation, the maximum would therefore be realized just before impact. In analyzing the problem of plasma attenuation, all calculations were conducted at surface level under equilibrium conditions.

It was assumed that no attenuation was present when the plasma frequency was below the transmission frequency. However, total loss of transmission occurred when the plasma frequency equaled or was greater than the transmission frequency. For an S-band radio, this corresponds to a critical density of 10^{11} electrons per cubic centimeter.

At sea level the Martian atmosphere is assumed to consist of 15 percent CO_2 and 85 percent N_2 by volume. This assumed atmosphere was used since

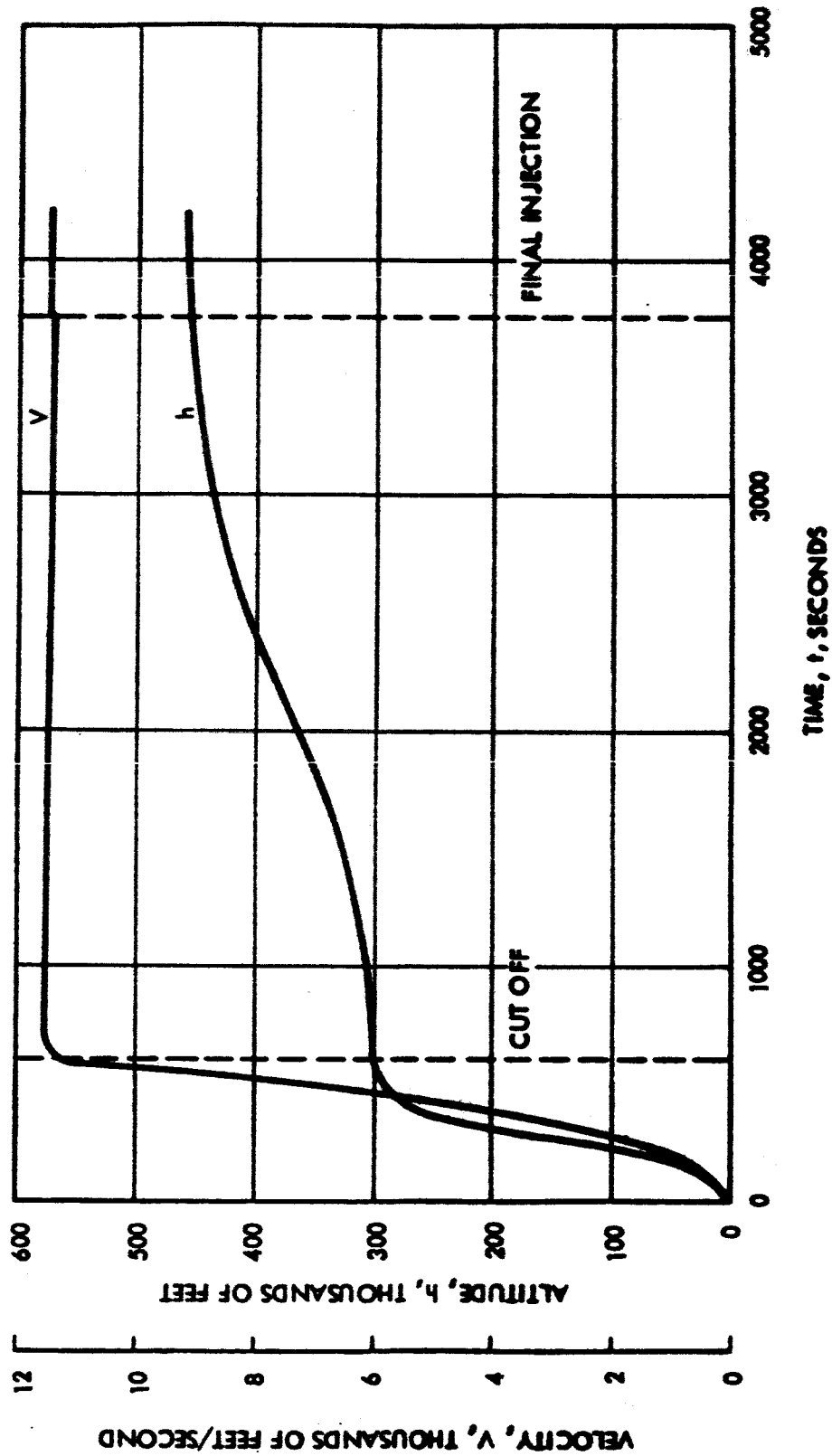


Figure 7.16 Martian Ascent Trajectories
Velocity and Altitude Histories
NASA Model 3 (10 mb) Atmosphere

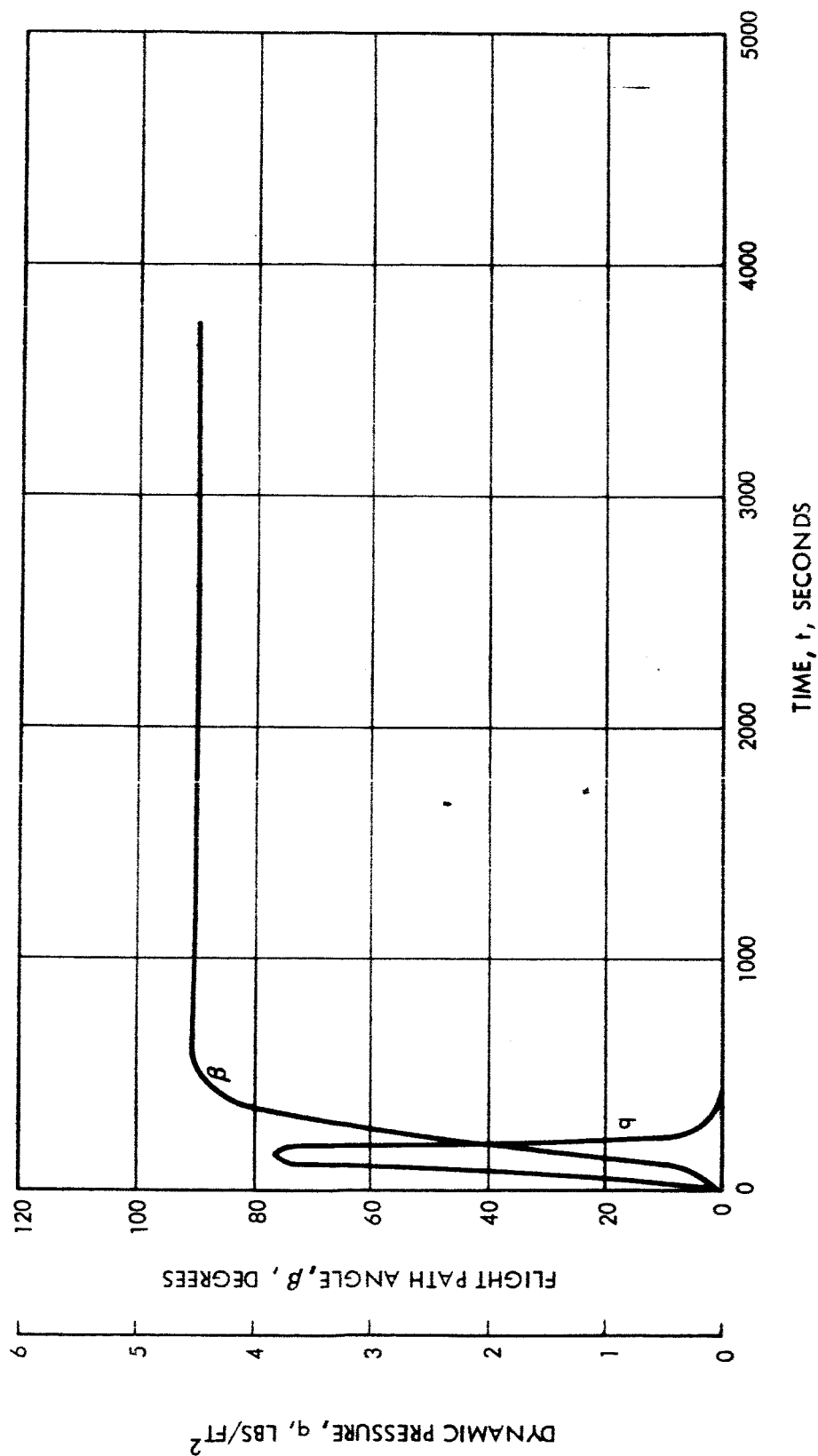


Figure 7.17 Martian Ascent Trajectory
Dynamic Pressure and Flight Path Angle Histories
NASA Model 3 (10 mb) Atmosphere

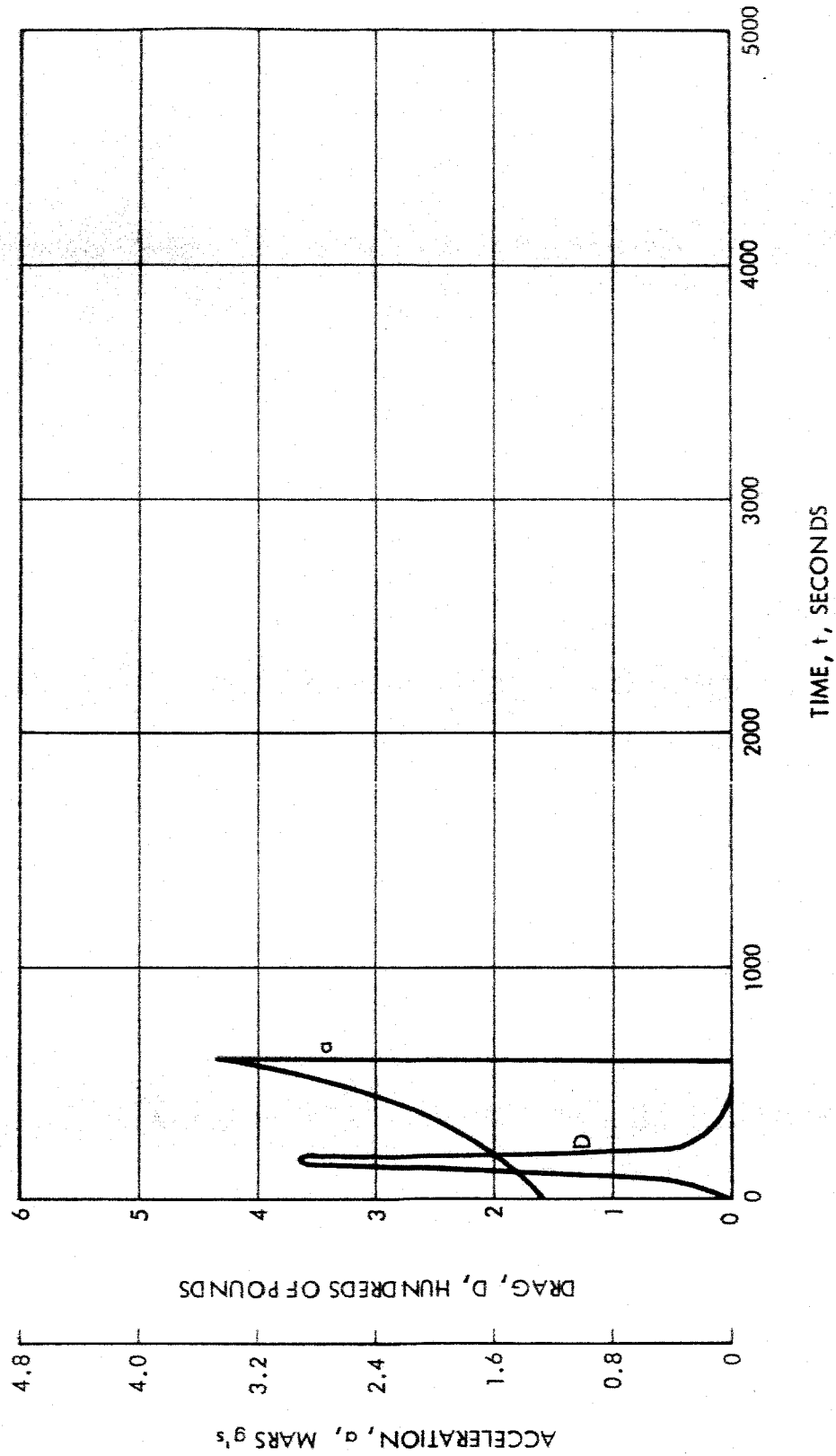


Figure 7.18 Martian Ascent Trajectory
Drag and Acceleration Histories
NASA Model 3 (10 mb) Atmosphere

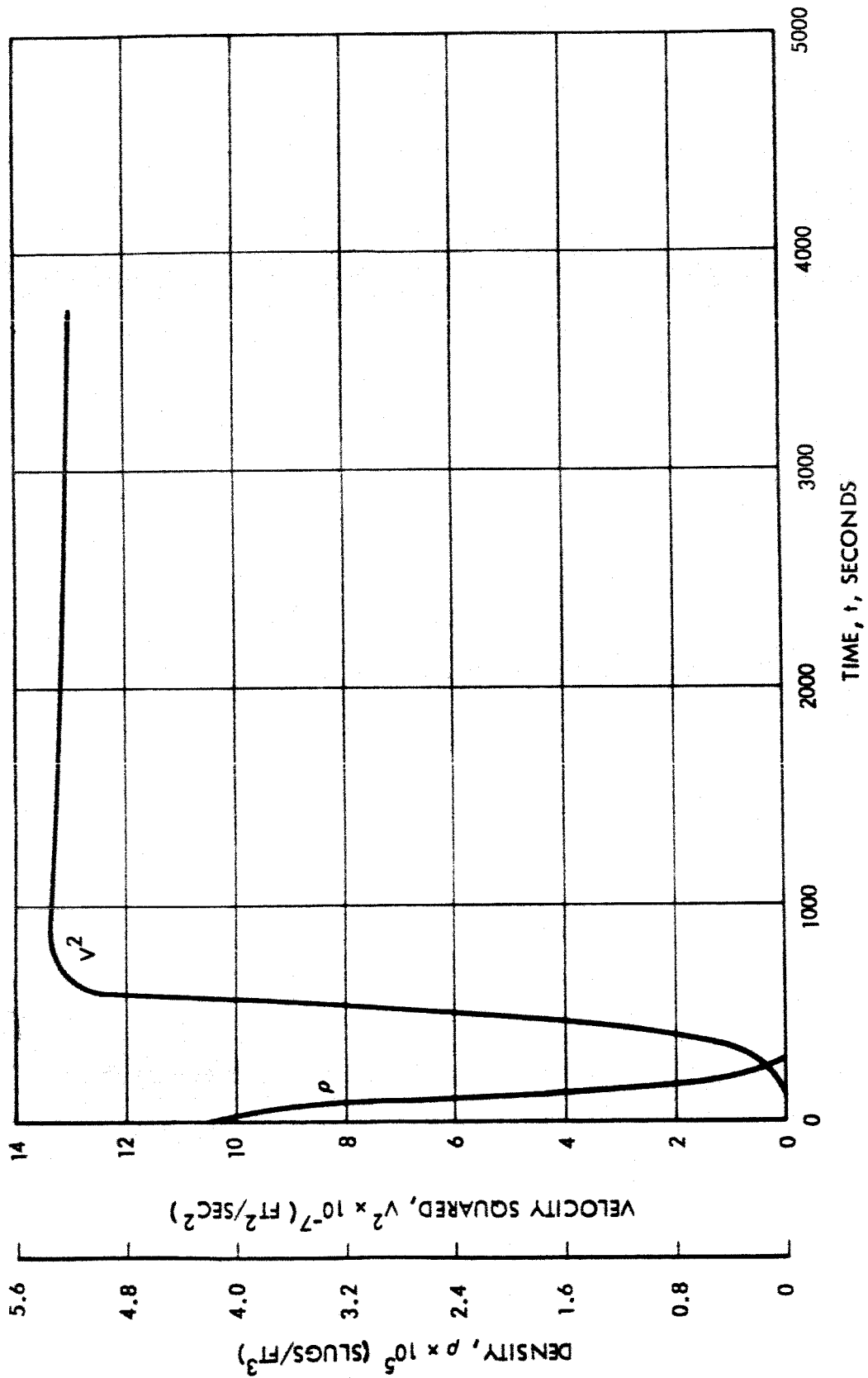


Figure 7.19 Martian Ascent Trajectory
Density and Velocity Squared Histories
NASA Model 3 (10 mb) Atmosphere

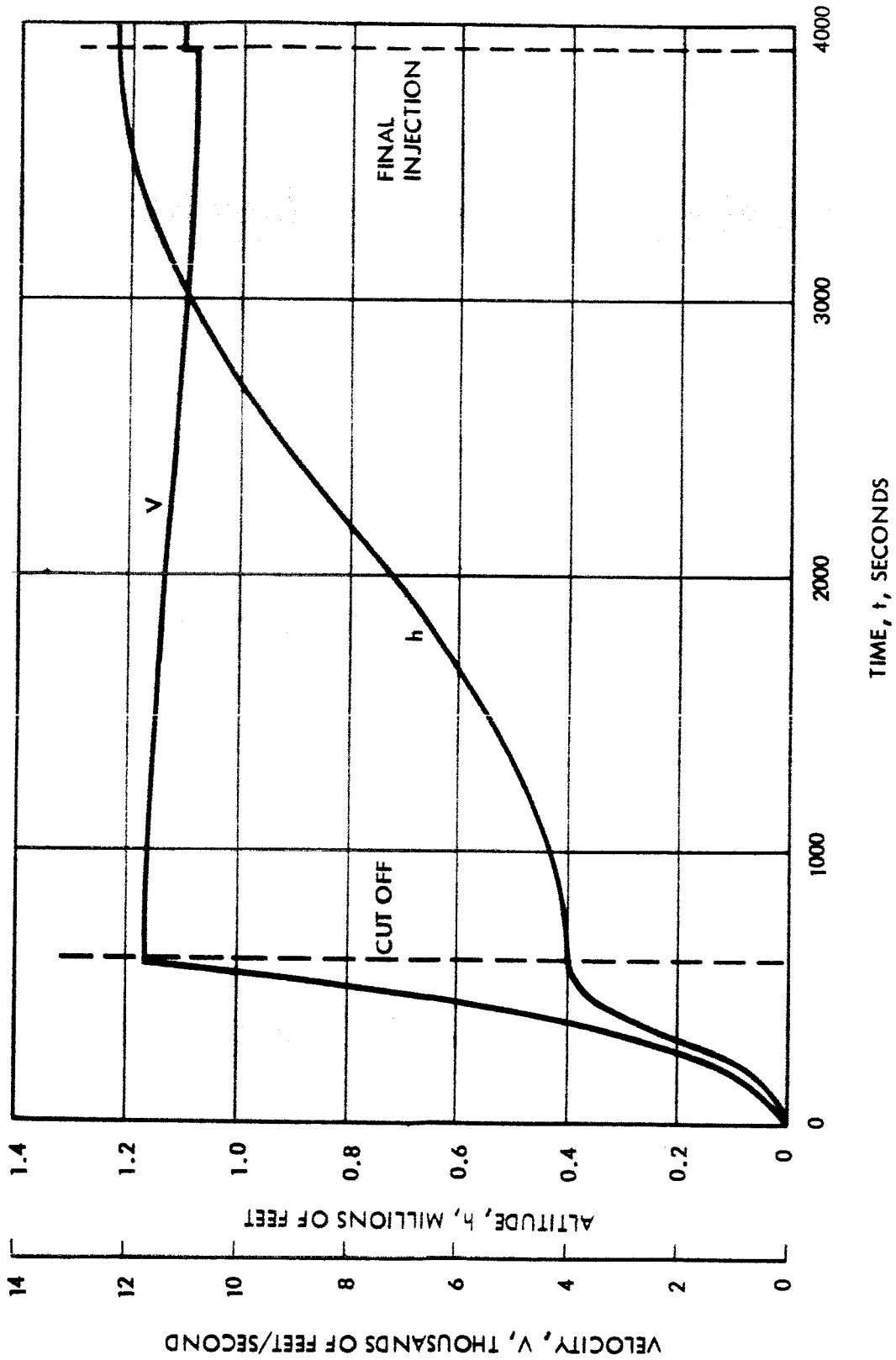


Figure 7.20 Martian Ascent Trajectory
Velocity and Altitude Histories
NASA Model 2 (25 mb) Atmosphere

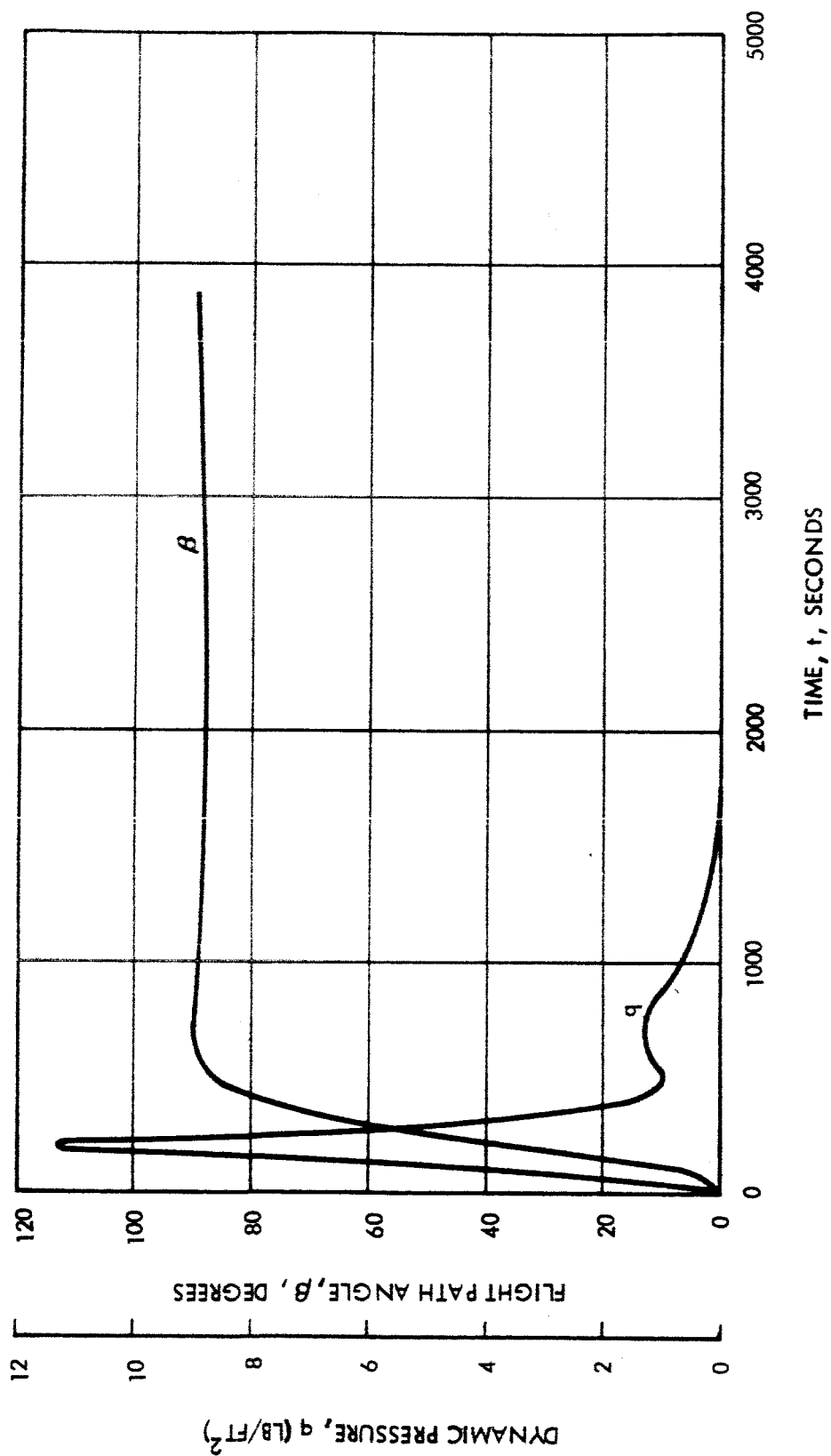


Figure 7.21 Martian Ascent Trajectory
Dynamic Pressure and Flight Path Angle Histories
NASA Model 2 (25 mb) Atmosphere

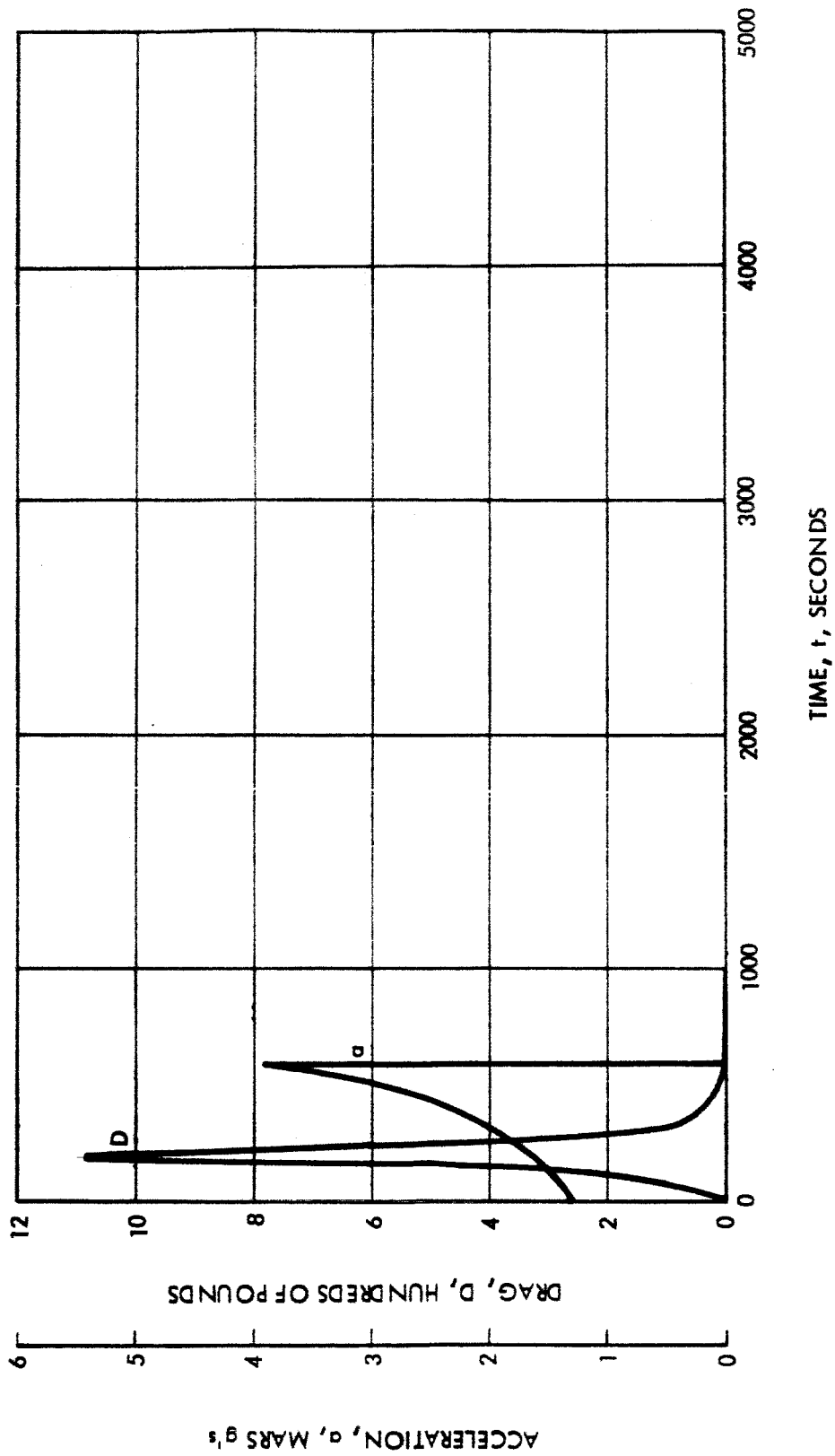


Figure 7.22 Martian Ascent Trajectory
Acceleration and Drag Histories
NASA Model 2 (25 mb) Atmosphere

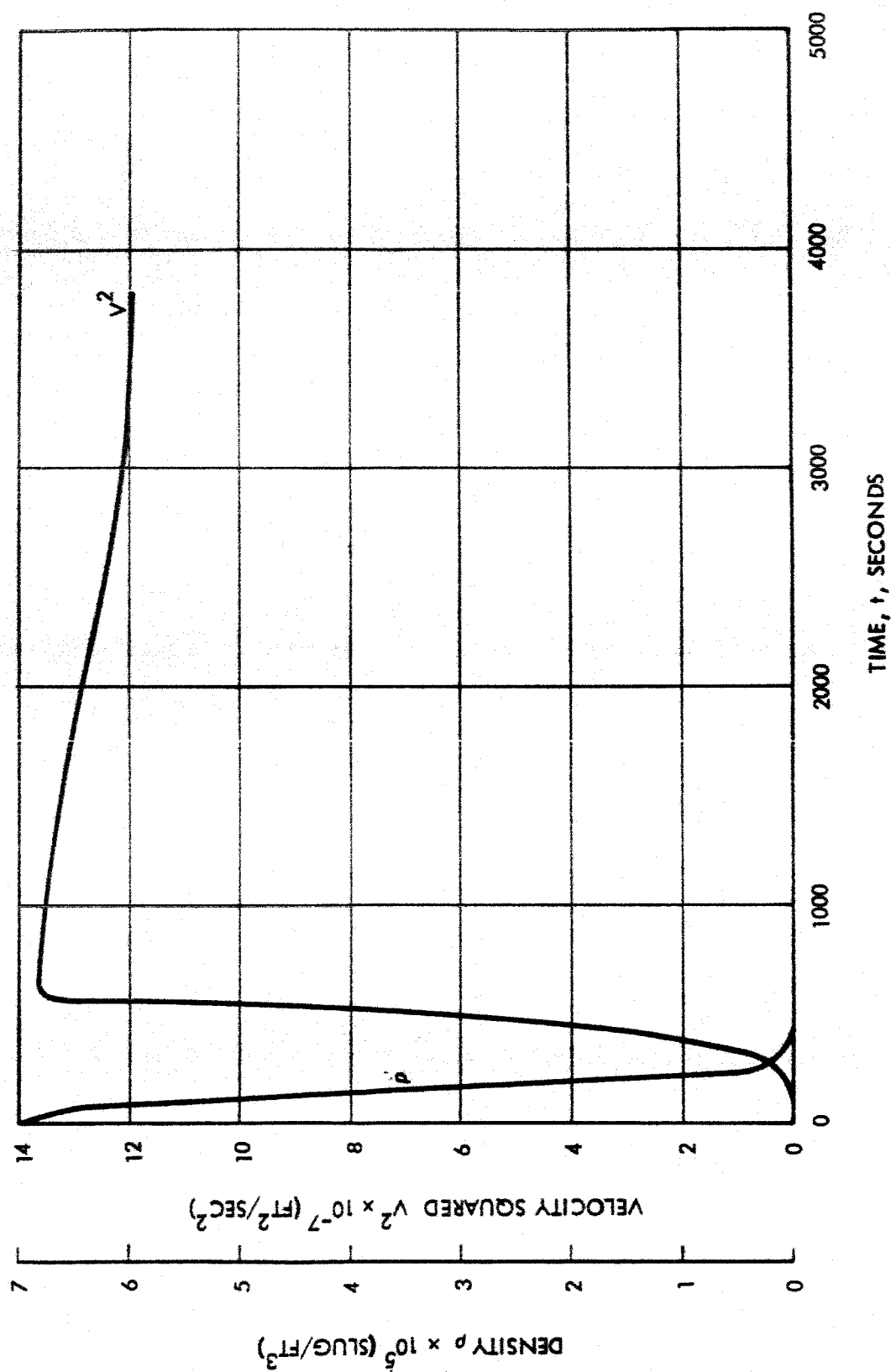


Figure 7.23 Martian Ascent Trajectory
Density and Velocity Squared Histories
NASA Model 2 (25 mb) Atmosphere

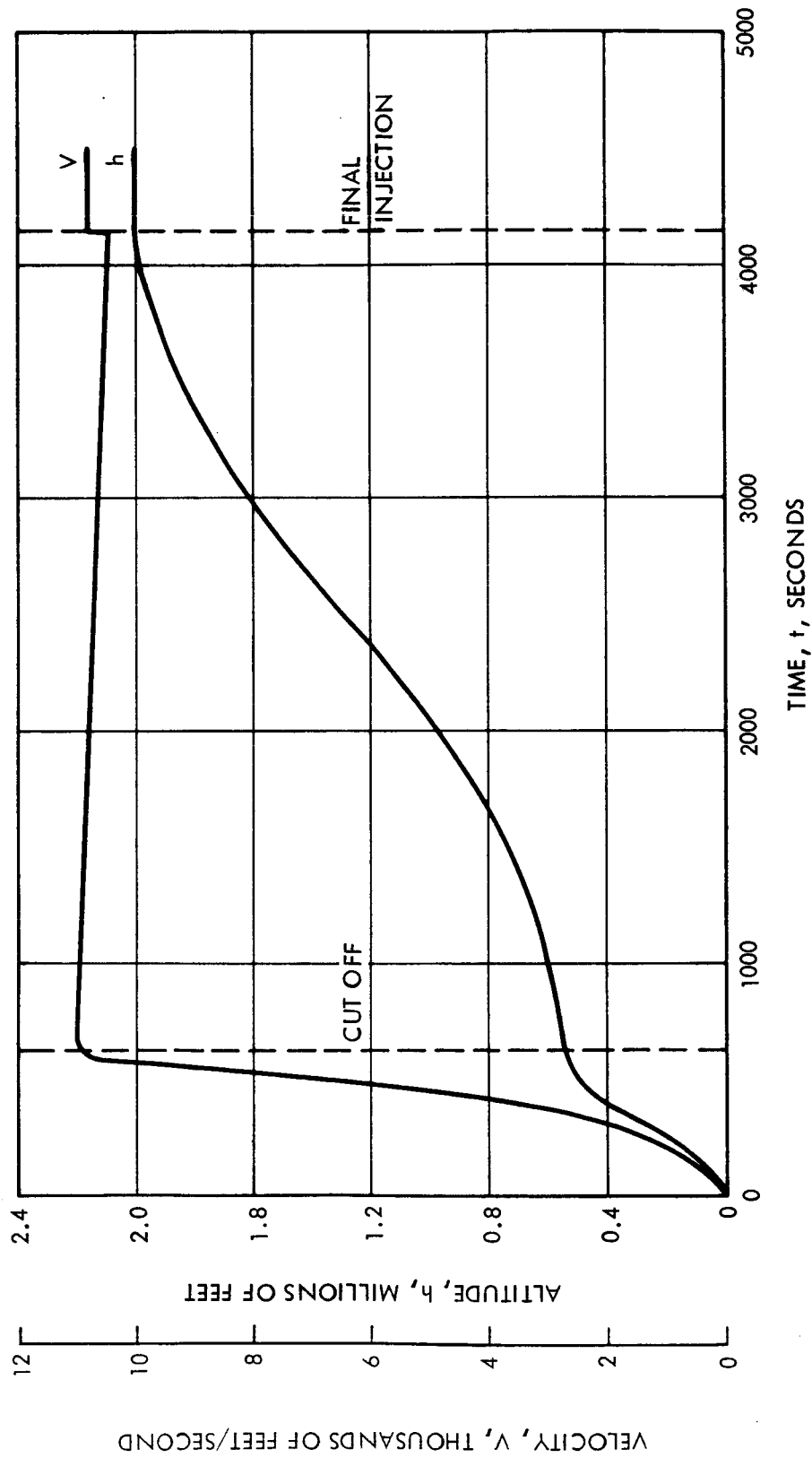


Figure 7.24 Martian Ascent Trajectory
Velocity and Altitude Histories
Schilling Model II (132 mb) Atmosphere

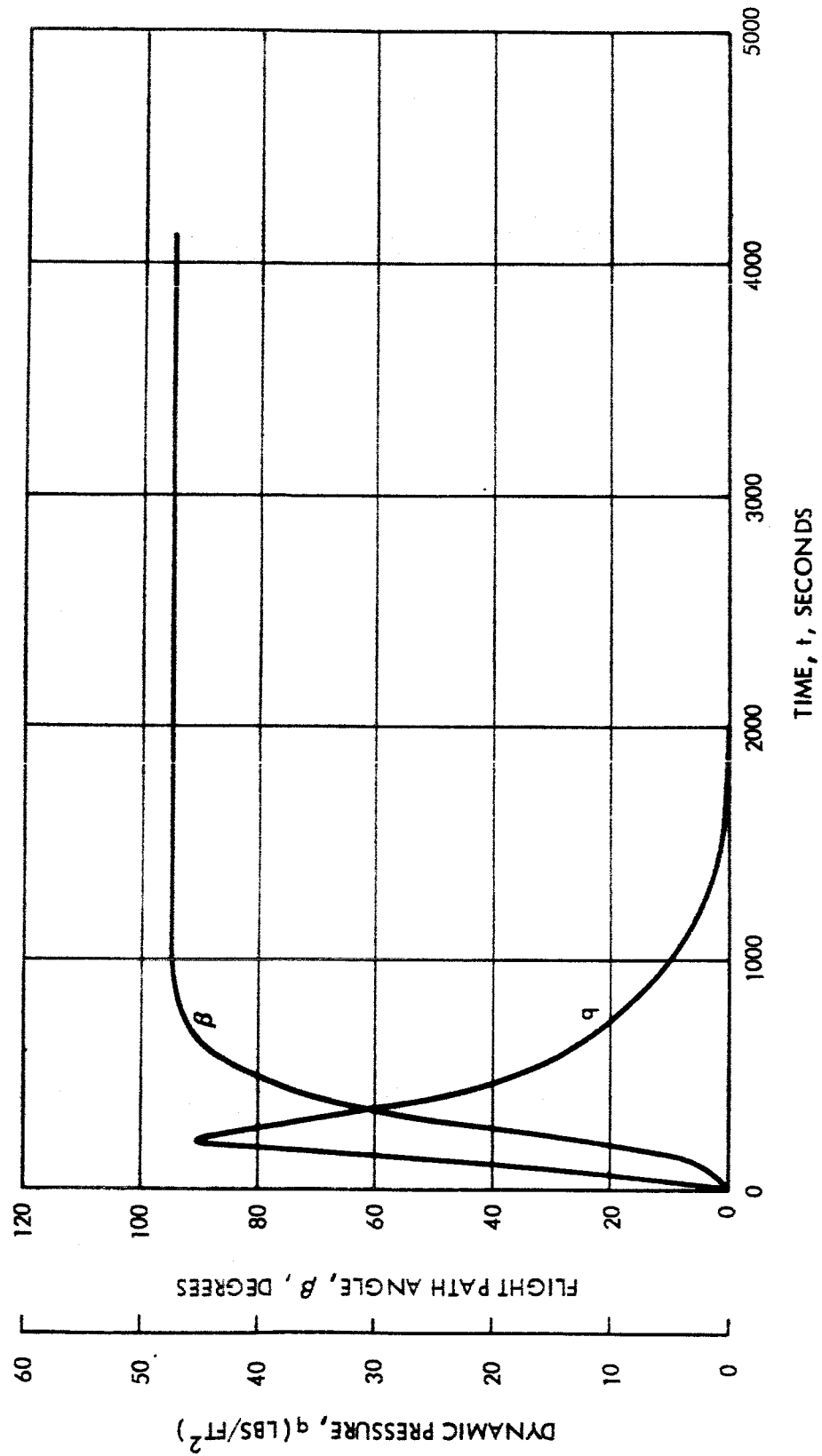


Figure 7.25 Martian Ascent Trajectory
Dynamic Pressure and Flight Path Histories
Schilling Model II 9132 mb) Atmosphere

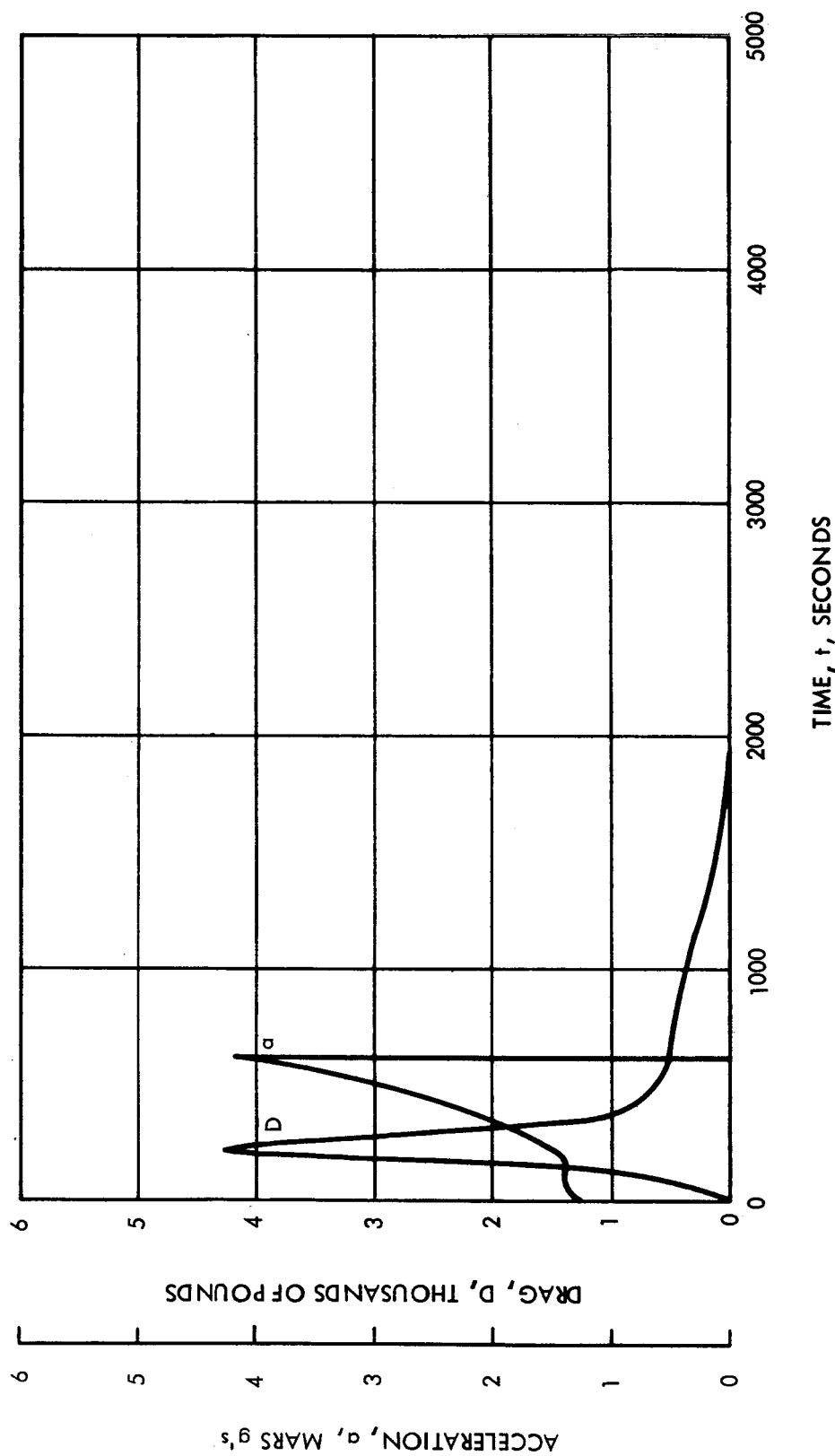


Figure 7.26 Martian Ascent Trajectory
 Drag and Acceleration Histories
 Schilling Model II (132 mb) Atmosphere

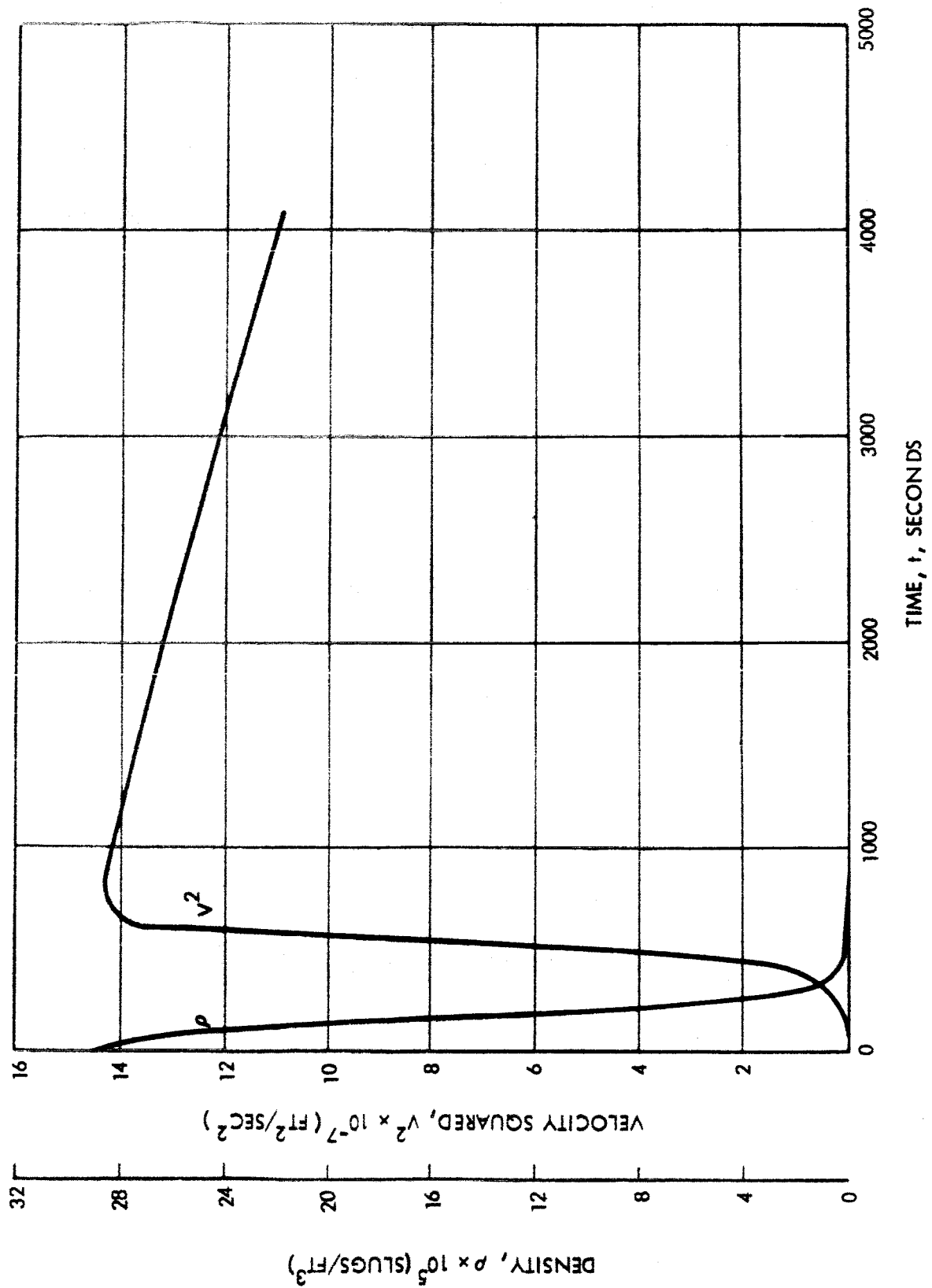


Figure 7.27 Martian Ascent Trajectory
Density and Velocity Squared Histories
Schilling Model II (132 mb) Atmosphere

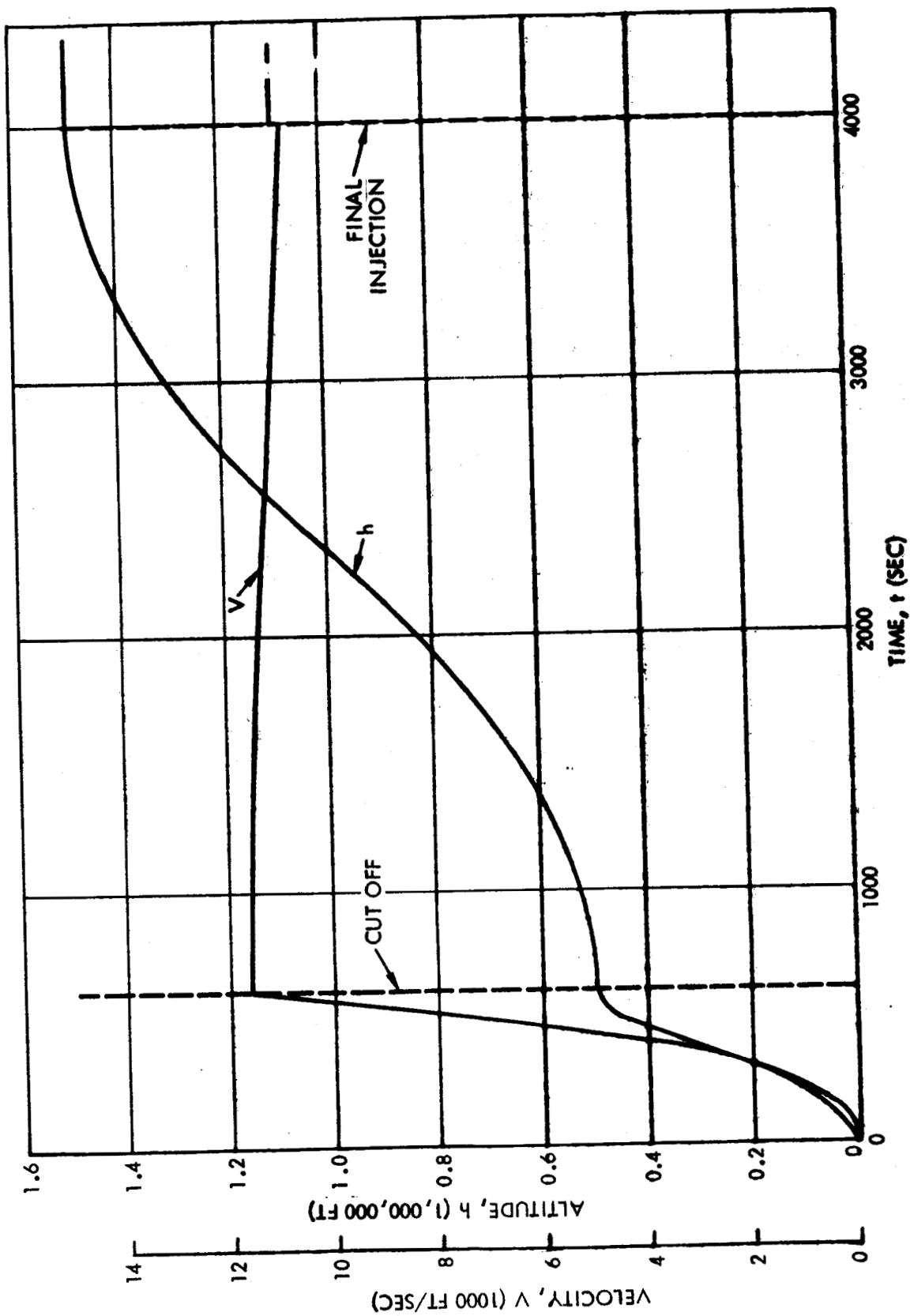


Figure 7.28 Martian Ascent Trajectory Velocity and Altitude Histories
Hybrid Atmosphere Model

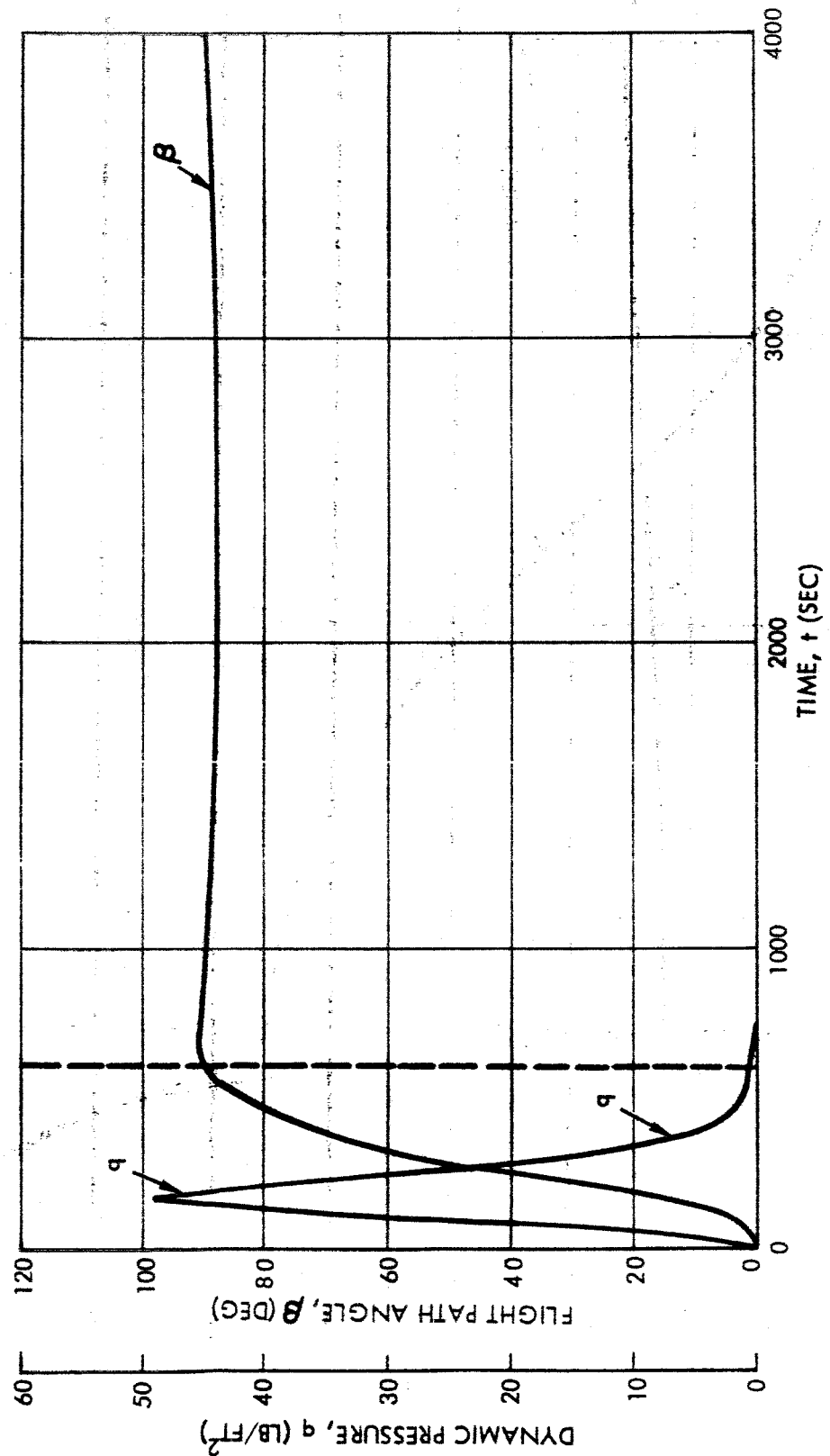


Figure 7.29 Martian Ascent Trajectory Dynamic Pressure and Flight Path Angle Histories
Hybrid Atmosphere Model

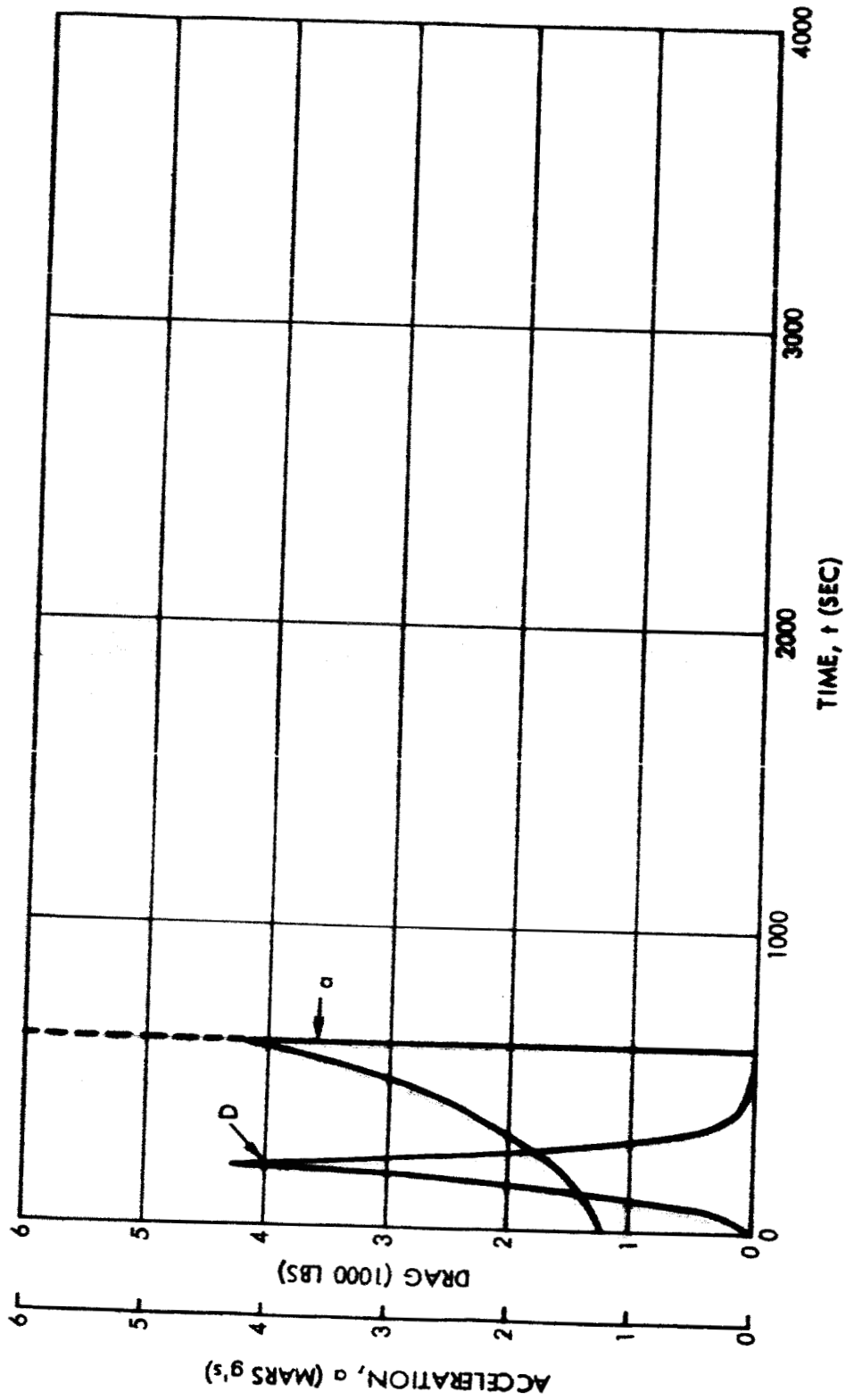


Figure 5.30 Martian Ascent Trajectory Acceleration and Drag Histories
Hybrid Atmosphere Model

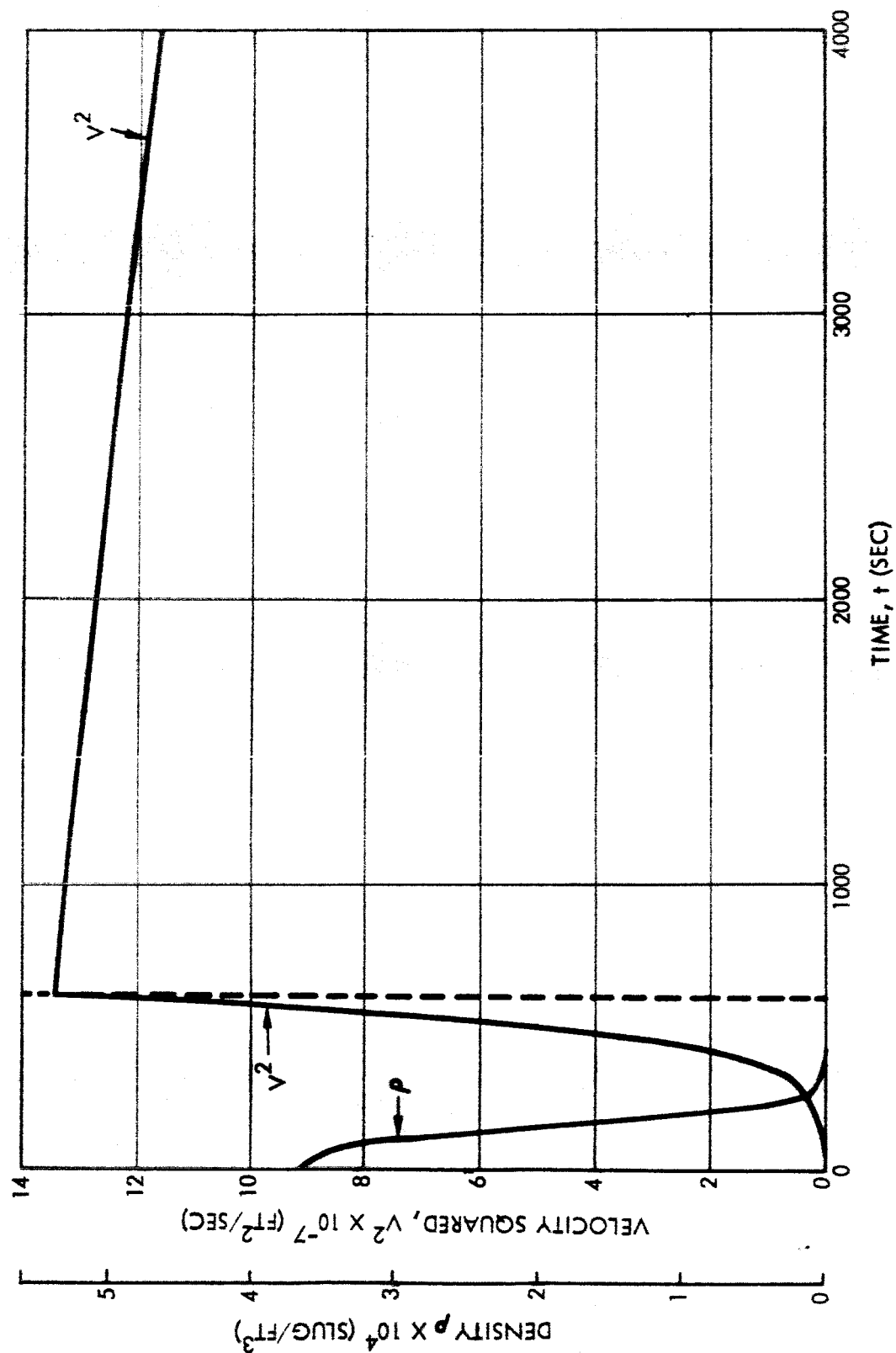


Figure 7.31 Martian Ascent Trajectory Density and Velocity Squared Histories
Hybrid Atmosphere Model

a complete Mollier diagram and equilibrium gas properties are available for it. Differences in composition will introduce minor changes in electron generation.

Inviscid Electron Generation

For the initial set of calculations it was assumed that the Mars Lander had a 10-inch diameter nose cap. This cap produces a strong shock, which in turn creates a significant amount of electrons at the stagnation point ($\sim 2 \times 10^{13}$ electrons/cc). On expansion to free-stream pressure, the inviscid electron concentration on the cylindrical portion of the lander, where the antenna window is located, is reduced to approximately 2×10^6 electrons/cc. Thus, no attenuation over the antenna is expected from the inviscid plasma at zero angle of attack.

At angles of attack, it was assumed that the pressure of the antenna window was equal to that experienced by an equivalent cone, which is defined as a cone with half angle equal to the angle of attack of the lander. The higher pressures give rise to higher electron densities since expansion from the stagnation condition is less. Thus, at an angle of attack of 15° , the expansion process is limited, such that 1.5×10^{11} electrons/cc are present at the antenna window. Blackout is assumed to occur at an angle of attack of 13° .

For the second set of calculations the Mars Lander was assumed to consist of a 30° cone, followed by the cylindrical section, where the antenna window is located. For this configuration, the electron concentration is significantly reduced. For example, at zero angle of attack the density at the antenna window is reduced to less than 10^4 electrons/cc. With a 30° cone instead of a spherical nose, the maximum angle of attack can be increased to 21° before any attenuation due to inviscid electron generated is experienced.

Boundary Layer Electron Generation

Although the Reynolds number (based on free stream conditions and the distance from the forward stagnation point to the location of the antenna window) is 4×10^7 , a turbulent boundary layer was assumed to exist at the window. This assumption is conservative. However, for a cold wall the ratio of peak to edge static enthalpy is 2 for turbulent boundary layers, while for a laminar boundary layer this ratio is 1.4. Hence, the difference in electron generation is not significant for present purposes.

For a Mars Lander with a 10-inch spherical nose cap, the maximum angle of attack before the critical electron density is realized is reduced from 13° to $5\frac{1}{2}^{\circ}$. With the 30° conical nose, the angle of attack at blackout is 15° . The $5\frac{1}{2}^{\circ}$ maximum angle of attack is believed to be too limited from the standpoint of maneuvering, while the 15° limit is more representative.

Electron Generation Due to Ablation Products

Since the Mars Lander is not assumed to decelerate during entry, it is expected that little ablation will occur with a 30° conical nose. Therefore, no attempt was made to account for the increase in peak boundary layer electron concentration due to contaminants, and the maximum tolerable angle of attack is taken from the uncontaminated calculation.

However, even with ablation, if the low ionization potential contaminants (e.g., sodium, potassium, and calcium) are kept to a minimum, the increase in electron concentration due to ablation products will be small.

Conclusions

With the assumption that blackout is attained as soon as any part of the plasma of the antenna window reaches the critical electron density, it is concluded that:

1. A spherical nose limits the maximum tolerable angle of attack to $5\frac{1}{2}^{\circ}$, which is not acceptable for maneuvering.
2. A 30° conical nose increases the maximum of 15° , which is more than adequate.

7.5 Power Breakdown of Antennas in Martian Atmosphere

Section 5 establishes a theoretical model Martian atmosphere and anticipated electrical CW breakdown power densities for the Martian surface pressure of 10 millibars and a theoretical electron density of 10^6 electrons per cubic centimeter. The power densities are:

<u>Frequency, mc</u>	<u>Breakdown Power Density (w/cm²)</u>
10,000	500
3,000	40
1,000	6

Estimates have been made concerning the likelihood of power breakdown in an antenna system consisting of a 3-foot parabolic reflector which is transmitting 20 watts CW at 2300 mc, and is located on the Martian surface.

The breakdown power density values listed above have been plotted in Figure 7.32 to allow interpolation to the 2300 mc frequency. The breakdown power density obtained through this technique is approximately 19 watts/cm².

In a 3-foot diameter parabola antenna system, the feed device will contain the highest density of r.f. power. Since the feed is not specified, it has been assumed that it will consist of a pyramidal horn which is fed by waveguide, which, in turn, is energized through a coaxial-to-waveguide transition.

The waveguide-to-coaxial transition will essentially consist of a monopole configuration, which has been treated by Scharfman and Morita (7.7).

The electric field at the tip of a monopole may be determined from:

$$E_t = \frac{91 I(O)}{a \sin \beta h} \text{ V/cm}$$

where

$$I(O) = \text{the current at the input terminal of the monopole} = \sqrt{\frac{P}{Z}} \quad P = 20 \text{ watts, } Z = 50 \text{ ohms.}$$

$$a = \text{the radius of the monopole, cm.}$$

$$\beta h = \text{monopole height, in wavelengths.}$$

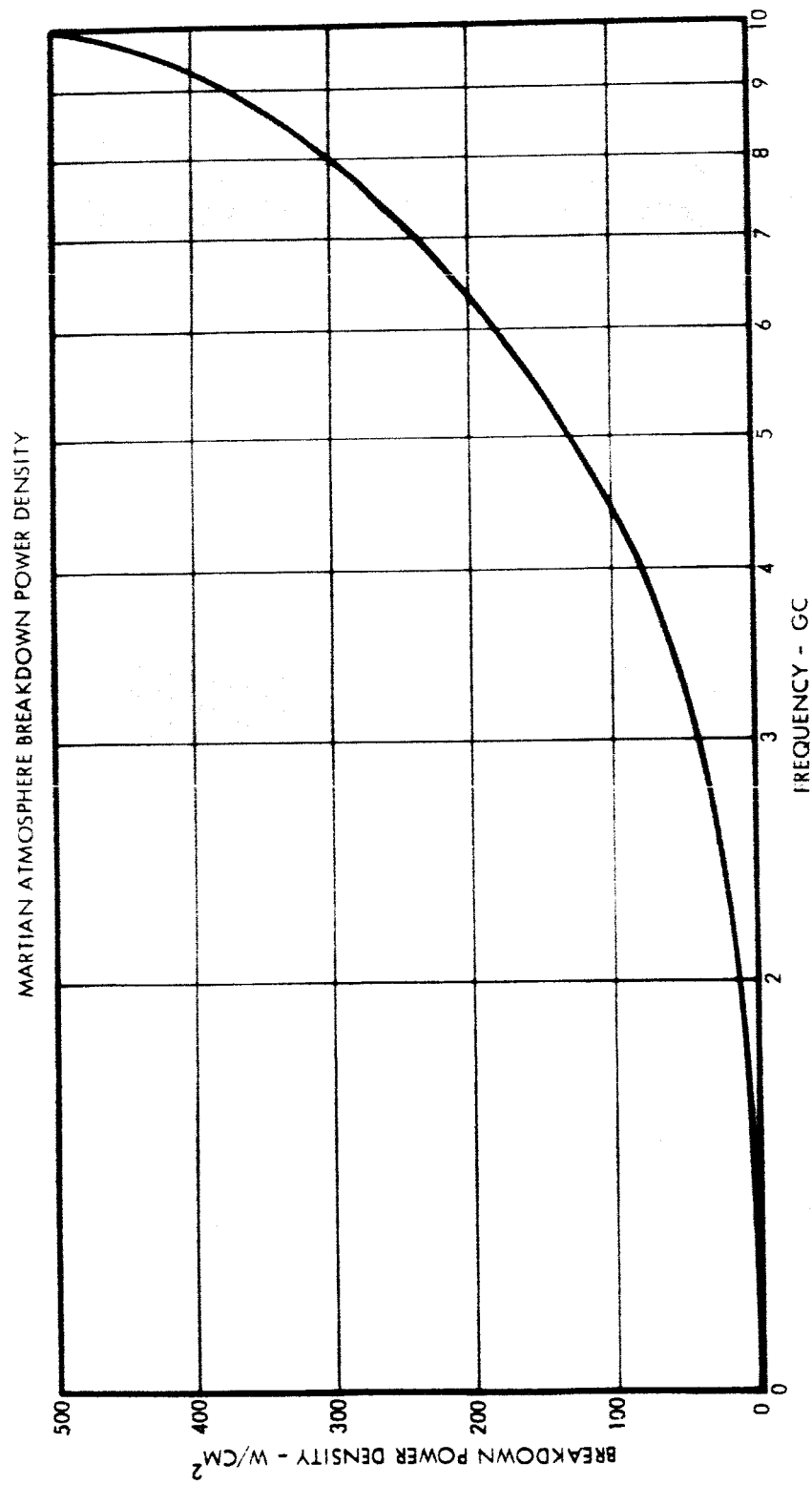


Figure 7.32 Martian Atmosphere Breakdown Power Density

For the case of $\beta h = \frac{\lambda}{4}$, $P = 20$ watts, $Z = 50$ ohms, $a = 0.0625$ in.

$$E_t = \frac{91 \sqrt{\frac{20}{50}}}{0.0625 \times 2.54 \sin 90^\circ}$$

$$E_t = 3.62 \text{ V/cm}$$

If this voltage density occurs inside a rectangular waveguide, WR 430, in which the characteristic impedance:

$$K = \frac{754 \frac{b}{a} \frac{\lambda_g}{\lambda_o}}{\lambda_o} = 754 \times 1.246 \times 0.5 = 470 \text{ ohms}$$

where

$$\frac{b}{a} = 0.5$$

$$\frac{\lambda_g}{\lambda_o} = 1.246 \text{ at } 2300 \text{ mc}$$

the corresponding power density is

$$P = \frac{E^2}{K} = \frac{(36.2)^2}{470} = 2.79 \text{ watts/cm}^2$$

This is nearly an order of magnitude less than that power density required to initiate breakdown. This will be the region of maximum power density in the feed system. It is concluded that there is little likelihood of antenna breakdown due to the presence of an ionization layer near the surface of Mars.

8. SURFACE MOBILITY

8.1 Typical Surface Rover Design

The early manned Mars mission can be expected to have at least limited surface mobility about the MEM landing site. While it is difficult at the present time to establish traverse range requirements for surface rovers, the gross surface features of Mars indicate that traverse ranges of a few hundred kilometers would provide opportunities for worthwhile junkets about the main landing site. More practically, the limited duration of the landing operation, which will not exceed one to two weeks for the initial missions because of overall mission trajectory constraints, will prevent extensive traverses about the main base. Traverse speed probably will be limited to 5 or 6 mph because of surface terrain conditions, and considerable time will be devoted to scientific examinations of surface phenomena. Hence, an upper limit of several hundred kilometers traverse range seems reasonable.

Many surface rover designs have been proposed for lunar explorations, and representative designs can be selected for application to the Mars landings. Assuming that a 3-man crew will be landed on the surface, a 2-man rover, capable of sustaining a 2-3 day traverse, should be provided, including modest experiment equipments, life support, communications, and navigation subsystems. It may be expected that a limited payload capacity will be required to return scientific samples to the main base.

A design meeting the above requirements is shown in Figure 8.1. A weight statement and pertinent design details are given in Table 8.1. The vehicle is designed for a nominal traverse speed of 5 mph. A fuel cell power supply is significantly superior to competitive systems, and is incorporated in the selected design.

8.2 Environmental Factors

The design described in Figure 8.1 will be examined for its sensitivity to the environmental factors on the Martian surface. The environmental factors of interest to the design and performance of the surface rover are:

Soil properties

- Frictional
- Cohesive
- Sinkage (or bearing)

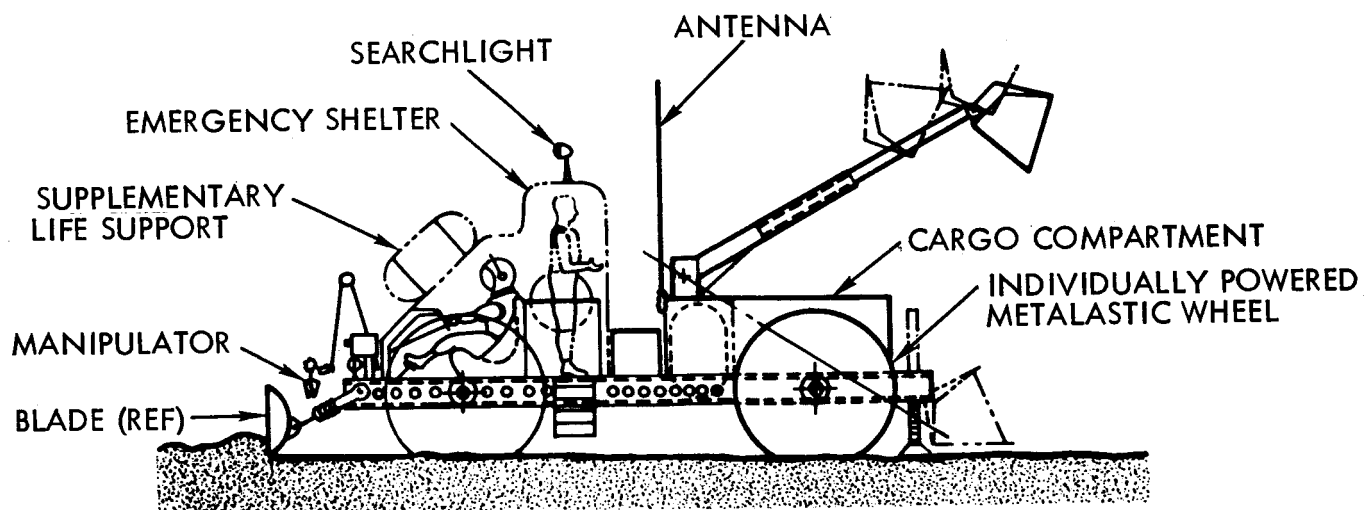
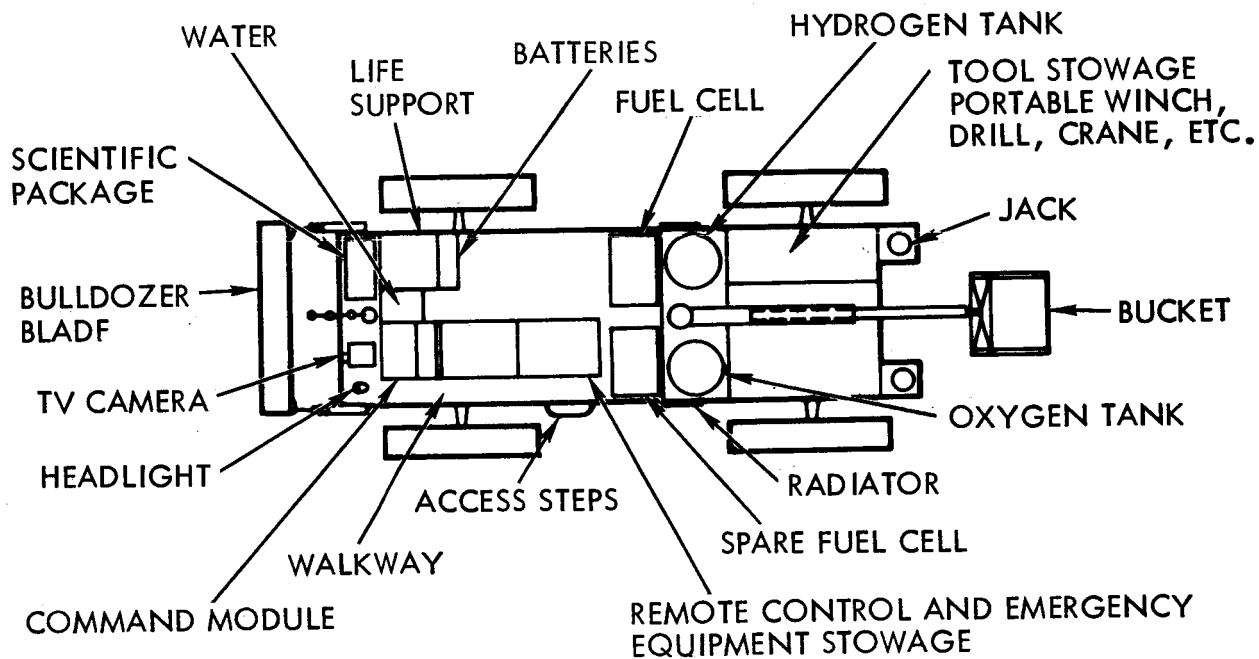


Figure 8.1 Surface Rover

TABLE 8.1 SURFACE ROVER CHARACTERISTICS
(Reference 8.1)

DESIGN FEATURES SUMMARY

1. Power supplied by one-kw hydrogen-oxygen fuel-cell system, tankage designed for one-year storage
2. Locomotion results from four individually powered metalastic wheels having an effective diameter of 150 in.
3. Chassis consists of a stiffened aluminum shell structure designed to support all landing loads in the stowed position and the dynamic loads of a 1500-lb payload during lunar operation
4. No deployment aids (assuming a 30-in. bus height), pallet or support structure are required of the bus
5. Vehicle is controlled remotely from MEM, and directly by man on vehicle (with and without a shelter)
6. Navigation and guidance system is capable of defining the vehicle's position to ± 1000 ft
7. Vehicle is capable of night and day operation

WEIGHT SUMMARY (MANNED VERSION)

Communications and instrumentation	200 lb
Power supply (inert weight of one-kw fuel cell)	150
Structure	240
Wheels, motors and transmissions	360
Guidance and control	80
Hold-down structure to bus	20
Life support equipment	
Fixed	50 lb
Variables	78
Two back packs	50
	178
Fuel and tankage (135 kw-hr, 120-lb reactants)	<u>272</u>
TOTAL	1500 lb

Features

- Crevices
- Bumps
- Obstacles
- Slope

Solar Cosmic Radiation

Atmosphere

- Temperature
- Density

Meteorology

- Winds
- Dust

Several environmental factors can be assessed quantitatively by determining their effects on system design and weight. In particular, soil properties and terrain features can be evaluated readily, but the effects of general meteorological factors such as dust can be discussed only in qualitative terms. Other interactions such as the effect of atmospheric pressure on the life support system are tedious to analyze in detail, and have a predictably small effect on overall system design. These interactions will not be treated in detail, although comments are made as to their general significance.

8.3 General Mobility Analysis¹

A surface rover of the general type described in Figure 8.1 must be designed so that it has sufficient traction power to overcome surface resistance, including obstacles, slopes, crevices, etc., and the soil can support its weight.

Traction Force

The general traction load carrying capacity of the soil is usually described in terms of its cohesion and friction characteristics, as illustrated in the following sketch.

1. The analyses in this section are based on References 8.2 and 8.3. Figures 8.2 - 8.8 and 8.12 - 8.14 are taken from these texts.

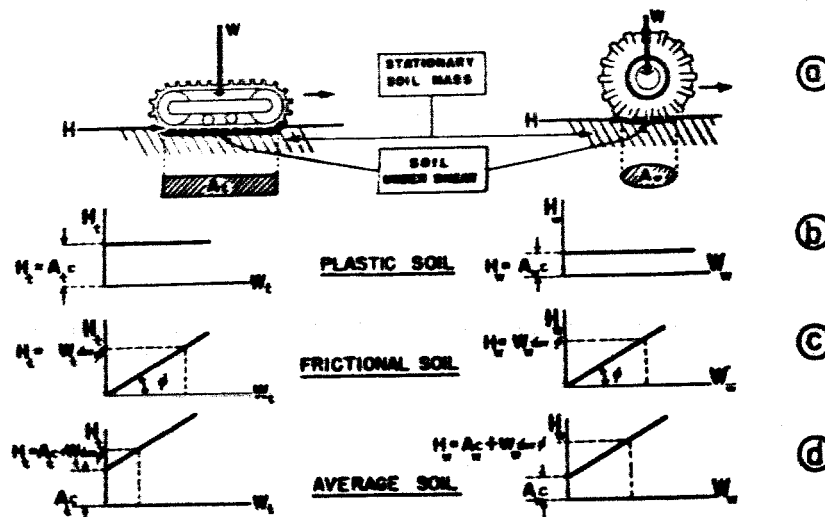


Figure 8.2 Soil Shear

The track or wheel develops a force, H , when loaded with a weight, W , due to the shearing strength of the soil. This force, H , is the gross tractive effort of the device. In plastic soils the tractive force H is essentially independent of the weight, whereas in purely frictional soils, the tractive force is directly proportional to the weight. Generally, a soil exhibits a combination of cohesive and frictional properties, as shown in part (c) of the figure. The total tractive force available is:

$$H = A_c + W \tan \phi$$

where ϕ is the so-called angle of friction. Test techniques for determining the values of c and ϕ for various soils is well established, and suffice to analyze soil stability characteristics, and traction capabilities of vehicles operating over these soils.

Flotation (Weight Bearing Capacity)

Whereas the parameters c and ϕ determine the traction capacity of a soil, additional parameters are required to determine the flotation, or weight bearing capacity, of the soil. The additional parameters are γ , the density of the soil, and b , the width of the track or tire of the vehicles. The equation giving the safe load that can be supported by soil is:

$$W_s = A (c N_c + \gamma z N_q + \frac{1}{2} \gamma b N_\gamma)$$

where A is the total foot-print area, z is the initial sinkage, and N_c , N_q and N_γ are constants which depend upon ϕ , the friction angle. Values for these constants are given in Figure 8.3.

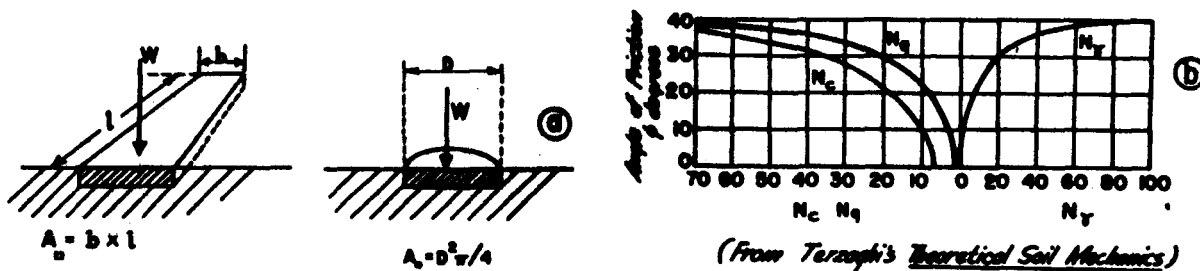


Figure 8.3 Soil Bearing Capacity

If sinkage is restricted to small values, so that the vehicle is prevented from breaking through the surface, the equation for safe loads becomes:

general conditions	$W_s = A c N_c + \frac{1}{2} A b \gamma N_\gamma$
cohesionless soil ($C = 0$)	$W_s = \frac{1}{2} A b \gamma N_\gamma$
frictionless soil ($\phi = 0$)	$W_s = A c N_c$

and the corresponding safe ground pressures for general conditions:

$$p = c N_c + \frac{1}{2} \gamma b N_\gamma$$

The latter equation can be modified slightly to account for non-rectangular plan forms.

It is important to note that the safe loads or ground pressures are not solely functions of soil properties. The shape of the track or tire has an important effect on the total weight or ground pressure that can be supported by a soil. Only in a strictly frictionless soil is the safe load independent of planform.

The above equations define the nature of flotation, which is a function of soil properties c , ϕ , and γ , and planform properties A and b . If the safe loads as determined by the above relations are exceeded, the vehicle breaks through to subsurface levels, and another set of soil values is required to determine the amount of sinkage, and the resistance of the soil to the movement of the vehicle. Generally speaking, off-road vehicles are faced with the problem of appreciable sinkage, and must be designed to overcome soil resistances encountered under these conditions. In this case, the concept of "flotation" is not well defined, and safe load must be defined in terms of allowable

sinkage. The case with appreciable sinkage is analyzed in the following paragraphs.

Safe Loads with Sinkage

If a track or tire is forced into the ground, the relationship between ground pressure, p , and sinkage depth, z , take the following form

$$p = k z^n$$

where k is function of soil properties and planform, and n is a coefficient of deformation. The factor k has been shown to take the form

$$k = B/b + C$$

where B and C are determined by the soil properties, and b is the track or tire width, as before. Extensive testing has shown good correlation of the above equation with load - sinkage test data. Typical sinkage test results are shown in Figure 8.4.

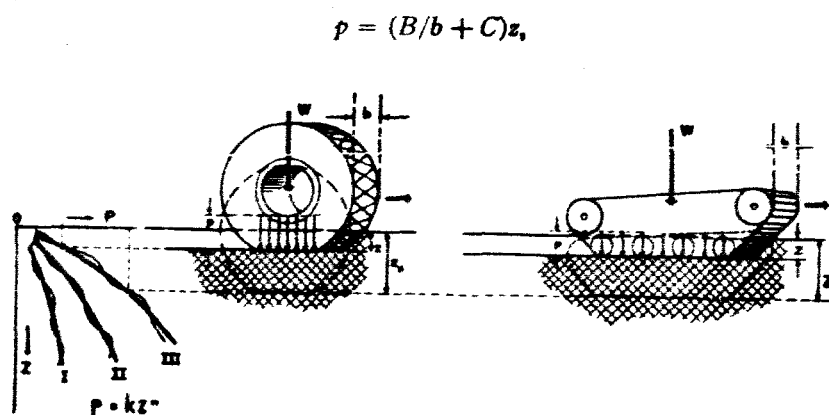


Figure 8.4 Load Sinkage Curves

The expression for the ground pressure becomes:

$$p = (k_c/b + k_\phi) z^n$$

This equation can be used to determine safe ground pressures or loads by specifying the allowable sinkage, which in turn is limited by the traction available to overcome resistance, and by chassis clearance.

We are thus led to the concept of general trafficability, which allows the designer to achieve a proper balance between traction capability and resistance.

If we subtract the rolling resistance from the traction force, the net drawbar pull capability can be derived. The net drawbar pull capability is an indication of the excess power the vehicle possesses for acceleration, and for negotiating bumps, slopes and crevices.

Before presenting the relations for net drawbar pull, a suitable expression for rolling resistance is required. Consider the following sketch:

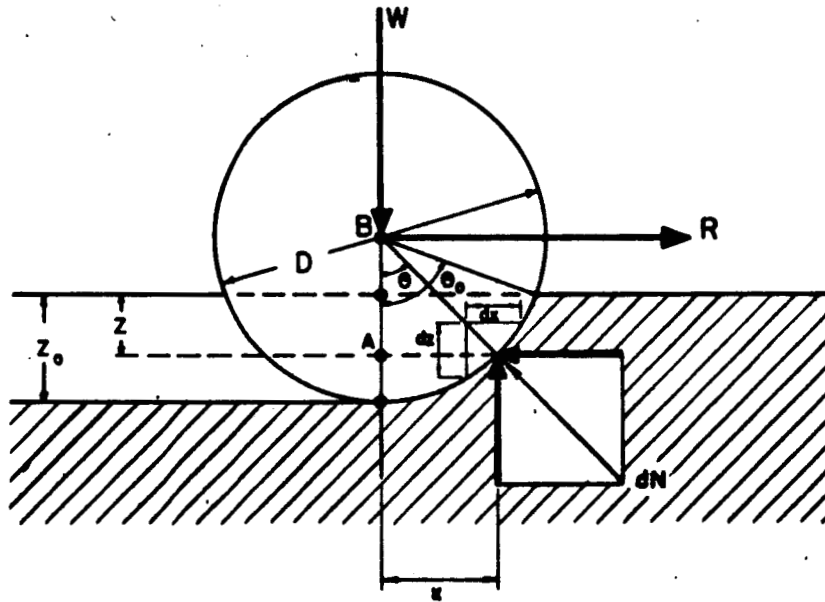


Figure 8.5 Relations for Rolling Resistance

The work spent in compressing the soil under the wheel to a depth z_0 is:

$$\begin{aligned}
 L &= \int_0^{z_0} p \, dz = \int_0^{z_0} k z^n \, dz \\
 &= k \frac{z_0^{n+1}}{n+1}
 \end{aligned}$$

If the distance rolled is ℓ and the width of the wheel is b , the work of compression is $Lb\ell$, and the work of traction is $R\ell$. Equating these gives

$$\begin{aligned}
 R &= Lb \\
 &= k b \frac{z_0^{n+1}}{n+1}
 \end{aligned}$$

$$\text{where } k = k_c/b + k_\phi$$

The wheel dimensions can be introduced into the above expressions by analyzing the free body diagram of Figure 8.5 in terms of load N and diameter D .

$$R - \int_0^{\theta_0} dN \sin \theta = 0$$

$$-W + \int_0^{\theta_0} dN \cos \theta = 0$$

where

$$dN \cos \theta = -p b dx$$

$$dN \sin \theta = p b dz$$

Integrating the above expressions and solving for the load gives

$$W = \frac{b k D z_0}{3} z_0^n (3-n)$$

$$z_0 = \frac{3W}{3-n} \frac{1}{b k D}^{\frac{2}{2n+1}}$$

By eliminating z_0 from the expressions for R and W , we can solve for R in terms of soil properties and planform dimensions:

$$R = \frac{1}{(3-n)^{\frac{2n+2}{2n+1}} (n+1) (k_c + b k_\phi)^{\frac{1}{2n+1}}} \left(\frac{3W}{D} \right)^{\frac{2n+2}{2n+1}}$$

$$= \frac{0.86}{\sqrt[3]{k_c + b k_\phi}} \frac{W^{4/3}}{D^{2/3}} \quad (n = 1)$$

$$= \frac{0.876}{k_c + b k_\phi} \frac{W^{3/2}}{D^{3/4}} \quad (n = 1/2)$$

The value of $n = 1/2$ is applicable to sandy type soils. For a rigid plate or track, the appropriate expression is

$$\begin{aligned}
 R &= \frac{1}{(n+1) (k_c + b k_\phi)^{1/n}} \left(\frac{W}{\ell} \right)^{\frac{n+1}{n}} \\
 &= \frac{0.5}{(k_c + b k_\phi)} - \left(\frac{W}{\ell} \right)^2 \quad (n = 1) \\
 &= \frac{0.667}{(k_c + b k_\phi)^2} \left(\frac{W}{\ell} \right)^3 \quad (n = 1/2)
 \end{aligned}$$

Net Drawbar Pull

The expression for net drawbar pull can now be set down as follows for a wheel:

$$\begin{aligned}
 DP &= H - R \\
 &= A c + W \tan \phi - \frac{1}{(3-n)^{\frac{2n+2}{2n+1}} (n+1) (k_c + b k_\phi)^{\frac{1}{2n+1}}} \left(\frac{3W}{D} \right)^{\frac{2n+2}{2n+1}}
 \end{aligned}$$

For a cleated track, the above expression becomes

$$\begin{aligned}
 DP &= 2 b \ell c \left(1 + \frac{2h}{b} \right) + (W \tan \phi) \left\{ 1 + 0.64 (h/b) \cot^{-1} (h/b) \right\} - \\
 &\quad \left[\frac{2}{(n+1) (k_c + b k_\phi)^{1/n}} \right] \left[\frac{W}{2\ell} \right]^{\frac{n+1}{n}}
 \end{aligned}$$

where a factor of 2 has been included to account for the two tracks. The term h , is the height of the spud or cleat.

The bulldozing resistance is not included in the above expressions. This factor can be important in certain types of soils, and can be approximated by the following expression:

$$R_b = \frac{b \sin(\alpha + \phi)}{2 \sin \alpha \cos \phi} \left[2 z c K_c + \gamma z^2 K_y \right]$$

where

$$K_c = (N_c - \tan \phi) \cos^2 \phi$$

$$K_y = \left[\frac{2 N_y}{\tan \phi} + 1 \right] \cos^2 \phi$$

$$\alpha = \cos^{-1} (1 - 2z/D)$$

The drawbar pull performance of the vehicle shown in Figure 8.1 will be explored parametrically in Section 8.6, however, the general deterioration of the vehicle trafficability in soft soils is shown in Figures 8.6 and 8.7. Figure 8.6 shows the comparative performance of various types of vehicles within given soil spectrums. The soil properties used correspond approximately to those of sandy loam. It can be seen that net drawbar pull decreases very rapidly in weak soils. Vehicles designed for stronger soils would be hopelessly bogged down if they encountered weak soils. Uncertainties in soil properties thus force the vehicle designer to provide for the worst case, although range penalties may be incurred by doing so.

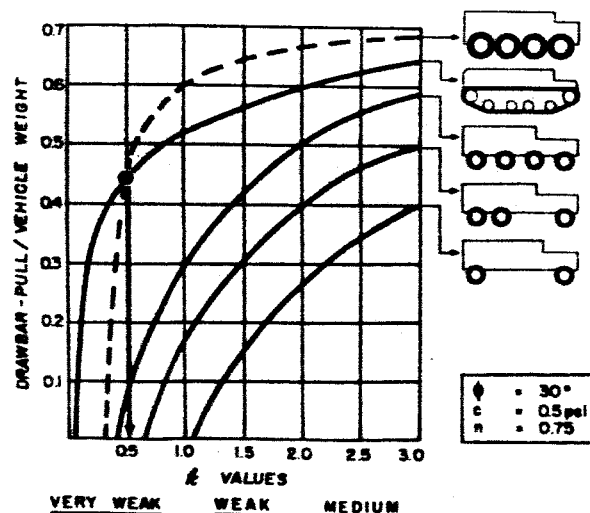


Figure 8.6 Comparative Performance of Various Types of Vehicles Within Given Soil Spectrum

This point is further illustrated in Figure 8.7, which shows the effect of track width on drawbar pull. Again, lack of knowledge of the soil conditions will force the designer to provide for weak soil capability.

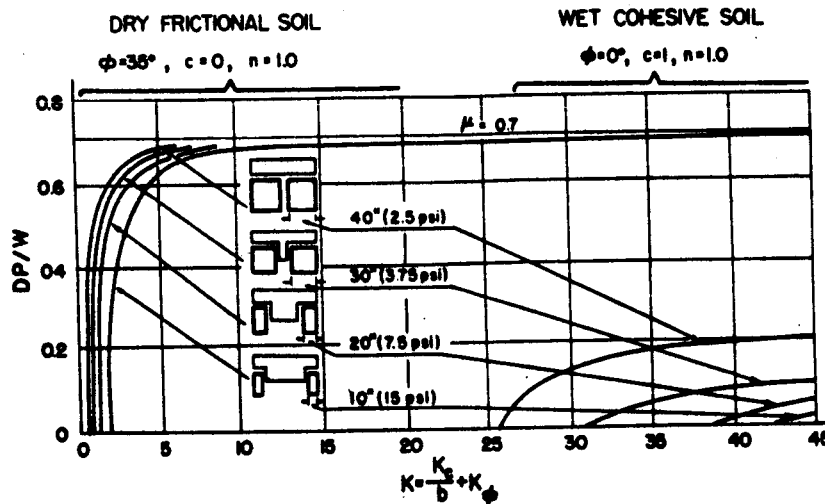


Figure 8.7 The Effect of Track Width on Performance

General approaches to vehicle design for various types of soil are shown in Figure 8.8.

8.4 Typical Soil Properties

Typical soil properties are given in Table 8.2.

TABLE 8.2 TYPICAL SOIL PROPERTIES

	Dry Sand	Natural Sandy Loam	Heavy Clay	Sandy Loam 19% Moisture	Firmly Settled Silt	Snow
ϕ (degrees)	31	30	20	36	10	18
c (psi)	0	1.1	1.5	0.6	6.5	0.1
k_{ϕ}	3.3	1.5	32.0	9.0		0.3
k_c	0	1.4	13.5	20.0		3.6
n	1.0	0.3	0.5	0.16		1.0
γ (lbs/cuin)	0.06					











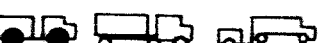
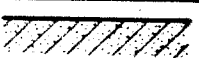

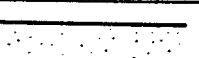
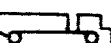
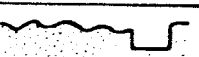



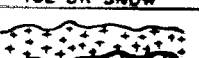
VEHICLE TYPE	MECHANICAL FEATURES OF SOIL MASS	GEOMETRY OF SOIL SURFACE
	 PAVED ROAD	IDEALLY SMOOTH
	 HARD GROUND	UNDULATORY IRREGULAR OBSTACLES
	 HARD GROUND	WALL AND DITCH TYPE OBSTACLES
	 COMPACT HARD SOIL	FLAT SURFACE
	 COMPACT HARD SOIL	UNDULATORY IRREGULAR
	 SOFT SOIL	FLAT SURFACE
	 LOOSE SOIL	
	 SOFT OR LOOSE SOIL	UNDULATORY IRREGULAR OBSTACLES
	 ICE OR SNOW	SMOOTH OR UNDULATORY
	 SNOW	ROUGH OBSTACLES

Figure 8.8 Approaches to Vehicle Design for Various Soil and Terrain Conditions

8.5 Vehicle Performance

Range Sensitivity

The range performance of the vehicle shown in Figure 8.1 will be analyzed and its sensitivity to soil and planform properties established.

The range of the vehicle is given by the following equation, assuming that the weight of the vehicle remains constant (the water generated by the fuel cell is kept on board for life support purposes):

$$\text{Range} = \left[\frac{W_f (\text{SFC}) \eta}{\frac{R V}{738} + k w_e \eta} \right] \frac{V}{1.098} \quad (\text{km})$$

where

W_f	=	Weight of fuel, lbs
SFC	=	kw - hr per lb of fuel
η	=	Mechanical and traction efficiency
R	=	Resistance
V	=	Vehicle velocity, fps
kw_e	=	Electric power for non-propulsion purposes

The resistance term includes that due to compression of the soil, bulldozing, negotiation of slopes, and negotiation of bumps. The expressions for compression and bulldozing resistance have been given; that due to negotiation of slopes and bumps is:

$$R_s = W \sin \theta \quad (\text{slopes})$$

$$R_{\text{bump}} = \frac{W V h N}{3280} \quad (\text{bumps})$$

where θ is the slope angle, h is the height of the bump and N is the bumps per kilometer of range. It is noted that W is in pounds as measured within the gravity field of the planet.

The range performance of the vehicle of Figure 8.1 is given in Figure 8.9a for various values of $k = k_c/b + k_\phi$, slope angle, and bump height. It is assumed that one-half the range is traversed at the slope angle, and the other half on flat terrain. One half the bump resistance is used, assuming that 50 percent of the potential energy is recovered. The resistance of the back wheels is assumed equal to that of the front wheels; 200 bumps per kilometer are assumed. Other values are:

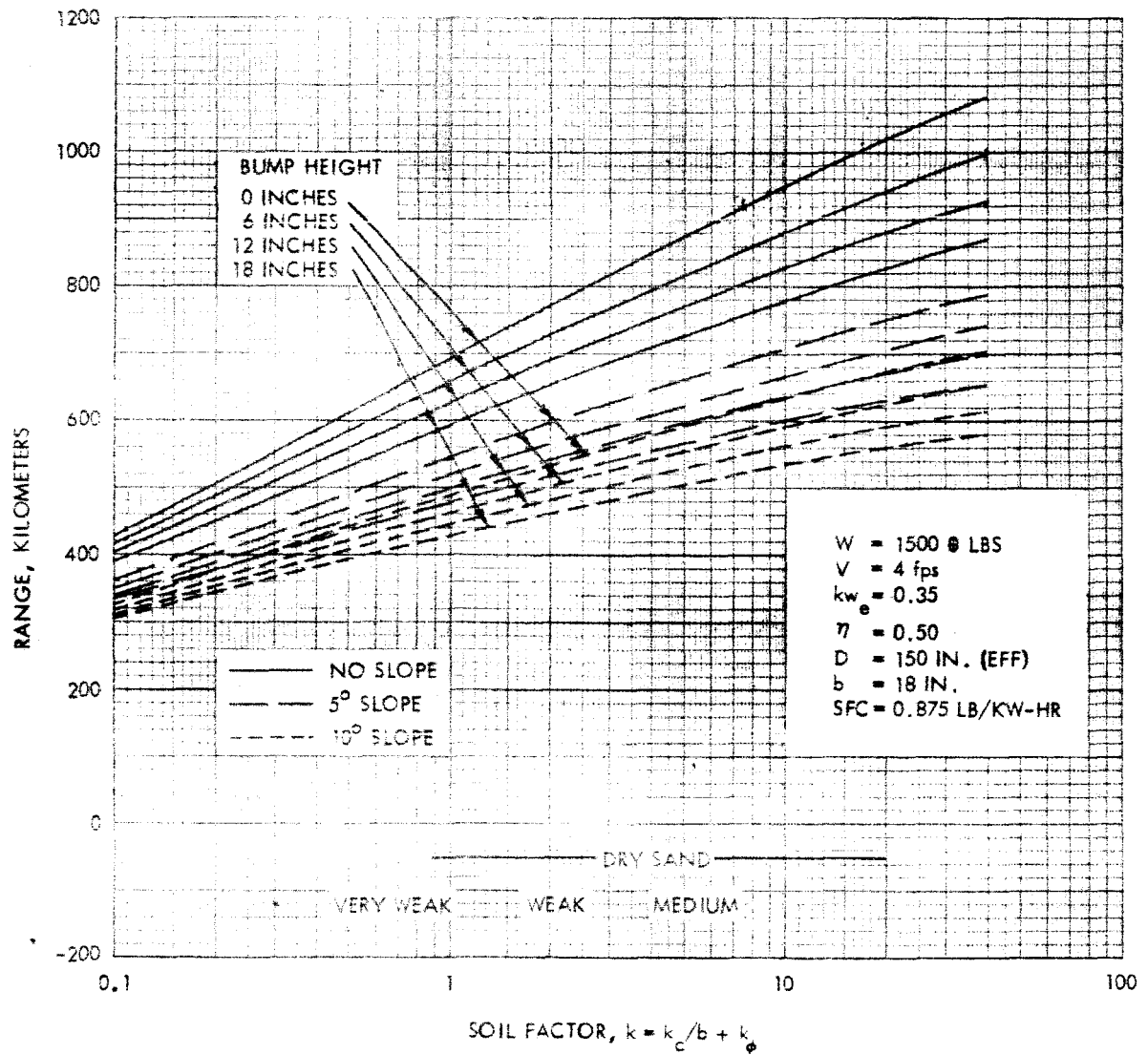


Figure 8.9a Effect of Terrain on Range

V	=	4 fps
SFC	=	0.875 kw - hr/lb
W_f	=	155 lbs (earth)
kw_e	=	0.350
η	=	0.50
n	=	1.0
D	=	150 inches (effective)
b	=	18 inches

The sensitivity to the various factors can be seen in Figure 8.9. Surface slope has a relatively large effect, as does the soil factor. Sinkage is given in Figure 8.9b.

Drawbar Sensitivity to Soil and Vehicle Design Factors

The vehicle design presented in Figure 8.1 was analyzed for its sensitivity to soil factors and design parameters using the equations given in the foregoing section. The parametric analyses were conducted by varying each factor in turn, while holding all other factors constant at the design value. The ranges of soil factors and design factors investigated covers the upper limits of probable values (see Table 8.2). The parametric analysis included bulldozing resistance, which was found to have a predominant effect on cohesive type soils, even on sandy soils with low cohesive properties. The range of factors is as follows.

Soil Factors

Φ ($\mu = \tan \phi$)	10°	25°	30°		
c (psi)			0	0.5	1.0
k_Φ		0.5	1.0	10	
k_c			0	15	30
γ (lbs/cuin)		0.04	0.06	0.10	
n	0	0.5	1.0		

Design Factors

b (in.)	5	10	18	
D (in.)	10	100	150	
W (\oplus lbs)		1000	1500	3000

In addition, a set of soil factors representative of the lunar surface was investigated.

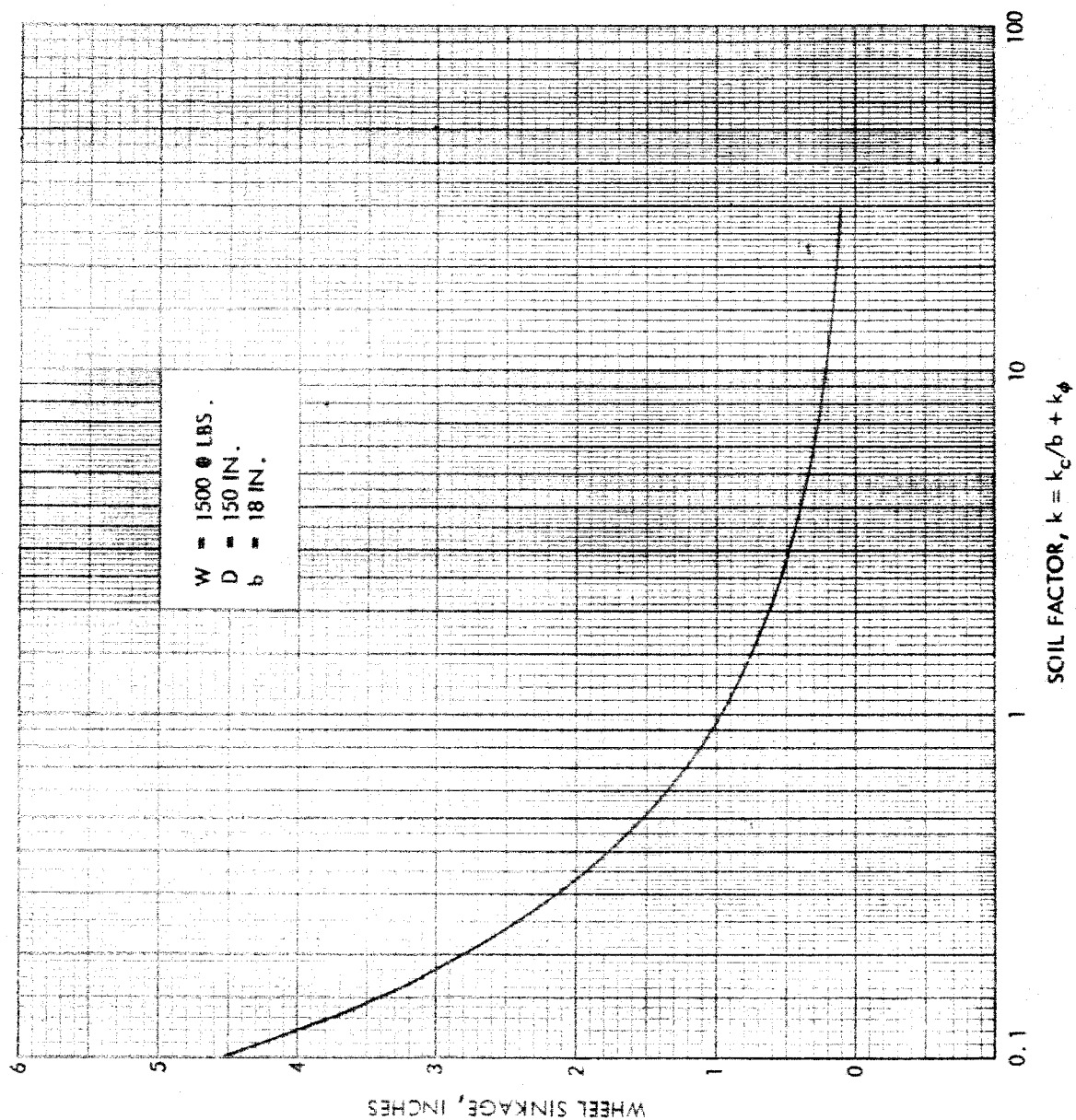


Figure 8.9b Effect of Terrain on Range - Wheel Sinkage

The results of the parametric analyses are shown in Figure 8.10 and 8.11. Figure 8.10 (a) (b) show the sensitivity of the drawbar pull of the vehicle to the various soil factors. The coefficient of friction does not have a large effect except at low values (snow has a $\mu \approx 0.10$). Soil density, on the other hand, may have a significant effect if density values increase to 0.008 - 0.10. Low values of k_ϕ , which are typical of very weak soils, has a disastrous effect on drawbar pull. Likewise, a very small degree of cohesiveness would reduce trafficability to zero. The factor n , also has a significant influence.

Drawbar pull for proposed models of the lunar surface are given in the following table.

TABLE 8.4 DRAWBAR PULL FOR VARIOUS MODELS
OF THE LUNAR SURFACE

Model	ϕ	$c = k_c$	k_ϕ	n	z (in.)	Drawbar Pull-lbs
1	32°	0	0.5	0.50	6.15	-3840
2	32	0	1.0	0.75	2.67	- 740
3	32	0	1.5	1.00	0.74	+ 184

Models 1 and 2 are indicative of very weak soils, which would completely immobilize the proposed vehicle.

Sensitivity to vehicle design parameters is shown in Figure 8.11. Wheel diameter (effective) has a significant influence, but the weight of the vehicle and the wheel width are not critical.

If cohesive type soils are anticipated, indeed soils with any degree of cohesiveness, a track type vehicle should be considered (see Figure 8.12).

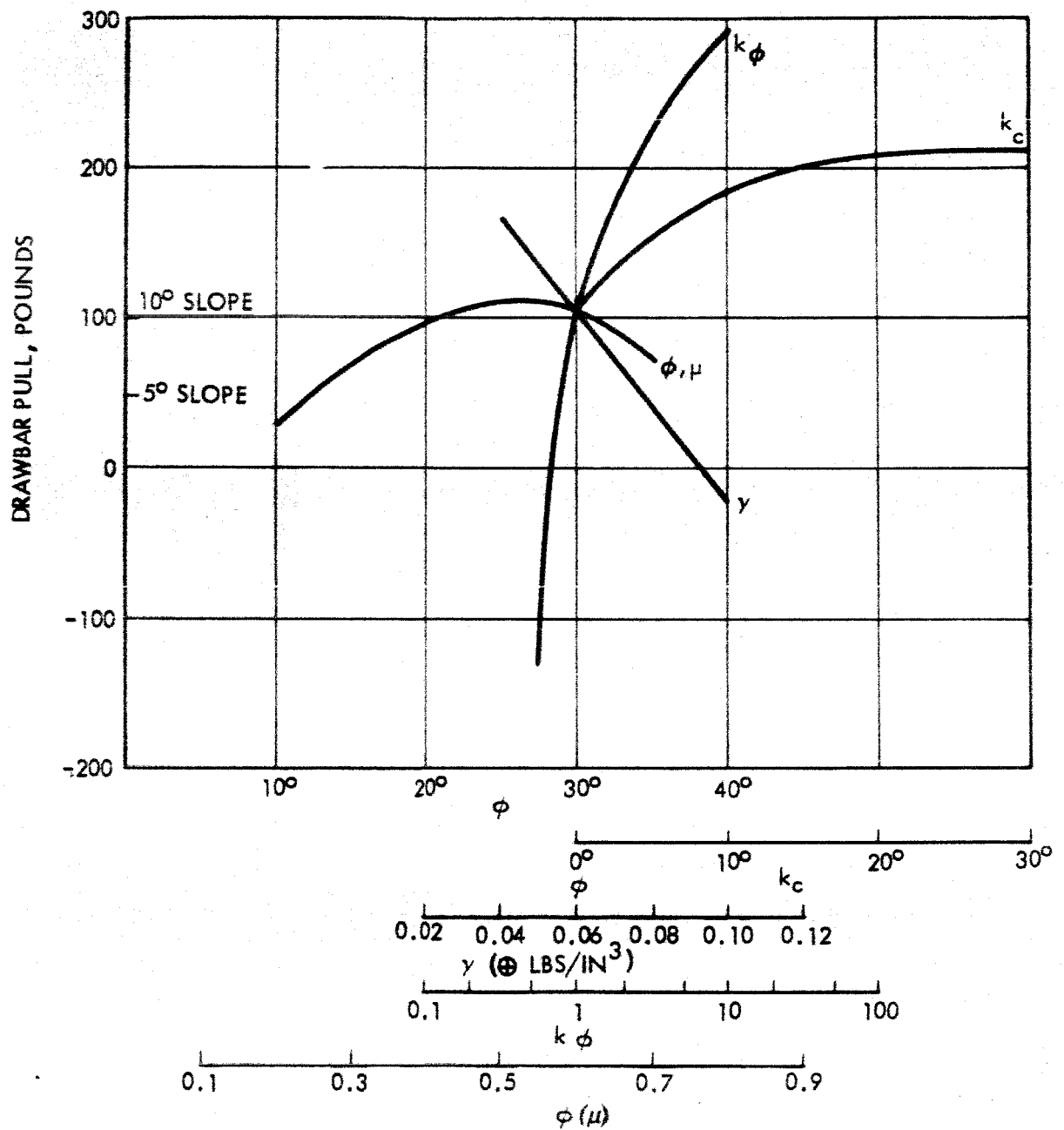


Figure 8.10a Drawbar Pull - Sensitivity to Soil

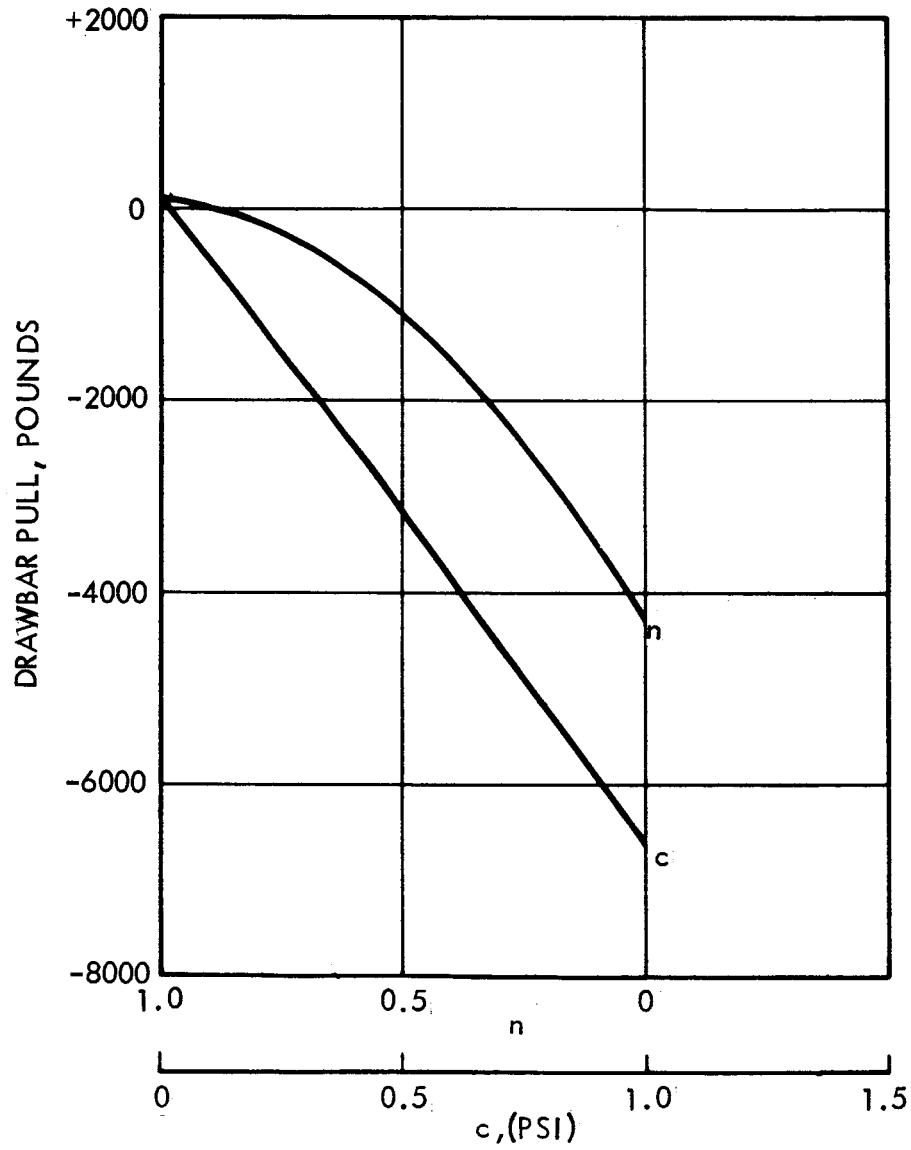


Figure 8.10 b Drawbar Pull - Sensitivity to Soil

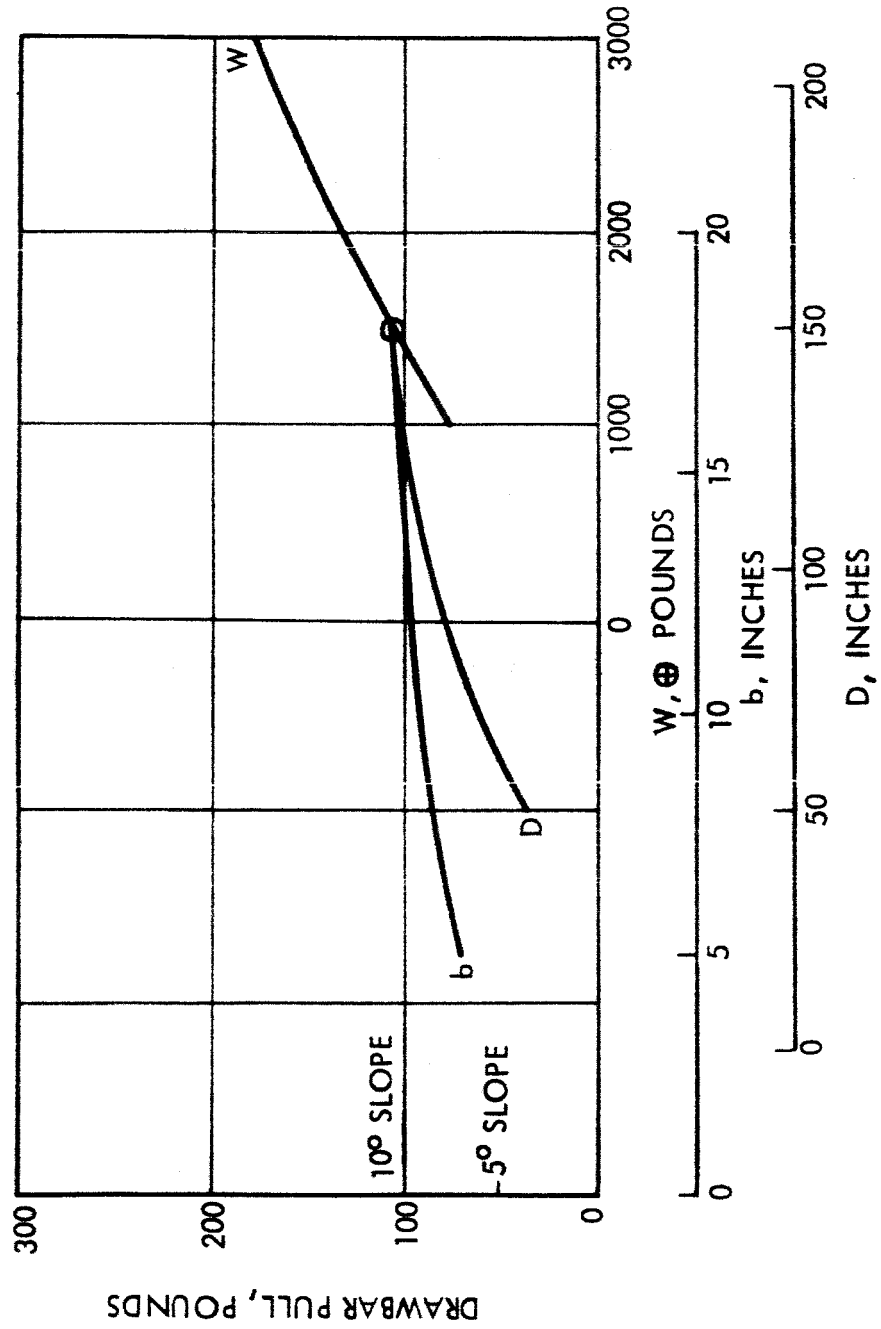


Figure 8.11 Drawbar Pull - Sensitivity to Vehicle Design

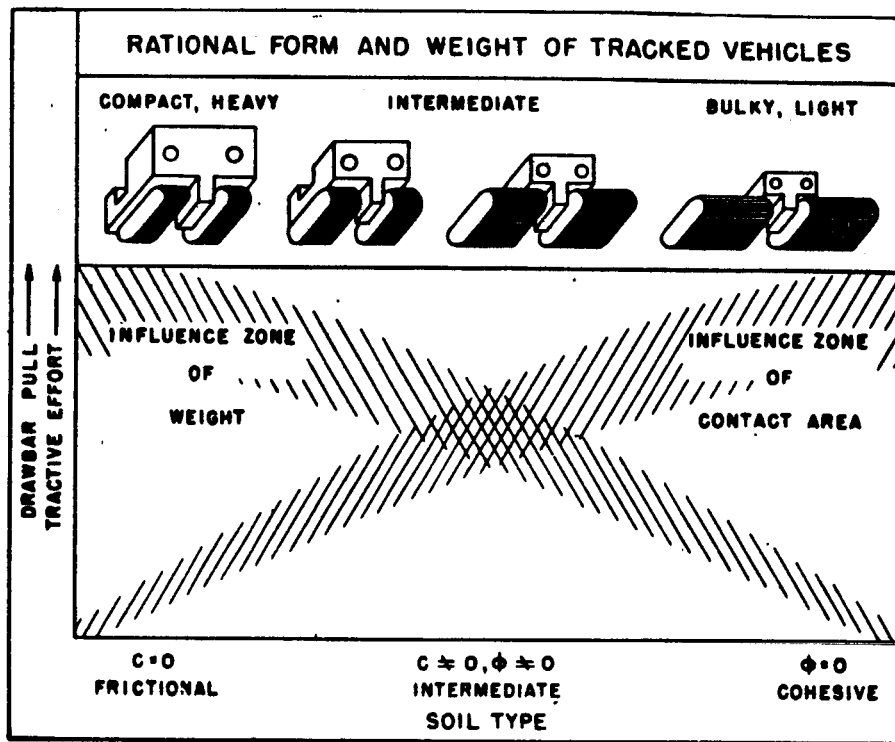


Figure 8.12 Use of Tracked Vehicles

The use of cleats is also very effective for vehicle applications in cohesive type soils, as shown in Figure 8.13.

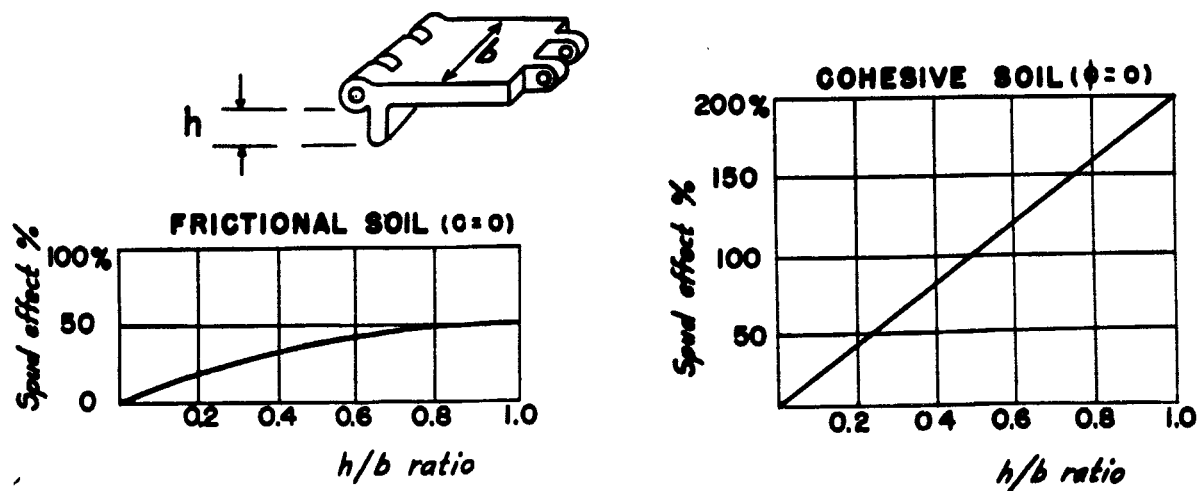


Figure 8.13 Use of Spuds

Vehicle Sensitivity to Terrain

The vehicle must have sufficient traction to negotiate bumps and crevices, and at least moderate slopes.

An analysis of the bump-climbing ability of the vehicle is given by the following equation for a 4-wheel vehicle driven by the rear wheels (bump crossed by the front wheels):

$$\frac{h}{D} = \frac{1}{2} \left\{ 1 - \frac{1}{1 + \mu^2 \left[\frac{S_1/S}{1 - S_1/S - uD/2S} \right]^2} \right\}$$

It can be seen that the height of the bump that can be negotiated, h , is a function of friction coefficient and center of gravity location. If the bump is encountered by the rear wheels the above equation becomes:

$$\frac{h}{D} = \frac{1}{2} \left(1 - \frac{1}{\sqrt{1 + \mu^2}} \right)$$

Ditch crossing capability can be analyzed in a similar manner. The resulting equations are the same as those given above, if the ditch width, ℓ , is taken as:

$$\frac{\ell}{D} = 2 \sqrt{\frac{h}{D} - \left(\frac{h}{D} \right)^2}$$

For a 4-wheel drive vehicle, the appropriate equation is as follows (bump crossed by front wheels):

$$\left(\frac{1}{\mu} - \frac{1 + \mu^2}{\mu} \frac{S_1}{S} - \frac{1}{2} \frac{D}{S} \right) \cos \alpha - \left(1 - \frac{1}{2} \mu \frac{D}{S} \right) \sin \alpha - \frac{1}{2} \mu \frac{D}{S} = 0$$

where $\alpha = \sin^{-1} (1 - 2h/D).$

If the rear wheels encounter a bump, the appropriate expression is:

$$\left[(\cos \beta - \mu \sin \beta) + \frac{1}{2} \mu \frac{D}{S} \right] \sin \alpha - \left[\left(\frac{1 + \mu^2}{\mu} \frac{S_1}{S} - \mu \right) \cos \beta \right. \\ \left. - \left(\frac{1 + \mu}{\mu} \frac{h}{s} + 1 \right) \sin \beta - \frac{1}{2} \frac{D}{S} \right] \cos \alpha \\ - \frac{1}{2} \mu \frac{D}{S} \left[(S - S_1) \cos \beta + h \sin \beta \right] = 0$$

The above expressions are graphed in Figure 8.14 for typical values of S_1/S . The conversion to give the ditch crossing capability is also given.

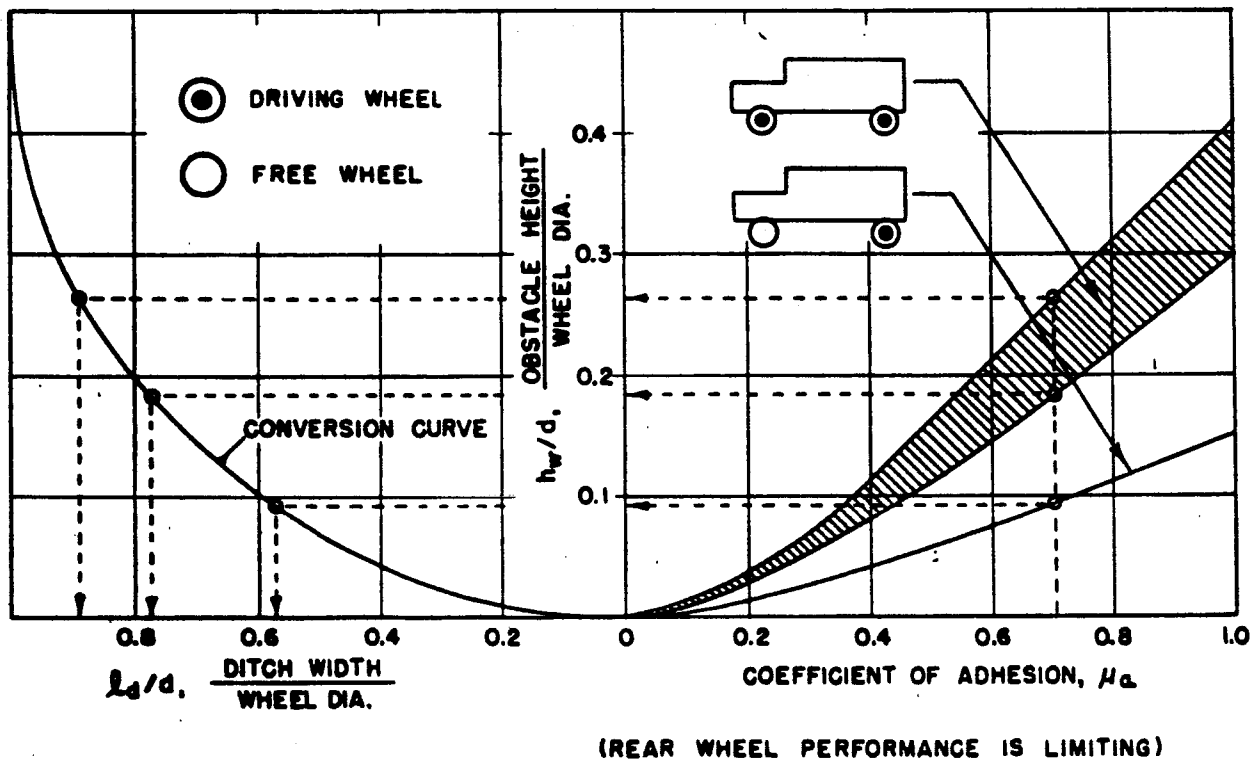


Figure 8.14 Bump and Crevice Crossing Capability

An additional factor of interest is that of maximum slope climbing ability. This is determined by the following

$$\theta_{\max} = \tan^{-1} \theta$$

Values for this expression are given below:

μ	θ
0.1	5.7
0.2	11.3
0.3	16.7
0.4	21.8
0.5	28.7
0.7	35.0
1.0	45.0

Rolling resistance, including that due to compression and bulldozing tend to indicate the maximum downhill slope that can be negotiated without slippage. Values of slope angle versus soil modulus are given below for the nominal case ($c = k_c = 0$):

k_ϕ	θ
0.5	54°
1.0	23°
10.0	3.3°

In the hard soils ($k_\phi > 10$) braking could be applied, as indicated by the table of allowable slope versus friction coefficient.

8.6 Rocket Boost Glide Vehicles for Surface Exploration

The surface rover vehicle described previously has a range limited to about 500 km, which may be inadequate for surface explorations subsequent to the initial landings. In addition, surface rovers may encounter soil conditions or terrain features that would limit their usefulness.

An attractive vehicle for extended range operations on Mars is the hyper-sonic boost glider, which is accelerated by rockets to a velocity and altitude sufficient for the craft to glide to a target location. The wings serve a two-

fold purpose in that they efficiently convert kinetic energy into useful range, and they reduce the terminal velocity to minimal values for final retro rocket touchdown. Ranges of several thousand kilometers can be achieved by the boost glider within reasonable weight limitations. The alternative to the boost glider is to equip the expedition with two or more Mars excursion modules (MEMs).

A brief discussion of the boost glider is given below.

Analysis

The range capability of a rocket-boosted hypersonic glide vehicle is given by Reference 8.4.

$$R = \frac{r_M}{2} \left(\frac{L}{D} \right) \ln \left(\frac{1}{1 - \frac{V_p^2}{g_M r_M}} \right) \quad (1)$$

where

V_p = boost velocity at end of powered flight, fps.

L/D = lift to drag ratio

r_M = radius of Mars

g_M = Mars acceleration due to gravity

This equation considers only the conversion of the kinetic energy of the glider's velocity at the end of the powered phase into range; the potential energy of altitude and the contribution to range of the powered flight are neglected.

Reference 8.5 indicates that trimmed L/D values of the order of 5 can be expected for high-performance hypersonic gliders. Substituting the appropriate values into Equation 1, the range as a function of required boost velocity was derived. A graph of the function is given in Figure 8.15. It is noted that a glide vehicle launched at the equator requires a boost velocity of 8000 fps in order to reach the pole.

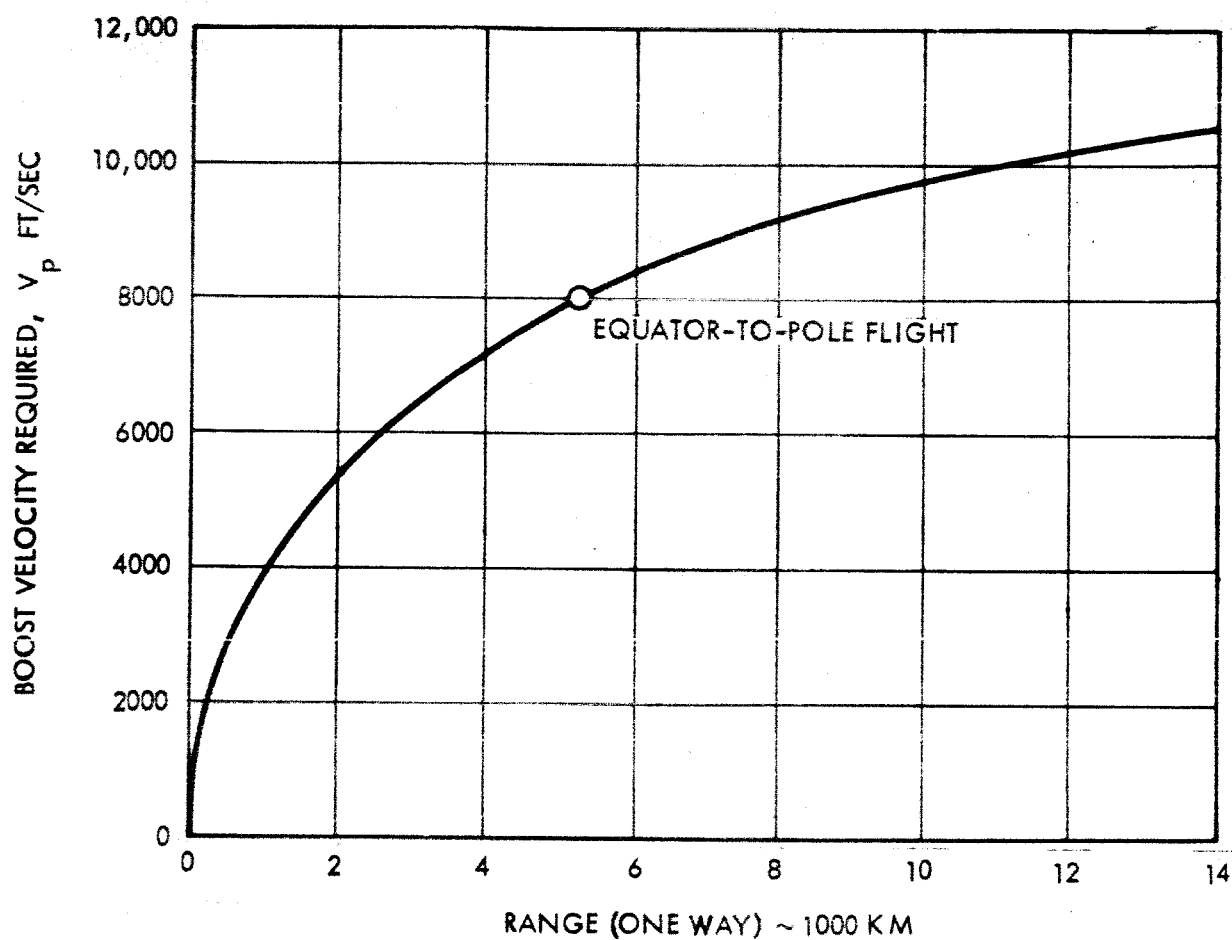
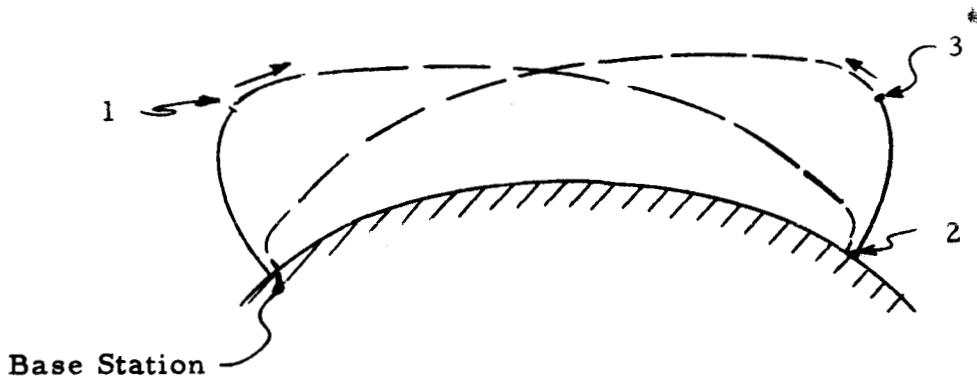


Figure 8.15 Mars Boost Glide Vehicle
Boost Velocity vs Range $L/D = 5.0$



The mass ratio for the boost phases is given by Reference 8.4 as:

$$\frac{m_1}{m_1} = \frac{m_2}{m_3} = e^{\left(\frac{V_p}{c}\right)} = e^{\left(\frac{V_p}{14,500 \text{ fps}}\right)} \quad (2)$$

where the thrust is assumed to be very large compared to the retarding aerodynamic and gravity forces. Assuming liquid H_2 and liquid F_2 as the propellants, ($I_{sp} = 450 \text{ sec}$), the rocket exhaust velocity is 14,500 fps.

As the vehicle progresses along the glide trajectory, the velocity continues to decrease. However, there will be a minimum velocity, V_{min} , for which the vehicle is no longer capable of developing lift equal to its weight. After the vehicle reaches its minimum level flight velocity, it will be decelerated to essentially zero forward velocity and will be designed for the capability of hovering for one minute before landing. Both of these maneuvers will be accomplished by means of rocket thrust.

The mass of fuel consumed during the deceleration maneuver for the outbound and the return phase will be:

$$m_{2_d} = \left(e^{\left(\frac{V_{min}}{c}\right)} - 1 \right) m_2 = \left(e^{\left(\frac{500 \text{ fps}}{14,500 \text{ fps}}\right)} - 1 \right) = .035 m_2 \quad (3)$$

$$m_{f_d} = \left(e^{\left(\frac{V_{min}}{c}\right)} - 1 \right) m_f = \left(e^{\left(\frac{500 \text{ fps}}{14,500 \text{ fps}}\right)} - 1 \right) = .035 m_f$$

where $V_{min} = 500 \text{ fps}$ has been assumed as a preliminary estimate.

The mass of fuel expended during the one minute hovering maneuver for each phase will be:

$$m_{2_h} = m_2 \frac{g_M \Delta t}{c} = m_2 \frac{(12.3)(60)}{14,500} = .05 m_2$$

$$m_{f_d} = m_f \frac{g_M \Delta t}{c} = m_f \frac{(12.3)(60)}{14,500} = .05 m_f$$
(4)

The ratio of initial to final mass for the complete flight is given by:

$$\frac{m_i}{m_f} = \underbrace{\frac{m_1}{m_1} \frac{m_1}{m_2} \left(\frac{m_2 + m_{2_d} + m_{2_h}}{m_2} \right)}_{\text{boost glide decelerate \& hover}} \underbrace{\frac{m_2}{m_3}}_{\text{boost}} \underbrace{\frac{m_3}{m_f} \left(\frac{m_f + m_{f_d} + m_{f_h}}{m_f} \right)}_{\text{glide decelerate \& hover}}$$
(5)

$$\frac{m_i}{m_f} = e^{\left(\frac{V_p}{14,500 \text{ fps}} \right) (1) (1.085)} \underbrace{\hspace{10em}}_{\text{outbound}} e^{\left(\frac{V_p}{14,500 \text{ fps}} \right) (1) (1.085)} \underbrace{\hspace{10em}}_{\text{return}}$$

Weight Estimate

A typical weight estimate for the glider in its final landed configuration is as follows:

2-men crew + life support equipment	500 earth lbs.
scientific payload, cameras, etc.	200 earth lbs.
navigation and communication gear	150 earth lbs.
structure	<u>1700</u> earth lbs.
final weight	2550 earth lbs.

Knowing the final weight, the initial weight of the complete launch vehicle can be calculated from Equation (5). The result is plotted as a function of total range (out and return) in Figure 8.16. The initial launch weight of the glider is 9050 \oplus lbs for an equator-to-pole and return flight (10,680 km).

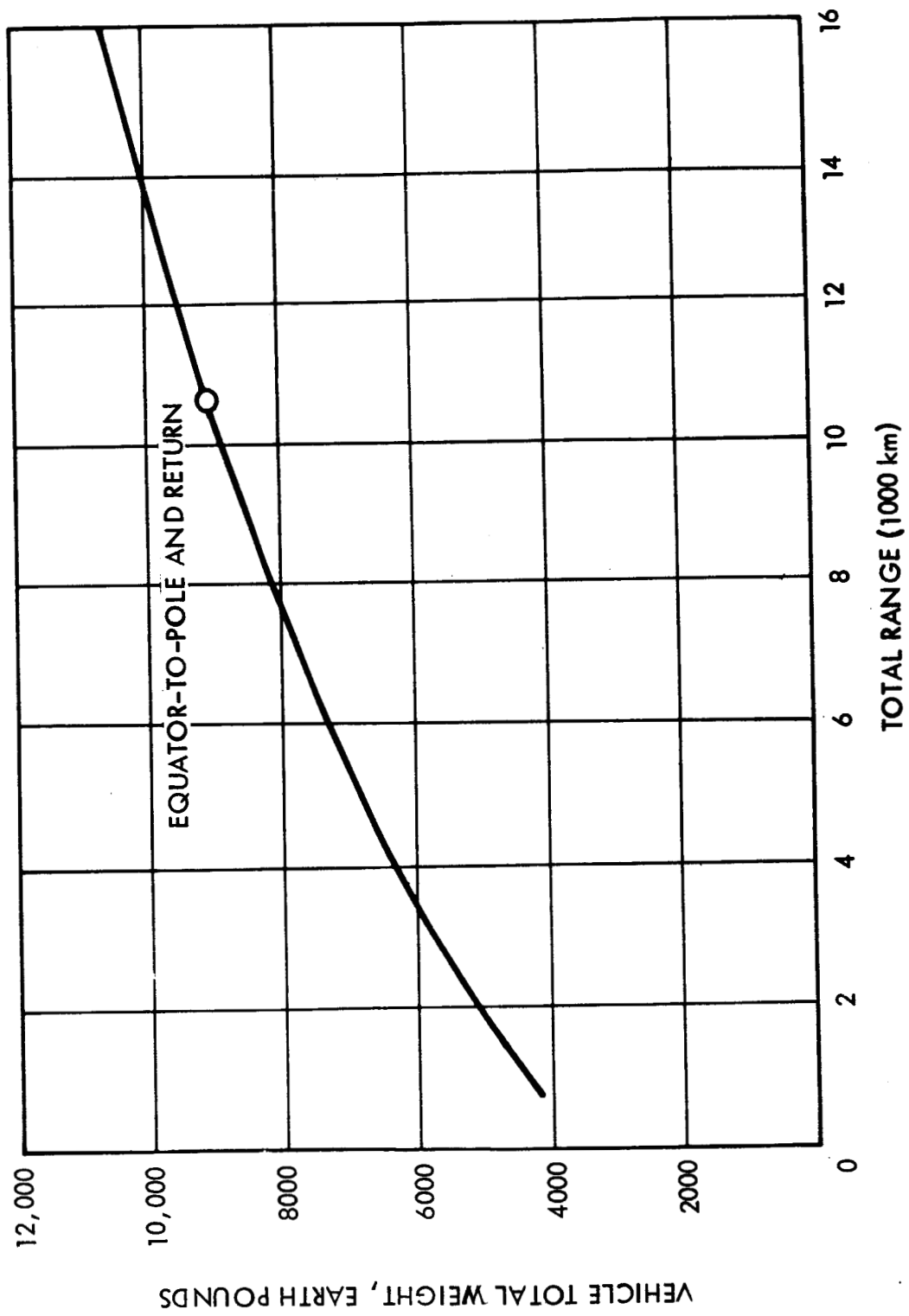


Figure 8.16 Mars Boost Glide Vehicle Weight Range Performance

Glider Design

By scaling Model 11 of Reference 8.5 to an appropriate size to accommodate the desired 2-man crew and payload, the resulting glider is approximately 35 feet long, has a 22.5-foot span, and a wing area of 375 square feet. The wing loading is $6.8 \oplus$ lbs/sq ft, or 2.6σ lbs/sq ft.

Assuming a $C_{L_{\max}} = 1.0$, the minimum level flight speed near the end of the return glide for the Model 2 (25 mb) atmosphere is:

$$V_{\min} = \left[\frac{2 W_M}{\rho C_{L_{\max}} S} \right]^{1/2} = 245 \text{ fps}$$

and for the Model 3 (10 mb) atmosphere, 368 fps.

During the (L/D) max portion of the glide, Reference 8.6 indicates that the trimmed aerodynamic coefficients of the glider will be:

$$\begin{aligned} (L/D)_{\max} &= 5.0 \\ C_L &= .97 \\ C_D &= .014 \\ \alpha &= 8^\circ \end{aligned}$$

A typical glider configuration and the associated launch vehicle configuration is shown in Figure 8.17.

Sensitivity to Environmental Factors

The boost glide vehicle is sensitive primarily to uncertainties in the atmosphere, and secondarily to uncertainties in terrain and soil conditions, which affect the touchdown maneuver. The latter effects are discussed in Section 7 in connection with the landing dynamics of the Mars excursion module.

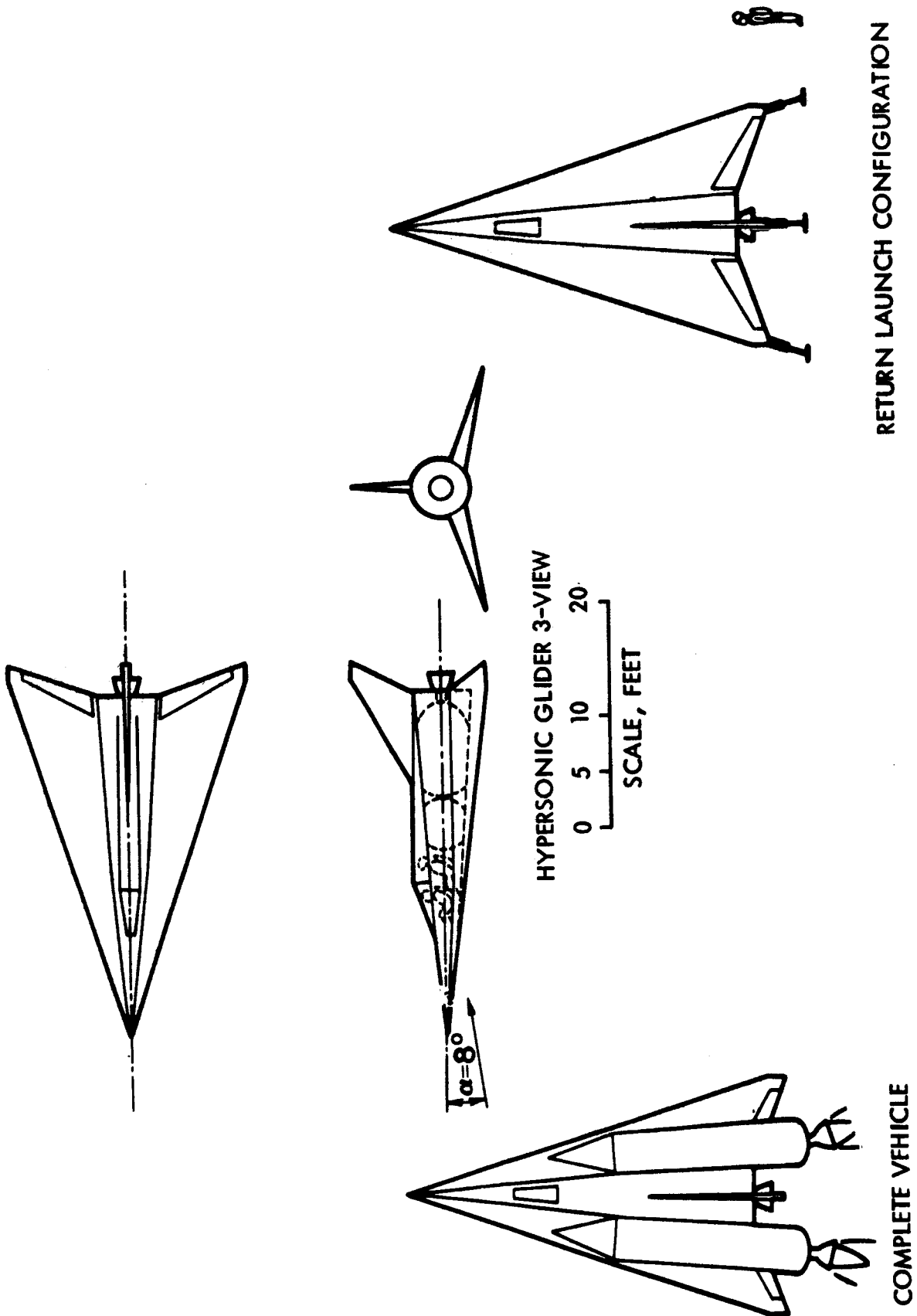


Figure 8.17 Mars Boost Glider

Uncertainties in the density of the atmosphere will affect the stalling speed of the vehicle and, hence, the magnitude of the retrorocket required for final touchdown. From the above analysis, the retro impulse required is seen to vary as $\sqrt{\rho}$. Hence, an uncertainty in density will lead to the following change in retro mass ratio.

$$\frac{M_r/M_o}{(M_r/M_o)_{\text{nom}}} = \sqrt{\frac{\rho_{\text{nom}}}{\rho}}$$

Conservatively, the mass required for terminal deceleration is 7 percent of the total mass for the Model 2 atmosphere. If instead the Model 3 atmosphere was encountered, the reduction in density to 59 percent of nominal would cause a 30 percent increase in retro propellant requirements. The gross weight of the vehicle would increase by 2.7 per retro, or 5.4 for the round trip. The effect on overall system weight in earth orbit is discussed in Section 10.

8.7 Surface Range Requirements

The question is raised as to surface traverse range requirements, which may be beyond the capabilities of the surface rover analyzed in Sections 8.1 - 8.5. Sagan (Reference 8.) has pointed out possible areas of interest for initial surface landings. These areas show marked changes in color pattern during the course of the seasons, as indicated in Figure 8.18 (from Reference 8.). Solis Lacus (1) and Syrtis Major (2) are areas of interest, based upon present knowledge. Other areas to be considered for exploration are noted in Figure 8.19.

It is evident that a surface rover cannot cover more than one of these sites, although by landing near the junctures of several areas displaying different surface characteristics, a variety of topographical features could be explored. The range of the surface rover vehicle described herein is approximately 500-600 km, depending on soil conditions. This range covers about 10 degrees of longitude along the martian equator.

Trips such as (1) (5) (6) 1 or 2, 3, 8, 2 require ranges of 8370 and 10,700 km, respectively, and are clearly beyond initial range capabilities. Trips to the polar caps from the equator require a range of about 9,500 km.

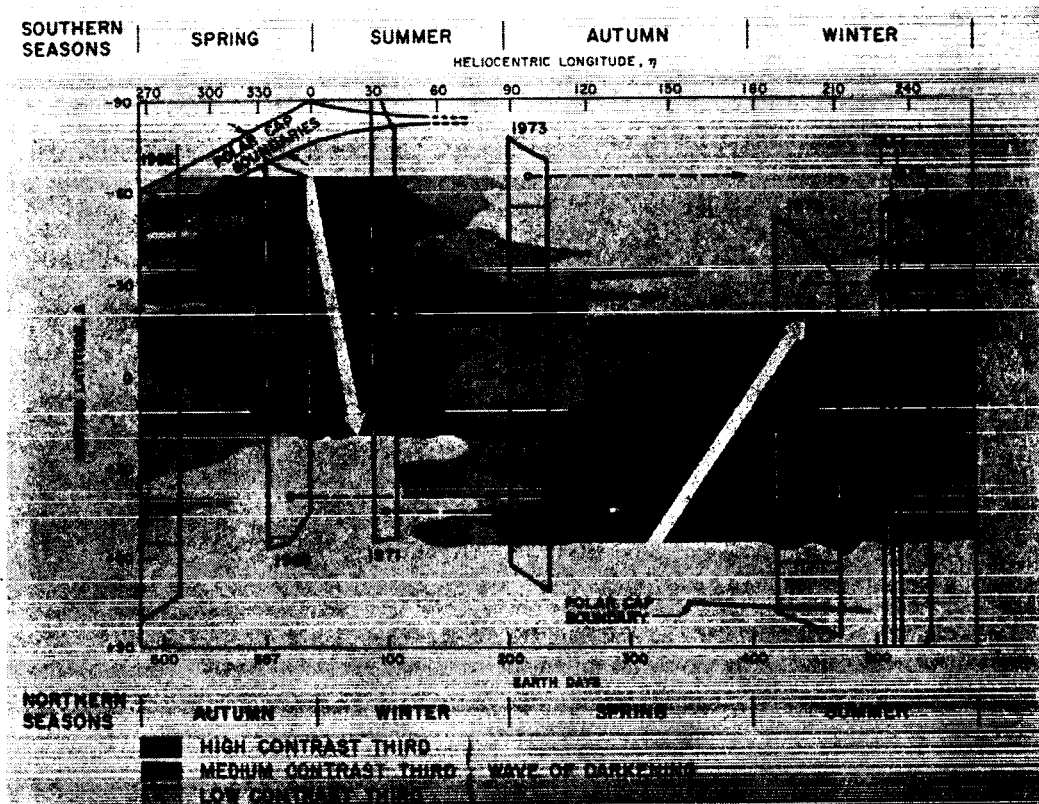


Figure 8.18 Seasonal Changes in Surface Features
(Sagan, Reference)

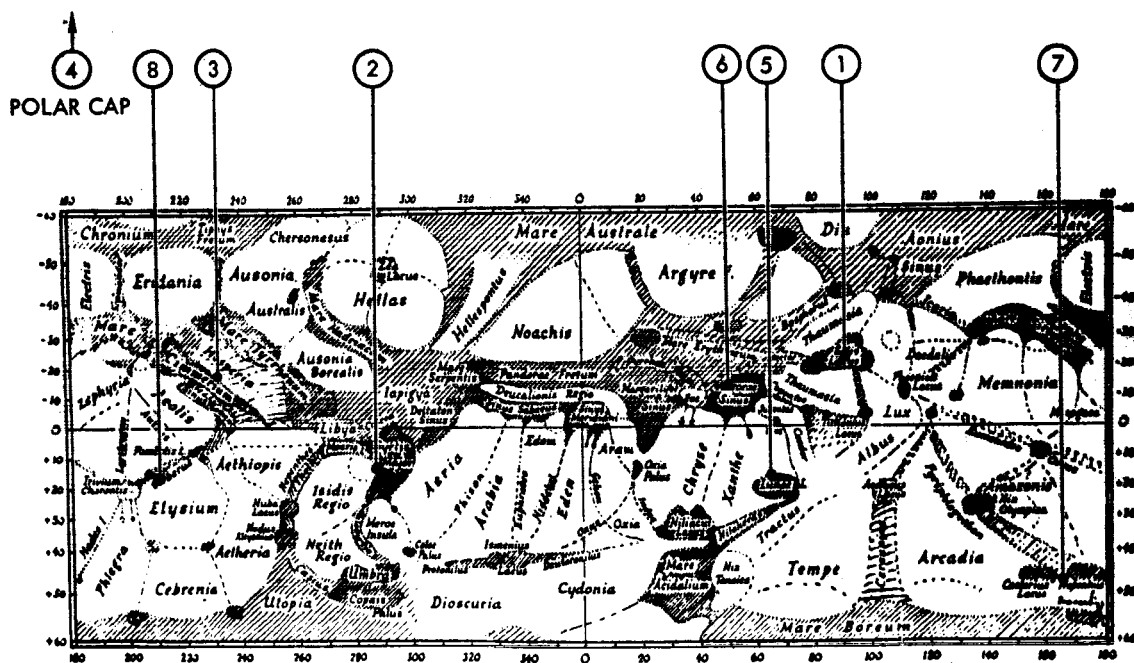


Figure 8.19 Surface Features
(de Vaucouleurs, Reference 5.12)

9. NUCLEAR AND METEOROID RADIATION EFFECTS

9.1 Nuclear Radiation9.1.1 Uncertainties in Radiation Dosages

The space radiation data now available indicate that the radiation hazard of a manned Mars mission appears to be tolerable, i.e., about 172 rads for the 14-month mission. However, there are a number of uncertainties associated with that result. Table 9.1 summarizes the results given in Section 5, together with an uncertainty associated with each major contribution to the dose.

Table 9.1 EXPECTED DOSAGES

<u>Events</u>	<u>Integrated Dose</u>	<u>Source Uncertainty</u>	<u>Calculation Uncertainty</u>	<u>Integrated Dose Plus Uncertainties</u>
Dose on Mars Surface				
Galactic cosmic rays per week	0.17 rad	-	-	-
Solar Cosmic rays per week	0.25 rad	-	-	-
One relativistic flare	40.0 rad	-	-	-
Total weekly trip dose	40.4 rad	+ 40 rad	+ 24 rad	104.4 rad
Dose in transit				
GCR	9 rad per yr	-	+ 5 rad	14 rad
SCR	104 rad per yr	+ 15 rad	+ 60 rad	179 rad
TOTAL Yearly Dose (Rad)	153	+ 55	+ 89	297
TOTAL Trip Dose (Rad)	172	+ 58	+ 100	330

A once per week "average" solar flare was assumed during the transit phase of the Mars mission. Since there is a wide variation in the intensity and energy spectrum of solar flare protons the concept of an "average" or "typical" flare is not very meaningful for calculating a radiation dose due to a single event. However, for a year's mission (52 events), the use of an average flare is justified and the associated statistical uncertainty in the number of flares would be ± 7 or approximately 15 percent uncertainty in the dose (± 15 rads).

One relativistic flare of the February 1956 type was assumed during the mission; this is also a potential source of error because flares of this nature are rare and unpredictable. However, it is extremely unlikely that there would be more than two

such flares during the mission, leading to an uncertainty of 40 rads in the accumulated dose due to this source.

Finally, an average of 22 gm/cm^2 of spacecraft shielding and a 30 gm/cm^2 (11 mb) of Mars atmosphere shielding was assumed in making the dose calculations. Accumulated dose calculations behind shields yield questionable results because of uncertainty in the secondary radiation generated due to interactions of the primary in the shielding. However, since the mean free path for nuclear interactions of space radiation is approximately 70 gm/cm^2 , the 22 gm/cm^2 and 30 gm/cm^2 shields used here are a small fraction of the nuclear mean free path. Consequently, the resulting dose calculation behind these thin shields is quite accurate even if the secondary radiation is ignored. One would expect one quarter to one third of the incident radiation to interact in the shield (or atmosphere) and the average number of secondary particles (protons and neutrons) produced of energy greater than 20 Mev, varies from about 1 to 4 as the incident proton energy varies from 100 Mev to 1 Bev. In the absence of interactions, (i. e., only ionization energy loss) the dose can be calculated precisely for a given source input. Hence, in the thin shield configuration (considered here), even if the secondary radiation is ignored completely and each interaction produced on the average of two secondary particles traveling in the forward direction and passing through the shield (this is unlikely), this would amount to about 60 percent increase in the dose. This degree of uncertainty in the dose behind the shield is in reasonable agreement with References 9.1 and 9.2, which quote an uncertainty of 100 percent in dose. It is also noted from various sources (c. f., Reference 9.3) that estimates of shield effectiveness vary by about a factor of 2. Hence, the uncertainties given in Table 9.1 appear reasonable.

The total uncertainty in dose behind a 22 gm/cm^2 shield is 158 rads, or a factor of 1.92. Obviously the additional shielding required to attenuate the dose from 330 rads to the original 172 rads constitutes a significant weight penalty.

In fact, the dose due to the relativistic flares would be nearly impossible to reduce to half levels as indicated by the following table for the 23 February 1956 flare:

Shield (gm/cm ²)	10	20	30	35
Dose (rads)	35-100	25-50	25-40	20-35

An optimization would indicate that a lesser shield weight penalty would result by reducing the dose principally by reducing the contributions from the solar cosmic radiation sources. Using the above table and estimates of shielding required to attenuate Bailey's model event (see Reference 9.4 Figure 3.1 - 3.5), an increase in shield thickness from 22 to 35 gm/cm² is indicated. Spacecraft gross weight in earth orbit would increase by 3.5 percent as a result.

The total uncertainty in solar shielding requirements due to the above factors, and to possible uncertainties in the recovery factor concept (it is estimated that only 10 percent of the damage due to radiation is irreparable, see NCRP Report No. 29, 1962) can amount to the following penalties in spacecraft gross weight:

	<u>Shield</u>	<u>Weight Penalty</u>
1. Nominal dose, 90% recovery	10 gm/cm ²	0%
2. Nominal dose, no recovery	22	4.8
3. Maximum dose, no recovery	35	8.3

The uncertainties in recovery factors are discussed in a following section.

9.1.2 Allowable Doses

A review of several analyses indicates that restrictions on radiation dosages to the blood forming organs tend to set the overall shielding requirements. Assuming that these organs can tolerate doses of 150 rems the dosimeter values inside the shield are 188 rads, assuming that the dose received by the organs is reduced by a factor of 2 with respect to that emanating from the shield, and RBE = 1.6. This value is slightly in excess of that estimated for the 22 gm/cm² shield.

The "design" dose established for Apollo is 54 rads, which corresponds to a skin dose of 108 rads if the body attenuation is 2. (Estimates of the body attenuation factor vary from 2 to 4. Assuming a body attenuation factor of 4 increases the allowable dose behind the shield to 216 rads.)

9.1.3 Recovery Factor

The following comments on recovery factors were made in Reference 9.5, which is a recent review of space environmental parameters in manned space flight. The review is an excellent and up-to-date analysis of the problems associated with space radiation shielding design.

"Enthusiasm for the extremely practical features of the equivalent residual dose concept must be moderated for a number of reasons.

It should be noted that the assumptions on which it is based and the constants employed have not been validated in man and are somewhat in conflict with a considerable body of present day radiobiological data. Furthermore, limited observations of fractionated exposure of man have indicated a disproportionately sensitive response of the hematopoietic system to a second acute exposure as long as 2 to 3 months after the first. Also, below normal peripheral blood counts have persisted in radiation accident victims for many months post exposure. In its present state, the equivalent residual dose concept is applicable only to generalized acute manifestations of radiation injury (as evidenced by hematopoietic end points and lethality in experimental animals), and lack of specific human data suggests prudent restriction of its use. . .

"Prediction of man's response is difficult enough when a regular pattern of protracted or fractionated exposure obtains, but when the erratic pattern of exposure likely to occur under most projected flight profiles is considered, the situation becomes virtually impossible on the basis of present knowledge. The prodromal symptoms and acute skin response will certainly benefit from dose protraction. The practical question related to progressive radiation debilitation is: To what extent will the hematopoietic system benefit and what are the significant time factors? The answer to this question is largely unknown at present. Nevertheless, equivalent residual dose calculations may be useful if limited to dose levels which are sufficiently small to have a low probability of significantly damaging the body's repair mechanisms. It is felt that potential response to small fractionated doses of less than 25 to 50 rems may be evaluated by allowing for recovery during exposure-free or very low-level (less than 2 rems/day) continuous exposure intervals of at least several weeks to several months duration.

No particular recovery constant is recommended for the ERD calculations except that it should be no greater than 2.5 percent per day and perhaps lower if it is to integrate all recovery processes acting over the first several months to a year. For higher daily doses and fractionated exposures, evaluation on the basis of simple unweighted dose accumulation would seem prudent. It is suggested, therefore, that a straight dose accumulation be used to evaluate potential acute and sub-acute hematopoietic response to fractionated exposures of about 50 rems or more per fraction and continuous exposures of greater than 2 rems/day."

9.1.4 Recommendations for Experimental Programs

Reference 9.5 makes the following recommendations for research in the subject fields:

1. Continuation of efforts to define and to predict the space radiation environment and, where possible, in terms amenable to assessment of radiation effects on living systems.
2. Collection and organization of all available data on human response to acute and chronic whole-body radiation exposure in a manner amenable to analysis for space operations needs.
3. Investigation of the dose-time-intensity dependency of the prodromal response of man, especially in the dose-rate range of about 0.1 to 100 rads/hr.
4. Investigation of the dynamics of progressive degeneration and repair of the hematopoietic system under acute and semi-acute radiation exposure conditions and establishment of the significant time factors for man. Only with such information will it be possible to establish a dependable equivalent residual dose concept for evaluation of net injury resulting from chronic and randomly fractionated acute exposure.
5. Continuation of investigations of the biological effects of high-energy charged particles and determination experimentally of the dynamics of early skin response to protons and alpha particles of sufficient energy to penetrate the epidermis.
6. Further investigation of the influence of nonhomogeneity of dose distribution (both topical and depth) on early and late response to acute and semi-acute radiation exposure.

7. Investigation of the effects of combined stress, especially the possible interface between weightlessness and early response to acute radiation exposure.
8. Continuation of the development of more sophisticated dosimetry directed toward producing measurements amenable to correlation with biological effects and expressed in units useful for prediction of specific radiation response.
9. In anticipation of the future of long-range missions, investigation of the cumulative effects of heavy charged particle interactions with biological systems and the significance of neural and behavioral response to acute and chronic radiation exposure.
10. Continuation of the search for drugs that are of practical prophylactic and therapeutic value against early and delayed radiation sequelae."

9.2 Meteoroid Flux

Status

An analysis of meteoroid flux models was given in Section 5.3. It was concluded that satellite data, which generally falls within the mass range below 10^{-6} grams, may be influenced by the dust cloud, believed to surround the Earth. The few data obtained from interplanetary space probes tend to indicate a much lower flux rate in this mass range.

The visual and radar meteoroid data obtained in the near-earth environment have established the flux rate in the 10^{-3} - 10^{-3} gram mass range to a reasonable degree of accuracy (within an order of magnitude). These data are representative of the flux rates to be expected in interplanetary space at 1 AU because all but a small percent of the particles have been determined with good accuracy to have hyperbolic velocities with respect to the Earth. These data are in the mass range of interest to the spacecraft designer, and provide a reasonable basis for shielding requirements. The greatest uncertainty remaining in the flux-mass models based on these data are the conversions from visual magnitudes, or radar energy data, to actual particle mass, although recent experiments have aided in reducing these uncertainties. The radar data in particular have contributed much to the better understanding of meteoroid phenomena.

The attempts to predict asteroid flux-mass models in the cismartian space are not well established, and cannot form the basis for any reasonable predictions at this time. The two attempts made to date vary by several orders of magnitude in flux rate. The higher prediction is very questionable. The problem essentially must be approached on a parametric basis until satellite data are obtained. Missions to this purpose are badly needed. In this regard, it might be noted that research on particle detectors and analyzers is much needed. More sophisticated detectors, capable of distinguishing between mass and velocity to a better degree are required.

Shielding Analysis

Shielding analyses are in an equally uncertain state because of lack of test data at velocities applicable to meteoroids in the 10^{-3} - 10^0 gram mass range (which can extend to 30 km/sec and above). Effectiveness of various shielding configurations at given velocity levels is currently the subject of considerable study, but many uncertainties remain.

To determine the particle mass for which the shielding is to be designed, assumptions must be made about the probability of encounter. If the probability, p , of encounter is small in comparison to unity, the following relation can be used to determine the allowable flux:

$$NAT \cong p$$

where A is the area in sq. meters, T is the time in seconds, and N is the flux in hits per m^2 -sec. If the vehicle has an outer shield to encase the aero entry system and Mars depart propellant tanks, a time of 200 days and an area of 5000 sq ft can be assumed for T and A in the above equation. The return to Earth will require an inner shield of about 2120 sq ft, exposed to the meteoroid environment for about 250 days. The outbound shield requirement is determining.

Assuming a probability of encounter of 0.01, a flux of 1×10^{-11} 9 hits per m^2 -sec. is obtained.

A flux-mass model is now required to determine the mass of particle to be protected against. Various models will be assumed for this purpose, as indicated below.

Shield thickness determinations require assumptions as to particle velocity and the thickness variation with mass and velocity. The relative effectiveness proposed shield configurations also must be assumed. For present purposes, it will be assumed that the following shielding model pertains:

$$t = 1.67 m^{1/3} \rho_m^{1/3} \left(\frac{V_m}{\rho_t S_t} \right)^{2/3} \frac{1}{R}$$

This model indicates that for a given velocity and shield effectiveness, R , shield thickness varies as the cube root of particle mass. This relation stems from the assumption that the particle craters out a volume of material proportional to its kinetic energy. The nominal shield weight is thus affected by particle mass uncertainty to the one-third power. Relative shield weights for various flux models are given below, based on the above scaling relations.

TABLE 9.1 METEOROID SHIELDING

MODEL	FLUX ($M^2 - SEC$)	SHIELD WEIGHT
STL SCALING LAW	$NM = 10^{-13.47}$	1.00
MSC ASTEROID	$NM = 10^{-12.66}$	1.54
NASA ORIGINAL	$NM = 10^{-12.15}$	2.36
NAA	$NM = 10^{-13.07}$	1.28
MSC COMETARY	$NM^{1.34} = 10^{-14.33}$	0.82

SHIELD WEIGHT $\propto M^{1/3}$

EQUAL PROBABILITY OF ENCOUNTER

Essentially, the range of weights can be bounded by the assumption of an order of magnitude uncertainty in flux rate. Uncertainties in velocity spectra and asteroid flux in the cismartian space will increase the above uncertainty in shield weight. Further analyses of the effect of observed velocity spectra on shield requirement (as related by the above equation) will be made during Phase II of the study.

It might be remarked that the operations in the vicinity of Mars are not expected to be critical from the standpoint of a possible dust cloud surrounding Mars because the velocities associated with any trapped dust cloud are small in comparison to interplanetary particle velocities, and because the dust cloud mass range is too small to be of concern in the shielding design, although solar array erosion effects may be significant.

In conclusion, it is emphasized that of all the environmental factors of concern to the designer of interplanetary manned spacecraft, the uncertainties in the nuclear and meteoroid radiation design requirements may lead to the greatest system weight penalties. Data leading to a more accurate definition of the environment, and means for protecting against the environment are much needed.

10. POTENTIAL CONTAMINATION HAZARD (Goldner)

10.1 Introduction

The assumption that some form of microscopic life exists on Mars raises the distinct possibility that the first manned mission could inadvertently bring back living organisms to Earth unless certain precautions are followed to prevent such an occurrence. It is also possible that Martian organisms could be harmful, either directly, by producing disease in man, animals or plants, or indirectly, by competing with the established biota of the Earth. The great epidemics of plague and smallpox during the Middle Ages serve as an example of the disasters which can result from the uncontrolled spread of disease organisms. The decimation of the American Indian by syphilis and tuberculosis is evidence of the destructive effects resulting from the lack of natural immunity to a particular pathogen. Although these are extreme examples, the possibility that extra-terrestrial organisms might exert a similar influence cannot be ignored, particularly in view of the adaptability and mutation rate of lower organisms.

Because of the inherent difficulty in reliably assessing the potential hazards of Martian organisms by unmanned probes, a protocol designed not only to protect the crew of the first manned mission to Mars but to prevent back contamination from Mars must be developed to adequately deal with this problem.

In the following sections various aspects of the technical problems are discussed with a presentation of the procedures required for minimizing the probability of transferring living organisms from Mars to Earth.

10.2 The Possibility of Life on Mars

The question of whether life exists on Mars has been the object of speculation for almost a century. Obviously, this problem will not be unequivocally resolved until Mars is investigated by automated probes instrumented with life detection devices or failing this, by a manned mission. We can, however, examine why life might be expected to exist on Mars, and from certain tentative theories or hypotheses based on our limited observations of the Martian atmosphere and terrain and our knowledge of the origin of life on our own planet.

The evidence for the existence of life on Mars has been collected from many sources. None of these pieces of evidence actually proves that life is present on Mars, but they do increase the probability that some form of life may exist. The changing colors of Mars - the greens, reds and browns which vary with the seasons - have been the subject of considerable speculation and could be attributed to the activities of living organisms. Polarization studies (10.1) have shown that the dark areas, in contrast to the bright areas, consist of small particles which are subject to seasonal variation. This suggests that if these areas are composed of microorganisms or vegetation, they change from an active form to a dormant form (perhaps spores) in response to the amount of moisture available.

The most compelling evidence to support the theory of living organisms is the reflected infrared light experiments of Sinton, who found that the dark regions show spectroscopic absorption bands at 3.43 microns which is the carbon-hydrogen stretching frequency of most organic molecules (10.2). Even this data, however, is open to interpretation.

Several proposals have been made to explain the dark or colored regions as a non-biological phenomena. The first of these is that the Martian atmosphere and particularly the white polar caps consist of nitrogen tetroxide instead of frozen water or carbon dioxide (10.3). The fact that spectroscopic studies have not detected oxides of nitrogen (10.4) and the inability of this theory to satisfy certain thermodynamic considerations tends to discount this explanation (10.5).

Secondly, it has been suggested that certain minerals might change color when they hydrate or dehydrate (10.6), but no known compounds on Earth undergo such wide variations in color as exhibited by the observed Martian regions.

Because of the lack of information regarding the Martian environment, investigators have approached the problem of the existence of life by indirect means. A great deal of study has been designed to determine whether terrestrial microorganisms are capable of surviving when subjected to what is believed to be a simulated Martian environment, with respect to temperature, atmosphere, soil composition, water, atmospheric pressure and freeze-thaw cycle conditions. The presence of terrestrial microorganisms in extreme environments such as

hot springs, arid deserts, brine and arctic regions strongly suggest that even the harsh environment of Mars could support some form of life. The results of experiments with these hypothetical models have demonstrated that bacteria are able to survive and even multiply in simulated Martian environments. For example, it was shown that spores of Clostridium botulinum survived and vegetative cells of Bacillus subtilis grew in various model environments (10.7). In another study, fungi and lichens collected from desert regions survived a simulated Martian environment (10.8). From these studies, the assumption can be made that if unadapted terrestrial species can survive the rigorous Martian environment, even through the process of natural selection, occurring over perhaps several billion years, indigenous Martian organisms, if present, probably occur in large numbers. Furthermore, there may be local microenvironments on Mars especially favorable to life where significant amounts of moisture and warmth are available through localized geothermal activity (10.9).

Another major line of investigation designed to explore the possibility of life on Mars is devoted to the manner in which life arose on Earth. If we assume that the theory of panspermia is invalid; i.e., that life was transported to Earth from another planet, then we must conclude that life arose on the primitive Earth independently. Since Mars was apparently created from the same cosmic dust cloud as the Earth, then conditions on Mars may have been at one time in its history similar to Earth and it is quite possible that life arose independently there as well. Oparin (10.10) proposed that life may have evolved in the oceans where large amounts of organic compounds were available. Accordingly, experiments have been made by many investigators to determine whether organic compounds can be evolved from the chemical compounds which are assumed to have been present on the primitive Earth. It is believed that the atmosphere of the primitive Earth, several billion years ago, was a reducing atmosphere consisting largely of methane, ammonia, water vapor, and hydrogen gas and that energy was available as heat from volcanic activity, ultraviolet radiation from the sun and electrical discharges originating from lightning. Experiments have, therefore, subjected synthetic reducing atmospheres to electrical discharges, and have shown that high energy phosphate molecules, amino acids, organic acids, pyrroles, purines, pyrimidines and various other

organic compounds can be formed. Recently, Ponomperuma (10.11) reported that the five nucleotides of DNA and RNA have been synthesized by applying an electrical discharge to water, ammonia, and methane at a comparatively low temperature (180°F). Some preliminary evidence was available that two or three nucleotides combined to begin building towards DNA or RNA. The study is being continued to search for catalysts or enzymes which might lead to more complex molecules, and eventually to a primitive form of organized living material. These investigations, while still incomplete, have answered many questions pertaining to the processes leading to the origin of life and offer some encouragement that some form of life exists on Mars.

Assuming that life does exist on Mars, we must now consider the nature of such life. It is more realistic to postulate that Martian life resembles terrestrial life at least with respect to basic physiology. The morphology of Martian life and even its molecular structure might differ markedly from terrestrial life forms, but considering the proposed mechanisms for the origin of life, it is probable that its metabolism is based on water and carbon.

Water has many properties which make it almost indispensable for our concept of life. For example, water has the important capacity to form hydrogen bonds which Pauling views as critical to the development of nucleic acids and proteins (10.12). Ammonia, in the liquid state, is the only other molecule known which approaches the characteristics of water, but several of its properties are not quite as suitable for the support of life as water. The high solubility of carbon dioxide in water and the ability of carbon dioxide to act as a buffer make it particularly suitable for life. The Martian atmosphere is believed to contain a high concentration of carbon dioxide (5 to 30% by volume) and small amounts of water.

Although silicon has been suggested as an alternative to carbon, silicon rarely forms multiple bonds and the Si-Si and Si-H links that do form are relatively unstable (10.13). Furthermore, there is no silicon compound known that resembles the properties of carbon dioxide. These and other reasons tend to minimize the probability of a silicon-based life, but it is not possible to eliminate this type of life chemistry at this time.

Because the dominant living organisms on Earth are microorganisms, it is reasonable to predict that this would also be true of Mars. Even if higher forms of life are present, it is difficult to envision a planet devoid of microorganisms because of their primary role in regulating the ecology of their environment and because of the evolutionary developmental sequence of living organisms. In considering what the physiological properties of Martian microorganisms might be, we must again use our knowledge of terrestrial organisms as a basis. Mars probably contains only trace amounts of oxygen, but is rich in carbon dioxide relative to Earth and receives a great deal of light energy from the sun. This suggests that photosynthesis, of the type carried out by anaerobic photosynthetic bacteria, may be one type of microorganism adapted to Martian conditions. These bacteria use light energy to reduce carbon dioxide and oxidize such substrates as reduced sulfur compounds. This type of photosynthesis does not evolve oxygen and is not dependent upon organic substrates. In addition to the photoautotrophic mode of nutrition, chemoautotrophic bacteria are capable of utilizing the oxygen from such compounds as carbon dioxide, nitrates and sulfates and oxidizing inorganic hydrogen. Finally, there are the anaerobic heterotrophs that metabolize organic compounds both as a source of energy and of carbon. Other ecological schemes, not known on Earth, but theoretically possible, may exist on Mars. Photosynthetic organisms on Mars could conceivably oxidize ammonia, for example.

10.3 The Possibility of Potentially Harmful Organisms on Mars

In the event Mars does contain a microflora, it is necessary to consider whether such organisms might be potentially harmful to either the lander crews exploring the surface of Mars or to life on Earth. Although there are thousands of microbial species on Earth, only a small minority of these are pathogenic to man, animals and plants. Most microbial species are either free-living and completely innocuous to higher forms of life (saprophytes) or live in certain regions in plants and animals without producing disease (commensals or indigenous microorganisms). Occasionally commensals will infect the host, but only under special circumstances.

Pathogenic organisms are those species which through a long period of evolution and adaption have adopted a parasitic mode of existence which causes disease in the host. Pathogens must have the ability to gain access and to multiply in the tissues (invasiveness). Once the pathogens have overcome the defense mechanisms of the host, they then produce chemical substances deleterious to the physiology of the host, such as powerful toxins. In addition, the invading organism may secrete certain substances other than toxins, and enzymes that have the capacity to induce or retard the coagulation of plasma or lymph, to destroy red and white blood cells, increase the permeability of tissue spaces or produce hyperallergic and other harmful immunochemical reactions. Many pathogenic organisms, exclusive of the viruses, can exist in a viable state outside the host for various periods of time, though often with a loss in virulence. Others lose their virulence when cultured in an artificial media, illustrating the dependency of pathogens on a suitable host.

Considering the specialized physiological requirements of pathogens and the characteristics such organisms must possess to produce disease, the probability of Martian microorganisms being pathogenic to man or terrestrial animals and plants is rather remote. The very small proportion of terrestrial organisms that are pathogenic even though the Earth is inhabited by thousands of different species of higher forms of life indicates that pathogenicity is a highly specialized mode of existence. Accordingly, in the probable absence of higher organisms on Mars that resemble terrestrial life, the process of natural selection which resulted in the evolutionary development of pathogens is non-existent.

In order for a Martian microorganism to be pathogenic, it would have to possess those characteristics necessary to overcome the normal defense mechanisms of a higher organism and produce a substance such as a toxin which is deleterious to the host without the advantage afforded by evolutionary processes. It should be mentioned that there exists a special type of pathogen which although not actually invasive, produces disease. The bacteria that produces tetanus and gas gangrene remain dormant in the soil as spores, and normally do not proliferate until they lodge in deep wounds where conditions are favorable to their growth. There they produce a toxin which is extremely lethal. The possibility exists that certain Martian microorganisms could similarly produce chemicals deleterious

to higher terrestrial forms of life. Thus, invasiveness would not necessarily be a prerequisite for pathogenicity in this case.

The problem, then, resolves itself more into determining whether Martian organisms are potentially pathogenic rather than pathogenic in their present state. Owing to the extremely high reproductive rate of microorganisms, the mutation rate is accordingly higher than any other form of life. Moreover, microorganisms have several adaptive mechanisms that enable them to rapidly adjust to new and even unfavorable environments. A familiar example is the development of resistant pathogenic strains to antibiotics such as penicillin in a relatively short period of time. However, even if Martian organisms have a high mutation rate, only a small percentage of mutations are beneficial to an organism. Nevertheless, it is possible that the mutant form, if better adapted to its new environment will, under the influence of natural selection, replace its parent strain and establish an ecological niche which may be harmful or pathogenic to terrestrial life.

Aside from whatever purely pathogenic effects Martian microorganisms may exert, the introduction of these organisms into the terrestrial environment may result in a serious imbalance in the ecology of Earth, provided that they can compete successfully with established terrestrial microorganisms. This occurrence could be potentially more harmful to man than possible pathogens. Microorganisms are responsible for most of the turnover of organic and inorganic matter on Earth and all forms of higher life are dependent upon the role of microorganisms. For example, microorganisms produce 80% of all the oxygen and 90% of all the carbon dioxide in our atmosphere. Moreover, activities of microorganisms govern most of the chemical and physical properties of soil and live in a highly complex ecology with other species of organisms. If, through the processes of mutation or adaption, Martian microorganisms manage to establish an ecological niche, this could result in a change, perhaps deleterious, in the basic ecology of Earth, or at least in certain environments. As an example, since Mars is a colder planet and considerably more arid than Earth, it is possible that Martian microorganisms might be more competitive than terrestrial organisms with respect to these aspects of their physiology provided that all other functions are equal. Or Martian organisms could utilize as a nutrient a substance not

ordinarily attacked by terrestrial organisms, and thus compete effectively by virtue of their nutritional capabilities. However, even when large populations of alien bacteria are added to soil, the new organisms rarely become established and die within a short period of time. Competition is usually too keen in the complex ecology of the soil for foreign organisms to establish a niche. There are, however, areas of Earth where the microbial population is sparse, such as desert regions, and Martian organisms might have an opportunity to become established provided conditions are suitable for their survival.

10.4 The Study of Martian Organisms by Unmanned Probes

The manned mission to Mars will be preceded by the Voyager program consisting of a series of unmanned lander probes designed to determine the presence of life. Most of the life-detection experiments planned are based on the assumption that the biochemistry of Martian life is similar to ours. Because of payload limitations, the early experiments must be relatively simple, compact and light-weight, and will attempt to establish the existence or non-existence of life without providing a great deal of information regarding the nature of this life. Later, as payload capacity is increased through advances in rocket power, more sophisticated experiments are planned which can deal with the problems of defining and investigating new and perhaps exotic forms of extraterrestrial life. The types of experiments that are being planned are both varied and extensive and, if successful, would be able to preliminarily identify and characterize Martian life with respect to its morphology, physiology, biochemistry, and ecology. Although these studies will immensely increase our knowledge of Martian life, many limitations are inherent and it will not be until samples of Martian life are actually brought back to laboratories on Earth for prolonged and extensive analysis that comprehensive information will be provided. The problems involved in ascertaining the pathogenicity or particularly the potential pathogenicity of an organism by remote instrumentation are formidable and it is doubtful that meaningful experiments could be designed which would rule out the existence of harmful organisms within an acceptable level of confidence. To gain information regarding the pathogenicity of Martian organisms to higher terrestrial forms of life, living small mammals, or intact plants should preferably serve as indicators, rather than parts of organisms such as red blood cells or tissue cultures. Even soil

saphophytes can attack tissue cultures, but these organisms are innocuous to a living animal because the defense mechanisms of the animal are intact. Provided that the maintenance of a living animal is feasible in an unmanned experiment and that infection by Martian organisms could be determined and properly interpreted, this type of experimentation would still not provide an assessment of the ability of such organisms to adapt and mutate to pathogenic strains. Furthermore, no living system other than man himself can serve as a reliable indication of pathogenicity as few animal pathogens can be transmitted to man. While there are a large variety of diagnostic procedures used to identify pathogenic organisms, these are quite specific, dependent upon known systems, and probably would not serve as reliable indicators of the pathogenicity of extraterrestrial organisms. Conceivably, ecological experiments could more readily be designed which might ascertain the ability of Martian microorganisms to compete and interact with terrestrial microorganisms, but even this approach is likely to be inconclusive and difficult to interpret due to the complexity of ecological relationships.

Thus, while it is possible to perform unmanned experiments that may give some indications of the nature of Martian life, the inherent technical difficulties and unreliability associated with gaining meaningful information by remote telemetry from unknown forms of life, dictate that defensive measures be undertaken to prevent the back contamination from early Martian missions until such organisms can be comprehensively examined and all potential hazards eliminated.

Unmanned Decontamination Studies

The ultimate success of any decontamination procedure depends upon a knowledge of the resistance of microorganisms to the particular method of sterilization. Without such information, the choice of decontaminants for the manned Martian mission will be selected on results obtained with terrestrial organisms, and these methods may not be effective against Martian organisms. It is conceivable, for example, that Martian organisms might be considerably more resistant to ultraviolet radiation due to the probable lack of atmospheric shielding on Mars.

It is imperative, therefore, that experiments be conducted with unmanned probes to evaluate the resistance of tolerance of Martian microorganisms to such well-known decontaminants as heat, ionizing radiations, chemical agents, etc. These studies could be conducted without necessarily identifying or determining the potential pathogenicity of Martian organisms. Several of the life detection experiments planned for the Voyager program could readily be modified to include sterilization studies.

10.5 Prevention of Back Contamination

By thoroughly understanding the sources of contamination, it is possible to recommend procedures which will control back contamination from Mars. If life does exist on Mars it must be assumed that it is widespread throughout the environment, as it is on Earth, rather than confined to limited areas. Therefore, four possible sources of contamination must be considered:

1. Samples collected for scientific investigation
2. Space suits, equipment, etc.
3. Crew members
4. Martian Excursion Module (MEM)

It should be recognized that it is virtually impossible to ascertain whether a complex piece of hardware is sterile because the actual item cannot be tested for sterility in a nondestructive manner. Such items as listed above can only be considered sterile in the sense that there is a certain low probability of viable contamination. That probability can be made as low as desired within the capabilities of the prescribed procedures.

10.5.1 Entry Airlock System

A means of access and exit for the crew to and from the MEM must be provided which will not admit contaminants to the command station of the MEM and will provide for decontamination of necessary personnel and support equipment. This can be accomplished with an airlock system which would serve as the transitional interface between members of the landing party and the command station. Not only is it mandatory that back contamination be minimized, but it

is equally important that the contamination of Mars with terrestrial organisms be prevented. Contamination of Mars with terrestrial microorganisms would destroy a unique opportunity for the exploration and study of extraterrestrial life. Thus an entry-exit airlock system would serve a dual function.

The probability of airborne contaminants from the Martian environment entering the airlock can be reduced by maintaining a higher than ambient static pressure in the airlock. Similarly, contamination of the command station can be minimized by maintaining the command station at a higher pressure than the airlock. A constant flow of decontaminated air (which flows counter to the movement of the personnel entering the command station) can be accomplished by providing a supply of decontaminated air to the command station and airlock and by providing various means of venting at both inner and outer portals. To admit personnel into the airlock and command station, and to minimize fluctuations in the pressure differential between the contaminated and uncontaminated areas, various portal devices can be used. All should be designed to open and shut rapidly while providing the minimum aperture necessary to pass a man's body.

10.5.2 Decontamination of Crew Members

Decontamination within the airlock should involve removing, deactivating, or destroying contaminants from exposed personnel to such a degree that the probability that contaminants will be introduced into the command station is very remote, perhaps as low as 10^{-4} .

Members of the landing exploratory party could be protected from all physical contact with the Martian environment by means of a self-contained life support suit. There should be little chance of contamination of the skin or inhalation of contaminants provided that the suit contains an adequate atmosphere filtration system. The problem of decontamination of personnel will then be largely confined to decontamination of the surface and subsurface areas of the suit. It is possible that members of the landing party will remain in the suits for the duration of the mission without entering the command station. If this protocol is followed, decontamination procedures would only have to be followed once just prior to the return flight. In the event crew members re-entry the excursion

module intermittently for purposes of rest, eating, and other functions, the same procedures must be followed each time. There is a substantial body of information pertaining to decontamination under special situations which can be directly applied to this problem. These include BW agent decontamination, protection of personnel who work with pathogenic organisms, and removal of particulate contamination from personnel and equipment entering clean rooms.

Three sequential types of procedures for the decontamination of exposed personnel appear to be pertinent:

- Destruction of contaminants without removal from space suit
- Removal from space suit with subsequent destruction of contaminants
- Removal from surface of the body

Destruction of Contaminants

Clearly, destruction without need for physical removal from the space suit would be the safest, most reliable, and simplest procedure. However, it is important to insure that adequate destruction of the microorganisms does not materially damage or reduce the reliability of the suit. Furthermore, known methods require a considerable time of exposure to the disinfectant for a high percent kill, often of the order of many hours or more.

Examples of such treatment are: a) exposure to volatile toxicants such as ethylene oxide or betapropiolactone; b) saturation with solutions of strong oxidizing agents (permanganate, chlorine and other halogens) or biocides (phenols, formaldehyde, etc.); and, c) exposure of radiation (ultraviolet light and soft X-rays). The last methods will sterilize surface areas, but will not decontaminate cracks or crevices which are shadowed by portions of the surface area. Another approach is to incorporate biocides directly into the material of the suit which could render the suit self-sterilizing.

Heat is an effective method of killing microorganisms, particularly spores, which are resistant to many chemical biocides. The suit might be designed so that limited surface areas can be heated to temperatures required for sterilization.

A useful approach to reducing the numbers of organisms present on the surface of the suit would be to help protect the suit from contamination by means of a non-porous protective shield which could be discarded prior to entrance of personnel into the airlock. Any method that reduces the number of organisms on the surface of the suit will reduce the probability of viable organisms remaining after the sterilization procedure.

In spite of the limitations of presently known methods of decontamination without prior removal of the agent, the directness of the approach and the margin of safety afforded to the crew members is so advantageous as to warrant further investigation into new methods that are rapid and effective.

Removal of Contaminants From Suit

Contaminants could be removed from the surface of the suit fairly rapidly, without immediate destruction. The contaminants could then be destroyed by any one of the methods previously discussed without the hazard of damaging the suit. This approach offers the advantage of permitting personnel to remove the suit and enter the command station without long delays. Rapid entry is particularly important if crew members must frequently enter the command station.

Removal of contaminants could be accomplished by the use of a high speed shower or scrubber containing a mixture of a disinfectant and a detergent to expedite the washing procedure. A further method might involve the transfer of the contaminant from the suit back to the outside environment by means of a high-efficiency low-volume flow vacuum cleaning device. Thus, upon entering the airlock, personnel would be able to remove many of the loosely adherent organisms from the surface of the suit by proper use of this method as a pretreatment prior to other chemical or physical disinfecting agents.

Removal from Body Surface

Even though rigid precautions must be taken to prevent contamination of the skin and other areas of the body, the possibility of accidental contamination must be considered and appropriate precautions taken. Therefore, a showering procedure might be used as a first cleansing step immediately after the crew member discards the suit, regardless of previous processing. Multistage showers with a

decontaminant or detergent contained in the first stage followed by possibly a mechanical flushing system and then a clear rinse should be considered. The shower could be followed by hot air drying in conjunction with ultraviolet irradiation.

Techniques which greatly reduce the quantity of water required to accomplish decontamination are very desirable. Certain quantities of water, however, will probably always be required. The possibility of reclaiming contaminated water, therefore, deserves consideration.

10.5.3 Decontamination of Equipment

Non-expendable equipment will be required to undergo decontamination before it is permitted into the command station of the MEM. Small items could be placed in impermeable bags or enclosures and treated with germicidal vapors or solutions. Large items could be sprayed or immersed in germicidal solutions. Heat treatment would be applicable provided the materials are compatible with heat. Equipment which is porous and difficult to decontaminate (gaskets, seals, etc.) should be discarded instead of assuming the risk of inadequate decontamination. If this is not practical, the items must be placed in perfectly sealed containers for later decontamination.

10.5.4 Decontamination of Samples

Samples of the Martian soil, subsoil, rocks, etc., will be collected and brought back to Earth for investigation and represent a prime source of contamination. Samples should be collected in containers that can be perfectly sealed against leaks. Before the sample containers are permitted into the command station, the surfaces should be decontaminated in the airlock by applying germicidal solutions or vapors. Heat would be precluded due to possible destruction of the contents unless the container is thermally insulated to protect the contents from the effects of heat.

If it is necessary to examine the samples during the return voyage, this should be carried out in sterile glove boxes and hoods under the most rigid conditions of isolation. The same precautions should apply once the samples reach Earth.

10.5.5 Sterilization of Air and Surfaces Within Airlock

A means of sterilizing the air within the airlock is essential, as particles with diameters of less than 10 microns can remain suspended in the air. A useful and effective technique of air disinfection is direct ultraviolet irradiation of both room air and room surfaces. Hospital studies have shown that ultraviolet lamps have a disinfectant effect with sprayed bacteria equivalent to 29 to 169 air changes per hour.

Sterilization of surfaces could be accomplished by washing or spraying with germicidal solutions or vapors. All surfaces should be constructed of tough, dust resistant, non-porous, easily washed materials. It is also essential that the airlock contain no cracks or crevices that might protect contaminants from sterilization procedures.

The maintenance of the proper flow of air in the airlock is essential for reducing the probability of the spread of contaminants to the command station and requires sensitive methods to monitor the flow of air. The use of a higher air pressure in "clean" areas and a lower air pressure in contaminated areas is also an effective means of reducing the spread of airborne particles.

10.5.6 Decontamination of MEM

The exterior of the MEM will be heavily contaminated and represents a potential source of contamination to the orbiting Main Mission Module during the rendezvous and docking operation. Transfer of contaminants can be minimized, however, by designing the spacecraft in such a manner that the MEM is completely isolated from the Main Mission Module except at the airlock where the transfer of decontaminated crew members and equipment can be made. Earth entry and landing will be made in the Earth Entry Module precluding the need to sterilize the surface of the MEM which will remain in Earth orbit with the Main Mission Module. Any subsequent attempt to return the excursion module to Earth will require that it be received in a strict isolation environment and decontamination procedures applied.

10.5.7 Isolation of Exposed Personnel

Because it is impossible to predict the nature and epidemiology of potential Martians pathogens, those personnel who have been exposed to the Martian

environment should be placed in strict quarantine from each other and the remainder of the crew. Even healthy individuals who do not show symptoms of a disease can act as carriers of pathogens. Micro-organisms can be disseminated from the respiratory tracts of exposed individuals without they themselves being infected in the sense that they show symptoms of the disease. Droplets of body fluids laden with microorganisms emanate from the mouth and nose during talking, coughing, and sneezing. These droplets may be transmitted directly to other personnel, or more commonly, will fall to the floor where they are dehydrated and thereby transformed into very small "droplet nuclei." These nuclei later may become resuspended in the air and inhaled by others.

Because exhaled droplets are relatively large particles, the spread of contaminants from the respiratory tract could be diminished by wearing face masks or dust respirators which cover the mouth and nose.

Human faces are a potential source of many pathogens even in the absence of clinical symptoms. Normal methods of waste disposal, such as flush toilets, are likely to aerosolize inherent microorganisms; therefore, special methods of collection and disposal will be necessary. The use of germicidal chemicals or heat are efficient methods for sterilizing human wastes.

Quarantine measures should be put into effect immediately upon return from Mars and extended for a lengthy period of time, perhaps four or five weeks. If no disease symptoms appear during this period, isolation may be relaxed but exposed crew members should continue to wear face masks and wastes should be isolated and sterilized as an added precaution against the spread of infection.

11. SYSTEM ANALYSIS

11.1 Mission Modes

As stated in Section 3, several mission modes were studied to determine the sensitivity of these missions to uncertainties in the Martian and Cis-martian environments. The missions analyzed included Mars orbit rendezvous, flyby, and direct lander modes, with aerodynamic or retro capture at Mars, and with chemical or nuclear propulsion. The matrix of mission cases is given in Table 11.1. It is noted that a range of mission opportunities was studied, to illustrate the change in sensitivities over the cycle of favorable to unfavorable opportunities. 1982 was chosen as the nominal mission. Aerodynamic braking at Earth was assumed in all cases.

Table 11.1 MISSION MODES

CASE	MODE	CREW	MISSIONS
MARS ORBIT RENDEZVOUS	C-A-C-A ^{1,2}	7	1975-1990
	N-A-C-A	7	1975-1990
	C-C-C-A	7	1982
	N-N-N-A	7	1982
MARS FLY BY	C-A	3	1980
	N-A	3	1980
MARS DIRECT LANDING	C-A-C-A	7	1982
	N-A-N-A	7	1982

1. DEPART EARTH - CHEMICAL (NUCLEAR)
ARRIVE MARS - AERO (RETRO)
DEPART MARS - CHEMICAL
ARRIVE EARTH - AERO.

2. 10-DAY STOPOVER

11.2 Mission Sensitivity Factors

Approach

The sensitivity analysis was performed by first determining the sensitivity of the manned Mars system, as described in Section 4, to changes in those system design parameters that are sensitive to environmental factors. This step in the overall analysis yields "sensitivity factors," that can be used to relate changes in the environment to changes in system weight (or cost):

$$\begin{aligned} \text{Change in system weight} &= \left(\frac{\% \text{ Change in system weight, } W_o}{\% \text{ Change in environment}} \right) \% \text{ Change in environment} \\ &= SF \times \% \text{ Change in environment} \end{aligned}$$

Where possible, changes in the environment were related to changes in system component weights: for example, atmosphere density can be related to parachute and retro system weight for the MEM, and changes in MEM weight can be related to changes in overall system weight through the sensitivity factors. As shown in Table 11.2, interactions between environmental factors and the overall system weight can be related through four system elements: propellant tank weight (or micrometeoroid shielding weight), main spacecraft weight (which includes solar radiation shielding), aero entry system weight, and MEM weight. Hence, sensitivity factors are required to link these four system elements to the overall spacecraft weight in Earth orbit.

$$SF_1 = \frac{\% \text{ Change in } W_o}{\% \text{ Change in Structure Factor, } \sigma} = \frac{\Delta W_o}{\Delta \sigma}$$

$$SF_2 = \frac{\% \text{ Change in } W_o}{\% \text{ Change in Mission Module Wt, } W_{MMM}} = \frac{\Delta W_o}{\Delta W_{MMM}}$$

$$SF_3 = \frac{\% \text{ Change in } W_o}{\% \text{ Change in Aero Entry System Wt, } W_{Aero}} = \frac{\Delta W_o}{\Delta W_{Aero}}$$

$$SF_4 = \frac{\% \text{ Change in } W_o}{\% \text{ Change in MEM Wt, } W_{MEM}} = \frac{\Delta W_o}{\Delta W_{MEM}}$$

TABLE 11.2 MANNED MARS MISSION SENSITIVITY FACTORS

Determine Change in Earth Orbit Weight due to Change in:

	$\Delta\sigma$ (Tank Struc)	Δ MMM	ΔW_{Aero}	ΔW_{MEM}
Atmosphere				
Aero Corridors			X	
Aero Heating			X	
MEM Descent				X
MEM Ascent				X
Parking Orbit				X
Meteorology				
Winds				X
Dust		X		
Observation		X		X
Surface				
MEM Impact				X
Surface Rover				X
Solar Radiation		X		X
Micrometeoroid Flux	X	X		

Scaling Laws

Sets of scaling laws were developed during recent studies of the manned Mars mission (References 1.1 and 11.1), which are directly applicable for deriving the four general sensitivity factors outlined above. These scaling laws are presented in Appendix C. The general design criteria followed in the scaling laws are given in Table 11.3. The computations are performed on 7094 machines, and take into account gravity losses for major propulsion maneuvers, engine size optimization based on gravity loss - engine weight relations, propellant boiloff, jettisoning operations, navigation and attitude control propellant requirements, variation in solar radiation shielding with mission year and distance of approach to the sun, and parking orbit circularization allowances. A complete discussion of the calculation procedures is given in the cited references.

TABLE 11.3 MISSION DESIGN CRITERIA

• EARTH RECOVERED PAYLOAD	— 10,000 LBS
• MISSION MODULE (7-MEN)	— 85,000 LBS AT 1 AU — 65,000 LBS (FLY BY)
• MARS EXCURSION MODULE	— 50,000 LBS
• LIFE SUPPORT EXPENDABLES	— 39 LBS/DAY
• STOPOVER TIME	— 10 DAYS
• PROPULSION	
NUCLEAR I_{SP}	— 800 SEC
$H_2 - F_2$ I_{SP}	— 450 SEC
STORABLE I_{SP}	— 330 SEC
• MIDCOURSE CORRECTION	— 100 M/SEC EACH LEG
• ATTITUDE CONTROL	— 1% EACH LEG; 0.2% CAPTURE
• MICROMETEOROID PROTECTION	
• OPTIMUM PROPELLANT INSULATION	

Mission Optimization

Spacecraft performing Mars stopover missions have a wide choice of paths and calendar dates available to them. Each combination of calendar date of departure and trip duration (both inbound and outbound) requires a different transfer trajectory, which has unique values of departure and arrival velocities. These combination of velocities determine the spacecraft aerodynamic and propulsion system performance requirements. To select an optimum mission profile for any given mode, it is necessary to trade-off the effects of changes in mission characteristic velocities, or trajectories, to determine those combinations that minimize overall system weight (or cost).

It is mandatory that this optimization be performed for each and every mission. For example, if the spacecraft design is altered from the nominal to

accommodate an uncertainty in the environment (e. g. , heavier meteoroid shielding), the trajectory paths and calendar dates must be reoptimized for the now heavier spacecraft. In other words, having altered the spacecraft design in some way, it is necessary to select a new trajectory profile if the spacecraft is to perform the mission in the most efficient manner. Failure to do so can completely obscure the effects of the design change, and give erroneous sensitivity factors.

STL has developed an analytical method for optimizing trajectory profiles for any given set of vehicle scaling laws and mission mode (see Reference 1. 1). Use is made of differential equations, which contain vehicle weight - velocity exchange ratios and derivatives of mission characteristic velocities with respect to launch date and trip duration. The process does not require total trip duration constraints (although these can be introduced if desired) and has been generalized to include launch hold allowances, arbitrary aero/retro braking modes and dwell time at Mars. Variable thrust-to-weight ratios can be selected to minimize engine weight, and secondary propulsion maneuvers can be inserted (such as midcourse corrections and parking orbit circularization allowances).

The sensitivity factors summarized in the following section have been minimized by the foregoing optimization procedures.

Sensitivity Factors

The results of the sensitivity factor analysis are presented in Tables 11. 4 and 11. 5, and in Figures 11. 1 and 11. 2.

Tables 11. 4 and 11. 5 summarize vehicle gross weights for the combinations of mission modes listed in Table 11. 1, and design parameter variations given in Table 11. 2. It is noted that allowances for Earth launch delays are not included in the performance computations; this does not affect the sensitivity factors significantly.

The nominal mission performance is given in the top rows of Table 11. 4 and 11. 5 for the various missions. The second row gives the spacecraft gross weights and sensitivity factors for a 100 percent increase in meteoroid shielding, that is,

$$\sigma_M = 2 (\sigma_M)_{\text{nom}}$$

As an example, the sensitivity factor for the 1982 mission is computed as follows (Table 11. 4):

Table 11.4 SENSITIVITY FACTORS

$$\frac{W}{SF} = \frac{\text{WEIGHT (MILLION LBS)}}{\text{SENSITIVITY FACTOR}} = \frac{\% \text{ CHANGE IN WEIGHT}}{\% \text{ CHANGE IN FACTOR}}$$

MISSION	1975	1978	1980	1982	1984	1986	1988	1990
NOMINAL W	1.691	1.704	1.554	1.341	1.206	1.194	1.399	1.704
NOMINAL + $\Delta \sigma_M$ ($2 \times \sigma_M$)	1.749 0.034	1.761 0.034	1.604 0.032	1.397 0.042	1.238 0.027	1.225 0.026	1.461 0.045	1.760 0.033
NOMINAL + ΔW_{MEM} (80,000 LB)	1.794 0.101	1.806 0.100	1.651 0.104	1.448 0.133	1.296 0.124	1.283 0.125	1.490 0.108	1.805 0.099
NOMINAL + ΔW_{AERO} (.50)	1.794 0.092	1.820 0.102	1.660 0.103	1.448 0.120	1.290 0.105	1.267 0.092	1.476 0.083	1.803 0.087
NOMINAL + ΔW_{MMM} (100,000)	1.870 0.605	1.881 0.592	1.713 0.585	1.497 0.665	1.333 0.600	1.321 0.608	1.546 0.600	1.879 0.587

NOMINALS

$$\sigma = \text{STRUCTURAL FACTOR} = \frac{\text{JETTISON WEIGHT}}{\text{STAGE GROSS WEIGHT}} \quad (\text{STL MICRO METEOROID SHIELD ALLOWANCE})$$

$$W_{MEM} = \text{WEIGHT OF MEM} = 50,000 \text{ LBS}$$

$$W_{AERO} = \text{WEIGHT OF MARS AERO ENTRY SYSTEM (K = 0.3)}$$

$$W_{MMM} = \text{WEIGHT OF MARS MISSION MODULE} = 85,000 \text{ LBS.}$$

NOTE: 10-DAY STOPOVER

TABLE 10.5 SENSITIVITY FACTORS (1982 MISSION)
(10-Day Stopover)

$$W = \text{WEIGHT (MILLION LBS)} \quad SF = \text{SENSITIVITY FACTOR} = \frac{\% \text{ CHANGE IN WEIGHT}}{\% \text{ CHANGE IN FACTOR}}$$

	MODE	MARS ORBIT RENDEZVOUS			FLYBY *			DIRECT LANDING	
		CACA	NANA	CCCA	NNNA	CA	NA	NANA	CACA
NOMINAL	W	1.341	.997	3.147	1.708	.443	.299	2.175	5.222
NOMINAL + $\Delta\sigma$ (EARTH DEPART)	W SF	- -	- -	- -	- -	0.498 0.124	0.317 0.057	- -	- -
NOMINAL + $\Delta\sigma$ (MARS ARRIVE & MARS DEPART)	W SF	- -	- -	3.363 0.069	1.851 0.085	- -	- -	- -	- -
NOMINAL + $\Delta\sigma$ (MARS DEPART)	W SF	1.397 0.042	1.023 0.026	- -	- -	- -	- -	2.578 0.185	6.144 0.177
NOMINAL + ΔW_{MEM} (80,000 LB)	W SF	1.448 0.133	1.063 0.111	3.315 0.089	1.821 0.110	- -	- -	- -	- -
NOMINAL + ΔW_{PROBE} (10,000 LB)	W SF	- -	- -	- -	- -	0.459 0.035	0.310 0.038	- -	- -
NOMINAL + ΔW_{AERO} (.50)	W SF	1.448 0.120	1.055 0.087	- -	- -	- -	- -	2.340 0.114	5.638 0.120
NOMINAL + ΔW_{AERO} (1.0)	W SF	- -	1.232 0.101	- -	- -	- -	- -	2.882 0.140	6.933 0.141
NOMINAL + ΔW_{MMM} (100,000 LB)	W SF	1.497 0.665	1.067 0.400	3.476 0.598	1.849 0.470	- -	- -	2.378 0.533	5.771 0.600
NOMINAL + ΔW_{MMM} (80,000)	W SF	- -	- -	- -	- -	0.493 0.490	0.333 0.494	- -	- -

* 1980

MARS ORBIT RENDEZVOUS MODE
C-A-C-A

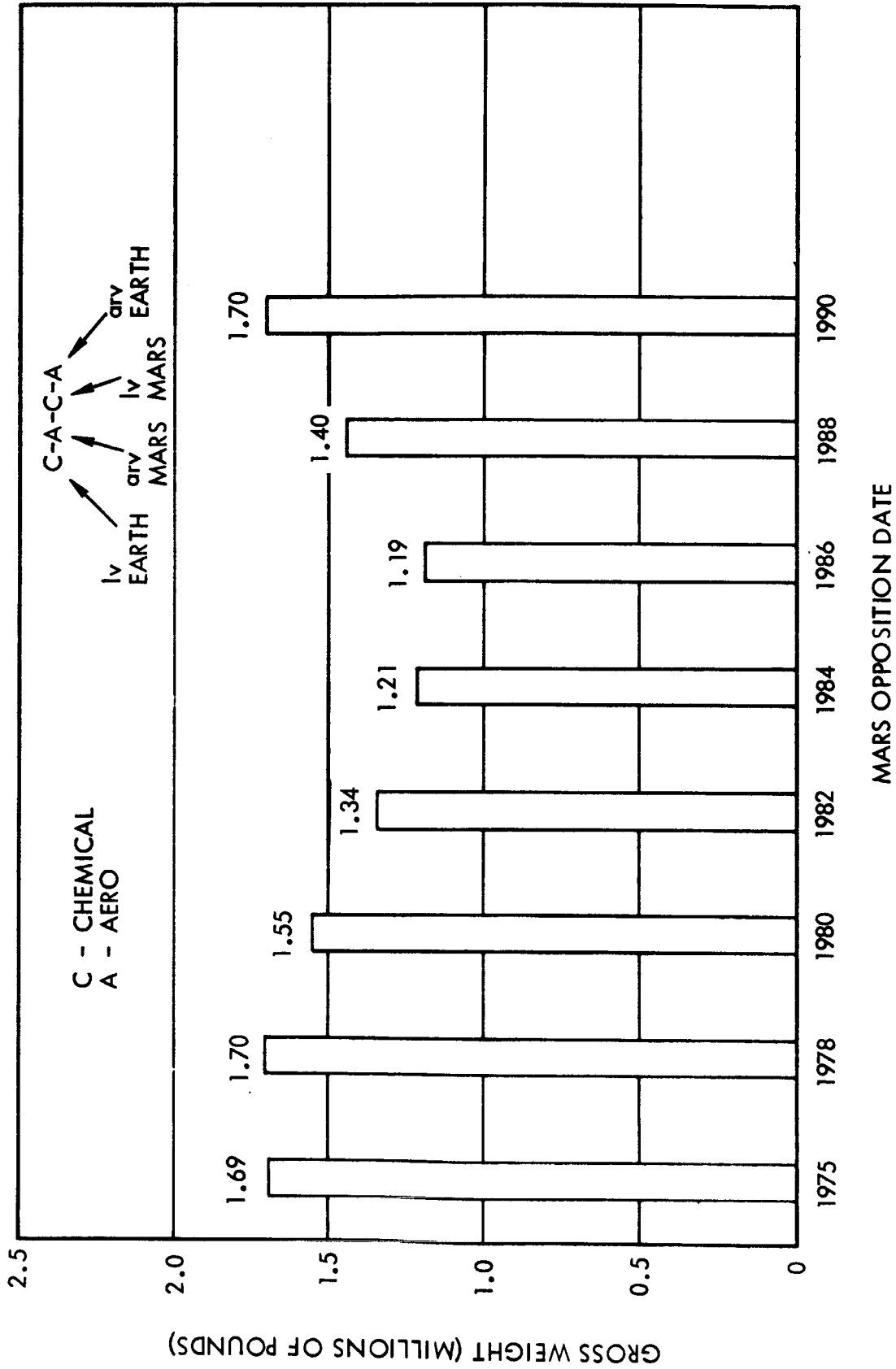


Figure 11.1 Comparison of Mission Gross Weight (10-Day Stopover)

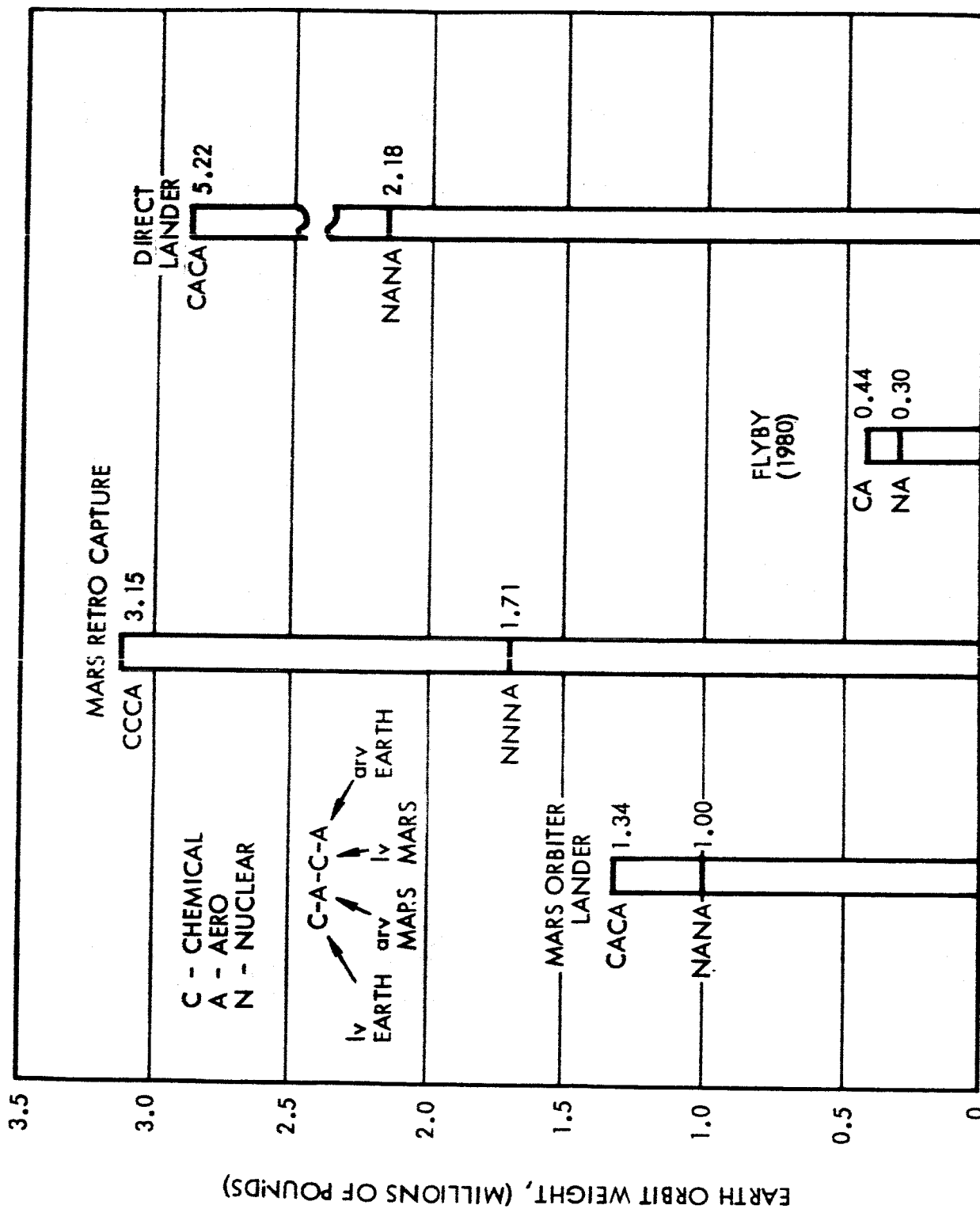


Figure 11.2 Comparison of Mission Modes
(1982 Mission 10-Day Stopover)

$$\begin{aligned}
 SF &= \frac{\% \text{ Change in system weight, } W}{\% \text{ Change in meteoroid shielding weight}} \\
 &= \frac{\frac{1.397 - 1.341}{1.341} (100)}{\frac{2 (\Delta \sigma_M)_{\text{nom}} - (\Delta \sigma_M)_{\text{nom}}}{(\Delta \sigma_M)_{\text{nom}}} (100)} \\
 &= 0.042
 \end{aligned}$$

The remaining values are calculated in a similar manner.

The third row gives the gross weights and sensitivity factors for a 60 percent increase in MEM weight, from 50,000 lbs to 80,000 lbs. In the fourth row a 66.7 percent increase in Mars aero entry system weight (from a scaling factor $K = 0.3$ to $K = 0.5$) is analyzed; the last row shows the effect of increasing the main mission module from a nominal 85,000 lbs to 100,000 lbs.

It is noted that the values of the increases in system component weights assumed as a means for computing the sensitivity factors, are arbitrary. The sensitivity factors must be multiplied by actual changes in system design brought about by the uncertainties in the environment to determine the system-environment interactions.

The sensitivity factors given in Tables 11.4 and 11.5 are valid (remain constant) for the range of design changes given above. This range of changes was not exceeded during the evaluation of the possible environmental changes. In general, the sensitivity factors remain constant over fairly wide ranges of design changes, as demonstrated in Figure 11.3 (from Reference 11.1).

The spacecraft gross weights are summarized in Figures 11.1 and 11.2. Figure 11.1 shows the variation in vehicle weight over the range of mission opportunities from 1975 to 1990, which covers a cycle of favorable to unfavorable opportunities. The weights range from 1.19 to 1.70 million pounds. It is noted that 1982 is an opportune time to commence the manned Mars landings because of reduced system requirements, which persist throughout the remainder of the decade. Nuclear systems (at least for earth depart) could be introduced into the program toward the late 1980s to make the unfavorable opportunities of the 1990s less difficult.

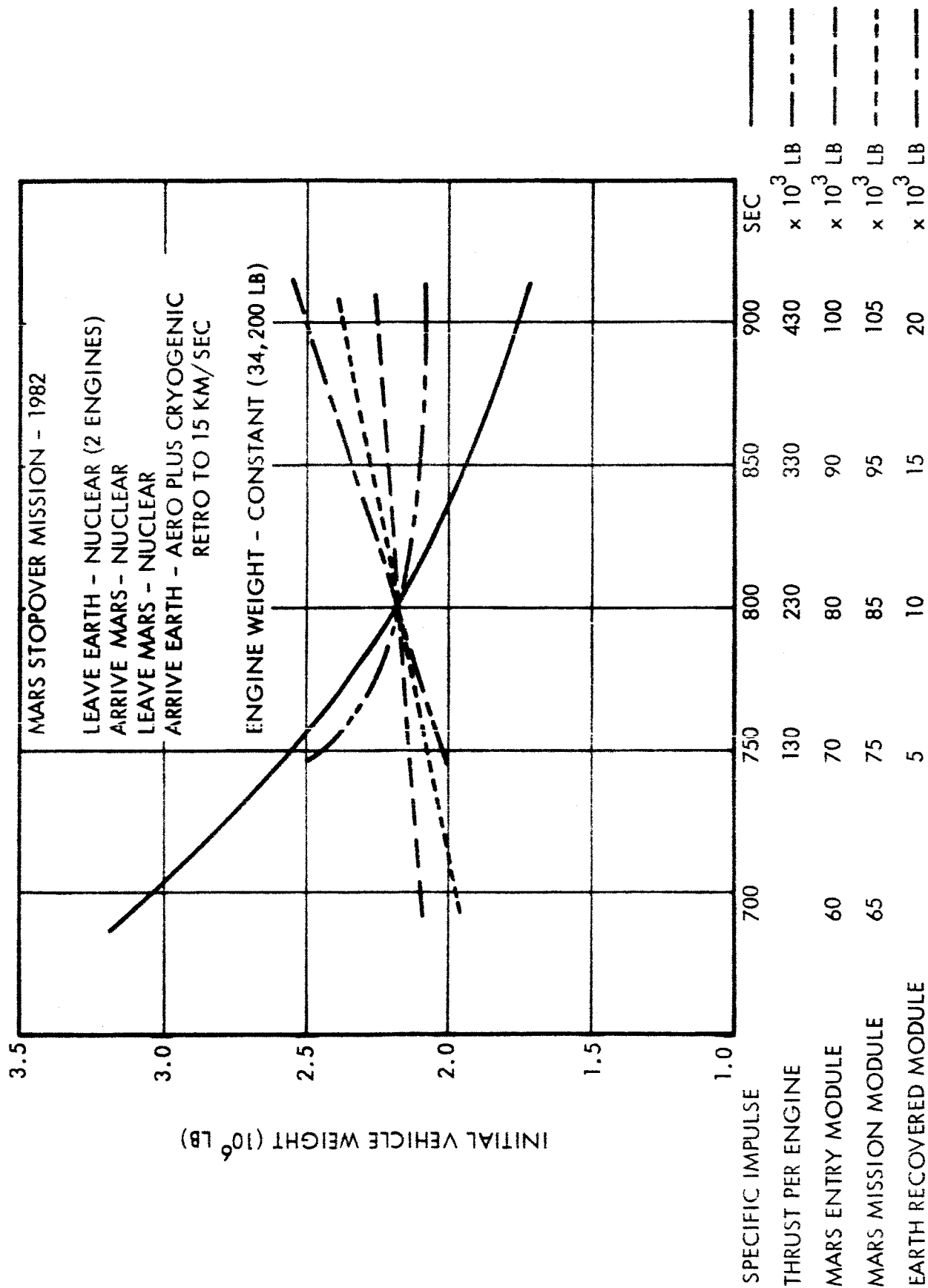


Figure 11.3 Sensitivity Analysis - Typical Results

Figure 11.2 shows the variation in gross weight with mission mode for the 1982 opportunity. A nuclear-hydrogen system reduces gross weight by 25 percent for the aero braking mode (from 1.34 to 1.00 million lbs), and by 45 percent for the retro braking mode. The retro braking mode more than doubles gross weight; a nuclear retro braking mode is 28 percent heavier than a chemical aero braking mode (from 1.34 to 1.71 million lbs). The direct landers are extremely heavy.

11.3 System Weight Sensitivity

The results of the analyses of mission-environment interactions are summarized in this section, and combined with the sensitivity factors to obtain the effects on spacecraft gross weight.

Atmosphere Uncertainties

Uncertainties in the atmosphere of the order of 10 percent will cause small changes in the design weight of the main spacecraft aero entry system. The vehicle must have a slightly greater lift-to-drag ratio capability (from 0.20 to 0.24), and some increase in heat protection (about 420 lbs) to the nominal shield weight of 28,880 lbs. Hence, a 10 percent uncertainty in the atmosphere increases aero entry system weight by 1.45 percent, which results in an increase in spacecraft gross weight in earth orbit, W_o , of (1982 CACA mission):

$$\begin{aligned} SF &= 0.120 \\ \text{Change in } W_o &= 1.46 \times 0.120 \\ &= 0.18\% \end{aligned}$$

Under the worst possible conditions, the aero entry system would be required to accommodate both the Schilling II Upper Limit atmosphere and the Model 3 (10 mb) atmosphere. In this case the L/D requirements would increase from 0.1 to 0.3, and heat shielding would increase by 4,000 lbs. The resulting increase in spacecraft gross weight is 1.81 percent.

The MEM is also sensitive to the atmosphere, particularly to surface density. A change of 10 percent in surface density will increase parachute weights by 10 percent, which increases the MEM weight by 0.15 percent. The resulting change in spacecraft gross weight, W_o , is $0.15 \times SF = 0.15 \times 0.133 = 0.02$ percent. If the decelerator system is designed for the nominal, Model 2 (25 mb) atmosphere, but is modified to accommodate the Model 3 (10 mb) atmosphere, the resulting increases in MEM and spacecraft gross weights are 1.1 and 0.14 percent,

respectively. In addition, the MEM ascent propulsion system must be sized to accommodate the higher drag losses. A 10 percent change from the Model 2 (25 mb) nominal atmosphere results in a 1.8 percent increase in MEM weight, whereas allowance for the Schilling II Upper limit atmosphere results in a 17.4 percent increase. Corresponding increases in spacecraft gross weight are 0.24 and 2.37 percent, respectively.

Combined effects of the atmosphere on the spacecraft aero capture system, MEM decelerator, and MEM ascent propulsion system, result in increases in spacecraft gross weight in earth orbit of 0.42 percent for a 10 percent uncertainty in the atmosphere, and 4.18 percent for the worst combination of atmospheres considered.

The corresponding interactions for all mission modes are summarized in Table 11.6. The direct landers are affected strongly by atmosphere uncertainties, as might be expected. The retro landers are only slightly less sensitive.

Winds

The effects of winds on MEM weights were given in Figure 7.10, and the corresponding effects on spacecraft gross weight in Table 11.6.

Meteoroid Protection

The effects of altering the meteoroid protection on the spacecraft gross weight are complicated by the multiple shields required for the aero entry system: a meteoroid shield must be placed around the shield during the transit out to Mars; this outer shield is jettisoned prior to entry at Mars. The aerodynamic heat protection shield is jettisoned immediately after capture; hence, a second meteoroid shield is required to protect the spacecraft during the return passage. Allowances for changes in meteoroid shielding for the main mission module and aero entry system are handled like changes in module weight and aero entry system weight, respectively. Allowances for propellant tank shielding are handled directly by the appropriate sensitivity factors (see Tables 11.4 and 11.5).

As an example, an analysis is given of the effects of meteoroid shielding on the 1982 CA CA mission. The total area of the spacecraft at Mars entry is 4280 sq ft. The nominal meteoroid shield weighs about 1 lb/sq ft, so that the outer

TABLE 11.6 SENSITIVITY SUMMARY

	CACA		RETRO AT MARS		FLYBY		DIRECT	
	1982		1986		CA		CACA	
					NA		NANA	
UNCERTAINTY IN ATMOSPHERE								
CAPTURE	1.8	1.4	1.3	0	--	--	0.2	1.7
MEM	2.5	2.3	2.1	1.7	--	--	4.8	3.8
COMBINED	4.3	3.7	3.4	1.7	<1.0	<1.0	6.0	4.6
EFFECT OF WINDS								
50% WINDS (GRADIENT)	0.3(0.4)*	0.3(0.4)*	0.3(0.3)*	0.2(0.2)*			2.4(2.8)*	2.4(2.8)
MAX WINDS (NO GRADIENT)	0.3(0.2)	0.3(0.2)	0.3(0.2)	0.2(0.1)			2.3(1.6)	2.3(1.6)
MAX WINDS (GRADIENT)	0.7(1.1)	0.7(1.0)	0.6(0.9)	0.5(0.7)			5.6(8.0)	5.6(8.0)
MAX WINDS (GRADIENT, NO RANGE MAKEUP)	0.2(0.2)	0.2(0.2)	0.1(0.1)	0.1(0.1)	<1.0	<1.0	1.3(1.2)	1.3(1.2)
MICROMETEOROID DOUBLE THICKNESS	7.5	5.4	4.8	8.9	14.6	7.9	21.4	20.8
MSC/STL (Cometary)	7.4	5.7	4.8	6.8	10.0	6.5	14.5	14.3
SOLAR COSMIC RADIATION HALF THICKNESS (90% RECOVERY)	-4.8	-6.5	-3.9	-6.5	-9.1	-9.1	-5.2	-5.8
UNCERTAINTY IN SHIELD EFFECTIVENESS & FLUX	3.5	4.7	2.8	4.7	6.6	6.6	3.7	4.2
TOTAL UNCERTAINTY	8.3	11.2	6.7	11.2	15.7	15.7	8.9	10.0

* Sch Upper Limit

shield weighs 4,280 lbs. The inner shield covers only the main mission module and not the flare, and weighs 2120 lbs. If the shield weight is doubled, the following allowances must be made:

$$\text{Outer shield: } (SF)_{\text{Aero}} \frac{4,280}{(W_{\text{Aero}})_{\text{nom}}} = (0.120 \frac{4,280}{30,490}) = 1.68\%$$

$$\text{Inner shield: } (SF)_{\text{MMM}} \frac{2120}{W_{\text{MMM}}} = (0.665) \frac{2120}{85000} = 1.66\%$$

$$\text{Tanks: } (SF)_{\text{met}} 100\% = (0.042) 100 = 4.20\%$$

The total effect on spacecraft gross weight is 7.54 percent. Similar analyses for other mission modes are summarized in Table 11.6. Discussions of the assumptions of the various models are given in Section 9.2. It seems reasonable to assume, however, that uncertainties in the meteoroid models should not exceed one order of magnitude.

Solar Cosmic Radiation

Effects of uncertainties in solar cosmic radiation on spacecraft weight are evaluated directly in terms of changes in main mission module weight. The nominal shelter has a 22 gm/sq cm shield; if maximum recovery factors are assumed, the shield thickness could be reduced, possibly to 10 gm/sq cm, or to about half the original value.

11.5 System Weight Sensitivity Summary

It can be concluded that, from an overall system weight standpoint, the three most significant environmental factors are atmosphere, meteoroid flux and velocity spectra, and solar radiation flux, although the significance of the latter effect is due in large part to the lack of design information necessary to protect against assumed radiation fluxes.

Spacecraft weight alone may not be the most significant effect on system design. Of equal importance are:

- o Requirements for aero entry system lift-to-drag ratio.
- o Navigation accuracies (including allowances for seasonal and diurnal effects).
- o Knowledge of surface features for landing site selection.
- o Knowledge of soil conditions and local terrain, which have an interaction on MEM impact attenuator design and surface rover design (and feasibility).
- o Knowledge of surface ionization, which could have a strong effect on equipment design and development, as well as the validity of unmanned probe flyby measurements of the atmosphere by means of rf attenuation experiments.

The above factors are discussed in the following sections, and qualitative assessments of experiment priorities made.

12. PRIORITY RATINGS

The foregoing analyses established the sensitivities of the manned Mars mission system to uncertainties in the Martian and Cismartian environment. The interactions between the environment and the manned Mars mission system were established by gathering and analyzing available data on the martian and interplanetary environments. Upper and lower bounds were placed upon the environment data in an effort to establish limits on the uncertainties in each environmental factor. It was not possible to establish meaningful bounds on all environmental factors, and in some cases a parametric approach was used, that is, ranges of uncertainties in environmental factors were assumed and examined for the effect on mission system design.

The designs were analyzed to determine the effects of uncertainties in the environmental factors on the system design, particularly in terms of the gross weight of the system. The results of the mission weight sensitivity analysis were given in Table 11.6.

12.1 Evaluation Factors

As noted previously, factors other than system weight can influence the manned mission.

1) Design Feasibility

Mission systems or subsystems can fail because they are based on inaccurate design criteria. Mission success can be jeopardized by these factors. Examples are: inadequate shielding against solar radiation environment, and, of lesser importance, surface rovers designed for surface properties considerably different than the actual surface properties. The possible existence of a surface ionization layer can lead to electrical system breakdown if adequate equipment design and testing is not provided for. Items such as these which involve questions of feasibility, or which represent vitally needed design criteria, must be given a high priority.

However, it is difficult to assign numerical ratings within such a category because all items relate to mission success, although some items could lead to catastrophic failures whereas others would compromise the accomplishment of some scientific objective.

2) System Weight

This category of interactions can be related to increases in spacecraft gross weight depending upon the uncertainty in the environmental factors. The uncertainty in the Martian atmosphere falls within this category. The properties of the Martian atmosphere affect many elements of the mission, including the lift-to-drag ratio of the main spacecraft, the altitude of the parking orbit, the lander impact velocity, and the amount of propulsion required to return the manned lander to orbit. Fortunately, reasonable bounds can be placed on the possible variations in the atmosphere making it possible to adjust the design of the spacecraft to accommodate the uncertainties. Hence, the uncertainties in the atmosphere can be converted into system weight penalties. Additional examples of environmental factors that can be assessed in terms of overall mission weight penalties include allowances for uncertainties in the winds, which generally require an increased propulsion capability in the Mars excursion module to negate drift range and velocity at impact.

In general, the difference between factors in Categories (1) and (2) lies in the fact that the uncertainties in the environmental factors in Category (1) cannot be bounded. As a result, it is not known whether the spacecraft can be altered sufficiently to accommodate the uncertainties. Items in Category (2) can be bounded with reasonable confidence and the spacecraft design altered to accommodate the uncertainties.

3) Mission Operations

Environmental factors in Category (3) affect the operation of the spacecraft. For example, the uncertainty in the density and scale height of the atmosphere affect the parking orbit altitude of the main spacecraft. This factor must be determined to a reasonable degree of certainty to assure proper lifetime in the orbit, etc. Additional items in this category are the diurnal and seasonal variations in the atmosphere. The meteorology of Mars also can affect the operation of the lander craft, which might be scheduled to avoid dust storms over desirable landing sites, etc.

4) Mission System Development

The final category of environmental factors includes those which influence the development of the mission system. An important factor in this category uncovered during the sensitivity analysis is the possible existence of an ionization layer near the surface of Mars, which could create problems in the operation of the electrical apparatus aboard the Mars excursion module, causing electrical breakdown and possible difficulties in communication. Such difficulties can be avoided if the existence and nature of such an ionization belt is verified and steps are taken during the development program to prevent interference from such ionization environments. The existence and nature of dust storms on the Martian surface will also necessitate development tests to assure satisfactory operation of surface equipments in the dust environment.

12.2 Experiment Priorities

A numerical rating system was used to aid in establishing priorities for the measurements of the Martian and Cismartian environment factors. Each environmental factor was rated in each of the four categories discussed above:

- o Design feasibility
- o System weight
- o Mission operations
- o System development

The results of the analysis are given in Table 12.1. The most important factor was assigned a priority value of 3 and the lowest a value of 1. Of the four factors discussed above, that of design feasibility is the most important and cannot be compared on a numerical basis with the other four categories; hence, the ratings are not summed "horizontally." It is essential that environmental factors which affect the design feasibility of the manned systems be measured by the unmanned precursors. Items which affect the gross weight of the manned spacecraft system must be taken into account in the ordering of experiment priorities, but failure to make these measurements accurately should not result in catastrophic failure of the manned system.

12.2.1 Solar Cosmic Radiation Environment

The results indicate that most important factor affecting the design of the manned spacecraft system is the solar cosmic radiation environment.

Solar cosmic radiation is important, not only because it has a large influence on the weight of the manned system, but because it is very difficult with the present state of knowledge of the radiation environment and effectiveness of manned shields to establish design criteria for protection against the radiation environment that will assure mission success. The three factors entering into the establishment of meaningful design criteria for the solar radiation shielding are: the radiation environment to which the manned system will be exposed, the effectiveness and behavior of the shield in attenuating the radiation, and the physiological reaction of the crew to the radiation environment. Large uncertainties exist in the definition of the radiation environment. Although measurements of the environment are being made on the present Mariner 4 spacecraft, additional measurements must be given a high priority on Voyager and other unmanned precursor spacecraft. Sufficient experiments must be conducted to establish a statistically meaningful model of solar events including the large relativistic flare.

Table 12.1 ENVIRONMENT PRIORITIES

	DESIGN FEASIBILITY	WEIGHT PENALTY	OPERATIONAL CRITERIA	DEVELOPMENT CRITERIA	EXPERIMENT ACCURACY
ATMOSPHERE					
THERMO PRESSURE	2	2	1	1	50%
TEMPERATURE					
CHEMICAL COMP					
ELECTRICAL PROP					
IONOSPHERE	-	2	-	-	
SURFACE IONIZATION	-	2	2	-	
DIURNAL AND SEASONAL EFFECTS	1	1	1	1	
METEOROLOGY					
WINDS	2	1	2	-	50%
CLOUDS	-	-	1	-	
DUST STORMS	1	1	1	-	
CLIMATE	1	-	1	1	
SURFACE CONDITIONS					
SURFACE COMP	2	1	2	2	25%
SOIL PROPERTIES	2	1	2	2	
TOPOGRAPHY	1	1	2	2	
RADIOACTIVITY	1	-	1	1	
SEISMIC ACT	1	-	-	-	
AREOLOGY					
(SEE SURFACE CONDITIONS)					
BIOLOGY	2	1	2	2	
RADIATION ENVIRONMENT					
COSMIC RAD SURFACE	2	1	2	1	20%
COSMIC RAD - CISMARTIAN	3	3	3	3	
UV RAD AT SURFACE	1	-	2	-	
METEOROID ENVIRONMENT					
	2	3	1	1	60%
GENERAL					
ALBEDO - ABSORP	1	1	-	1	
MAG FIELD	1	-	-	-	
GRAV FIELD	1	1	1	-	
	3	HIGH PRIORITY			
	1	LOW PRIORITY			

A lower degree of uncertainty is associated with the effectiveness of radiation shielding; however, even here, additional experimental work must be carried out in ground-based laboratories to establish the effectiveness of shields. An uncertainty of about 100 percent in shielding effectiveness exists at present for high energy solar events.

Many unknowns exist in our knowledge of the response of the crew to high energy radiations. It has been the practice during the course of studies of the manned Mars mission to assume that crews exposed to large doses of radiation over the course of the trip tend to recover from the effects of the radiations according to recovery models proposed by Blair and others. These recovery models presume that irreparable damage from typical radiations is of the order of 10 percent, and is characterized by recovery half lives of the order 3 to 4 weeks. The amount of irreparable damage assumed by these typical recovery models is based upon animal experiments in which the subjects were exposed primarily to x-rays and fast neutrons. These recovery models have not been tested for radiation doses typical of those that might be experienced during the long duration planetary missions. Additional experiments must be carried out in this area.

In summary, many uncertainties exist in our knowledge of the solar cosmic radiation environment, the effectiveness of shields, and in man's response to the probable radiation environment to which he will be exposed. Experiment programs must be designed and carried out to reduce these uncertainties, and to establish better and more precise design criteria.

Ratings:	Design Feasibility	3
	System Weight	3
	Mission Operations	3
	System Development	3

Meteoroid Environment

The second priority environmental factor is that of the meteoroid hazard. The environment-mission system interaction analysis summarized in Table 11.6 indicates that the uncertainties in the meteoroid environment can have a large effect upon system weight. Problems associated with measurements of this environmental factor are given below. A more complete discussion of this effect is given in Volume II.

Although there are fairly large uncertainties in the meteoroid environment, the environment can be bounded within reasonable limits. Furthermore, particle velocities, which have a dominant effect upon shielding design, tend to decrease with increasing distance from the center of the solar system, so that the meteoroid environment will be less hostile even though the flux rates are predicted to be those of the near-Earth environment. Because of the large uncertainties in the environment, particularly as the inner reaches of the asteroid belt are encountered in the vicinity of Mars, attempts should be made to reduce the uncertainties as much as possible, particularly with respect to the velocity spectra of the meteoroid flux.

The best and most meaningful data available are those based upon visual and radar observations from ground based stations at the Earth. Over the past 15 years a very large number of measurements have been made, of the order of 15,000 to 20,000, giving meaningful data on the velocities, the masses, the visual magnitudes and the characteristics of the interplanetary orbits of the particles. The data are especially useful because the velocity spectra of the particles can be obtained, and because the range of masses of the particles observed extend down to the sizes that can be expected to be encountered during the trip to Mars. The estimates of flux made from these measurements are accurate to within 1 to 2 orders of magnitude.

The data thus obtained applies only to the near-Earth environment, however. The problem is to extrapolate the flux models based upon these data to the interplanetary and near-Mars regions. At the present time, reliable models do not exist; lack of information on velocity spectra of particles in Earth-Mars space is especially serious.

Experiments must be designed not only to measure the flux in the regions of interest but also the velocity spectra as well. A complete new approach must be taken to the measurement of the meteoroid environment. The current attempts to make these measurements with Pegasus-type satellites are inadequate because they give falacious readings when operated in the presence of trapped radiation belts in the vicinity of the planets, and are not able to obtain information about the velocities of the particles. Experiments that can be placed onboard the Voyager spacecraft using conventional sensor techniques are likewise not meaningful for application to the design of the manned planetary

system because the sizes of particles likely to be encountered with the small sensor areas are not applicable to the design of the manned system. TRW has recently proposed a new approach to the measurement of the meteoroid environment which is capable of measuring velocities to a reasonably high degree of accuracy, and of sensing particles in large numbers, in the sizes of interest to the design of the manned system.

It is recommended that additional analytical research be carried out in the field of meteoroid flux analyses in an attempt to predict more accurately the velocity spectra of the interplanetary particles and particles which may be trapped near the target planets. Possible approaches are described in Appendix A to Volume II.

Ratings:	Design Feasibility	2
	System Weight	3
	Mission Operations	1
	System Development	1

Martian Atmosphere

Uncertainties in the Martian atmosphere have not been given a top priority rating because although the atmosphere has a significant influence on many facets of the design of the manned system, the degree of interaction can be estimated reasonably well from the extreme upper and lower bounds established for the atmosphere and accommodated with system design changes. The most significant interaction with the design of the manned system is the increase in the lift-to-drag ratio on the atmospheric braking versions of the manned system. The lift-to-drag ratio requirement is dictated by the navigation corridor, which is not particularly stringent for the entry velocities expected for the Mars aerodynamic capture mode. The lift-to-drag ratio affects heat protection provisions and the location of the center of gravity, which may have a pronounced effect on the general layout of equipments within the spacecraft. The equipment location problem is not difficult for low values of lift-to-drag ratio, but can become difficult if lift-to-drag ratios in excess of 0.4 are required. A more complete discussion of these problems is given in Section 6.

In summary, the atmosphere has a significant influence on the design of the spacecraft, but reasonable upper and lower bounds can be established for the properties of the atmosphere, and the uncertainties accommodated by proper design of the spacecraft system.

Ratings:	Design Feasibility	2
	System Weight	2
	Mission Operations	1
	System Development	1

Bio-Contamination

One of the most difficult environmental factors to analyze is that of possible bio-contamination which will influence the operations of the lander crews, and possibly the altitude of the parking orbit. The two aspects of the bio-contamination problem to be considered are: the possible contamination of the Mars biological forms by the lander crews, thus interfering with or invalidating experiments to search for and analyze the nature of the life forms on Mars; secondly, there may be life forms present on Mars which would be dangerous to the lander crews or to the entire crew if such hostile life forms were introduced into the main spacecraft. Conceivably, these hostile life forms could be brought back to Earth if the crew was unaware of their presence and could not take appropriate steps to prevent their introduction into the Earth's environment.

The problem of measuring or analyzing the possible bio-contamination environment is especially difficult because it requires obtaining statistically meaningful data, which may require a fairly large number of experiments to be performed over several precursor missions.

At the present time it seems more fruitful to establish decontamination procedures that will assure that pathogens are not introduced into the Martian environment, or back into the earth environment, than it is to define with high confidence the exact nature of the bioenvironment at Mars. Decontamination procedures are required in any case, and probably can be relied upon to satisfy the biocontamination constraints on the early missions.

Ratings:	Design Feasibility	2
	System Weight	1
	Mission Operations	2
	System Development	2

Surface Conditions

The composition, soil strength and bearing properties of the soil are reasonably high priority items. The analyses reported in Section 8 indicated that the performance of surface rover vehicles could be seriously reduced if clayey type of surface soils are encountered on Mars. The clayey soils would greatly reduce the trafficability of the surface rover because of the relatively high coefficients of cohesion. Although the surface rovers could be designed to overcome soils of this type, the range of surface rovers able to cope with the clayey soils is considerably less than that of rovers designed for operation in sandy or more stable soils. Lacking data on the nature of the soil, it would be necessary to equip the surface rovers with track running gear. System weight reductions could be accomplished if it were known with a reasonable degree of certainty that clayey or sticky soils would not be encountered. The nature of the soil would not adversely affect the design of the impact gear of the Mars excursion module unless an extremely soft material were encountered such as a frothy material predicted for the lunar surface.

In general, the topological features of Mars must be established by photographic reconnaissance from unmanned precursor orbiter systems, and by unmanned landers equipped with cameras. Although the requirements for extensive photographic analyses of the surface of Mars cannot be readily assigned numerical ratings based upon sensitivity analyses of the manned system, it nonetheless constitutes an important requirement which will tend to dominate the precursor missions to a large extent, principally because of the large amount of data that must be returned to Earth for analysis purposes. It can be expected that the scientific community will desire a thorough analysis of the surface features of Mars before they will endorse the selection of one or more primary landing sites for the manned missions. Consequently, all precursor missions should be equipped with television systems or photographic systems so that a maximum amount of data can be obtained from each mission within the limitations of the communication systems.

Ratings:	Design Feasibility	2
	System Weight	1
	Mission Operations	2
	System Development	2

Reduced Priority Environmental Factors

Table 12.1 indicates that the remaining environmental factors will not have a dominating influence on the selection of unmanned precursor systems; however, several of these environmental factors in this reduced priority category should be taken into account when selecting the experiment payloads for the unmanned precursors. Among these are the analysis of the wind structures on Mars, which influence the design of the Mars excursion modules, the frequency and extent of dust storms, which may have a significant influence on the operations of the lander crews. The measurement of winds, particularly at high altitudes above the Martian surface pose a difficult problem for the unmanned precursor missions. In general, the densities expected at 20,000 to 30,000 feet above the Martian surface are very low, making it necessary to use large, heavy balloon systems to operate at these altitudes for the measurements of winds.

The general area of meteorological experiments for Mars requires the accumulation of a relatively large amount of data, which will impose severe requirements on the communication systems of the unmanned precursor vehicles. At the present time, the state of the art of conducting meteorological experiments from satellite systems is not advanced to the point where a complete analysis of the meteorology of a planet can be established from these measurements alone. It is necessary to augment these satellite systems with a reasonably large number of lander stations which are read out by the satellite system. In general, this area will be of strong interest to the scientific community but will be of relatively moderate importance to the design of the manned system. In relation to the complexity introduced into the unmanned precursor systems both in terms of numbers of satellites and lander systems as well as in terms of the large amount of data that must be gathered and communicated to the Earth, the complete analysis of the meteorology of Mars will

13. CONCLUSIONS

The following conclusions can be drawn from the analyses and results derived in this report:

1. The priorities for the experiments in the order of their importance are: solar cosmic radiation environment, meteoroid environment, and atmospheric properties.
2. Nuclear radiation dosages appear to be within limits prescribed for the Apollo mission, assuming a shield of 22 gm/cm^2 . Recovery effectiveness, if realizable, could reduce the shield to 10 gm/cm^2 , resulting in a 4.8 percent reduction of spacecraft gross weight. The Mars atmosphere contributes somewhat to shielding against nuclear radiation, and does not cause peaking of total secondary radiations. Uncertainties in shielding effectiveness, and in the radiation environment could cause increases in shield thickness to 35 gm/cm^2 which would increase spacecraft gross weight by 3.5 percent. Total uncertainties could thus amount to 8.3 percent. A comprehensive experiment program should be performed in earth-based facilities to establish shielding effectiveness and man's tolerance to the solar radiation environment.
3. The uncertainties in the Martian environment as bounded by the Schilling II Upper Limit Model (132 mb) and the NASA Engineering Model 3 (10 mb) can reduce the entry corridor in the worst case from 74.5 km to 21.9 km for a spacecraft having a lift-to-drag ratio capability of 0.3, and to 46 km for $L/D = 0.4$. Corridor reduction due to roll requirements are negligible, but uncertainties in diurnal effects on atmosphere scale height and density, which were not calculated directly for the Martian atmosphere, could reduce the corridor by an additional 10 km, based on Earth entry analyses. The corridor accuracy attainable with state-of-the-art navigation systems is estimated to be 5.4 km (3σ), which is within the capabilities of the $L/D = 0.3$ aero entry system, unless the diurnal effects are greater than 10-15 km.

4. Aero heating shield requirements are not stringent (amounting to about 7 percent of the spacecraft weight at Mars entry) and do not vary greatly with L/D, up to about $L/D = 0.3$ to 0.4 . About 4000 lbs additional shielding is required if L/D is increased from 0.1 to 0.3. The greatest effect on shielding is due to uncertainties in scale height, which determine the length of time the shield is retained after entry until a safe jettisoning altitude is reached. Uncertainties in composition are not important, except for the effect of composition on density variation with altitude. Radiative heating effects are reduced to a minimum by sharply pointing the forebody of the spacecraft.
5. Atmosphere surface density can affect the design of the Mars Excursion Module in the areas of decelerator sizes and weights, and in ascent trajectory shaping and propellant requirements. Decelerator (parachute plus retro) weights can be increased by 1.8 percent in the worst case, leading to 0.1 percent increase in spacecraft gross weight. Ascent trajectory losses are affected appreciably because of parking orbit altitude variation with density. Increases of 2.3 percent in spacecraft gross weight can be brought about in the worst case.
6. The lander touchdown dynamics can be affected by soil conditions and terrain characteristics, but to a minor degree. Landing gear designs can be adopted which minimize these effects with little increase in weight.
7. Winds can have a substantial effect on landing operations, due to reduced vision because of dust, excessive drift rates, which must be nulled before impact, and propulsion requirements to null drift velocity and drift range. In the worst case spacecraft gross weights could increase by 0.7 percent due to winds. Drift meters must be installed to permit drift cancellation. The effects of winds on MEM ascent are small because of the small dynamic pressures generated.
8. Uncertainties in meteoroid flux mass models can amount to one order of magnitude, resulting in shielding weight increases of about 100 percent. The resulting increase in spacecraft gross weight is 7.5 percent.

It is noted that meteoroid flux and shielding effectiveness uncertainties have a relatively large effect on mission weight, and should be reduced by precursor missions.

9. Surface rover performance could be seriously affected by unusually weak or sticky soils. These effects can be minimized by proper design techniques, particularly the use of wide track techniques, but range performance would be reduced.
10. The presence of a strong ionization belt at the surface of Mars has been predicted. This belt could affect the proper functioning of electrical equipment, and communication radiators. It also interjects an uncertainty in Mariner 4 measurements of the atmosphere by radio attenuation techniques.
11. Biological contamination interactions could influence surface operations to a large extent. Decontamination procedures have been established to avoid harmful contaminations of the Martian environment, and of the lander crews.
12. Experiment priorities as determined from the foregoing analysis are:
 - a. Solar cosmic radiation and shielding effectiveness
 - b. Micrometeoroid flux and shielding effectiveness
 - c. Determination of atmosphere properties
 - d. Surface features and soil properties

14. REFERENCES

- 1.1 R. L. Sohn, ed., "Manned Mars Landing and Return Mission." Space Technology Laboratories Report 8572-6011-RU-000. 28 March 1964. Contract NAS 2-1409.
- 2.1 Anon., "Mars Environmental Handbook." Space Technology Laboratories Report 9990-6856-TU-000. December 1964.
- 5.1 Kuiper, G. P., "Composition and Structure of the Martian Atmosphere," presented at 45th Annual Meeting, A. G. U., April 21-24, 1964.
- 5.2 Spinrad, H., G. Munch, and L. Kaplan, "High Resolution Spectroscopy of Mars," presented at 45th Annual Meeting, A. G. U., April 21-24, 1964.
Kaplan, L., G. Munch, and H. Spinrad, "An Analysis of the Spectrum of Mars," *Astrophys. J.* 139, 1 (1964).
- 5.3 Colthup, N. B., "Identification of Aldehyde in Mars Vegetation Regions," *Science* 134, 529 (1961).
- 5.4 Kuiper, G. P., "Planetary Atmospheres and Their Origin," Atmospheres of the Earth and Planets, ed. Kuiper (University of Chicago Press, Chicago, 1952), Chapt. 12.
- 5.5 Slipher, E. C., Mars (Sky Publishing Corp., Cambridge, Mass., 1960), p. 32.
- 5.6 de Vaucouleurs, G., Physics and Medicine of the Atmosphere and Space, ed. O. O. Benson, Jr., and H. Strughold (John Wiley and Sons, Inc., New York, 1960), p. 590.
- 5.7 Dorsey, H. G., Jr., "Arctic Meteorology," Compendium of Meteorology, ed. T. F. Malone (American Meteorological Society, Boston, 1951), p. 947.
- 5.8 G. M. Levin, D. E. Evans, V. Stevens, "NASA Engineering Models of the Mars Atmosphere for Entry Vehicle Design." NASA TN D-2525. November 1964.

5. 9 JPL TR 32-675, "Determination of Some Physical Properties of the Atmosphere of Mars from Changes in the Doppler Signal of a Spacecraft in an Earth-Occultation Trajectory," October 15, 1964.
5. 10 Gifford, F. , Jr. , "The Surface Temperature Climate of Mars," Atmosphys. J. 123 154-161 (1956).
5. 11 Hess, S. L. , "Mars as an Astronautical Objective," Advances in Space Science and Technology, Vol. 3, ed. F. I. Ordway (Academic Press, New York, 1961), p. 170.
5. 12 de Vaucouleurs, G. , "The Physical Environment of Mars," Physics and Medicine of the Atmosphere and Space, ed. O. O. Benson, Jr. and H. Strughold (John Wiley and Sons, Inc. , New York, 1960), p. 596.
5. 13 de Vaucouleurs, G. , Physics of the Planet Mars (Faber and Faber Ltd. , London, 1954), pp. 290-292.
5. 14 Sinton, W. M. and J. Strong, "Radiometric Observations of Mars," Astrophys. J. 131, 459-469 (1960).
5. 15 Shaefer, H. J. , Aerospace Medicine 34, 1, Jan. 1963.
5. 16 Foelsche, T. , TN D-1383, NASA, Washington, D. C. , 1962.
5. 17 Tilson, S. , Science and Technology, January 1964, p. 28.
5. 18 Neher, H. V. , Phys. Rev. 107, 588 (1956).
5. 19 Shen, S. P. , G. E. Report R64-SD1, January 1964.
5. 20 D. K. Bailey, Time Variations of the Energy Spectrum of Solar Cosmic Rays in Relation to the Radiation Hazard in Space, J. Geophys. Res. 69:391-396 (1962)
5. 21 Whipple, F. L. , "Dust and Meteorites." Astronautics, Vol. 7, No. 8, August 1962, p. 40.
5. 22 Whipple, F. L. , "On Meteoroids and Penetration." AAS Preprint 63-29. January 1963. Presented at the AAS Interplanetary Missions Conference, Los Angeles.
5. 23 Hamermesh, B. , "Micrometeoroids." Space Physics, p. 270. Wiley 1964.
6. 1 Levin, George, Dallas E. Evans, and Victor Stevens, "NASA Engineering Models of the Mars Atmosphere for Entry Vehicle Design." NASA TN D-2525, November 1964.

- 6.2 Schilling, G. F. , "Limiting Model Atmospheres of Mars." RAND Report R-402-JPL, August 1962.
- 6.3 Carlson, Robert W., and Byron L. Swenson, "Maneuvering Flight Within Earth-Entry Corridors at Hyperbolic Speeds." AIAA Preprint No. 65-19, January 1965.
- 6.4 Chapman, Dean R. , "An Analysis of the Corridor and Guidance Requirements for Supercircular Entry into Planetary Atmospheres," NASA TR R-55, 1960.
- 6.5 Myer, H. G. , "Equilibrium Radiant Heating in a Model Planetary Atmosphere Including Absorption Considerations," TRW Space Technology Laboratories Report 9990-6716-RU-000, July 1964.
- 6.6 Myer, H. G. , "Radiation from Shock-Heated Air Part I. Equilibrium Radiation," TRW Space Technology Laboratories Report 6130-0001-NU-P01, October 1961.
- 6.7 Rollin, E. A. , and J. P. Griest, "STL Aerodynamic Heating Program Computer Analysis," STL CDRC Report 9852.22-8, 1 October 1963.
- 6.8 Hoshizaki, H. , "Heat Transfer in Planetary Atmospheres at Super-Satellite Speeds," ARS Journal, October 1962.
- 6.9 Prieb, S. L. and A. H. Silver, "Receding Boundary Heat Flow," STL CDRC Report 9852.22-15, 15 June 1963.
- 7.1 "Development Contract Proposal for the Surveyor Spacecraft," Space Technology Laboratories, Inc.
- 7.2 "Direct Flight Study Using Saturn C-5 for Apollo Project," Space Technology Laboratories, NASw-516, 24 October 1962.
- 7.3 "Study of Spacecraft Bus for Lunar Logistics System, Appendix I," Space Technology Laboratories, Inc., NASw-530, 22 December 1962.
- 7.4 J. Alper, "Multi-Mission Module, Dynamics Analyses," Space Technology Laboratories Memo 64-9713.6-8, 31 January 1964.
- 7.5 Helgostam, "The Requirements for Efficient Mars Launch Trajectories," AIAA Preprint No. 64-15.

- 7.6 Wolverton, Flight Performance Handbook for Orbital Operations, published by Space Technology Laboratories, Inc. under contract number NAS 8-863 to NASA, Huntsville, September 1961.
- 7.7 ASTIA AD 240961 SRI Technical Report 69, "Voltage Breakdown of Antennas at High Altitudes", by W. E. Scharfman and T. Morita.
- 8.1 Anon, "Studies of Lunar Logistics System Payload Performance, Volume I, Technical". Grumman Report PDR-344-2b, 7 January 1963.
- 8.2 M. G. Bekker, "Off-the-Road-Locomotion", University of Michigan Press, Ann Arbor, 1960.
- 8.3 M. G. Bekker, "Theory of Land Locomotion", University of Michigan Press, Ann Arbor, 1957.
- 8.4 A. J. Eggers, H. Julian Allen, and S. E. Neice, "A Comparative Analysis of the Performance of Long-Range Hyper-Velocity Vehicles", NASA TN4046, October 1957.
- 8.5 C. H. McLeelan and C. L. Ladson, "A Summary of the Aerodynamic Performance of Hypersonic Gliders", NASA TM X-237, March 1960.
- 8.6 R. W. Rainey, D. E. Fetterman, and R. Smith, "Summary of the Static Stability and Control Results of a Hypersonic Glider Investigation", NASA TM X-277, May 1960.
- 8.7 Swan, P. R., Sagan, C., "Martian Landing Sites for the Voyager Mission". Journal of Spacecraft and Rockets, Vol. 2, No. 1 January-February 1965, p. 18
- 9.1 A. L. Jones, et al, "Study of Subsystems Required for a Mars Mission Module". NAA Report SID-64-1-2. 2 January 1964. Vol. 2.

- 9.2 Private communication, A. Kelton, DAC. 9 June 1965.
- 9.3 J. R. Lilley, W. R. Yucker, "Charge, A Space Radiation Shielding Code". Douglas Report SM-46335. April 1965.
- 9.4 "Manned Mars Landing and Return Mission Study", NAA SID 64-619-3. April 1964.
- 9.5 "A Special Report on Radiation Biology and Space Environmental Parameters in Manned Spacecraft Design and Operations". Sponsored by McDonnell Aircraft and Los Alamos Scientific Laboratory. Published by Aerospace Medicine. February 1965. Vol. 36, No. 2.
- 10.1 Dollfus, A., "The Nature of the Surface of Mars", Publ. Astron. Soc. Pac. 70, 56 (1958)
- 10.2 Sinton, W., "Further Evidence of Vegetation of Mars", Science 130, 1234 (1959)
- 10.3 Kiess, C. C., S. Karrer, and H. K. Kiess, Publ. Astron. Soc. Pac., 72, 256 (1960)
- 10.4 Urey, H. C., Handbuch der Physik, Vol. 52, S. Fluge, ed., (Springer Verlag, Berlin, 1959), p. 385
- 10.5 Arrhenius, S., The Destinies of the Stars, (Putnam, New York, 1918)
- 10.7 Hawrylewicz, E. J., and R. Ehrlich, "Studies with Microorganisms and Plants Under Simulated Martian Environments:", presented at the Am. Assoc. Advan. Sci., Denver, Colo., 26-30 Dec. 1961.
- 10.8 Hagen, C. A., and R. Jones, "Life in Extraterrestrial Environments", NASA N64-11293, Nov. 1964.
- 10.9 Lederberg, J., and C. Sagan, "Microenvironments for Life on Mars", Proc. Natl. Acad. Sci., U. W., 48, 1473 (1962)

- 10.10 Oparin, A. I., The Origin of Life, 3rd ed. (Academic Press, New York, N. Y., 1957)
- 10.11 Ponnampereuma, C., Los Angeles Times, July 11, 1963, p. 1
- 10.12 Pauling, L., The Nature of the Chemical Bond, 2nd ed., (Cornell Univ. Press, Ithaca, N.Y., 1950)
- 10.13 Sidgewick, N. V., The Chemical Elements and Their Compounds, (Oxford Univ. Press, New York, N.Y., 1950)
- 11.1 Chovit, A. R., et al, "Mission Oriented Advanced Nuclear System Parameters Study, Vol. II, Detailed Technical Report, Mission and Vehicle Analysis; TRW Space Technology Laboratories Report No. 8423-6006-RU000, March 1965.
- A.1 Van Tassel, R. A., and Salisbury, T. W., "The Composition of the Martian Surface", Icarus 3, 264 (1964)
- A.2 Slipher, E. C., Mars (Sky Publishing Corp., Cambridge, Mass., 1962), p. 168.
- A.3 Wilson, A. G., "Direct Photography in the Exploration of Planetary Atmospheres," Appendix 1, The Atmospheres of Mars and Venus, W. W. Kellogg and C. Sagan (National Academy of Sciences - National Research Council, Washington, D. C., Publication 944, 1961), p. 67.
- A.4 Dollfus, A., "Polarization Studies of Planets," Planets and Satellites, Vol. III of The Solar System, eds. Kuiper and Middlehurst (University of Chicago Press, Chicago, 1961), Chapter 9.
- A.5 Dollfus, A., "Visual and Photographic Studies of Planets at the Pic du Midi," Planets and Satellites, Vol. III of The Solar System, eds. Kuiper and Middlehurst (University of Chicago Press, Chicago, 1961), Chapt. 15.

- A.6 Ryan, J. A., "Notes on the Martian Yellow Clouds," J. Geophys. Res. 69, 3759 (1964).
- A.7 de Vaucouleurs, G., Physics of the Planet Mars, (Faber and Faber, London, 1954), p. 343.
- A.8 Spinrad, H., G. Munch, and L. D. Kaplan, "The Detection of Water Vapor on Mars," Astrophys. J. 137, 1319 (1963).
- A.9 Hess, S., "A Meteorological Approach to the Question of Water Vapor on Mars and the Mass of the Martian Atmosphere," Pub. A. Soc. Pac., 60, 289-302 (1948).
- A.10 Kuiper, G. P., "Composition and Structure of the Martian Atmosphere," presented at 45th Annual Meeting, A. G. U., April 21-24, 1964.
- B.1 de Vaucouleurs, G., "The Physical Ephemeris of Mars," Icarus 3, 236-247 (1964).
- B.2 de Vaucouleurs, G., "Geometric and Photometric Parameters of the Terrestrial Planets," Icarus 3, 187-235 (1964).
- B.3 Lamar, D. L., "Optical Ellipticity and Internal Structure of Mars," Icarus 1, 258 (1962); also Report RM-3127-JPL (RAND Corp., Santa Monica, Calif.), 1962.
- B.4 Kuiper, G. P., "Limits of Completeness," Planets and Satellites, Vol. III of the Solar System, eds. Kuiper and Middlehurst (University of Chicago Press, Chicago, 1961), Chapt. 12.
- B.5 Redmond, J. C. and F. F. Fish, "The Luni-Tidal Interval in Mars and the Secular Acceleration of Phobos," Icarus 3, 87-91 (1964).
- B.6 Jeffreys, H., "The Density Distributions of the Inner Planets," M. N. Roy, Astron. Soc., Geophys. Sup., 4, 62 (1937).
- B.7 Singer, S. F., "Some Considerations of Expected Radiation Belts of Planets Mars and Venus," ASTIA Doc. AD-240811, January 1960. (Also, Advances in the Astronautical Sciences, ed. Amer. Astronaut. Soc. (Macmillan Co., New York, 1961), Vol. 6, pp. 781-793).

APPENDIX A. MARTIAN ENVIRONMENT

A.1 Surface Markings

The visual surface markings of the planet Mars can be categorized as (1) the white polar cap regions, (2) the bright pinkish and orange areas, and (3) the dark areas. Below is a brief summary of the characteristics of these types of surface features, and some of the physical data and hypothetical explanations pertinent to them. Figure 8.19 is a map of the prominent surface markings (after de Vaucouleurs) on a mercator projection.

Polar Cap Regions

The polar cap regions appear visually as brilliant white areas possessing an apparent reflection coefficient of 0.153 ($\lambda = 0.43 \mu$) at 70° incidence, which would correspond to a reflection coefficient at normal incidence of 0.447 if the albedo of the atmosphere is neglected. Since the reflection coefficient of snow in this spectral range is about 0.9, it is generally conceded that the polar caps may be thin deposits of hoarfrost combined with ordinary ice, and the relative amounts of these forms of crystallized water may vary considerably with the martian seasons. Experiments have virtually eliminated the possibility that the polar caps are condensed CO_2 .

The thickness of the polar caps is still a matter of dispute. In the absence of experimental determination of the water content of Mars, other than upper bounds, the thickness may be between a few millimeters to perhaps ten centimeters.

The caps alternate between North and South polar regions with season. In local summer, they almost completely disappear, thus indicating the existence of a mechanism for water transfer across the equator.

The connection between seasonal variations in the brightness of dark areas and polar cap disappearance has been noted by many observers. As the polar cap shrinks, a dark band or fringe appears at its edge. The caps recede in regular fashion, leaving behind dark bands and white patches indicative of polar area depressions and elevated areas. The darkening radiates and propagates in a fairly reproducible fashion from the receding cap into the temperate zone with advancing summer, and eventually spills across the equator into the other hemisphere. With the arrival of full summer, the polar area turns pale again.

The darkening seems to follow along certain fixed arteries. There is little doubt of correlation between polar cap recession and the reproducible darkening along these "channels," but the mechanism involved is unknown, although speculations (liquid or vaporous water transfer in depressed fissures, by porosity, by a vegetation process, by artificial "canals") have been advanced.

Bright Areas

The bright areas of the surface of Mars comprise more than one-half the total surface area. These areas appear visually as orange-pink in color, with some variations locally over the surface.

The spectrum of visible light reflected from these areas resembles quite closely that of red sandstone. However, differences occur in the near infrared ($\lambda \sim 1-2 \mu$). It has been suggested on this basis that the composition may be felsite mixed with felsitic rhyolite. Polarization studies have led to the hypothesis of a composition of finely powdered limonite (iron hydroxide). The occurrence of meteorological phenomena (yellow cloud formations and movements) over these areas is consistent with dust storm formation over terrestrial deserts, and lends some support to the hypothesis of finely-grained dusty composition of the surface in bright areas.

The most acceptable hypothetical surface composition has been until recently limonite $[\text{FeO}(\text{OH}) \cdot n\text{H}_2\text{O} + \text{Fe}_2\text{O}_3 \cdot n\text{H}_2\text{O}]$. However, Van Tassel and Salisbury (Reference A.1) have shown by laboratory experiments that the spectrometric measurements which lead to the limonite hypothesis are ambiguous. They argue that the martian surface materials could well be composed primarily of finely divided grains of silicates, or of coarse-grained silicates coated with finely divided limonite without changing the observed spectrometric characteristics.

Dark Areas

The dark areas appear as irregularly variable visual features of the surface. Because of their low surface brightness and geometrically limited extent, the dark areas are very difficult to study by precise physical techniques. Therefore, the physical data on these areas are of low quality, and are often of doubtful value. Thus, the majority of observations available are visual.

The dark areas cover approximately one-third of the total martian surface area. They appear predominantly in a belt south of the equator, but project in some places into the northern hemisphere. There are also a few large dark areas

(oases), north of the equator, unconnected to the dark belts. Visually, dark areas appear greenish-grey, dark blue, deep purple or violet-grey. Some of these color mixtures may be due to contrast effects with the surrounding bright orange-pink areas.

The extent and geometrical shape of portions of the dark areas have been observed to change with season, along with their photometric properties (tint and polarization of reflected light). These areas become darker in spring and summer, and fade in winter. The darkening has been observed to advance from the receding polar cap toward the equator and into the opposite hemisphere.

A difference in the infrared spectrum of the bright and dark areas has been observed. Weak absorption bands in the region between $\lambda = 3.5-3.8 \mu$ appear in the spectrum of the dark areas, but not in that of the bright areas. It has been suggested that these absorption bands may indicate the presence of organic molecules in the dark areas.

There are many hypotheses concerning the nature of the dark areas. These include (1) the existence of lichen-like vegetation, (2) ancient oceanic beds, (3) lava fields with a variable covering of dust from the bright areas, and (4) regions of dark volcanic dust deposits. All of these hypotheses are subject to some reasonable criticism, and none appears very acceptable at present.

The occurrence of dark streaks on the bright areas of Mars has been reported. These markings are too small to be photographed, and there is great controversy concerning their existence and interpretation. They have been called "canals," but the great variability in visual data reported concerning their locations, extents and other features places this "surface feature" in the realm of pure speculation.

Volcanos

It has been suggested that the shape and changes of visual surface markings can be explained on the basis of ash and lava excreted and ejected by active volcanos on Mars. In particular, irregular morphology of certain of the dark areas has been ascribed to the fall-out of volcanic dust carried by the martian wind and atmospheric circulation systems. If such interpretations were true, it would indicate a wide-spread vulcanism on Mars only slightly in excess of terrestrial volcanic activity.

However, there have been strong criticisms of the vulcanism theory. At this time there is little believable evidence for the existence of volcanic activity on Mars, and a majority of observers specializing in this planet are of the opinion that such activity is either of minor significance, or non-existent. However, one observation of a small, brilliant spot on Mars has been reported to have persisted for more than one hour in December, 1951. This observation is unfirmed and isolated.

Mountains and Valleys

Approximately three-fourths of the surface of Mars is covered by the bright areas. Their relief must be flat, or at best gently rising, since no prominences have ever been consistently observed under favorable shadow conditions at the terminator, under oblique illumination. It has been concluded that there can be no mountains higher than 6 to 14 thousand feet anywhere on the planet. However, localized regions (small, bright spots) consistently appear at fixed places on the planet (Nix Olympica, Mountains of Mitchel). These can be interpreted as isolated peaks of sufficient elevation to produce or accrue condensations of frost or clouds.

Direct observation of declivities interpretable as valley-like or canyon-like structure has not been made.

Plains

The bright areas of Mars have been best explained as sandy deserts or bare areas covered by a silicated dust mixture of iron oxide. This would generally explain their uniformity and permanence. The mean visual albedo of Mars of approximately 0.15 is very similar to that of terrestrial desert areas.

In summary it appears that the interpretation of the bright areas of Mars as relatively reliefless desert plains of unproven mineralogical composition is most consistent with available physical data.

There is no trustworthy evidence concerning the probable soil mechanical properties of the surface, such as grain size, depth of dust or grains, soil bearing strength, and so forth.

Aerosols and Clouds

No statistical data appear to exist about the frequency of occurrence of aerosol particles that are suspended in the atmosphere, or of clouds. Usually martian surface features are visible from the Earth's surface at wavelengths

greater than $\lambda 4550 \text{ \AA}$, but the surface is usually obscured at wavelengths less than $\lambda 4550 \text{ \AA}$ (Reference A. 2). This type of obscuration, generally called the blue or violet haze, clears occasionally for one to five days to reveal surface markings over a small fraction of the disc, or even the entire disc. The blue haze may disappear in a few hours. The clearings usually occur near opposition, or in the presence of yellow clouds (Reference A. 3).

The clouds are frequently classified as blue, white, or yellow, even though other colors may appear. The blue clouds appear bright through a blue filter. Blue clouds are usually present in the equatorial zones near the terminators. However, the clouds disappear during midday (Reference A. 4). The blue clouds are also generally present in the vicinity of the autumn-winter polar regions, but cannot be seen through red filters.

The white clouds appear white to the eye and can be seen through either blue or red filters. Dollfus (Reference A. 4) also believes that these clouds are composed of small crystals, similar to those of cirrus clouds on the earth. The most conspicuous example of all the white cloud types begins to form during autumn over the winter pole. Eventually the cloud completely covers the polar ice cap, and extends into the temperate latitude of the winter hemisphere to approximately 45° . The polar cloud disappears soon after the vernal equinox. It also appears to be transparent to red light.

The white cloud may occur in other regions as tenuous haze, scarcely distinguishable from blue haze, or as bright clouds. The clouds sometimes appear, but rarely, along the terminators. Since white clouds appear sometimes in the afternoon, or in fixed areas, one type of the clouds may be convective. White clouds have been observed to move at speeds up to 10 m sec^{-1} and may be associated with traveling cyclones that are similar to those that appear on the earth at midlatitudes. The white clouds sometimes extend around the globe a few thousand kilometers and exist for weeks. (See Reference A. 5 for discussion of white clouds).

Yellow clouds appear bright through yellow or red filters, but are inconspicuous through blue filters. They are believed to be dust that has been swept up from the orange-red surface (Reference A. 5), and the clouds usually appear near perihelion. The clouds may cover only a small fraction of the disc and last only one or two days. Because of the short lifetime of the clouds,

Ryan shows that the dust grains may be as large as a few hundred microns in diameter. On a few occasions the yellow clouds cover the whole visible planet and last for several weeks. Slipher says that most yellow clouds extend to a height of 30 km. The apparent speed of the yellow clouds is less than 25 m sec^{-1} (Reference A. 7).

A. 2 Atmospheric Circulation

A model of the general atmospheric circulation is of interest here, principally because it specifies the mean seasonal winds. Such specifications for Mars are largely speculative, however. One expects a weak flow from the winter hemisphere to the summer hemisphere at low elevations and a reverse flow at high elevations within the troposphere, which seems to be within about 30 km of the ground. The surface winds are expected to be light and variable. In the winter hemisphere the winds are expected to increase with increasing height at the rate of about 1 m sec^{-1} per km and flow from west to east. The winds in the summer hemisphere are expected to increase with height at about the same rate, but to flow in the opposite direction -- from east to west. One must always remember that for small time and space intervals the wind velocities are expected to depart strongly from those of the mean model.

The observed martian wind velocities are commonly deduced from the apparent movement of clouds, but such data may not yield reliable estimates of the true wind speed. The martian clouds that have been used to estimate wind velocities would seem to lie within the troposphere, or below about 30 km, and at some distance above the surface, perhaps one km. The white clouds move at a rate less than 10 m sec^{-1} (Reference A. 3). The speed of yellow clouds as a function of their duration is shown in Figure A.1. Initially, the clouds move at the speed of 25 m sec^{-1} but slow to $2-3 \text{ m sec}^{-1}$ after five days.

Estimates of high surface wind speeds that would be required to initiate dust storms have been made by Ryan (Reference A. 6). The minimum wind speeds required to start dust storms are given in Table A.1. The pressures refer to the atmospheric pressure at the ground for martian model atmospheres. The speeds in the 80 mb column are less than some of the observed speeds of yellow clouds. However, speeds as large as those entered in the 25 mb column have not been observed on Mars. If the martian surface pressure is as low as 10 mb, which is possible, even stronger winds would be required to initiate dust storms. Stronger winds than have been observed can occur, though on a scale too small to have been observed from the earth.

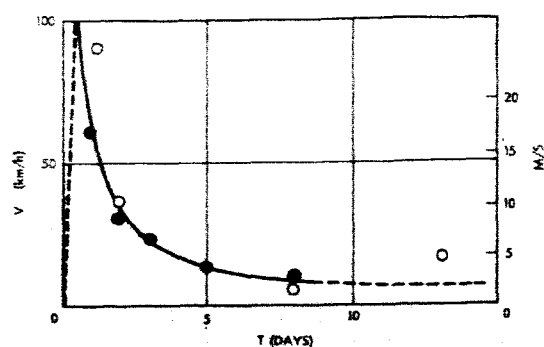


Figure A.1 Speed of Large Yellow Clouds

TABLE A.1 MINIMUM HORIZONTAL WIND SPEED REQUIRED TO INITIATE DUST STORMS

Height (M)	25 mb	80 mb
1	26	11
5	31	14
10	33	15
100	40	18

A. 3 Atmospheric Water Substance

Prior to 1963 all evidence for the presence of water substance on the surface or in the atmosphere of Mars was based on indirect inference. The several attempts to detect water vapor on Mars by spectroscopic techniques were universally unsuccessful except insofar as they served to set somewhat conjectural upper bounds to the water vapor content of the martian atmosphere.

The Kaplan, Münch and Spinrad Determination

In 1963, Kaplan, Münch and Spinrad (Reference A. 8) announced the detection of "faint but unmistakable lines which have been ascribed to (Doppler shifted absorption by) H_2O in Mars' atmosphere." Their conclusions, however, were based upon a study of a single spectral plate obtained during favorable low humidity conditions on the night of 12-13 April 1963. They claim to have ascertained, by visual inspection of the plate, the presence of martian H_2O lines as faint red-shifted components in a number of the stronger (telluric) lines of the (2, 1, 1) water vapor band near 8200 \AA . Their reproduced microphotometer tracings admittedly do not illustrate convincingly the presence of these martian H_2O lines. The above authors claim, however, that once the presence of red-shifted components have been visually ascertained from the plate, their presence also becomes apparent in the microphotometer tracings.

In their preliminary announcement, Kaplan, Münch and Spinrad listed a total of eleven lines as having detectable components red-shifted by the expected amount to be attributable to absorption in the martian atmosphere. They also briefly mentioned, however, the possibility of some of the lines arising from blends with Fraunhofer or telluric lines. In a later study, they eliminated two of the eleven original lines as possibly arising from blends of weak Doppler

shifted Fraunhofer lines with ordinarily non-detectably weak telluric lines. Ultimately, they based their analysis of water vapor abundance in the martian atmosphere upon the average "equivalent width" of 0.006 cm^{-1} for three definitely unblended lines at 8176.98 \AA , 8189.27 \AA and 8226.96 \AA . By comparison of this average equivalent width with laboratory determined line strengths and "curves of growth" for the strongest spectral lines in the (2, 1, 1) band, they infer the existence of $5 \times 10^{-3} \text{ gm cm}^{-2}$ of martian atmosphere water vapor in their optical path. Then, allowing for a double slant traversal of the martian atmosphere with a mean secant factor of 1.8, they predict that the abundance of water vapor in the martian atmosphere is equivalent to $(1.4 + 0.7) \times 10^{-3} \text{ gm cm}^{-3}$ cross section of vertical optical path. Or, in the somewhat awkward units conventionally utilized for specification of water vapor abundance.

The Kaplan-Munch-Spinrad

$$\begin{array}{l} \text{Martian Water Vapor} \\ \text{Abundance} \end{array} = (1.4 + 0.7) \times 10^{-3} \text{ precipitable-cm}$$

They are careful to point out, however, that better data is required for more definitive measurements of martian atmosphere water vapor abundance. They expect to obtain such data in an extensive and thorough study planned for the more favorable 1965 opposition.

Indirect Inferences of Martian Water Substance

In 1952 Kuiper (Reference 5.4) found the polar caps of Mars to have reflection spectra consistent with a thin layer of H_2O frost. The polarization of the light reflected from the polar caps was observed and interpreted by Dollfus (Reference A.5) as also providing evidence for the existence of H_2O ice on the martian surface. At the temperatures and vapor pressures estimated to prevail on Mars, phase transitions of H_2O would be directly from ice to vapor. The seasonal variations observed in the extent of the martian polar caps imply, moreover, a net transport of H_2O between both poles. It then appears reasonable that, at least sometime during the cycle, a significant fraction of the total martian polar cap water substance must exist in the form of atmospheric water vapor. On this basis de Vaucouleurs (Reference A.7) has estimated "an atmospheric water content of the order of 0.01 precip. -cm or less." Sagan (Reference A.8) has suggested the value of 0.001 precip. -cm, based on the sublimation rate and assumed temperature of a polar cap. An amount of this order of magnitude suffices, according to Hess (Reference A.9), to explain the nocturnal and limb

clouds observed on Mars. In a recent presentation, Kuiper (Reference A.10) stated that observations made during a polarization study of light scattered by the martian haze were compatible with ice particles of approximately 0.35 micron diameter, but not with quartz particles. He said that a very rapid variation of particle size was indicated by the time variation of the observed polarization and intensity pattern of the scattered light.

The general conclusions of several investigators including de Vaucouleurs and Hess is that the martian atmosphere probably contains up to 0.01 precip. -cm of water substance, with an uncertainty of approximately one order of magnitude. It is believed, however, that most of this water substance is distributed within the ice crystal clouds, and that the residual amount in the form of true atmospheric water vapor may be as low as 0.001 precip. -cm. It will be seen that the Kaplan, Munch and Spinrad determination of 0.0014 precip. -cm is compatible with this latter inference.

APPENDIX B. SOME PHYSICAL PROPERTIES OF MARS

B.1 Mass

The mass of a planet is determined in either of two ways: by observation of the gravitational perturbations which it exerts on the motions of the other planets, and of the asteroids; and by observation of the planet's satellites. Both methods are applicable to Mars.

Neither method gives the planetary mass directly, but rather its ratio to that of the sun. The best current estimate of this ratio for Mars, that of Van den Bosch, later improved by Clemence, was obtained by observation of the satellites. It is

$$\frac{\text{Mass of Mars}}{\text{Mass of Sun}} = \frac{1}{3\ 088\ 000 \pm 3000} = (3.238 \pm 0.003) \times 10^{-7}$$

This value has been adopted as standard by JPL.

Measurement of the astronomical unit (e. g., by radar observation of Venus) makes possible a determination of the value of GM for the Sun. This value may be combined with the above mass ratio to yield GM for Mars. The current JPL numbers are

$$\text{Astronomical unit} = 1.49599 \times 10^{13} \text{ cm.}$$

$$\text{GM (Sun)} = 1.32715 \times 10^{26} \text{ cm}^3 \text{ sec}^{-2}.$$

and finally

$$\text{GM (Mars)} = (4.298 \pm 0.004) \times 10^{19} \text{ cm}^3 \text{ sec}^{-2}.$$

The value of GM for Mars should suffice for most applications. The actual value of the mass is obtained from the additional knowledge of the universal gravitational constant, G. The most accurate determination is that of Heyl and Chrzanowski,

$$G = (6.673 \pm 0.003) \times 10^{-8} \text{ cm}^3 \text{ gm}^{-1} \text{ sec}^{-2}.$$

This gives

$$\text{Mass of Mars} = (6.441 \pm 0.007) \times 10^{26} \text{ gm.}$$

B.2 Rotational Data

The sidereal rotational period adopted by the American Ephemeris and Nautical Almanac is the 1953 determination by Ashbrook, $24^{\text{h}} 37^{\text{m}} 22^{\text{s}}.6689 \pm 0^{\text{s}}.0026$, ephemeris time.

B. 3 Physical Ephemeris

Data needed in expressing measurements of observed markings on Mars in areocentric coordinates (latitude and longitude on Mars) are collectively referred to as the physical ephemeris of Mars. These data, too complex to be summarized here, are given in an excellent recent review by de Vaucouleurs (Reference B.1).

B. 4 Geometric Figure

Determination of the polar and equatorial diameters of Mars is a very difficult task. Measured values depend on the wavelength of the light used in the observation, the phase of illumination of the disc, atmospheric refraction and haze, surface markings (in particular the polar caps), the assumed law of limb darkening, "seeing," and other effects. Several of these phenomena have different effects on the measured polar and equatorial diameters, thereby rendering visual observations of the flattening somewhat precarious. These problems are discussed in a recent review by de Vaucouleurs (Reference B. 2).

The best determinations of the polar and equatorial diameters of the surface of Mars are given by de Vaucouleurs as

Polar Diameter:	6700 ± 20 km
Equatorial Diameter:	6750 ± 20 km

Optical observations of the ellipticity as mentioned above, are subject to many errors. The best weighted mean for the optical ellipticity is given by de Vaucouleurs as

$$f(\text{optical}) = 0.0105 \pm 0.0007.$$

The equatorial bulge of Mars, caused by the centrifugal force of rotation, produces a noncentral gravitational field, which results in a motion of the nodes of the satellite orbits. These motions have been accurately measured (see below) and may be used to determine the dynamical ellipticity. This quantity is defined as the ellipticity of a homogeneous planet with the given satellite motions. For Mars, it has the value

$$f(\text{dynamical}) = 0.00525,$$

as given by de Vaucouleurs. This is just half the optical value. The discrepancy is discussed in terms of the internal structure of Mars by D. L. Lamar (Reference B. 3).

B. 5 Density

From the values given above for the mass and polar and equatorial diameters, the mean density of Mars is found to be

$$\text{Mean Density} = 4.030 \pm 0.005 \text{ gm cm}^{-3}$$

B. 6 Natural Satellites

Mars possesses two known natural satellites, Phobos and Deimos. A fruitless attempt to discover additional satellites is described by Kuiper (Reference B. 4).

The principal data concerning the satellites are given in the following table.

TABLE B.1 PROPERTIES OF PHOBOS AND DEIMOS

	<u>Phobos</u>	<u>Deimos</u>
Sidereal Period	7 ^h 39 ^m 13. ^s 85	30 ^h 17 ^m 54. ^s 87
Semi-major Axis of Orbit, A. U.	6.27×10^{-5}	1.570×10^{-4}
Semi-major Axis of Orbit, km	9.38×10^3	2.349×10^4
Eccentricity of Orbit	0.021	0.003
Inclination to Mars' Equator, degrees	1.12 - 1.14	0.85 - 2.69
Annual motion of Node, degrees	-158.5 ± 0.5	-6.2795 ± 0.0007

The secular acceleration of Phobos, which amounts to $+(1.882 \pm 0.26) \times 10^{-3} \text{ deg yr}^{-2}$, is discussed by J. C. Redmond and F. F. Fish (Reference B. 5). These authors find that certain parameters of Phobos may be expected to lie between the bound indicated by the following table.

TABLE B.2 PROPERTIES OF PHOBOS

Geometric Albedo	0.100	- 0.154
Equivalent Radius, km	7.8	- 6.4
Density, gm cm ⁻³	3.8	- 2.8
Mass, gm	7.6×10^{18}	- 3.1×10^{18}

There is at present no evidence concerning the shape of Phobos and Deimos.

Kuiper mentions that photographically Phobos is 1.2 magnitudes brighter than Deimos. This implies that Phobos is brighter by a factor of 3.0, larger in equivalent radius by a factor of 1.7, and more massive by a factor of 5, than Deimos, if their composition is the same.

B. 7 Internal Structure

In the absence of geophysical data such as those derived from seismology, tectonophysics, heat flux measurements, and the like, one can only speculate on the internal constitution of the extraterrestrial planets. Even with the wealth of data accumulated by geophysicists in the case of Earth, there are still many controversies about the details of Earth's internal structure.

The only data bearing on the internal structure of Mars are those of an indirect nature, such as the dynamical flattening (oblateness) and the mass. From these astronomical data, some models have been hypothesized.

Jeffreys (Reference B. 6) has considered the problem of deducing the density distribution within Mars from the following astronomical data

$$\text{Mass} = 6.43 \times 10^{26} \text{ gm.}$$

$$\text{Diameter} = 6.77 \times 10^8 \text{ cm.}$$

$$\text{Density} = 3.958 \text{ (mean).}$$

He finds that such data can be explained almost equally well by either of two assumptions: (1) a once-discontinuous density variation with no central high density core; (2) the assumption of a small ferrous core of areocentric radius 1400 km, and with two Earth-like discontinuities.

These density distributions are shown in Figure B.1 (after Jeffreys). In both once-discontinuous and twice-discontinuous distributions, it was assumed that the density-pressure relation is the same as that indicated by data pertinent to Earth.

The model involving a ferrous core gives a total planetary mass only 2 percent different from the astronomically determined mass, and an ellipticity $\epsilon_d = 0.00487$, compared to the value $\epsilon_d = 0.00521$ deduced from the ephemerides of the martian satellites Phobos and Deimos. The mass discrepancy can be removed by a small change in core radius. On the other hand, the model involving no core leads to a mass some 10 percent too small, a discrepancy which can be removed only by large changes in the location of the sub-crustal discontinuity. This model also leads to $\epsilon_d = 0.00566$. It would appear from these considerations that the Earth-like model involving a ferrous core more closely satisfies the available astronomical data, but only direct measurements of seismic events can confirm the nature of internal structure.

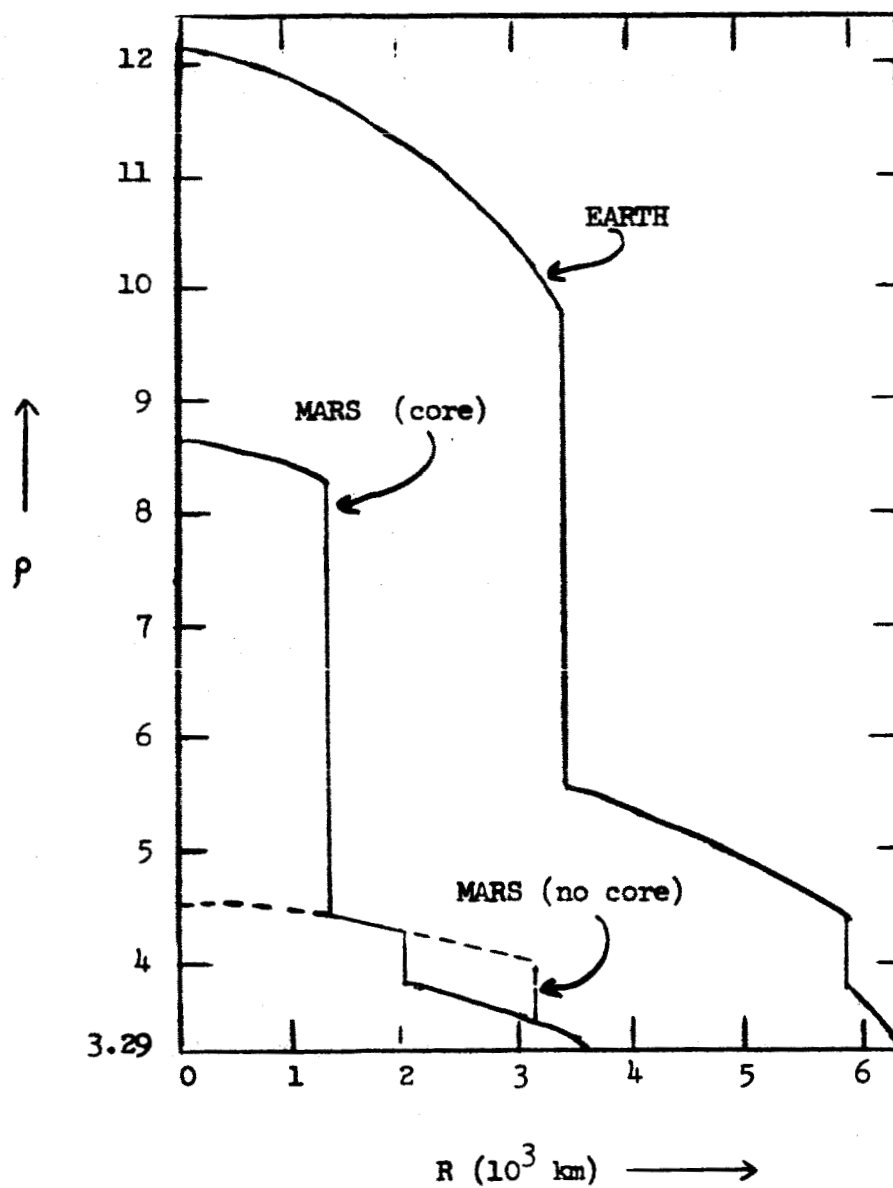


Figure B.1 Density Distribution in Two Models of Mars' Internal Structure, and a Model for Earth. (After H. Jeffreys, Reference B.6)

Lamar (Reference B. 3) has also considered density distribution models in some detail. His viewpoint is that the optical value ϵ_o is geometrically correct (represents the physical shape of the planetary surface) while ϵ_d determines the planetary gravitational field. This requires that the equatorial bulge observed optically must be compensated isostatically by variations in crustal thickness. His conclusions are: that one is not justified to assert that Mars has a more homogeneous density distribution than that of Earth; that it is likely that Mars has a core; the percentage of (low density) crustal rock in Mars must be an order of magnitude greater than that in Earth (0.3%); that the base of the martian crust is best represented by a change in phase basalt \longrightarrow eclogite, rather than a change in chemical composition.

In summary, the nature of the internal structure of Mars remains at best highly speculative, and only planetary probes properly equipped with seismological instrumentation are likely to produce new data necessary to help clarify the situation.

B. 8 Magnetic Field

There exist no physical data which indicate that Mars possesses a magnetic field of planetary origin. Singer has advanced the hypothesis that the equivalent magnetic moment of a planetary body may be proportional to its volume. He then uses the measured magnetic field $B_o \approx 0.3$ gauss at the equatorial surface of the Earth to compute the magnetic moment $M_E = 6.1 \times 10^{25}$ gauss-cm³. The magnetic moment of Mars would then be

$$M_M = M_E \left(\frac{R_M}{R_E} \right)^3 \quad (1)$$

where $R_M = 3400$ km is the mean radius of Mars,

$R_E = 6400$ km is the mean radius of Earth.

The hypothesis leads to $M_M = 9.2 \times 10^{24}$ gauss-cm³ for the magnetic moment of Mars. The equatorial magnetic field of Mars is then

$$B_M = M_M / R^3 \quad (2)$$

where R is the areocentric distance.

One should view with some skepticism this analog calculation based upon such a questionable hypothesis. The Mariner-2 spacecraft failed to detect any planetary contribution to the magnetic field during the Venus flyby, although the hypothetical calculation just discussed leads to magnetic field strengths easily detectable by the magnetometer on Mariner-2. One can argue that because Venus rotates very slowly (if at all) compared to Earth, while Mars rotates at a rate nearly equal to that of the Earth, the dependence of magnetic moment on volume may be a more valid hypothesis in the case of Mars. This remains to be proved. Mariner-4 will pass within about 8600 km of the surface, or an areocentric distance of about $3.5 R_M$ (Mars' radii). The field there would be $B \approx 0.007$ gauss = 700 γ , if one believes the volume calculation of Equation (1). Since the residual spacecraft field of Mariner-4 is less than 30 γ , such a field will be detectable.

If one assumes the alternate theory of geomagnetism, that is, the theory of convection currents in the Earth's molten ferrous core, then one would expect a smaller field than that given by Equation (2) for Mars. As a crude estimate, if the magnetic moment of a planet is proportional to the volume of the central core, the surface equatorial field of Mars would then be

$$B_{oM} = \left[\frac{R_{CM}}{R_{CE}} \cdot \frac{R_E}{R_M} \right]^3 B_{oE} \quad (3)$$

where R_{CM} and R_{CE} are the core radii of Mars and Earth, R_M and R_E are the corresponding planetary radii, and $B_{oE} = 0.3$ gauss is the surface equatorial field of Earth. There are two models of density distribution of Mars that can fit the astronomical data. One has no core ($R_{CM} = 0$) in which case (3) yields zero martian magnetic field. The other model has $R_{CM} \approx 1400$ km. Since $R_{CE} \approx 3500$ km, and $R_M = 3400$ km, $R_E = 6400$ km, one has

$$B_{oM} = 0.43 B_{oE} = 0.13 \text{ gauss} \quad (4)$$

$$B_M(R) = (0.13) \left(\frac{R_M}{R} \right)^3 \text{ gauss}$$

At the Mariner-4 flyby distance of $R = 3.5 R_M = 12000$ km (areocentric) one expects

$$B_M \sim 0.003 \text{ gauss} = 300 \gamma$$

which should be easily detectable.

In summary, it must be stated that no direct or even indirect evidence of a martian magnetic field is available. No adequate theory of the origin of the geomagnetic field, let alone an areomagnetic field, exists. Therefore, any estimates of such a martian field must be viewed with suspicion. Mariner-4 will fly by Mars in July of 1965 at an areocentric distance of some 12,000 km, and should give good magnetic field data provided the instruments and telemetry continue to function.

B. 9 Radiation Belts

There is no direct evidence for the existence of trapped particle belts (analogous to the Van Allen belts around Earth) around Mars.

There exists one highly speculative calculation (Reference B. 7), based on very arbitrary assumptions concerning the magnetic field and particle source functions, of a hypothetical radiation belt around Mars. It seems that a reasonable upper limit, for purposes of dosage calculations and the like, would be to assume energetic particle fluxes in martian belts not exceeding those measured for Earth. The degree of over-estimation involved in such an assumption is unknown.

APPENDIX C. MARS MISSION CRITERIA

Earthlanded Payload - 10,000 lbs

Basic Mission Module (7 man) - 68,700 lbs

Basic Solar Shield (1 Au) - 16,300 lbs¹

Mars Lander (MEM) - 50,000 lbs

Mars Orbit Return Module - 1,500 lbs

Life Support Expendables - 39 lbs/day

Solar Shield - Total Weight (W_s) - lbs¹

$$\text{Active Year (1986) } W_s = 9076 + \frac{5238}{R_p - 0.271}$$

$$\text{Intermediate Year (1982) } W_s = 12672 + \frac{2615}{R_p - 0.272}$$

$$\text{Quiet Year (1978) } W_s = 16300$$

Stopover Time - 10 days

Nuclear Isp - 800 sec

Cryogenic Chemical (H_2F_2) Isp - 450 sec

Storable Chemical Isp - 330 sec

Midcourse Correction - 100 M/sec. each leg
Storable Propellant

Circularizing Velocity After Aerodynamic Braking at Mars - 130 M/sec
Storable Propellant

Attitude Control - 1% each leg
0.2% Capture Orbit

Optimum Cryogenic Insulation/boiloff

Aerodynamic Mars Braking Scaling Law

$$W_{\text{Heat Shield}} = K (0.001386 \Delta V^2 + 0.00916 \Delta V + 0.2019) W_{\text{initial}}$$

Aerodynamic Earth Braking Scaling Law

$$W_{\text{initial}} = 38.43 \Delta V^2 - 144.36 \Delta V + 12,800$$

(ΔV - Km/sec)

1. Reduced to 75 percent of these values for 22 gm/cm² shield.

Propellant Tank Scaling Laws:

$$\text{Leave Earth - H}_2 - W_{p \text{ max}} = 342,500 \text{ lbs}$$

$$W_j = 0.16644 W_p + 6420$$

$$\text{Leave Earth, Arrive Mars, Leave Mars - H}_2\text{F}_2 - W_{p \text{ max}} = 400,000 \text{ lbs}$$

$$W_j = .03701 W_p + 0.259 T^{1/3} (.00569 W_p + 970)^{4/3}$$

$$+ 6334 \text{ (400,000 lbs max)}$$

$$A_o = .001915 W_p + 547$$

$$A_F = .003774 W_p + 429$$

Outbound Midcourse and Circularizing at Mars - Storable

$$W_j = 0.1154 W_p + 0.0259 (T)^{1/3} (0.00656 W_p + 489)^{4/3} + 1190$$

$$\text{Arrive Mars/Leave Mars - H}_2 - W_{p \text{ max}} = 342,500 \text{ lbs}$$

$$W_j = 0.12 W_p + 0.01492 (T)^{1/3} (0.02577 W_p + 493)^{4/3} + 8368$$

$$\text{Leave Mars - Storable - } W_{p \text{ max}} = 800,000 \text{ lbs}$$

$$W_j = 0.0284 W_p + 0.01492 T^{1/3} (0.0027 W_p + 1374)^{4/3} + 12,646$$

Inbound Midcourse - Storable

$$W_j = 0.0665 W_p + 937$$

FLYBY MISSION CRITERIA

Earth Landed Payload - 8500 lbs

Mission Module (3 man) - 65,000 lbs

Planet Probe - 10,000 lbs

Life Support Expendables - 20 lbs/day

Planet Passage Altitude: Mars - 1000 km ($R_d = 1.3$)

Venus - 1000 km ($R_d = 1.16$)

Nuclear I_{sp} - 800 sec

Cryogenic Chemical (H_2F_2) I_{sp} - 450 sec

Storable Chemical I_{sp} - 330 sec

Midcourse Correction - 200 m/sec outbound leg
300 m/sec inbound leg

Attitude Control - 1% each leg

Optimum Cryogenic Insulation/boiloff

Aerodynamic Earth Backing Scaling Law

$$W_{initial} = 38.43 \Delta V^2 - 144.36 \Delta V + 12,000$$

(ΔV km/sec)

Propellant Tank Scaling Laws:

Same as Stopover Mission